Development of Confined Rubberised Concrete for High Ductility Structural Applications

A thesis presented for the degree of

Doctor of Philosophy in Civil and Structural Engineering

at The University of Sheffield

By

Samar Raffoul

Sheffield

October 2017

To mom and dad

for your unconditional love and support

for giving endlessly

for always being there

Abstract

The global environmental and economic implications of the disposal of waste tyres have prompted research exploring valuable outlets for their components. Concrete is an inherently brittle material and can benefit from tyre rubber properties to achieve higher ductility and energy dissipation for special applications in locations of high deformation demands, such as coupling beams. Despite the prospective benefits, the use of rubber as partial mineral aggregate replacement negatively affects concrete workability and strength. Recent research has shown that the external confinement of RuC can benefit from its high lateral expansion and mitigate the drawbacks of RuC, leading to high strength. Nevertheless, the majority of this research is limited to low rubber contents, which restricts the deformability potential of confined rubberised concrete (CRuC).

This research aims to advance the understanding on unconfined and FRP-confined RuC, developed with high rubber contents and optimised mix parameters, leading the way for new high-strength high-deformability concrete elements.

More than forty RuC mixes were investigated experimentally to develop an understanding of the effect of rubber and various concrete mix parameters on RuC fresh properties and short-term compressive strength. An "optimum" RuC mix with adequate workability and strength at all rubber contents was developed for further study.

The influence of rubber (content and type) on the stress-strain behaviour of the optimised RuC mix was investigated in a second parametric study involving more than 60 cylinders. The addition of rubber to concrete led to high lateral strains and premature failure, particularly at high rubber contents, which can be exploited to activate external confinement. The mix with high rubber content (60% total aggregate replacement) was identified as most suitable for study to maximise the deformability in RuC.

The use of Aramid or Carbon FRP sheets as external confinement to high rubber contents RuC was examined experimentally under monotonic and cyclic uniaxial compression. This led to the development of constitutive models to accurately predict the performance of confined rubberised concrete (CRuC) subject to monotonic or cyclic loading. CRuC led to unprecedented axial strains (>6%) and compressive strength above 90 MPa, indicating high potential for its use in a variety of structural applications.

Acknowledgements

Table of Contents

List of Figures

Chapter 1. Introduction

Chapter 2. Optimisation of rubberised concrete with high rubber content

Chapter 3. Unconfined and FRP-confined rubberised concrete in axial compression

Chapter 4. Constitutive model for passively confined rubberised concrete

Chapter 5. Cyclic behaviour of FRP-confined rubberised concrete cylinders

List of Tables

List of Acronyms

AFRP	aramid fibre reinforced polymer;
AVG	average;
BSE	backscattered electron;
C	coarse rubber content (as a percentage of coarse aggregate volume);
CA	coarse mineral aggregate;
CFRP	carbon fibre reinforced polymer;
CR	coarse rubber;
CRuC	confined rubberised concrete;
EDS	energy dispersive X-ray spectroscopy;
F	fine rubber content (as a percentage of fine aggregate volume);
FA	fine mineral aggregate;
FR	fine rubber;
FRP	fibre reinforced polymer;
F&C	fine and coarse rubber content (as a percentage of total aggregate volume);
GFRP	glass fibre reinforced polymer;
ITZ	interfacial transition zone;
LOP	limit of proportionality;
LVDT	linear variable differential transformer;
P	plasticiser;
PFA	pulverised fuel ash;
RC	reinforced concrete;
RuC	rubberised concrete;
SCRuC	self-compacting rubberised concrete;
SD	standard deviation;
SEM	scanning electron microscopy;
SF	silica fume;
SG	specific gravity;
SP	superplasticiser;
SSD	saturated surface dry;
VSI	visual stability index;
w/b	water to binder ratio;

List of Symbols

Chapter 1. Introduction

μ_δ	displacement ductility;
μ_k	curvature ductility;
ε_{cu}	ultimate strain capacity of concrete in compression;

Chapter 2. Optimisation of rubberised concrete with high rubber content

ε	voids content
ϕ	solid concentration

Chapter 3. Unconfined and FRP-confined rubberised concrete in axial compression

E_c	concrete initial modulus of elasticity;
E_f	tensile modulus of elasticity of FRP fibres;
f_c	unconfined concrete compressive strength;
f_{cc}	confined concrete compressive strength;
f_f	tensile strength of the FRP coupon;
t_f	thickness of one layer of FRP sheet;
ε_a	axial compressive strain (taken as negative for compression);
ε_{cclLOP}	confined concrete hoop lateral strain at LOP;
ε_{ccLOP}	confined concrete axial compressive strain at LOP;
ε_{cclu}	confined concrete ultimate hoop lateral strain;
ε_{ccu}	confined concrete ultimate axial compressive strain;
ε_{cLOP}	unconfined concrete axial compressive strain at LOP;
ε_{clp}	unconfined concrete hoop lateral strains at peak stress;
ε_{cp}	unconfined concrete axial compressive strain at peak stress;
ε_{fu}	ultimate elongation of FRP coupons (in direct tension);
ε_l	hoop lateral strain (taken as positive for tension);
ε_{vol}	volumetric strain;

D	cylinder diameter;
E_c	concrete secant modulus of elasticity at various stress and strain values;
E_{co}	concrete initial modulus of elasticity;
E_f	tensile modulus of elasticity of FRP fibres;
E_{sec}	concrete secant modulus of elasticity at peak stress and strain;
$E_{sec,\omega}$	secant modulus (E_{sec}) of actively confined concrete at corresponding ω_w;
K_j	confining stiffness;
K_{jn}	confining stiffness normalised to the unconfined concrete strength;
n	number of layers of FRP confinement;
f_c	axial compressive stress in confined/unconfined concrete;
f_{co}	compressive strength of unconfined concrete;
f_{cc}	compressive strength of confined concrete;
$f_{cc,\omega}$	ultimate compressive stress of actively confined concrete at corresponding ω_w;
f_{cr}	critical stress;
f_l	lateral confinement pressure;
f_f	tensile strength of the FRP coupon;
t_f	dry fibre thickness of FRP sheet;
β	FRP confinement effectiveness factor;
ε_{ax}	cylinder axial strain (in absolute value);
ε_c	axial strain in confined/unconfined concrete in compression;
ε_{cc}	ultimate axial strain in FRP confined concrete in compression;
$\varepsilon_{cc,\omega}$	ultimate axial strain in actively confined concrete at corresponding ω_w;
ε_{ccl}	ultimate hoop lateral strain in FRP confined concrete in compression;
ε_{co}	axial strain at peak stress in the unconfined confined;
ε_{cr}	axial strain in FRP confined concrete at critical stress;
ε_{fu}	ultimate elongation of FRP coupons (in direct tension);
ε_l	lateral strain in confined concrete at different levels of stress;
ε_{lat}	cylinder lateral strain (in absolute value);
ε_{lcr}	lateral strain in FRP confined concrete at critical stress;
ε_{vol}	volumetric strain;
v	initial Poisson's ratio;
v_{cr}	Poisson's ratio at critical stress;
ω_w	mechanical volumetric confinement ratio;

Chapter 5. Cyclic behaviour of FRP-confined rubberised concrete cylinders

D	cylinder diameter;
$E_{c,0}$	concrete initial modulus of elasticity;
$E_{c,f}$	gradient of the linear portion of the envelope curve (i.e. after the critical point);
E_f	tensile modulus of elasticity of the FRP fibres;
$E_{c,i}$	initial gradient of the softening part of each reloading curve;
$E_{re,i}$	reloading secant modulus;
K_{jn}	normalised confining stiffness;
Φ_i	ratio of strength degradation;
n	number of FRP confining layers;
n_0	shape parameter that defines the curvature of the transition zone in the envelop curve;
$n_{0,i}$	shape parameter that defines the curvature of the softening part of the reloading curve;
$n_{re,i}$	shape parameter that defines the curvature of the hardening part of the reloading curve;
$n_{un,i}$	shape parameter that defines the curvature of the unloading curve;
f_0	intercept of the second (linear) part of the envelope curve with the y-axis;
$f_{0,i}$	intercept of the vertical at $(\varepsilon_{inf}, f_{inf})$ with the envelope curve for each reloading curve;
f_c	axial compressive stress in confined or unconfined concrete;
f_{cc}	compressive strength of confined concrete;
f_{co}	unconfined concrete compressive strength;
f_{cr}	critical stress;
f_f	tensile strength of the FRP coupon;
$f_{inf,i}$	axial compressive stress at the inflection point of each reloading curve;
$f_{new,i}$	reloading stress at $\varepsilon_{un,i}$ of the corresponding cycle;
$f_{re,i}$	axial stress upon intersection of reloading curve with the envelope;
$f_{un,i}$	axial stress at unloading;
t_f	dry fibre thickness of FRP sheet;
β	confinement effectiveness factor;
ε_c	axial compressive strain in confined or unconfined concrete;
ε_{cc}	confined concrete ultimate axial strain;
ε_{cl}	confined concrete ultimate hoop strain;
ε_{co}	axial strain at peak stress in unconfined confined;
ε_{cr}	axial strain at critical stress;
$\varepsilon_{inf,i}$	axial compressive strain at the inflection point of each reloading curve;
ε_{fu}	ultimate elongation of FRP coupons (in direct tension);

$\varepsilon_{pl,i}$ residual plastic strain upon full unloading;

$\varepsilon_{re,i}$ axial strain upon intersection of each reloading curve with the envelope;

$\varepsilon_{un,i}$ axial strain at unloading;

ω_w mechanical volumetric confinement ratio;

Chapter 1

Introduction

1.1   RESEARCH MOTIVATION

Current annual global production of tyres exceeds 2.9 billion units per year and with the rapid growth of developing countries, this production rate is predicted to further increase (Freedonia, 2014). The disposal of waste tyres or waste tyre by-products is governed by stringent environmental protocols in most developed countries. For instance, the European Landfill Directive (Council Directive 1999/31/EC) prohibits the disposal of waste tyre products in landfills, whilst a subsequent directive (Council Directive 2008/98/EC) encourages waste reuse rather than recycling. This has increased efforts to find viable alternative solutions for waste tyre rubber disposal. On the other hand, in many developing countries, waste tyres are often disposed of in landfills leading to significant threats to the environment and public health (WBCSD, 2008; Sienkiewicz *et al.*, 2012). Hence from an environmental and economical point of view, a global outlet for waste tyre disposal is essential for both developed and developing countries.

The past few years have seen a surge in the research investigating uses for waste tyre by-products, including vulcanised rubber (forming around 70-80% of the tyre by mass (Sienkiewicz *et al.*, 2012)), steel and textile reinforcement in concrete (Pilakoutas *et al.*, 2015). A typical tyre cross-section is shown in Figure 1. These by-products are derivatives from highly engineered products and have excellent properties. Concrete is the most widely used material in the construction industry with a global annual production exceeding 25 gigatonnes per annum (Gursel *et al.*, 2014). The use of tyre components in concrete can therefore create a major outlet for waste tyres worldwide and mitigate many environmental problems. Nevertheless, the physical and mechanical characteristics of tyre rubber have been the chief incentive behind the development of rubberised concrete (RuC).
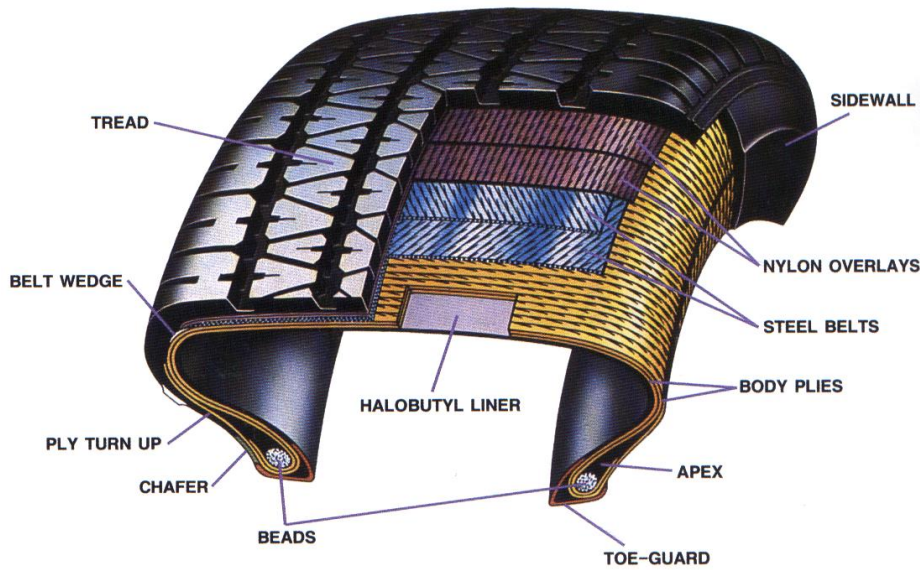
Figure 1. Typical constituents of tyres (ETRma, 2010)

Concrete is an inherently brittle material but reinforced concrete structures can achieve some ductility by using appropriately detailed steel reinforcement. The ductility of structural systems is generally described as their ability to offer resistance in the inelastic domain, i.e. to sustain high inelastic deformations and absorb energy through plasticity and hysteresis in critical elements of the structure with minimum degradation in its structural strength and stiffness (Paulay and Priestley, 1992; Elghazouli, 2016). Global ductility is related to element displacement ductility (μ_δ) and this in turn is dependent on the curvature ductility (μ_k) of key sections. In reinforced concrete elements, μ_k is limited by the ultimate strain capacity of concrete in compression (ε_{cu}), around 0.004 in normal strength concrete (Paulay and Priestley, 1992). This limits overall deformability and special devices are normally required in locations of high deformation demands.

Rubber particles are characterised with high energy absorption capacity, flexibility and an ability to maintain their volume when compressed as well as high abrasion resistance, sound absorption capacity, electrical and heat insulation and low unit weight (Freakley and Payne, 1978; Leblanc, 2002; Fröhlich, Niedermeier and Luginsland, 2005; ETRma, 2010).

Research shows that intrinsic mechanical properties of rubber can be utilised to achieve high ductility and deformability (higher ε_{cu}) in RuC (Zheng, Huo and Yuan, 2008; Najim and Hall, 2010; Mohammadi, Khabbaz and Vessalas, 2014). The successful development of highly deformable RuC can be of great value to engineers as it can be used for valuable structural applications as follows:

i) Coupling beams (in coupled wall systems), which are designed to reduce the base moments of individual walls and dissipate large amounts of energy. Coupling beams attract high ductility demand and must avoid excessive strength degradation due to load cycles (Elghazouli, 2016).

ii) Plastic hinge zones for energy dissipation in reinforced concrete frame systems

iii) Short columns for higher deformability

iv) Integral or semi-integral bridge elements, where highly deformable concrete elements can be used in abutments, piers and transition slabs, eliminating the need for discontinuous bridge elements (e.g. bearings or movement joints).

v) Base isolation systems, which necessitate high energy dissipation capacity to isolate superstructures and maintain their integrity under extreme loading.

vi) Pile sections, to accommodate lateral displacement demands at interfaces between different soil layers.

Rubberised concrete offers other distinct advantages, compared to conventional concrete, including a reduced unit weight (Pierce and Blackwell, 2003), enhanced toughness (Goulias and Ali, 1998), higher vibration damping capacity (Najim and Hall, 2012), improved resistance to fatigue (Liu *et al.*, 2013) and impact (Atahan and Yücel, 2012), higher freeze/thaw resistance (Richardson, Coventry and Ward, 2012; Gesoğlu *et al.*, 2014), as well as increased sound, thermal and electric insulation (Sukontasukkul, 2009; Issa and Salem, 2013), which make it attractive for variety of other applications.

Nonetheless, the use of rubber in concrete leads to several material and technological issues that have, to date, deterred its development for structural applications (Khatib and Bayomy, 1999; Khaloo, Dehestani and Rahmatabadi, 2008).

Current applications for RuC are limited to:

i)   Non-structural applications such as in lightweight fills (Pierce and Blackwell, 2003; Argyroudis *et al.*, 2016), concrete pedestrian blocks (Ling, 2012; Da Silva *et al.*, 2015), lightweight concrete blocks (Mohammed *et al.*, 2012), and concrete panels for thermal or acoustic insulation (Sukontasukkul, 2009; Holmes, Browne and Montague, 2014; Pastor *et al.*, 2014; Ghizdăveț *et al.*, 2016), and

ii) Applications with low-medium compressive strength requirements, where the reduced weight, vibration damping capacity and resistance to impact and cyclic loads are required. Examples include applications in concrete road pavements (Hernández-Olivares *et al.*, 2007; Meddah, Beddar and Bali, 2014; Mohammadi, Khabbaz and Vessalas, 2014; Liu *et al.*, 2015) or road-side barriers (Elchalakani, Aly and Abu-Aisheh, 2016).

1.2   SCIENTIFIC BACKGROUND

Rubber in concrete has been shown to lead to undesirable losses in workability and consistency, degradation in strength and stiffness, premature cracking and an increase in lateral expansion, predominantly at higher rubber contents (Toutanji, 1996; Khatib and Bayomy, 1999; Li *et al.*, 2004; Batayneh, Marie and Asi, 2008; Reda Taha *et al.*, 2008; Turatsinze and Garros, 2008; Ganjian, Khorami and Maghsoudi, 2009). The effect of rubber on some fresh concrete properties and mechanical properties is described in 1.2.1 and 1.2.2, respectively.

The reduction in RuC strength due to the incorporation of rubber has been a major obstacle to its development for structural applications (refer to 1.2.2). This reduction is predominantly

attributed to the rubber softness and high Poisson's ratio (around 0.5), which alters the overall volumetric behaviour of the concrete. When subjected to axial stress, the rubber expands laterally at a higher rate than the surrounding concrete, leading to the development of tensile stresses and the premature micro-cracking in the vicinity of the rubber particles (Khatib and Bayomy, 1999; Reda Taha *et al.*, 2008; Ganjian, Khorami and Maghsoudi, 2009). Provided these lateral dilations are controlled, losses in strength can be reduced. This can be achieved by confinement, as will be discussed in 1.2.3.

The following sections (1.2.1-1.2.3) provide additional literature on rubberised concrete that is relevant to this research. Since the structural applications with the most potential for Confined Rubberised Concrete (CRuC) are associated with energy dissipation due to dynamic loads, a brief review on the research on cyclically loaded CRuC is provided in section 1.2.3.

1.2.1 Fresh properties of rubberised concrete

Compared to concrete with conventional mineral aggregates, RuC generally exhibits lower workability, demonstrated by a reduced slump and an increase in air content, segregation and bleeding (Toutanji, 1996; Li *et al.*, 2004). This effect on concrete workability was found to be more significant for larger rubber contents (Mohammadi, Khabbaz and Vessalas, 2014) and more evident when large rubber chips are used to replace coarse aggregates as opposed to fine rubber replacing sand (Khaloo, Dehestani and Rahmatabadi, 2008; Reda Taha *et al.*, 2008; Güneyisi *et al.*, 2016). On the contrary, Khatib and Bayomy (1999) found that replacing high volumes of sand with rubber was more detrimental to the mix flowability. This can be attributed to the significant contribution of sand to concrete flowability (Neville, 1995; Fung, Kwan and Wong, 2009), as well as the rubber relatively high surface area to weight ratio, which can lead to flocculation and inter-particular surface forces among fine rubber particles (Sukontasukkul and Chaikaew, 2006; Wong and Kwan, 2008; Fennis, Walraven and den Uijl, 2013).

This detrimental effect that the rubber particles have on concrete has been attributed to physical and mechanical properties of the rubber particles including: i) the rough surface of the shredded particles, leading to excessive friction with the cement paste and increasing their tendency to interlock (Eldin and Senouci, 1994); ii) rubber contamination (with steel wires or textile fabric); iii) low density of rubber, compared to other concrete components (Atahan and Yücel, 2012); iv) rubber hydrophobicity (Mohammadi, Khabbaz and Vessalas, 2014); and v) flocculation among the fine rubber particles (Neville and Brooks, 1990; Sukontasukkul and Chaikaew, 2006). Additional information on the properties of rubber particles can be found in Appendix A.

Research on rubberised concrete has often used the fresh concrete slump as a qualitative measure for workability (Toutanji, 1996; Khatib and Bayomy, 1999; Güneyisi, Gesoğlu and Özturan, 2004; Najim and Hall, 2010). Workability, however, is defined as the ability to mix, cast and consolidate a fresh concrete mixture whilst preserving its homogeneity and hence, the use of slump as a sole measure of the quality of concrete has led to misperceptions and inappropriate comparisons of the effect of rubber on the concrete performance. For example, whilst a highly fluid mix (i.e. with high slump) was often viewed as a positive quality in fresh RuC performance, it can also be associated with rubber floating and segregation, if the concrete mix parameters were not appropriately modified, due to the relatively low density of the rubber compared to mineral aggregates (Khatib and Bayomy, 1999; Turatsinze and Garros, 2008; Topçu and Bilir, 2009; Ismail and Hassan, 2015).

The rheology of concrete is affected by several mix parameters, apart from rubber type and volume, such as the ratio of coarse to fine mineral aggregates, the content of cement and other binder materials, the water and admixture contents as well as the preparation and casting techniques (Najim and Hall, 2010; Ismail and Hassan, 2015). These parameters affect the packing of the concrete mix, which in turn influences the pore structure and the mix flowability and cohesion of the fresh concrete (De Larrard, 1999). Compared to conventional mineral aggregates, rubber particles have very different shape and surface characteristics and therefore

the use of traditional mix approaches might not be effective in avoiding the severity of the effect of rubber on concrete properties. A review on the significance of granular particles on concrete performance can be found in Appendix B. Limited research exists on the use of rubber in concrete with self-compacting properties, often designed to satisfy the demand for resistance to segregation and high flowability in a concrete mixture (Bignozzi and Sandrolini, 2006; Turatsinze and Garros, 2008; Najim and Hall, 2012). Turatsinze and Garros (2008) report that the use of self-compacting rubberised concrete (SCRuC), optimised using fine calcareous fillers, can improve the slump and the resistance to segregation of the RuC mix. Similarly, Bignozzi and Sandrolini (2006) and Ismail and Hassan, 2015 reported superior fresh properties for SCRuC, where large volumes of rubber could be suitably used in the concrete. To promote particle packing other researchers have sought to replace the concrete mineral aggregates with rubber particles of similar gradation (Sukontasukkul and Chaikaew, 2006; Pedro, De Brito and Veiga, 2012) or with gap graded particles (Youssf *et al.*, 2014). However, the influence of rubber on the packing of the concrete mixture has not been studied sufficiently. As it stands, the majority of researchers use rubber in concrete as a direct replacement of mineral aggregates without modifying other mix parameters (Mohammadi, Khabbaz and Vessalas, 2014). Hence, there is a need to better understand the fresh properties of RuC and develop techniques to optimise the mix designs with high rubber contents.

1.2.2 Rubberised concrete mechanical properties

Research shows that the use of high rubber contents in concrete can lead to up to 90% reduction in the RuC compressive strength, when compared to the original concrete mix (Toutanji, 1996; Khatib and Bayomy, 1999; Batayneh, Marie and Asi, 2008). The reduction in RuC strength is influenced by a variety of parameters including: the rubber content, size and shape, as well as the aforementioned mix parameters that influence the concrete workability and pore structure (see section 1.2.2).

The large number of parameters influencing RuC strength has led to large disparities among the results in the literature and makes it difficult to quantify the influence of rubber on concrete strength (see Chapter 2, Fig.1). One common issue in the literature on RuC is that researchers erroneously compare different coarse or fine aggregate replacements by considering the percent by volume of either fine or coarse aggregate replacement, rather than total aggregate replacement. These concrete mixes often differ in their aggregate content and the coarse to fine aggregate ratio and thus their direct comparison is unsuitable (Bignozzi and Sandrolini, 2006).

The lower strength of RuC has been mainly attributed to:

i)   the high Poisson's ratio and softness of the rubber particles, which, when compressed, undergo higher lateral expansion than the surrounding mix leading to high stress concentration and micro-cracking (Khatib and Bayomy, 1999; Li *et al.*, 2004; Ganjian, Khorami and Maghsoudi, 2009).

ii) the presence of a weak bond at the rubber-cement paste interphase transition zone (ITZ). This is attributed to the rubber hydrophobicity, which is intensified by the presence of Zinc Stearate, often added to the tyres to improve their service life (Segre, Monteiro and Sposito, 2002). According to Eldin and Senouci (1993), this lack of good bond leads the rubber to act as a void and reduces stress-transfer in the mix. This notion, however, has been disputed by many others who report the development of interlock of the rough surface of the rubber particles with the cement paste (Turatsinze, Granju and Bonnet, 2006; Reda Taha *et al.*, 2008).

iii) segregation and non-homogeneity of the hardened concrete, mainly caused by the rubber low density (Ganjian, Khorami and Maghsoudi, 2009). This effect is less evident in mixes that were appropriately designed to accommodate the rubber aggregates (Ismail and Hassan, 2015).

iv) high porosity and air void ratio in the concrete mix (Khaloo, Dehestani and Rahmatabadi, 2008). This is due to the combined effect of rubber hydrophobicity, surface characteristics and inadequate packing of the concrete constituents.

To offset the effect of rubber on RuC compressive strength, various physical/chemical pre-treatments have been used (Chou, Yang, *et al.*, 2010; Dong, Huang and Shu, 2013; Najim and Hall, 2013; Onuaguluchi and Panesar, 2014; Ossola and Wojcik, 2014). Rubber has been pre-washed with water (Richardson, Coventry and Ward, 2012), or pre-treated with sodium hydroxide (NaOH) (Segre, Monteiro and Sposito, 2002; Meddah, Beddar and Bali, 2014), organic waste sulfur (C_2S) (Chou, Lin, *et al.*, 2010), or polyvinyl alcohol (Ganesan, Raj and Shashikala, 2013). Other methods included partial oxidation of the crumb rubber (Chou, Yang, *et al.*, 2010) and the use of a silane coupling agent (Huang, Shu and Cao, 2013). Despite some success with some pre-treatments (increase in strength ranging between 3-40%), the results are mostly inconclusive, as often mixes with pre-treated rubber are not compared with control RuC mixes with untreated rubber (Ganesan, Raj and Shashikala, 2013). Additionally, the influence of the chemical pre-treatments on the concrete durability, cost and environmental impact has not been extensively investigated.

Previous research shows that the influence of rubber on the concrete stress-strain performance of RuC is more evident at high rubber contents (Batayneh, Marie and Asi, 2008; Khaloo, Dehestani and Rahmatabadi, 2008; Atahan and Yücel, 2012). According to Batayneh, Marie and Asi (2008), the replacement of fine aggregates by up to 40% by volume led to a significant reduction in strength and a brittle behaviour similar to that of conventional concrete. A further increase in rubber content (above 60% sand volume), however, led to a fundamental change in the overall stress-strain behaviour resulting in a more ductile material. Future work, however, is needed to further investigate the influence of rubber volume on the concrete stress-strain behaviour including its lateral expansion (volumetric behaviour).

It is evident from the above literature that to benefit from the high deformability potential of RuC, high rubber contents must be used. Nevertheless, as shown in 1.2.1 and 1.2.2, such high rubber contents lead to significant influence on the concrete fresh and hardened properties. Whilst the fresh properties may be improved by optimising the concrete mix design and particle gradation, further action is required to enhance the strength of high rubber content RuC, making it suitable for structural applications where enhanced deformability is required.

1.2.3   Confined rubberised concrete

It is well known that the lateral confinement of concrete can significantly improve its strength and axial strain capacities (Mander, Priestley and R.Park, 1988). For such mechanism to be effective, however, sufficient lateral expansion has to occur in the concrete. Therefore, it is anticipated that the high lateral expansion developed in RuC with high rubber contents at low load levels can be exploited to activate the confining effect at earlier stages of loading. At present, steel and fibre reinforced polymer (FRP) materials are commonly used as external confinement to retrofit damaged structures and strengthen undamaged deficient structures (Garcia *et al.*, 2015).

FRP-confined concrete is characterised by a bi-linear stress-strain response, where the second (linear) gradient of the curve is controlled by the normalised FRP confining stiffness (Teng *et al.*, 2003; Papastergiou, 2010). The failure of FRP-confined conventional concrete is generally governed by the strain capacity of the FRP sheet, normally around 60-80% of its ultimate strain capacity in direct tension (Matthys, Toutanji and Taerwe, 2006). Hence, the stiffness and ultimate strain capacity of the confining material play a significant role in the strength and deformability potential of the confined material. The typical properties of commonly used confining materials are shown in Figure 2.
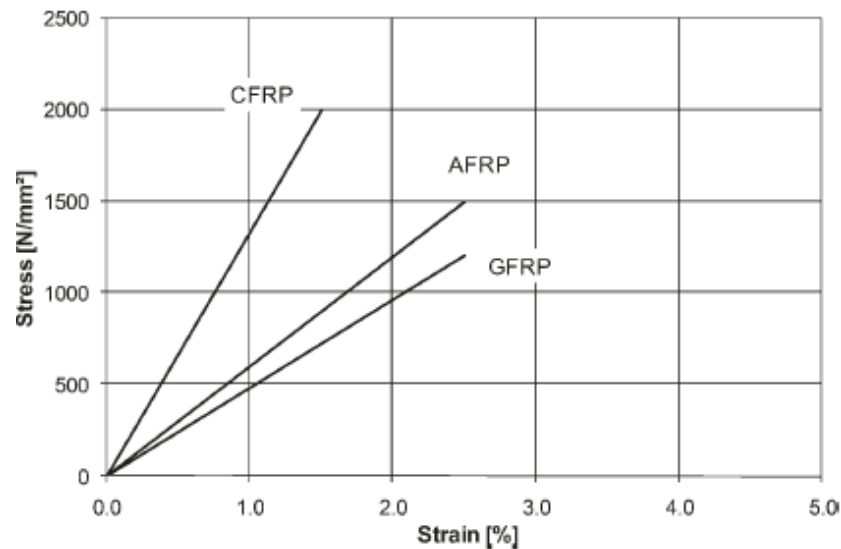
Figure 2. Typical stress-strain diagram of FRP fibres in tension along their principle axes (Model Code, 2010)

Recent studies have investigated the use of different confining materials as external confinement for RuC (Li, Pang and Ibekwe, 2011; Duarte *et al.*, 2015; Moustafa and ElGawady, 2016). For instance, Youssf *et al.* (2014) and Li, Pang and Ibekwe (2011) report that casting RuC in Carbon and Glass FRP tubes, respectively, leads to high compressive strength (>110 MPa). While the strength of such concrete is suitable for most structural applications, its influence on the concrete ductility was minimal, when compared to conventional concrete (Lam and Teng, 2004). Duarte *et al.* (2016) reported significant improvements to the ductility of columns (up to 50%) when casting RuC in cold-formed steel tubes. Nonetheless, according to Duarte *et al.* (2016), a lower dilation angle was observed for RuC, which led to the RuC columns being less effectively confined by the steel tubes, when compared to conventional concrete columns.

It must be noted that the previous studies adopted only limited rubber contents up to 10% of total aggregate (Youssf *et al.*, 2014), 30% of fine aggregate (Li, Pang and Ibekwe, 2011) or 15% of the total aggregate (Duarte *et al.*, 2016). This limited rubber content (in essence, all under 15% of the total aggregate), is insufficient to produce high lateral dilations necessary to

mobilise early the passive confinement. To date, the effect of confining optimised RuC with high rubber contents > 20% of the total aggregate content has not yet been investigated.

As shown in Figure 2, AFRP sheets incorporate both high stiffness and tensile strain capacity (intermediate properties between CFRP and GFRP fibres). This higher strain capacity of AFRP can allow the development of higher deformations, compared to CFRP, while maintaining higher strength than that achieved by GFRP. Despite the excellent performance of Aramid FRP (AFRP) as a confining material (Ozbakkaloglu and Akin, 2012), to date, no research has been reported on AFRP CRuC and thus further research is needed.

Of particular importance for the targeted applications of CRuC (see section 1.1) is to investigate for its performance under cyclic loading. Duarte *et al.* (2016) and Youssf, ElGawady and Mills (2016) show that CRuC columns subjected to both axial load and bending show remarkable ductility (up to 40% increase in ductility factor for 15% total aggregate replacement with rubber); nevertheless, no research can be found on the parameters of the uniaxial cyclic behaviour of AFRP/CFRP CRuC needed for the accurate modelling of structural elements.

The high confinement effectiveness and high strain capacity of CRuC (Li, Pang and Ibekwe, 2011) means that previous constitutive models for conventional concrete may not be suitable to predict the performance. Further research is needed to develop constitutive models that can accurately describe the cyclic mechanical behaviour of RuC confined with suitable confining materials, leading the way for the development of new deformable elements and relevant design guidelines.

1.3   AIM AND OBJECTIVES

The aim of this research is to advance the understanding on optimised unconfined and FRP-confined rubberised concrete, opening the way for the development of new high-strength high-deformability concrete elements.

To achieve this aim, experimental and analytical work for both confined and unconfined concrete was carried out. A breakdown of the principal objectives of this research is given in the following:

1. Identify the effect of concrete mix parameters, rubber content and type on the properties of RuC by conducting an extensive experimental parametric study.

2. Design RuC mixes that can accommodate high rubber volumes with minimum effect on the concrete fresh performance and mechanical properties.

3. Examine the effect of rubber content and type on the stress-strain behaviour of unconfined concrete through an experimental parametric study.

4. Identify a suitable RuC mix with high deformability potential for confined applications.

5. Examine the effect of different types and level of FRP confinement, cylinder size, and different loading conditions (monotonic or cyclic) on CRuC performance through an experimental parametric study.

6. Assess degradation parameters of CRuC subjected to cyclic loading.

7. Examine existing constitutive models for conventional confined concrete and assess their potential to describe the behaviour of CRuC.

8. Develop constitutive models for CRuC subject to monotonic or cyclic loading

1.4   RESEARCH SIGNIFICANCE

The successful development of CRuC for uses in special structural applications where there is high deformation demand addresses global challenges such as the environmental and economic impact of waste tyre disposal and structural safety requirements in the construction industry (as described in 1.1).

This study contributes to a larger research project, Anagennisi (http://anagennisi.org/wordpress/) funded by the 7th Framework Programme of the European Commission, which aims to reuse all the tyre components in concrete for valuable structural applications (Pilakoutas *et al.*, 2015). The collective work of the project partners means that an extensive experimental database ranging from small, medium and large scale tests has been created allowing the broader understanding of the material's performance. As part of the project, a life cycle analysis, design recommendations, demonstration project and dissemination events regarding the use of tyre rubber, steel fibres and textile fibres have also been carried out. In principle, the collective work achieved through the Anagennisi project has contributed to advance knowledge in the following areas:

- ❖ Consolidation of existing fragmented research on rubberised concrete.

- ❖ Further the understanding of rubberised concrete as a material through appropriate characterisation and constitutive models.

- ❖ Progress the understanding of the effect of particle packing on RuC fresh and hardened state mechanical properties.

- ❖ Provide confidence in the material's potential, through contributing to preliminary design recommendations, dissemination works and demonstration projects to address industry and end-user concerns.

- ❖ Develop and demonstrate the performance of highly deformable concrete.

- ❖ Establish the potential benefits of CRuC in structural applications (e.g. in base isolation, short columns or integral bridges), which could inspire future research.

The work presented in this thesis has contributed to the above outputs and led to the development of i) an optimal mix design for CRuC, ii) an extensive set of high quality data that provide experimental evidence of the effect of critical parameters on the fresh and hardened

properties of unconfined RuC and FRP CRuC, and iii) analytical constitutive models for CRuC subjected to both monotonic and cyclic loading suitable for analysis and design.

1.5   THESIS LAYOUT

This thesis will be presented in an "alternative thesis" format and consists of two main types of chapters:

1. Chapter 1 (Introduction) and Chapter 6 (Conclusions and recommendations for future research) are written following the conventional thesis format

2. Chapters 2-5 are based on self-contained journal papers; two published (2,3), one submitted (4) and one in preparation (5); with small alterations where necessary to suit the overall flow of the thesis

Additional information on the properties of rubber are provided in Appendix A. Appendix B provides the relevant literature on the particle packing of concrete mineral aggregates. Appendix C includes photos of the fresh concrete mixes during the optimisation practice. Appendix D includes instrumentation details. Appendix E and F include data from the experimental tests on CRuC subjected to monotonic and cyclic loading, respectively. Finally, Appendix G incudes specimens' photos (before and after failure) that could not be included in the main chapters of the thesis (journal papers), due to space limitations.

A brief description of the thesis chapters and how they contribute to the objectives is provided as follows:

Chapter Two is based on Raffoul *et al.* (2016) and addresses objectives 1-2. It comprises an experimental investigation on the effect of tyre rubber particles on the properties of concrete. More than 40 rubberised concrete mixes were examined to develop an understanding of the effect of rubber and other mix parameters on RuC fresh properties and short-term compressive

behaviour. The parameters investigated were rubber content, type of mineral aggregate replacement, type of binder material, water or admixture content, and rubber surface pre-treatments. Microstructural analysis is used to examine the rubber-cement paste bond at the Interphase Transition Zone (ITZ). This study leads to the development of an "optimum" RuC mix, combining high workability and adequate compressive strength at all rubber contents. Following research investigates the effect of rubber content and type on the stress-strain performance of the optimised RuC mix.

Chapter Three is based on Raffoul *et al.* (2017a), and addresses objectives 3-4. More than sixty confined and unconfined cylinders, cast using the optimised concrete mix parameters described in chapter two, were tested in uniaxial compression. The stress-strain behaviour of unconfined rubberised concrete with various rubber contents was examined to develop an understanding of RuC performance. A suitable mix possessing the highest deformability potential, by sustaining high lateral strains that can be exploited to effectively activate the confinement, is identified for further study. To achieve this, the mix is expected to have high rubber contents, which was only possible following the previous optimisation practice (Chapter two). Cylinders cast using the selected mix were confined with two or three layers of AFRP sheets and tested in uniaxial compression. The use of additional confining materials and configurations will be discussed in Chapter four.

Chapter Four is based on Raffoul *et al.* (2017b) (submitted) and addresses objectives 5,7 and 8. Examines the suitability of existing confinement models and assesses their potential use for modelling CRuC monotonic behaviour. It proposes a unified analytical constitutive model for RuC confined with AFRP or CFRP sheets. More than 38 CRuC cylinders with high rubber content (60% total aggregate replacement) were cast and tested in uniaxial compression under monotonic and cyclic loading. Parameters investigated were the amount and type of external confinement as well as the cylinder size. Additional work on the cyclic behaviour of AFRP and

CFRP CRuC, which is of particular importance for the targeted applications of the material (see 1.1), is presented in Chapter five.

Chapter Five is based on Raffoul *et al.* (2017c) (under preparation) and addresses objectives 5-8. It investigates the key parameters that govern the cyclic behaviour of FRP CRuC. This study is based on the large experimental study on cyclically loaded AFRP and CFRP rubberised concrete cylinders (Chapter 4). The results are analysed in terms of the effect of loading history on the shape of the cyclic unloading and reloading stress-strain curves, the concrete strength and stiffness degradation, the concrete ultimate stress and strain capacity. The results of this analysis are used to develop a constitutive model that can predict the behaviour of AFRP and CFRP CRuC subject to cyclic loading.

Chapter Six comprises concluding remarks based on Chapters 2-5. Additional comments and recommendations for future work are also provided.

1.6   REFERENCES

Argyroudis, S., Palaiochorinou, A., Mitoulis, S. and Pitilakis, D., (2016). Use of rubberised backfills for improving the seismic response of integral abutment bridges. *Bulletin of Earthquake Engineering*. **14**(12), 3573–3590. Available from: doi: 10.1007/s10518-016-0018-1.

Atahan, A. O. and Yücel, A. O., (2012). Crumb rubber in concrete: Static and dynamic evaluation. *Construction and Building Materials*. **36**, 617–622.

Batayneh, M. K., Marie, I. and Asi, I., (2008). Promoting the use of crumb rubber concrete in developing countries. *Waste Management*. **28**(11), 2171–2176.

Bignozzi, M. C. and Sandrolini, F., (2006). Tyre rubber waste recycling in self-compacting concrete. *Cement and Concrete Research*. **36**(4), 735–739.

Chou, L. H., Yang, C. K., Lee, M. T. and Shu, C. C., (2010). Effects of partial oxidation of crumb rubber on properties of rubberized mortar. *Composites Part B: Engineering*. **41**(8), 613–616.

Chou, L. H., Lin, C. N., Lu, C. K., Lee, C. H. and Lee, M. T., (2010). Improving rubber concrete by waste organic sulfur compounds. *Waste Management & Research*. **28**(1), 29–35.

Council Directive 1999/31/EC of 26 April 1999 on *the Landfill of Waste*.

Council Directive 2008/98/EC of 19 November 2008 on *Waste and Repealing Certain Directives*.

Dong, Q., Huang, B. and Shu, X., (2013). Rubber modified concrete improved by chemically active coating and silane coupling agent. *Construction and Building Materials*. **48**, 116–123.

Duarte, A. P. C., Silva, B. A., Silvestre, N., de Brito, J., Julio, E. and Castro, J. M., (2015). Experimental study on short rubberized concrete-filled steel tubes under cyclic loading. *Composite Structures*. **136**, 394-404.

Duarte, A. P. C., Silva. B. A., Silvestre, N., de Brito, J., Julio, E. and Castro, J.M., (2016). Tests and design of short steel tubes filled with rubberised concrete. *Engineering Structures*. **112**, 274–286.

Elchalakani, M., Aly, T. and Abu-Aisheh, E., (2016). Mechanical properties of rubberised concrete for road side barriers. *Australian Journal of Civil Engineering*. **14**(1), 1–12.

Eldin, N. N. and Senouci, A. B., (1993). Observations on rubberized concrete behavior. *Cement, Concrete and Aggregates*. ASTM International. **15**(1), 74–84.

Eldin, N. N. and Senouci, A. B., (1994). Measurement and prediction of the strength of rubberized concrete. *Cement and Concrete Composites*. **16**(4), 287–298.

Elghazouli, A., (2016). *Seismic design of buildings to Eurocode 8*. 2nd ed. CRC Press.

European Tyre & Rubber manufacturers' association (ETRma). (2012). Reinforcing Fillers in the Rubber Industry - Assessment as potential nanomaterials with focus on tyres. [online] Available from; http://www.etrma.org/uploads/Modules/Documentsmanager/201201-etrma-fact-sheet---carbon-black-and-silica-2.pdf

Fennis, S., Walraven, J. C. and den Uijl, J. A., (2013). Compaction-interaction packing model: regarding the effect of fillers in concrete mixture design. *Materials and structures*. **46**(3), 463–478.

fib Model Code (Fédération internationale du béton), (2010). Model Code for Concrete Structures 2010. *Berlin, Germany*.

Freakley, P. K. and Payne, A. R., (1978). *Theory and practice of engineering with rubber*. Applied Science Publishers London.

Freedonia., (2014). World Tyres: Industry study with Forecasts for 2017 & 2022. [online]. *The Freedonia Group* [Viewed 2 October 2017]. Available from: https://www.freedoniagroup.com/industry-study/world-tires-3357.htm.

Fröhlich, J., Niedermeier, W. and Luginsland, H.-D., (2005). The effect of filler–filler and filler–elastomer interaction on rubber reinforcement. *Composites Part A: Applied Science and Manufacturing*. **36**(4), 449–460.

Fung, W. W. S., Kwan, A. K. H. and Wong, H. H. C., (2009). Wet packing of crushed rock fine aggregate. *Materials and structures*. **42**(5), 631–643.

Ganesan, N., Raj, B. and Shashikala, A. P., (2013). Behavior of Self-Consolidating Rubberized Concrete Beam-Column Joints. *ACI Materials Journal.* **110**(6), 697–704.

Ganjian, E., Khorami, M. and Maghsoudi, A. A., (2009). Scrap-tyre-rubber replacement for aggregate and filler in concrete. *Construction and Building Materials*. **23**(5), 1828–1836.

Garcia, R., Pilakoutas, K., Hajirasouliha, I., Guadagnini, M., Kyriakides, N. and Ciupala, M. A., (2015). Seismic retrofitting of RC buildings using CFRP and post-tensioned metal straps: shake table tests. *Bulletin of Earthquake Engineering*. **15**(8), 1–27.

Gesoğlu, M., Güneyisi, E., Khoshnaw, G. and İpek, S., (2014). Abrasion and freezing–thawing resistance of pervious concretes containing waste rubbers. *Construction and Building Materials*. **73**, 19–24.

Ghizdăveţ, Z., Ştefan, B. M., Nastac, D., Vasile, O. and Bratu, M., (2016). Sound absorbing materials made by embedding crumb rubber waste in a concrete matrix. *Construction and Building Materials*. **124**, 755–763.

Goulias, D. G. and Ali, A. H., (1998). Evaluation of rubber-filled concrete and correlation between destructive and nondestructive testing results. *Cement, concrete and aggregates*. **20**(1), 140–144.

Güneyisi, E., Gesoglu, M., Naji, N. and İpek, S., (2016). Evaluation of the rheological behavior of fresh self-compacting rubberized concrete by using the Herschel–Bulkley and modified Bingham models. *Archives of Civil and Mechanical Engineering*. **16**(1), 9–19.

Güneyisi, E., Gesoğlu, M. and Özturan, T., (2004). Properties of rubberized concretes containing silica fume. *Cement and Concrete Research*. **34**(12), 2309–2317.

Gursel, A. P., Masanet, E., Horvath, A. and Stadel, A., (2014). Life-cycle inventory analysis of concrete production: a critical review. *Cement and Concrete Composites*. **51**, 38–48.

Hernández-Olivares, F., Barluenga, G., Parga-Landa, B., Bollati, M. and Witoszek, B., (2007). Fatigue behaviour of recycled tyre rubber-filled concrete and its implications in the design of rigid pavements. *Construction and Building Materials*. **21**(10), 1918–1927. Available from: doi: 10.1016/j.conbuildmat.2006.06.030.

Holmes, N., Browne, A. and Montague, C., (2014). Acoustic properties of concrete panels with crumb rubber as a fine aggregate replacement. *Construction and Building Materials.* **73**, 195–204.

Huang, B., Shu, X. and Cao, J., (2013). A two-staged surface treatment to improve properties of rubber modified cement composites. *Construction and Building Materials*. **40**, 270–274.

Ismail, M. K. and Hassan, A. A. A., (2015). Influence of Mixture Composition and Type of Cementitious Materials on Enhancing the Fresh Properties and Stability of Self-Consolidating Rubberized Concrete. *Journal of Materials in Civil engineering*. **28**(1). Available from: doi:10.1061/(ASCE)MT.1943-5533.0001338.

Issa, C. A. and Salem, G., (2013). Utilization of recycled crumb rubber as fine aggregates in concrete mix design. *Construction and Building Materials.* **42**, 48–52.

Khaloo, A. R., Dehestani, M. and Rahmatabadi, P., (2008). Mechanical properties of concrete containing a high volume of tire–rubber particles. *Waste Management.* **28**(12), 2472–2482.

Khatib, Z. K. and Bayomy, F. M., (1999). Rubberized Portland cement concrete. *Journal of Materials in Civil engineering*. **11**(3), 206–213.

Lam, L. and Teng, J. G., (2004). Ultimate condition of fiber reinforced polymer-confined concrete. *Journal of Composites for Construction.* **8**(6), 539–548.

De Larrard, F., (1999). *Concrete mixture proportioning: A scientific approach*. London, UK: E & FN Spon.

Leblanc, J. L., (2002). Rubber–filler interactions and rheological properties in filled compounds. *Progress in polymer science.* **27**(4), 627–687.

Li, G., Stubblefield, M. A., Garrick, G., Eggers, J., Abadie, C. and Huang, B., (2004). Development of waste tire modified concrete. *Cement and Concrete Research.* **34**(12), 2283–2289.

Li, G., Pang, S.-S. and Ibekwe, S. I., (2011). FRP tube encased rubberized concrete cylinders. *Materials and structures.* **44**(1), 233–243.

Ling, T. C., (2012). Effects of compaction method and rubber content on the properties of concrete paving blocks. *Construction and Building Materials*. **28**(1), 164–175. Available from: doi: 10.1016/j.conbuildmat.2011.08.069.

Liu, F., Zheng, W., Li, L., Feng, W. and Ning, G., (2013). Mechanical and fatigue performance of rubber concrete. *Construction and Building Materials*. **47**, 711–719.

Liu, F., Meng, L. Y., Ning, G. F. and Li, L. J., (2015). Fatigue performance of rubber-modified

recycled aggregate concrete (RRAC) for pavement. *Construction and Building Materials*. **95**, 207–217. Available from: doi: 10.1016/j.conbuildmat.2015.07.042.

Mander, J. B., Priestley, M. J. N. and Park, R., (1988). Theoretical Stress Strain Model for Confined Concrete. *Journal of Structural Engineering*. **114**(8), 1804–1825. Available from: doi: 10.1061/(ASCE)0733-9445(1988)114:8(1804).

Matthys, S., Toutanji, H. and Taerwe, L., (2006). Stress – Strain Behavior of Large-Scale Circular Columns Confined with FRP Composites. *Journal of Structural Engineering*. **132**(1), 123–133. Avaliable from: doi: 10.1061/(ASCE)0733-9445(2006)132:1(123).

Meddah, A., Beddar, M. and Bali, A., (2014). Use of shredded rubber tire aggregates for roller compacted concrete pavement. *Journal of Cleaner Production*. **72**, 187–192.

Mohammadi, I., Khabbaz, H. and Vessalas, K., (2014). In-depth assessment of Crumb Rubber Concrete (CRC) prepared by water-soaking treatment method for rigid pavements. *Construction and Building Materials*. **71**, 456–471.

Mohammed, B. S., Hossain, K. M. A., Swee, J. T. E., Wong, G. and Abdullahi, M., (2012). Properties of crumb rubber hollow concrete block. *Journal of Cleaner Production*. **23**(1), 57–67.

Moustafa, A. and ElGawady, M. A., (2016). Strain Rate Effect on Properties of Rubberized Concrete Confined with Glass Fiber–Reinforced Polymers. *Journal of Composites for Construction*. **20**(5), p. 04016014.

Najim, K. B. and Hall, M. R., (2010). A review of the fresh/hardened properties and applications for plain-(PRC) and self-compacting rubberised concrete (SCRC). *Construction and Building Materials*. **24**(11), 2043–2051.

Najim, K. B. and Hall, M. R., (2012). Mechanical and dynamic properties of self-compacting crumb rubber modified concrete. *Construction and Building Materials*. **27**(1), 521–530.

Najim, K. B. and Hall, M. R., (2013). Crumb rubber aggregate coatings/pre-treatments and their effects on interfacial bonding, air entrapment and fracture toughness in self-compacting rubberised concrete (SCRC). *Materials and structures*. **46**(12), 2029–2043.

Neville, A. M., (1995). *Properties of Concrete*. Essex: Pearson Education Limited.

Neville, A. M. and Brooks, J. J., (1990). *Concrete Technology Revised Edition-2001 Standards Update*. Harlow: Pearson Education Limited.

Onuaguluchi, O. and Panesar, D. K., (2014). Hardened properties of concrete mixtures containing pre-coated crumb rubber and silica fume. *Journal of Cleaner Production*. **82**, 125–

131. Available from: doi: 10.1016/j.jclepro.2014.06.068.

Ossola, G. and Wojcik, A., (2014). UV modification of tire rubber for use in cementitious composites. *Cement and Concrete Composites*. **52**, 34–41. Available from: doi: 10.1016/j.cemconcomp.2014.04.004.

Ozbakkaloglu, T. and Akin, E., (2012). Behavior of FRP-Confined Normal- and High-Strength Concrete under Cyclic Axial Compression. *Journal of Composites for Construction*. **16**(4), 451–463. Avaialble from: doi: 10.1061/(ASCE)CC.1943-5614.0000273.

Papastergiou, P., (2010). *A confinement model for concrete wrapped or pretensioned with FRP*. Ph.D. thesis, University of Sheffield.

Pastor, J. M., García, L. D., Quintana, S. and Peña, J., (2014). Glass reinforced concrete panels containing recycled tyres: Evaluation of the acoustic properties of for their use as sound barriers. *Construction and Building Materials*. **54**, 541–549. Available from: doi: 10.1016/j.conbuildmat.2013.12.040.

Paulay, T. and Priestley, M. J. N., (1992). *Seismic Design Of Reinforced Concrete And Masonry Buildings*. John Wiley & Sons, Inc.

Pedro, D., De Brito, J. and Veiga, R., (2012). Mortars Made with Fine Granulate from Shredded Tires. *Journal of Materials in Civil engineering*. **25**(4), 519–529.

Pierce, C. E. and Blackwell, M. C., (2003). Potential of scrap tire rubber as lightweight aggregate in flowable fill. *Waste Management*. **23**(3), 197–208.

Pilakoutas, K., Raffoul, S., Papastergiou, P., Garcia, R., Guadagnini, M. and Hajirasouliha, I., (2015). A study of the reuse of all tyre components in concrete: The Anagennisi project. *In the International conference on sustainable structural concrete*. La Plata, Argentina, 2015.

Raffoul, S., Garcia, R., Pilakoutas, K., Guadagnini, M., Medina, N. F., (2016). Optimisation of rubberised concrete with high rubber content: An experimental investigation. *Construction and Building Materials*. **124**, 391-404. Available from: doi: 10.1016/j.conbuildmat.2016.07.054.

Raffoul, S., Garcia, R., Escolano-Margarit, D., Guadagnini, M., Hajirasouliha, I., Pilakoutas, K., (2017a) Behaviour of unconfined and FRP-confined rubberised concrete in axial compression. *Construction and Building Materials*. **147**, 388–397. Available from: doi: 10.1016/j.conbuildmat.2017.04.175.

Raffoul, S., Escolano-Margarit, D., Garcia, R., Guadagnini, M., Pilakoutas, K., (2017b). Constitutive model for passively confined rubberized concrete. s*ubmitted to Journal of Composites for Construction*.

Raffoul, S. Escolano-Margarit, D., Garcia, R., Guadagnini, M., Pilakoutas, K., (2017c). Cyclic behaviour of FRP-confined rubberised concrete cylinders. *under preparation, to be submitted to Cement and Concrete Composites.*

Reda Taha, M. M., El-Dieb, A. S., Abd El-Wahab, M. A. and Abdel-Hameed, M. E., (2008). Mechanical, fracture, and microstructural investigations of rubber concrete. *Journal of Materials in Civil engineering.* **20**(10), 640–649.

Richardson, A. E., Coventry, K. A. and Ward, G., (2012). Freeze/thaw protection of concrete with optimum rubber crumb content. *Journal of Cleaner Production.* **23**(1), 96–103.

Segre, N., Monteiro, P. J. M., and Sposito, G., (2002). Surface characterization of recycled tire rubber to be used in cement paste matrix. *Journal of colloid and interface science.* **248**(2), 521–523.

Shulman, V., (2004). *Tyre recycling* (Vol. 15). iSmithers Rapra Publishing.

Sienkiewicz, M., Kucinska-Lipka, J., Janik, H. and Balas, A., (2012). Progress in used tyres management in the European Union: a review. *Waste Management.* **32**(10), 1742–1751.

Da Silva, F. M., Barbosa, L. A. G., Lintz, R. C. C. and Jacintho, A. E. P., (2015). Investigation on the properties of concrete tactile paving blocks made with recycled tire rubber. *Construction and Building Materials.* **91**, 71–79.

Sukontasukkul, P., (2009). Use of crumb rubber to improve thermal and sound properties of pre-cast concrete panel. *Construction and Building Materials.* **23**(2), 1084–1092.

Sukontasukkul, P. and Chaikaew, C., (2006). Properties of concrete pedestrian block mixed with crumb rubber. *Construction and Building Materials.* **20**(7), 450–457.

Teng, J. G., Chen, J. F., Smith, S. T. and Lam, L., (2003). Behaviour and strength of FRP-strengthened RC structures: a state-of-the-art review. *Proceedings of the institution of civil engineers-structures and buildings.* **156**(1), 51–62.

Topçu, I. B. and Bilir, T., (2009). Experimental investigation of some fresh and hardened properties of rubberized self-compacting concrete. *Materials and Design.* **30**(8), 3056–3065. Available from: doi: 10.1016/j.matdes.2008.12.011.

Toutanji, H. A., (1996). The use of rubber tire particles in concrete to replace mineral aggregates. *Cement and Concrete Composites.* **18**(2), 135–139.

Turatsinze, A. and Garros, M., (2008). On the modulus of elasticity and strain capacity of self-compacting concrete incorporating rubber aggregates. *Resources, Conservation and Recycling.* **52**(10), 1209–1215.

Turatsinze, A., Granju, J. L. and Bonnet, S., (2006). Positive synergy between steel-fibres and rubber aggregates: effect on the resistance of cement-based mortars to shrinkage cracking. *Cement and Concrete Research*. **36**(9), 1692–1697.

WBCSD – World Business Council for Sustainable Development, (2008). Managing End-of-Life Tyres. [online] Available from: http://www.wbcsd.org/Projects/Tire-Industry-Project/Resources/Managing-End-of-Life-Tires.

Wong, H. H. C. and Kwan, A. K. H., (2008). Rheology of cement paste: role of excess water to solid surface area ratio. *Journal of Materials in Civil engineering*. **20**(2), 189–197.

Youssf, O., ElGawady, M. A., Mills, J. E. and Ma, X., (2014). An experimental investigation of crumb rubber concrete confined by fibre reinforced polymer tubes. *Construction and Building Materials*. **53**, 522–532.

Youssf, O., ElGawady, M. A. and Mills, J. E., (2016). Static cyclic behaviour of FRP-confined crumb rubber concrete columns. *Engineering Structures*. **113**, 371–387. Available from: doi: 10.1016/j.engstruct.2016.01.033.

Zheng, L., Huo, X. S. and Yuan, Y., (2008). Strength, modulus of elasticity, and brittleness index of rubberized concrete. *Journal of Materials in Civil Engineering*. **20**(11), 692–699.

Chapter 2

Optimisation of rubberised concrete with high rubber content

*Raffoul S., Garcia, R., Pilakoutas, K., Guadagnini, M. and Medina N.F. (2016). Optimisation of rubberised concrete with high rubber content: an experimental investigation. Construction and Building Materials. **124**, 391-404.*

This article investigates experimentally the behaviour of Rubberised Concrete (RuC) with high rubber content so as to fully utilise the mechanical properties of vulcanised rubber. The fresh properties and short-term uniaxial compressive strength of 40 rubberised concrete mixes were assessed. The parameters examined included the volume (0 to 100%) and type of mineral aggregate replacement (fine or coarse), water or admixture contents, type of binder, rubber particle properties, and rubber surface pre-treatments. Microstructural analysis using a Scanning Electron Microscope (SEM) was used to investigate bond between rubber and concrete at the Interface Transition Zone (ITZ). This initial study led to the development of an "optimum" RuC mix, comprising mix parameters leading to the highest workability and strength at all rubber contents. Compared to a non-optimised concrete with 100% replacement of fine aggregates with rubber, the compressive strength of concrete with optimised binder material and moderate water/binder ratio was enhanced by up to 160% and the workability was improved significantly. The optimisation proposed in this study will lead to workable high rubber content RuC suitable for sustainable high-value applications.

1 INTRODUCTION

Tyres used in the automotive industry are made with 70-80% highly durable vulcanised rubber, which cannot be easily recycled. Over 300 million tyres reach their service life every year in the EU alone, i.e. practically one waste tyre per person [1]. The inadequate disposal of rubber from scrap tyres is hazardous to the environment and human health and, as a result, stringent environmental legislations have been introduced to manage such "waste". For instance, the EU directives prohibit the disposal of scrap tyres in landfills and favour the reuse of waste materials ahead of recycling to minimise energy consumption (Landfill Directive 1991/31/EC [2] and Directive 2008/98/EC [3], respectively). This has increased efforts towards generating new applications for vulcanised rubber from scrap tyres [4-12]. In the past two decades, numerous studies have investigated the reuse of recovered tyre rubber in concrete to replace fractions of its mineral aggregates [5-12]. Whilst rubber is a valuable material with high strength, durability and elasticity, it can have a detrimental effect on some of the fresh and hardened mechanical properties of concrete.

In general, previous literature on the characteristics of RuC mixes is contradictory, highlighting the difficulty of achieving suitable mixes for construction. Whilst some researchers have reported satisfactory workability at all rubber contents and sizes [13, 14], others have measured zero slump at 50% [15] or 80% [16] aggregate replacement by volume. Previous experimental work often measures concrete workability through slump [17, 18]. Workability, however, is defined by the ease of mixing, placing and consolidating fresh concrete while maintaining adequate concrete homogeneity [19], and therefore, the overall stability (i.e. segregation and bleeding) of the fresh RuC mix has to be taken into account. Due to the relatively low density of rubber compared to mineral aggregates and cement, RuC cylinders with inadequate mix proportioning, consolidation or handling can exhibit a high concentration of rubber at the top upon vibration [20, 21]. The increase in porosity and entrapped air content (up to 30% at 25% rubber replacement by volume [20]) is conceivably the main reason behind the poor fresh

performance of RuC [22]. Such increase may be attributed to rubber hydrophobicity, irregular shape, rough texture, contamination, interlock among rubber particles and excessive friction with cement paste [23, 24]. Other factors include flocculation among fine rubber particles, particle gradation and moisture content [22].

The compressive strength of RuC reduces by up to 90% at high levels of rubber replacement (e.g. 100% sand replacement) [25]. The lower compressive strength of RuC can be attributed to the relatively high Poisson's ratio of rubber particles (nearly 0.5), the high porosity of the composite and the weak rubber-cement paste bond (or Interfacial Transition Zone, ITZ) [26, 27]. Other factors that reduce RuC strength include segregation, lower overall stiffness of the composite and casting and consolidation techniques [28]. While the strength of RuC with various rubber contents is well documented in the literature [14, 17, 24, 25, 29-31], the level of reduction in strength seems to be influenced by rubber content, size and properties, as well as other mix parameters and proportions (i.e. water to binder ratio (w/b), type of chemical admixture and binder material). As a consequence, results from compressive strength tests on RuC cylinders are difficult to compare due to their large scatter (Figure 1).
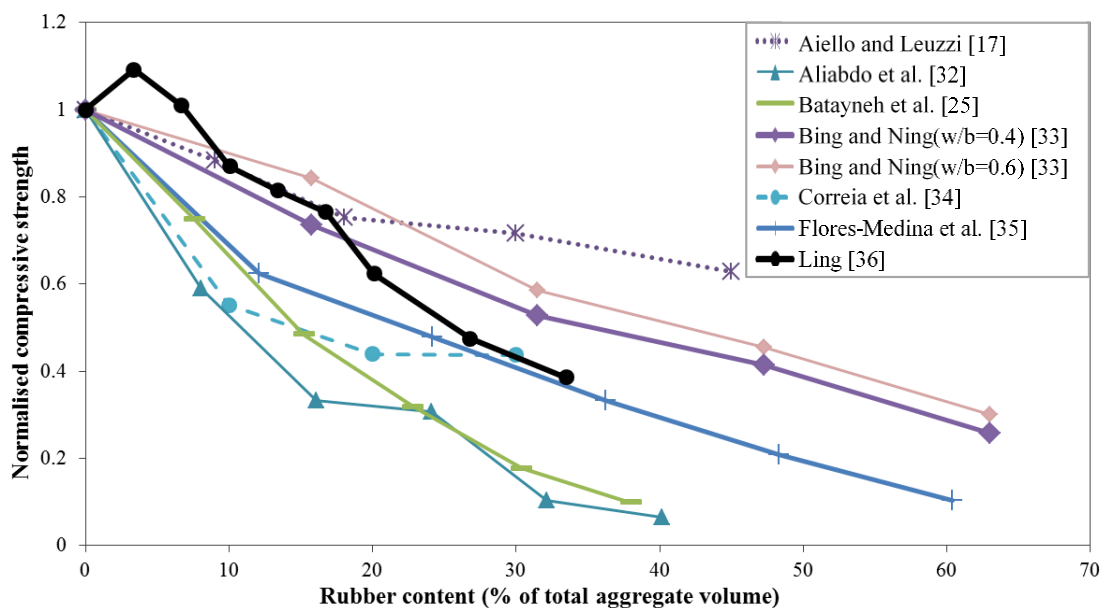

Figure 1. Normalised concrete compressive strength vs. rubber content (data from [17, 25, 32-36])

Whilst rubber hydrophobicity and surface texture are known to weaken the bond between rubber and cement paste, the bond strength and the load transfer mechanism at the rubber-cement paste interface is still unknown. Microstructural analysis of RuC revealed higher porosity in the matrix at the rubber-cement paste ITZ, as well as a larger ITZ, when compared to conventional concrete [37, 38]. In fact, the ITZ between rubber aggregates and cement paste increased from 6.65 μm to 13.44 μm at 10% and 50% sand volume replacement, respectively [38]. However, w/b was often varied with rubber content [38], which could possibly affect the hydration kinetics, mix porosity and ITZ density and width. Scanning Electron Microscopy (SEM) images have shown a lack of bonding (gap) between the rubber and cement paste at their ITZ, as well as limited hydration products surrounding the rubber particles [37-39]. Conversely, other studies show that rubber bonds well to the cement matrix [30, 40]. This good rubber-cement paste bond has been attributed to interlock at the rough surface of rubber particles [40].

It has been reported that zinc stearate (used to extend tyre service life in many developing countries) increases rubber hydrophobicity and leads to a porous and weak rubber-cement interface [41]. To improve rubber-cement paste chemical/physical bonding [18], several rubber pre-treatments have been investigated such as washing with water [21, 35, 42], polyvinyl alcohol [43], NaOH [13, 41, 44, 45], $Ca(OH)_2$ [46], silane coupling agents [47], organic sulphur compounds [48] or acid [40], as well as partial oxidation of the rubber surface [49], exposure to UV radiations [50] or pre-coating with cement [51], mortar [26], silica fume [39], limestone [52] or sand [45]. Despite some success in rubber pre-treatments (strength increase in the range of 3-40% [18, 26, 41, 51, 52]), results are often scattered and inconclusive, particularly when mixes with pre-treated rubber are not compared to mixes with as-received rubber [35, 42]. The effects of the pre-treatments on the concrete hydration reaction and long term durability have not been investigated. The pre-treatments are also often costly and time-consuming, and can only be justified if concrete performance is enhanced.

The significance of achieving an "ideal" packing of the concrete constituents on its rheology, durability and mechanical properties has been highlighted in the literature [53]. The packing of granular particles is influenced by their shape, texture, specific gravity, moisture condition and mixing, placing and consolidation techniques. To date, an appropriate method for characterising rubber particle properties does not exist, possibly due to the different types of rubber, levels of contamination and the lack of standard tests. For instance, the specific density of rubber reported in the literature varies between 0.5 and 1.3 [7, 28, 54]. The reported water absorption values vary between "negligible" [27, 55] up to 42.1% [33]. Nevertheless, rubber particles are broadly characterised with a flaky and elongated shape, a rough surface (i.e. high friction coefficient) and hydrophobicity that is likely to affect its packing with conventional aggregates [21, 56]. Due to their high surface area to weight ratios, it is also likely that ultra-fine rubber particles interact by surface and inter-particular forces [57]. To limit the influence of rubber size on concrete particle packing, mineral aggregates are often replaced with rubber particles of similar grading [58].

Based on the previous discussion, it is evident that the lack of consensus in the literature, insufficient understanding of RuC performance and adverse effects of rubber on concrete properties limit the development/use of rubber in structural concrete applications. To date, the use of RuC has been mainly limited to:

1) Non-structural applications such as road barriers [7], thin overlays [8], concrete panels [9], paving blocks [29, 31] and applications for thermal and acoustic insulation [5, 6], and

2) Low-medium compressive strength structural concrete with reduced weight and increased ductility, as well as resistance to vibrations, impact and cyclic loads [6, 10-12].

To minimise the negative impact of rubber on concrete strength, the use of small volumes of rubber (up to 25% of the total mineral aggregates) is often proposed [16, 59, 60]. This inhibits the benefits that high-quality rubber can have on the concrete toughness and ductility [61, 62]. The use of large amounts of rubber in concrete can also have a positive environmental impact

by reusing materials that would otherwise be considered waste. Therefore, from a structural and environmental perspective, further research is needed to mitigate the negative impact of large amounts of rubber on concrete characteristics.

This article investigates experimentally the behaviour of RuC with high rubber content so as to fully utilise the excellent mechanical properties of vulcanised rubber. The article describes an experimental programme that examines the parameters that influence the performance of RuC and describes a mix "optimisation" exercise. Subsequently, the study presents the main experimental results and analyses the factors influencing the fresh performance and compressive strength of RuC. Microstructural observations from scanning electron microscope (SEM) images are also presented and discussed. This research is part of the ongoing EU-funded collaborative research project Anagennisi (http://www.anagennisi.org/) that aims to develop innovative solutions to reuse all scrap tyre components. The results of this study are instrumental to understand the fundamental behaviour of RuC and contribute to the development of high-value structural applications.

2   EXPERIMENTAL PROGRAMME

A total of 40 rubberised concrete mixes and 180 standard cylinders (100×200mm) were produced. To optimise the mix proportions and achieve a RuC with satisfactory fresh properties and short-term compressive strength, the first part of the experimental study (Part 1) examined RuC produced using different water to binder ratios (w/b), binder materials, specimen preparation techniques, rubber treatments and admixture contents at a fixed rubber content of 40% of the fine aggregate volume. Based on the results of Part 1, an 'optimum mix' was selected for the second part of the study (Part 2) to investigate the effects of rubber contents and sizes on the concrete compressive strength. In Part 2, the rubber replaced a) volumes of either fine or coarse aggregates (0%, 10%, 20%, 40%, 60%, 80% and 100%), or b) volumes of both fine and coarse aggregates (20%, 40% and 60% total aggregate replacement).

2.1 Material Properties and Characterisation of Rubber Particles

High strength Portland Limestone Cement CEM II – 52.5 N (10-15% Limestone) conforming to BS EN 197-1 [63] was used as main binder to reduce the carbon footprint of the mixes. Alternative binder materials including Silica Fume (SF) (Undensified microsilica – Grade 940) [64] and Pulverised Fuel Ash (PFA) (BSEN 450 – 1, Class N Category B LOI) [65] were also examined. Two commercially available high range water-reducing admixtures were used [66, 67]. Round river washed gravel was used as coarse aggregate (Sizes: 5-10 mm and 10-20 mm; Specific gravity: 2.65; Absorption: 1.24%), whereas medium grade river washed sand was used as fine aggregate (Sizes: 0-5 mm; Specific gravity: 2.65; Absorption: 0.5%, Fineness modulus: 2.64). The rubber particles were recovered through mechanical shredding at ambient temperature and assorted in two types: a) fine (0-5mm) and coarse rubber (5-10mm) from car tyres and b) large rubber chips (10-20mm) from truck tyres. Fine rubber particles (0-5mm) were sorted in five size groups and a linear gradation was used to calculate their proportions. The rubber surface, particularly the large rubber chips, was jagged and contaminated with steel fibres and fluff, as shown in Figure 2b-c. The relative density of tyre rubber reported in the literature ranges from 0.51 [7] and up to 1.30 [28], therefore, the mass of rubber replacing the mineral aggregates was calculated assuming a relative density of 0.80.
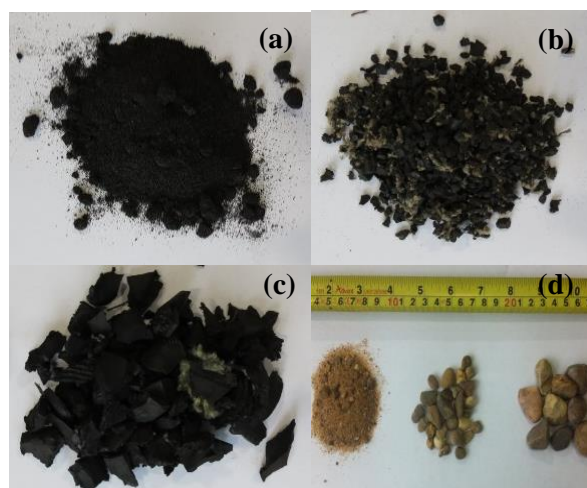
Figure 2. (a) Fine rubber (0-5mm), (b) coarse rubber (5-10mm), (c) coarse rubber (10-20mm) and (d) mineral aggregates used in the experimental programmes.

Table 1 summarises a typical composition of rubber crumbs as reported by the provider, whereas Figure 3 shows the particle size distribution of rubber and mineral aggregates obtained according to ASTM C136 [68].

Table 1. Chemical characterisation of rubber granulates and powder

COMPOSITION INFORMATION OF INGREDIENTS* (data provided by ADRIA [69])
Polymers: 40-55%
Include Natural Rubber (NR), Styrene-Butadiene Rubber (SBR), Isoprene Rubber (IIR), Isobutylene-Isoprene Rubber (IIR), Halogen Isobutylene-Isoprene Rubber (modified IIR), Polybutadiene Rubber (BR), and Acrilonitril-Butadiene Rubber (NBR)
Carbon black: 20-25%
Other (softener, filler): 20-40%

*Percentages of each constituent will vary according to mixture
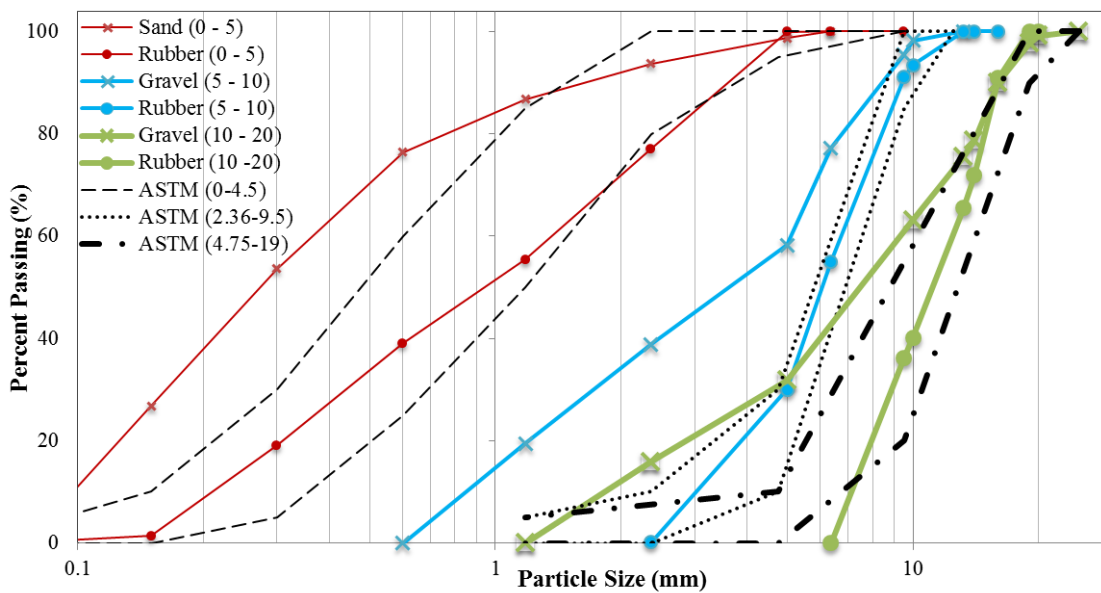
Figure 3. Particle size distribution of rubber and mineral aggregates and ASTM 33 boundaries for fine, medium and large coarse aggregates.

The rubber and mineral aggregate shape and physical properties were evaluated as follows: particle density and water absorption according to BS EN 1097-6-Annex C for lightweight aggregates [70]; bulk density according to BS EN 1097-3 [71]; and flakiness index according to BS EN 933-3 [72]. Particle density, water absorption and flakiness of fine rubber particles (0-

5mm) were not evaluated as these particles float and agglomerate, thus giving misleading results. The aggregate properties are shown in Table 2.

Table 2. Physical and mechanical properties of rubber and mineral aggregates

Material (size in mm)	Apparent density (g/cm³)	Oven dry density (g/cm³)	SSD* density (g/cm³)	Water absorption (%)	Specific gravity	Bulk density (g/cm³)	Flakiness Index
Rubber (0-5)	-	-	-	-	-	0.4-0.46	N/A
Rubber (5-10)	1.1-1.2	1.0-1.1	1.1-1.2	5.3-8.9	1.1	0.45	6.6-8.3
Rubber (10-20)	1.1	1.1	1.1	0.8-1.3	1.1	0.48	10.4-17.5
Gravel (5-10)	2.69	2.60	2.63	1.24	2.65	1.51	7.1
Gravel (10-20)	2.69	2.60	2.63	1.24	2.65	1.58	9.7
Sand (0-5)	2.65	2.62	2.63	0.50	2.65	1.78	N/A

*Saturated surface dry

The results in Table 2 indicate that the water absorption of the rubber particles was unexpectedly high, e.g. up to 8.9% for the 5-10mm coarse rubber particles. This could be due to the difficulty of achieving surface dry conditions and to the presence of contaminants (steel, fluff and others), which was particularly high for the 5-10mm rubber particles. It is also observed that all rubber particles had a relatively low uncompacted bulk density (0.40 to 0.48 g/cm³) in comparison to that of the mineral aggregates (1.51 to 1.78 g/cm³). This can be attributed to the lower specific gravity of the rubber, but also to a lower packing of the rubber aggregates. The lower bulk density of ultra-fine rubber particles (compared to the larger particles) could be caused by surface inter-particular forces, which lead to flocculation and agglomeration among fine rubber [57]. Nevertheless, more accurate data on particle density and size of fine rubber are required before any conclusions can be drawn. The 10-20mm coarse rubber particles had higher flakiness compared to the replaced gravel (Table 2). This high flakiness indicates that the conventional sieve analysis is not suitable to measure rubber particle sizes. For instance, rubber particles measuring 40mm in one dimension and 20mm in the other orthogonal dimensions would still pass through a 20mm sieve, thus providing a misrepresentation of the actual particle sizes.

2.2   Mix Design and Parameters

A typical bridge pier mix design with a target 28-day compressive strength of 40 MPa was used as reference (mix O), according to the proportions shown in Table 3. This mix was selected because the RuC investigated in this study can potentially be used in applications where vibration damping and/or energy dissipation are needed (e.g. integral bridges, earthquake resistant structures, etc.). Mix O was designed to be highly flowable with relatively high cement content, water to binder ratio (w/b=0.423) and fine to coarse aggregate ratio. The concrete constituents were mixed as follows: 1) the aggregates (both mineral and rubber) were dry-mixed for 30 seconds. All mineral aggregates were Saturated Surface Dry (SSD), whereas the rubber particles were mixed dry and as-received (excluding the mixes with pre-treated rubber); 2) half of the mixing water was added and mixed for another minute; 3) the mix was allowed to rest for three minutes; 4) the binder materials (including cement and other pozzolanic materials) and the remaining mixing water were then added followed by a gradual addition of the admixtures and 5) the concrete was then mixed for another three minutes.

Table 3. Mix design for the original mix (O).

Material	Original mix (O) Quantity/m³
CEM II – 52.5 MPa	425 kg
Aggregates 0/5mm	820 kg
Aggregates 5/10mm	364 kg
Aggregates 10/20mm	637 kg
Fine aggregate : coarse aggregate	1 : 1.22
Water	180 l
Plasticiser (P)	2.5 l
Superplasticiser (SP)	5.1 l

2.3   Part 1: Mix Optimisation

The original mix O was very segregated, non-homogeneous and non-cohesive when rubber was incorporated and, consequently, various mixes were attempted to achieve improved fresh properties and short-term compressive concrete strength. Table 4 summarises data from

representative mixes in Part 1 of the experimental programme while Table 5 shows the quantities of rubber and mineral aggregates used. In Table 4, the trial mixes are identified according to the different parameters examined: water to binder content (w/b=0.3-0.38 – mixes A), admixture content (B), rubber pre-treatments (C) and binder material (D). The number in the ID represents the mix trial number. For comparison purposes, a fixed rubber content of 40% was used to replace the sand aggregates (by volume) in all trial mixes. In this initial study, the parameters leading to the best mix performance in terms of workability and compressive strength were selected as the "optimised mix" parameters. Additional rubber contents of 10% and 100% were used to replace aggregates in the original mix O and mix D. Two rubber pre-treatments were examined. In mixes C.1 and C.2, the rubber was pre-washed with water to remove surface impurities, air dried and then stored in a closed container under standard laboratory conditions to maintain relatively constant moisture throughout the study. In mix C.3, the rubber was pre-coated with silica fume (SF) mixed with some water (10% of the cement weight). The pre-coated particles were then allowed to rest for 20 min before they were mixed with the aggregates and remaining concrete constituents, following the sequence described in section 2.2. In mixes D.1-D.4, SF and PFA were used to replace 20% of the cement by mass (10% each), based on optimal values in previous research [15], whilst w/b was maintained at 0.35.

Table 4. Representative trial RuC mixes examined in Part 1 (see aggregate quantities in Table 5).

Mix I.D.	Cement (kg/m³)	SF (kg/m³)	PFA (kg/m³)	Fine aggregate replacement (%)*	w/b	Other varied parameters
O.1	425	-	-	0	0.423	-
O.2	425	-	-	10	0.423	-
O.3	425	-	-	40	0.423	-
O.4	425	-	-	100	0.423	-
A.1	425	-	-	40	0.38	-
A.2	425	-	-	40	0.35	-
A.3	425	-	-	40	0.32	-
A.4	425	-	-	40	0.30	-
B.1	425	-	-	40	0.423	Admixtures reduced by 20%
B.2	425	-	-	40	0.423	SP reduced by 40%
B.3	425	-	-	40	0.423	P reduced by 80%
C.1	425	-	-	40	0.38	Rubber pre-washed
C.2	425	-	-	40	0.35	Rubber pre-washed
C.3	340	42.5	42.5	40	0.35	SF as pre-treatment
D.1	340	42.5	42.5	0	0.35	-
D.2	340	42.5	42.5	10	0.35	-
D.3	340	42.5	42.5	40	0.35	-
D.4	340	42.5	42.5	100	0.35	-

*No coarse aggregate replacement in the above mixes (0%). Coarse aggregate content=1001.0 kg/m³

2.4   Part 2: Variation in Rubber Contents

Based on the results from Part 1 of this study (see analysis in section 3), the "optimum mix" was selected to carry out an in-depth parametric study in Part 2 of the experimental programme. Rubber contents were varied from 0 to 100% of the fine aggregate (FA) or coarse aggregate (CA) volume. A combined replacement of both fine and coarse mineral aggregates (20%, 40% and 60% by volume) was also examined. Table 5 summarises the rubber and mineral aggregate proportions used for the RuC mixes examined in Part 2. All other mix parameters were fixed to the proportions in Table 4 of the optimised mix, later identified as mix D, based on its fresh and hardened concrete performance, as described in sections 3.1-3.7. In Table 5, the mixes are identified with an ID that indicates the volume of rubber replacing aggregates in percentage (0%-100%) followed by the type of aggregate replacement, i.e. "FR" for rubber replacing fine aggregates (0-5mm) or "CR" for rubber replacing coarse aggregates (5-20mm). The IDs

20CR20FR, 40CR40FR and 60CR60FR identify mixes with 20%, 40% and 60% combined replacement of CR and FR, respectively.

Table 5. Proportions of rubber and mineral aggregate at different levels of replacement

Replacement Type	Mix I.D.	Rubber Mass (kg/m³)		Mass of CA[a] (kg/m³)	Mass of FA[a] (kg/m³)
		CR	FR		
None	Plain	-	-	1001.0	820.0
Fine Rubber (FR)	10FR	-	24.8	1001.0	738.0
	20FR	-	49.5	1001.0	656.0
	40FR	-	99.0	1001.0	492.0
	60FR	-	148.5	1001.0	328.0
	80FR	-	198.0	1001.0	164.0
	100FR	-	247.6	1001.0	0.0
Coarse Rubber (CR)	10CR	30.2	-	900.9	820.0
	20CR	60.4	-	800.8	820.0
	40CR	120.9	-	600.6	820.0
	60CR	181.3	-	400.4	820.0
	80CR	241.8	-	200.2	820.0
	100CR	302.2	-	0.0	820.0
CR & FR	20CR20FR	60.4	50.0	800.8	656.0
	40CR40FR	120.9	99.0	600.6	492.0
	60CR60FR	181.3	148.5	400.4	328.0

[a]CA = coarse aggregate, FA = fine aggregate

2.5 Specimen Preparation

A total of 180 standard concrete cylinders (100×200mm) and 30 cubes (100mm) were cast according to BS EN 12390-2 [73]. The cubes were cast to examine the development of axial compressive concrete strength for the highest rubber content (60CR60FR) at 3, 7, 14, 28 and 52 days. All specimens were cast in two layers and vibrated on a vibrating table (15-20s per layer). After casting, all specimens were covered with plastic sheets and kept under standard laboratory conditions for 48hrs until demoulding. The specimens were then stored in a mist room until 24hrs prior to testing. As the casting face of most RuC cylinders was uneven, two methods for cylinder surface preparation were examined: 1) cutting and grinding the cylinder surface according to BS EN 12390-3 [74], and 2) casting of gypsum caps (ASTM C617 [75]). Figure 4a-b show the concrete cylinders before and after casting the gypsum caps. The caps failed prematurely during the tests, leading to local crushing and failure at the top/bottom of cylinders.

Conversely, surface cutting and grinding (Figure 4c-d) prevented local crushing and was used for testing the cylinders presented in this study.
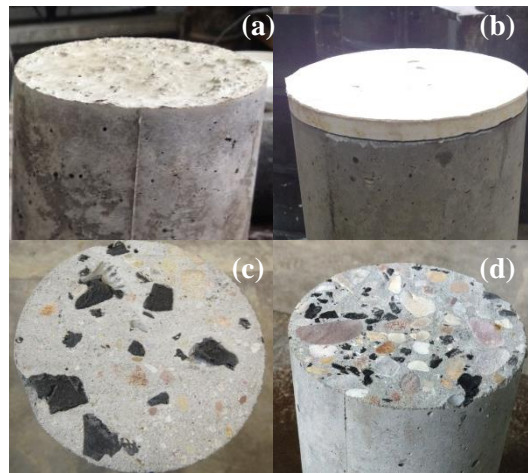

Figure 4. Cylinder without preparation (a), cylinder with gypsum cap (b) and cut cylinders from D mix with 10%CR (c) and 100% FR (d).

2.6   Test setup and instrumentation

As no standard method exists for measuring the fresh properties for RuC, these were evaluated using slump tests (BS EN 12350-2 [76]), flow table tests (BS EN 12350-5 [77]), or both depending on a visual assessment of the suitability of the test for each mix. Additionally, a visual stability index (VSI) was used to examine segregation and bleeding and to classify the mixes in descending order of stability (from 0 to 3) according to ASTM C1611 [78]. The hardened concrete density was obtained at the date of testing after air drying for 24hrs.

The cylinders and cubes were tested in uniaxial compression using a cube crusher of 3,000 kN capacity at a loading rate of 0.6 MPa/s according to BS EN 12390-2 [73]. However, the loading rate was reduced to 0.1 MPa/s to prevent prompt failure of (weaker) cylinders with higher rubber contents (above 80% sand or gravel replacement). To speed up the experimental programme, 150 cylinders were tested after 7 days of casting, while the rest were tested after 28 days. Two cylinders were tested for each mix in Phase 1 of the experimental programme,

whereas at least four cylinders were tested for each mix in Phase 2 to account for material variability.

High resolution scanning electron microscopy (SEM) and Energy Dispersive X-ray Spectroscopy (EDS) analyses were used to observe the microstructure of selected RuC samples. The images were obtained in backscattered electron (BSE) imaging mode. Cylindrical cores (25 mm dia×10mm height) were extracted by cutting at the mid-height of the RuC cylinders and then coring at their centre. The face of each core was polished manually using commercial sanding paper to achieve a surface roughness of about 6 μm. The samples were then polished gradually using diamond paste of 6, 3, 1 and 0.25 μm, and washed with isopropanol using an ultrasonic cleaner.

3   RESULTS AND ANALYSIS

Table 6 reports the following results from Part 1 of the experimental programme: a) slump of fresh mixes (when measurements were possible), b) average flow values, c) segregation, and d) 7-day compressive strength. Table 7 summarises the same results for Part 2 of the experimental programme, as well as the specific gravity and corresponding standard deviation (SD) of the 7-day compressive strength results. The variation in the average 7-day compressive strength of the tested cylinders as function of the content of rubber replacing the total aggregate volume is shown in Figure 5. The following sections summarise the most significant observations of the testing programmes and discuss the results listed in Tables 6 and 7 and Figure 5.

Table 6. Results - Part 1 of the experimental programme

Mix I.D.	Slump (mm)	Flow (mm)	Segregation (VSI)	Compressive strength at 7 days (MPa)
O.1	N/A[a]	700	0	46.8
O.2	N/A[a]	700	0	34.8
O.3	N/A[a]	685	2	14.1
O.4	N/A[a]	485	3	3.7
A.1	190	520	0	21.8
A.2	110	440	0	22.4
A.3	N/A[a]	N/A[a]	1	31.9
A.4	N/A[a]	N/A[a]	3	-[b]
B.1	N/A[a]	640	1	-[b]
B.2	N/A[a]	575	0	-[b]
B.3	N/A[a]	580	0	-[b]
C.1	N/A[a]	495	1	19.8
C.2	150	425	0	26.2
C.3	170	495	1	28.1
D.1	230	575	0	61.7
D.2	215	560	0	53.4
D.3	190	530	0	31.7
D.4	0	N/A[a]	2	9.6

[a] Mixes where flow or slump measurements were not possible
[b] No cylinders cast

Table 7. Results - Part 2 on optimum mix D with different rubber contents

Mix I.D.	Slump (mm)	Flow (mm)	Specific Gravity (SG)	Compressive strength 7day (MPa)	SD (%)
Plain	230	575	2.48	61.7	6.7
10FR	215	560	2.41	53.4	3.9
20FR	230	570	2.35	43.2	9.9
40FR	190	530	2.3	31.2	0.4
60FR	180	495	-	20.6	5.1
80FR	130	465	-	14.7	4.0
100FR	0	N/A[*]	2.13	9.6	7.4
10CR	N/A[*]	590	2.4	45.9	6.6
20CR	N/A[*]	535	2.34	32.7	18.5
40CR	45	N/A[*]	2.22	25.3	15.9
60CR	N/A[*]	510	2.2	15.8	27.1
80CR	40	N/A[*]	2.06	14.3	9.4
100CR	70	380	1.98	8.7	15.9
20CR20FR	210	490	2.22	32.0	3.2
40CR40FR	185	-	2.05	10.7	0.0
60CR60FR	40	410	1.94	7.1	16.8

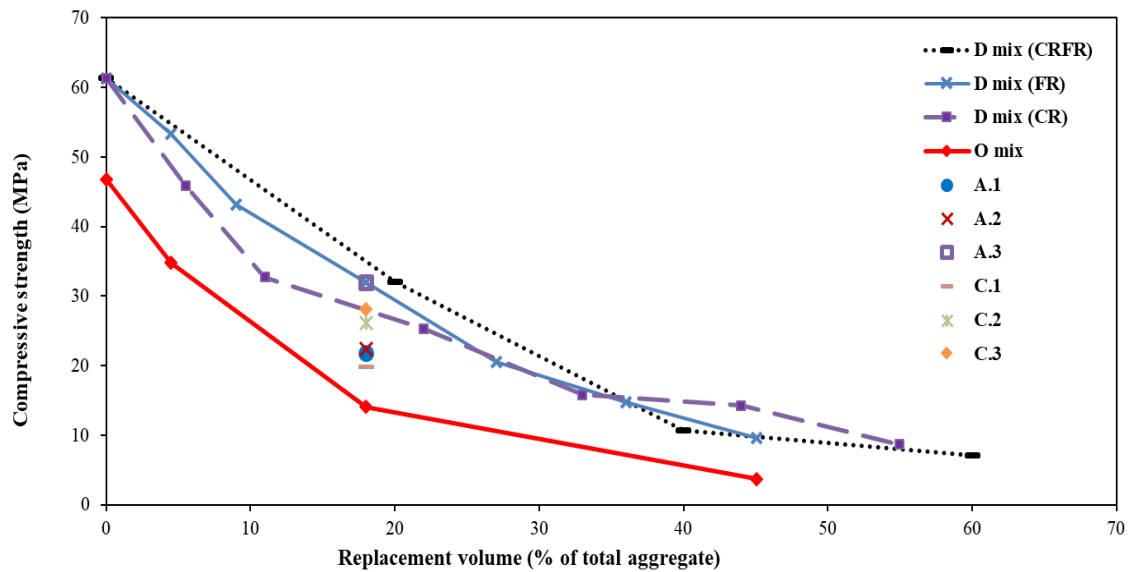[a] Flow or slump measurements were not possible

Figure 5. Average 7-day compressive strength of the tested cylinders as function of total aggregate replacement

3.1   Fresh Properties

The fresh properties of RuC mixes changed significantly with the addition of rubber, and therefore the mix design was adjusted to achieve a good flow and no segregation. Figure 6 shows the flow table results of mixes O and D (with CR or FR replacement) as a function of the total volume of replaced aggregate. The results indicate that rubber contents of 0% to 10% FR did not change the flow of the original mix O. However, the flow reduced by 30% at a 100% FR replacement, which equals 45% of the total aggregate volume. The latter mix was very harsh, unworkable and segregated, as shown in Figure 7a. Compared to the plain mix O, the plain mix D had much lower flowability (575 mm at 0% rubber replacement). Flow reduced by 34% for mix D with the highest rubber content (100% CR, or 55% replacement of the total aggregate volume). Despite the high rubber content in mix D (55% total aggregate replacement compared to 45% in mix O.4), the former was more cohesive and homogeneous, as shown in Figure 7b.
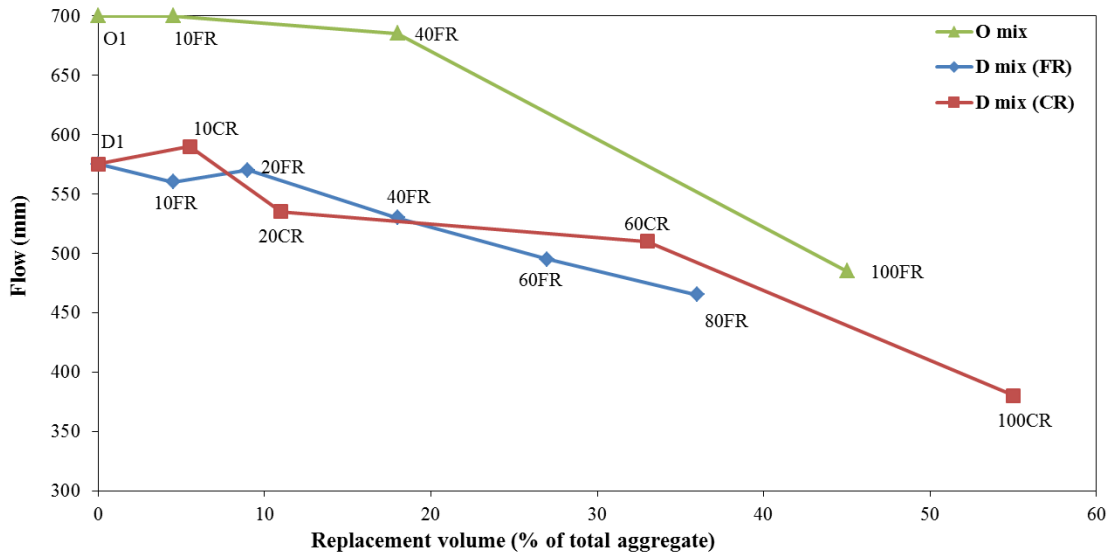
Figure 6. Flow table results for mixes O and D as function of total aggregate volume replacement
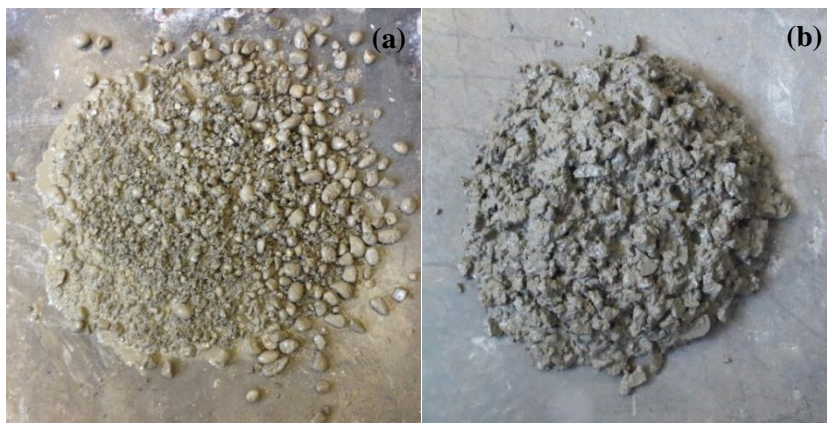
Figure 7. View of flow table test of (a) mix O at 100% FR and (b) mix D at 100% CR.

The slump/flow values and levels of segregation in Table 6 show that most mixes achieved acceptable flowability for casting and compacting purposes (except mixes O.4, A.3 and A.4). However, segregation and bleeding were evident in RuC mixes, as confirmed by: 1) shear failure in slump test, particularly in dryer mixes (an indication to harshness and lack of cohesion, Figure 8a), 2) separation of coarse aggregates from finer particles in flow table tests (Figure 8b), and 3) the presence of a mortar halo. A gleam was also observed at the surface of RuC mixes with high water content (B.1 and O.3), indicating bleeding. This can be attributed to rubber hydrophobicity, poor particle grading and concrete porosity.
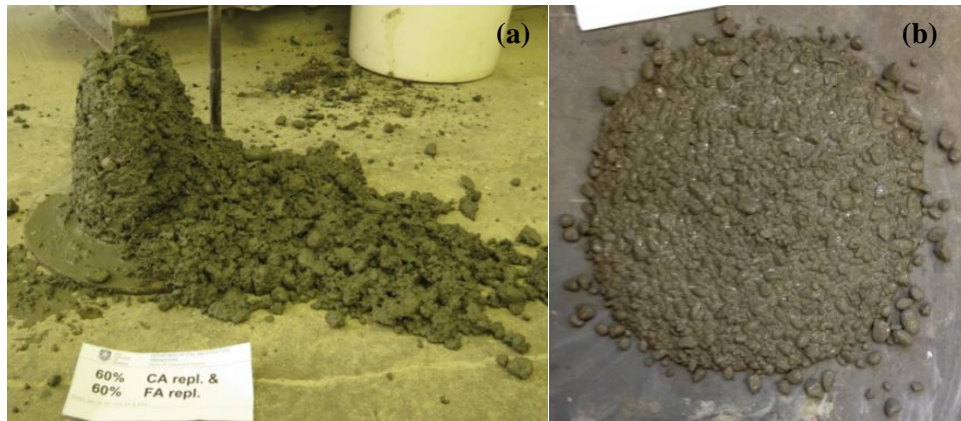
Figure 8. (a) Shear slump failure of 60C60F and (b) flowability test of C.3 with SF pre-treatment

The above results highlight the difficulty of achieving a highly flowable mix without compromising mix cohesion. To limit segregation and bleeding, sufficient water was added to hydrate the cement and superplasticisers were used to aid mix flowability and facilitate casting. The use of SF and PFA also limited segregation and bleeding and improved mix cohesion in mix D (Table 6). The effect of water/admixture content and binder materials on RuC performance is discussed in sections 3.3 and 3.4, respectively.

The optimisation of the mix proportions led to satisfactory fresh properties for RuC mixes at high rubber contents. Based on the results of this study, it is suggested to limit the w/b ratio to 0.35 and use SF and PFA to replace 20% of the cement mass (10% each).

3.2   Effect of rubber content

Figure 9 compares the average 7-day compressive strength of the original mix O and optimised mix D (normalised to the strength of corresponding mixes with no rubber, i.e. 42 MPa for mix O and 62 for mix D) as a function of rubber replacing total aggregate volume. Figure 9 indicates that the strength of the RuC mixes reduced for all rubber contents up to a maximum of 92% for mix O (100% FR or 45% of the total aggregates). This is in line with previous studies that report a 90% reduction in compressive strength as a result of full replacement of sand with rubber [25].
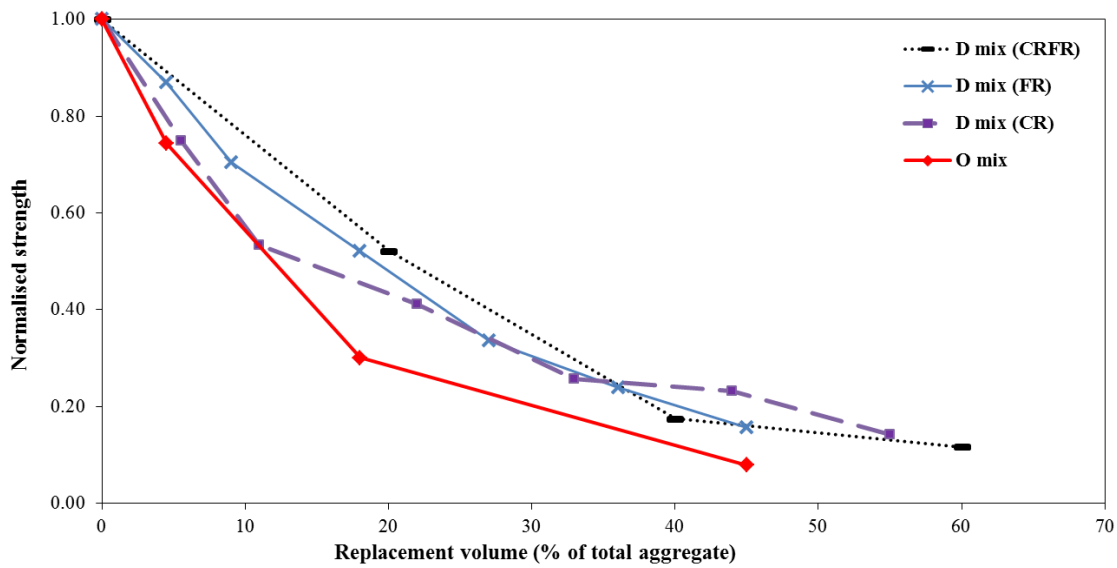
Figure 9. Variation in normalised strength of O mix and D mix with FR replacement, CR and both

The plain mix D with no rubber had SF and PFA and lower w/b and, consequently, it had higher compressive strength than the plain mix O (see Table 6). Nonetheless, Figure 9 shows that the reduction in compressive strength due to increasing rubber content was less severe in the optimised mix D. For instance, at 40% FR content (equivalent to 18% total aggregate replacement), the strength of mix O reduced by 70%, whereas the drop was 49% in mix D. Similar results were observed in mix D with CR replacement, as well as in mixes with combined replacement of CR and FR.

The reduction in strength shown in Figure 9 is consistent with the drop in slump and flow discussed in section 3.1. Such properties are affected by the higher air content and lower workability of RuC, which can be attributed to rubber hydrophobicity, texture and shape. The reduction in compressive strength can also be due to a) the lower stiffness of the rubber aggregates (relative to the substituted mineral aggregates), which leads to higher compressive stresses in the cement paste as rubber replacement is increased, and b) rubber high Poisson's ratio, which tends to induce lateral tensile stresses in the concrete surrounding the rubber particles. Moreover, the reduction in strength of mixes O.3 and D.3 (at similar 40% FR) was

70% and 49%, respectively (Figure 9). This suggests that strength reduction in RuC does not only depend on rubber content but also on other mix parameters and proportions.

Figure 10 shows the reduction in density as a function of rubber content. In this figure, the density (obtained from standard cylinders) is normalised with reference to the density of concrete mixes with no rubber. To allow direct comparisons, the rubber content is expressed as a percentage of the total mix aggregate content. The results indicate that regardless of the mix constituents, the concrete density reduced with increasing rubber volume. This reduction is in line with the reduced compressive strength of RuC mixtures and can be mainly attributed to the lower specific gravity (SG) of the rubber particles, but also to an increase in air content. The SG of mix O was 2.54, 2.41, 2.33 and 1.92, respectively at 0%, 10%, 40% and 100% FR replacement. The SG results from mix D (Table 7) show that the plain mix D had a lower density of 2.48 (compared to mix O) due to the use of SF and PFA. The SG reduced by 24% as the sand was fully replaced with FR (100% FR replacement) in mix O. At 100% FR and 100% CR replacement, the SG of mixes D was reduced to 2.13 (14% reduction) and 1.98 (20% reduction), respectively, compared to mixes without rubber. The data in Figure 10 and Table 7 indicate that, compared to mix O, the density of mix D (with optimised proportions) reduced more gradually with increasing rubber content. This suggests a more moderate increase in air content relative to the rubber content in the latter mix. As a result, the mix optimisation was proven effective at minimising the amount of air introduced in the mix.
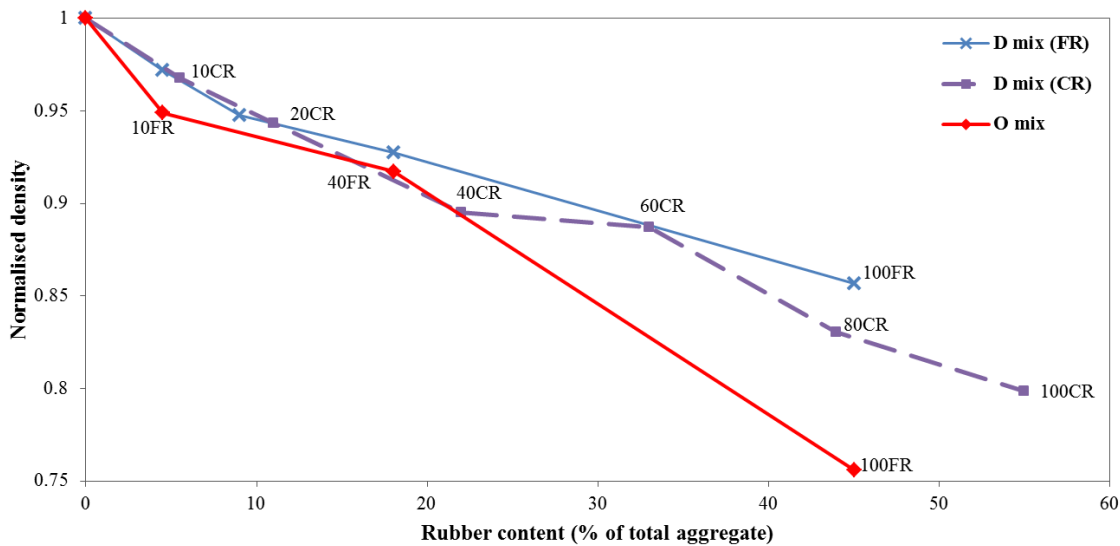
Figure 10. Variation of the density (normalised to the density of the corresponding plain mix) with rubber content for the original (O) and optimised (D) mixes.

To assess the effect of high rubber contents on the development of concrete compressive strength over time, cube compressive strengths at 3, 7, 14, 28 and 56 days were obtained for the optimised RuC mix with highest rubber content (60CR60FR). At least three cubes were tested per age and the maximum observed standard deviation was 1.6%. The results in Figure 11 indicate that the model proposed by Eurocode 2 (EC2) [79] estimates with reasonable accuracy the development of cube compressive strength of 60CR60FR RuC over time. However, further experimental results are necessary to fully confirm this conclusion.
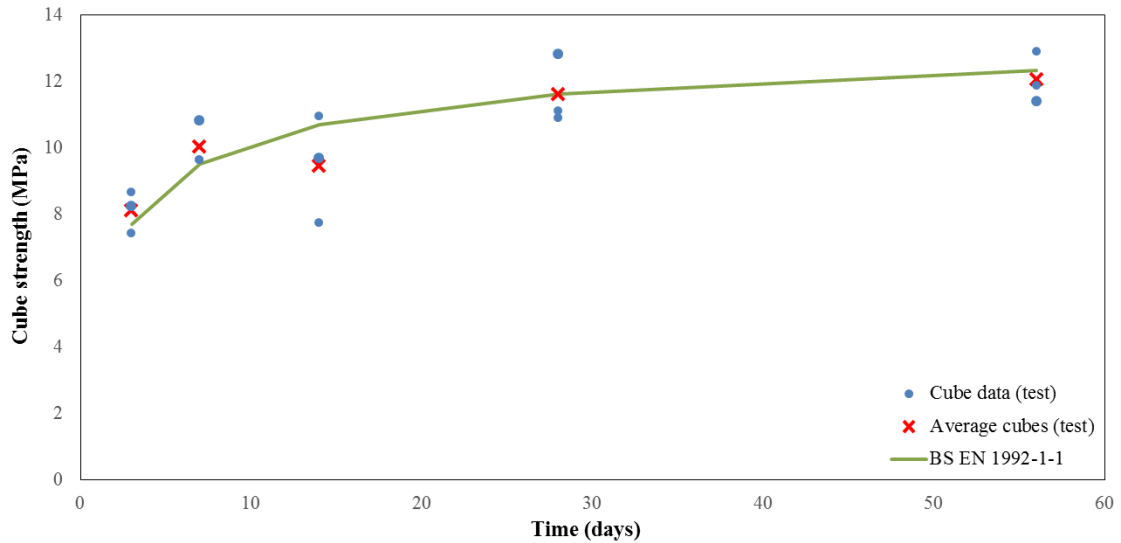
Figure 11. Development of cube strength at 3, 7, 14, 28 and 56 days (mix 60CR60FR)

3.3   Effect of water and admixture contents

The data in Table 6 show that at a rubber content of 40% FR, the fresh flow of mix O.3 (w/b=0.423) reduced from 685 mm to 520 mm, 420 mm and 'not flowable' for lower w/b contents (0.38 for mix A.1, 0.35 for A.2 and 0.32 for A.3, respectively). Figure 12 shows the effect of w/b on the fresh flow and compressive strength of RuC. Compared to mix O.3, the reduction in w/b also led to an increase in the 7-day compressive strength of mixes A.1, A.2 and A.3 by 55%, 59% and 126%, respectively. The reduction in w/b also resulted in significant improvements in mix cohesion and homogeneity. However, the use of w/b=0.30 (mix A.4) led to a very dry, unworkable, segregated and non-cohesive mix, and therefore no cylinders/cubes were cast. The extremely low flowability and the presence of segregation in mix A.3 (40% FR) indicated that such mix would behave inadequately at higher rubber contents. Therefore, a w/b of 0.35 was selected for Part 2 of the experimental programme.
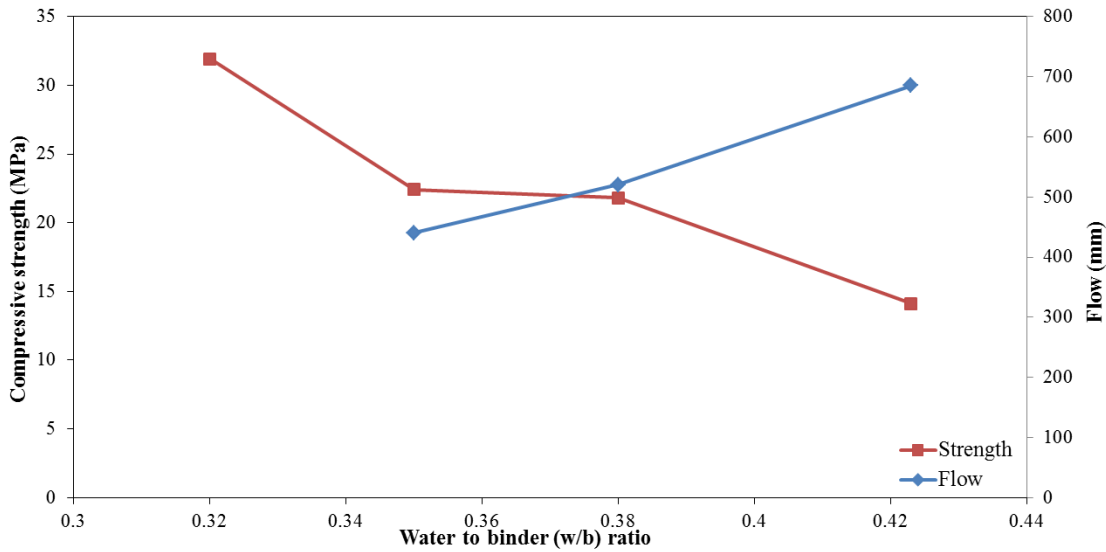
Figure 12. Variation of concrete flow and compressive strength with w/b at 40% FR content.

The mix water content also influences rubber distribution within the tested concrete cylinders. Figure 13a-b show the distribution of rubber in specimens of mixes O.3 and A.2 with 40% FR (w/b=0.423 and 0.35. respectively). It is shown that the rubber accumulated at the top of the cylinder cast in the original mix (O.3), whereas mix A.2 had a homogeneous distribution of rubber over the full cylinder height.
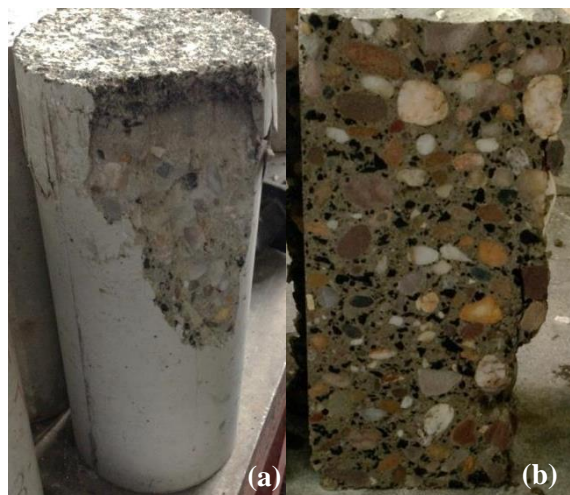

Figure 13. Rubber distribution in (a) Mix O.3 and (b) Mix A.2 with 40% fine rubber content.

The reduction of superplasticiser content by 40% (in mix B.2) reduced the flow (by up to 16%) but, more importantly, led to a reduction in mix segregation (segregation level reduced from 2 to 0) compared to mix O.3 with identical rubber content (see Table 6). However, due to the relatively high amount of lubricating water in the mixes and the rubber hydrophobicity, a thin gleam was observed at the surface of all B mixes, thus indicating bleeding. Based on the above observations, it is proposed to limit the w/b to the minimum required for cement hydration and use water reducing admixtures to achieve the necessary flowability. To maintain mix stability and homogeneity, flowability should be kept to a minimum. The reduced w/b is also recommended to prevent significant strength reduction.

3.4   Effect of rubber particle size

The results in Figure 6 (and Table 7) show that the fresh flowability of RuC is more affected by fine aggregate replacement than by coarse aggregate replacement, particularly at rubber contents above 20% of the total aggregates. At 100% FR replacement (45% of total aggregate volume), the mix was extremely dry and unworkable, whereas a flow of 380mm was achieved for the mix with 100% CR replacement (55% of total aggregate volume). This can be attributed to the filling effect of sand and its role in aiding mix flowability, as well as the excessive friction caused by the fine rubber particles, which have a rough surface and a larger surface area compared to coarse rubber particles with the same volume.

Figure 9 reveals a marginal difference in the compressive strength of the optimised mix D if coarse or fine rubber is used as aggregate replacement. Such difference varies with rubber content and seems to peak at around 10% total aggregate replacement, where CR led to compressive strength nearly 20% lower than the strength achieved using FR (strengths of 34 MPa vs. 42 MPa, respectively). This can be due to the load-bearing role of the larger coarse aggregates, which transfer loads directly within the specimens. However, for rubber contents ranging between 20% and 40% of the total aggregate, a similar concrete compressive strength was achieved regardless of type of rubber replacement. This is not in line with previous studies

reporting much lower compressive strength when replacing coarse aggregates as opposed to fine aggregates [24]. This deviation can be attributed to comparisons often being made between different amounts of rubber. Unfortunately, numerous previous studies express the rubber content as a fraction of the type of mineral aggregate replaced (coarse or fine), and therefore the actual amount of rubber in the mix could vary depending on the coarse to fine aggregate ratio, leading to comparisons among concretes with different overall rubber contents [61].

The standard deviation (SD) in compressive strength for mixes with FR replacement was 7.4% (mix D.4 with 100% FR, see Table 7). However, higher SD was observed for CR replacement, with a maximum of 27.1% at 60% CR. The higher variability associated with CR replacement may be attributed to the possible reduction in the amount of force that is transferred through direct contact in the stiffer mineral coarse aggregate, as well as to variations in stiffness across the cylinder. For instance, due to the larger size and lower quantity of CR particles (at an identical replacement level as FR), the particle distribution throughout the cylinder may vary significantly among test cylinders, leading to the observed higher variability.

The effects of combined replacement of coarse and fine aggregates (20CR20FR, 40CR40FR and 60CR60FR) on RuC fresh properties and compressive strength are shown in Table 7 and Figure 9, respectively. The compressive strength of mix 20CR20FR (20% total aggregate replacement - 32MPa) was higher than that achieved with 40FR or 40CR (18% and 22% total aggregate replacement, respectively) with strengths of 31.2 and 25.3 MPa, respectively, as shown in Figure 9. At 60% total aggregate replacement (60CR60FR), the strength reduction was similar to that observed in 100% FR or 100% CR replacement (45% and 55% of the total aggregates, respectively) despite having a higher overall rubber content. In terms of fresh properties, all mixes with combined CR and FR replacement had good workability with good cohesion and limited segregation. In particular, mix 60CR60FR had much better cohesion and homogeneity compared to mixes with total fine (100FR) or coarse aggregate (100CR) replacement.

The above observations indicate that, at low rubber contents, coarse aggregate replacement was more detrimental to the RuC compressive strength than fine aggregate replacement. This effect was not observed at higher rubber contents, where rubber properties seemed to control RuC behaviour regardless of the type of aggregate replaced. Whilst the compressive strength seems to be slightly more influenced by CR properties, the FR was slightly more detrimental to the concrete fresh properties, particularly at the higher rubber contents. The combined CR and FR replacement proved to be a suitable solution to maximise the rubber contents in RuC mixes without completely eliminating coarse or fine mineral aggregates, as well as to maintain satisfactory fresh properties and compressive strength. Mix 60CR60FR had a flow of 410mm, adequate cohesion and homogeneity and a compressive strength of around 7MPa. Such properties at high rubber contents were only achieved with the optimised mix and combining both CR and FR replacement. The 60CR60FR mix is instrumental for future studies by the authors in which high-rubber-content RuC cylinders are confined to achieve an environmentally friendly, high-ductility, high-deformability concrete.

3.5   Rubber pre-treatments

The results in Table 6 show that pre-washing rubber with water did not enhance the mix performance significantly. A minor reduction in flowability (3-5%) was observed in mixes C.1 and C.2 (with pre-washed rubber), respectively, compared to mixes A.1 and A.2 with the same amount of water directly added to the mix. Nonetheless, the strength and density of mixes C.1 and C.2 were comparable to mixes A.1 and A.2, respectively. These results confirm that pre-washing the rubber is not an effective solution to improve the rubber-cement paste bonding. Likewise, pre-coating the rubber with SF (mix C.3) rather than simply adding SF to the mix (mix D.3) did not improve mix performance. In fact, compared to mix C.3, mix D.3 had slightly higher slump, flow and strength (12%, 7% and 13%, respectively). Overall, the variation in performance and density of the mixes with pre-treated particles compared to mixes with as-received particles falls within the standard variation anticipated in normal concrete. Pre-

treatments are also often costly, time-consuming and aggressive to the concrete and rubber and should be only used if significant benefits are foreseen.

3.6   Effect of SF and PFA replacement

The partial replacement of cement with SF and PFA (10% each) improved significantly the concrete mix performance (Table 6). For instance, mix D (at w/b=0.35), had better fresh properties and compressive strength than the original mixes O and A (w/b=0.35) at all rubber contents. The improved mix performance due to binder material alone is evident by comparing mixes A.2 and D.3 at 40% FR, as the strength and flowability of the latter were 42% and 20% higher, respectively. The effectiveness of SF and PFA at enhancing RuC properties can be attributed to its filling effect (improved packing), as well as to its pozzolanic reaction with the cement hydration products. Previous research [80] indicates that fine SF particles also reduce bleeding, thus enhancing packing in the ITZ (which in turn increases the RuC strength). The effect of the fine fillers on the packing of the cementitious materials and RuC microstructure are discussed in sections 3.7 and 3.8, respectively.

3.7   Influence of water and binder in packing

The effect of optimising the water content and binder type on the packing of the concrete cementitious materials was examined using the wet packing method developed by Wong and Kwan [81]. Accordingly, the samples were prepared as follows: 1) Dry mix all binder materials for 2 min; 2) Place all the mixing water (based on selected w/b) in a bowl; 3) Add half the binder and admixtures to the bowl and mix at low speed for 3 min; 4) Divide the remaining binder and admixtures into four parts and add the portions (one after the other) to the bowl and mix for 3 minutes each; 5) Fill a (50mm dia × 100mm) cylindrical mould with the mixture to excess. The cylinder is either vibrated or left unconsolidated and the excess paste is removed; 6) Record the weight of the paste in the mould.

The binder mixes follow the proportions examined during the mix optimisation (see Table 3 and Table 4). Four representative mixes were selected to examine the influence of w/b and binder

material on the packing of the cementitious mixes: a) O – with w/b=0.423; b) A - 0.38 – with a w/b=0.38; c) A - 0.35 – with w/b=0.35 and d) D – with w/b=0.35 and SF and PFA each replacing 20% of the cement mass (10% each). The void contents (ε) and solid concentration (ϕ) for mixes with/without vibration are shown in Table 8.

Table 8. Voids ratio, air ratio and solid concentration of binder paste with/without vibration

Mix I.D.	Unconsolidated		Vibrated	
	Voids content $(\varepsilon)^a$	Solid Concentration $(\phi)^b$	Voids content (ε)	Solid Concentration (ϕ)
O	0.573	0.427	0.570	0.430
A–0.38	0.557	0.443	0.555	0.445
A–0.35	0.531	0.469	0.528	0.472
D	0.514	0.486	0.511	0.489

[a]Defined as the ratio of the volume of voids (voids content) to the bulk volume of the granular materials; [b]Ratio of the solid volume of the bulk granular material to its bulk volume [81]

Table 8 indicates that the solid concentration was slightly higher for all vibrated mixes compared to unconsolidated mixes. This increase in solid concentration is attributed to a decrease in voids and air content upon vibration (Table 8) and to the 'settling' of cementitious particles. As the w/b reduced from 0.423 (O) to 0.38 (A-0.38) and 0.35 (A-0.35), the solid concentration increased by 4% and 10%, respectively, indicating a better packing in the mix (vibrated and unconsolidated). The highest solid concentration (14% increase compared to O mix) was observed when SF and PFA were used to replace portions of the cement (see mix D, Table 8). Moreover, compared to mix A-0.35 (with identical w/b), the packing density of mix D increased by 4% for both consolidation types. This can be mainly attributed to the filling effect of SF and PFA [81].

The data in Table 8 show that the increase in solid concentration coincides with a reduction in voids content, thus indicating a reduction in the mix water requirement (to fill the voids) and, in turn, a higher compressive strength in mixes with higher packing densities. At a fixed water content, the excess water (not filling the voids) can increase the mix workability [81] up to the point where segregation and bleeding occur. This is in line with the flow table test results

summarised in Table 6. For example, the flow for mix D.3 (with SF and PFA binder) is 20% higher than that observed in mix A.2, despite having identical w/b (0.35) and rubber content (40% FR).

3.8 Microstructural observations

Figure 14a-d show 30x magnification images of RuC samples (at an age of 14 days) extracted from the following mixes: a) Mix D with alternative binder materials and w/b of 0.35, b) Mix O with w/b of 0.423, c) Mix A-0.35 with w/b of 0.35, and d) Mix A-0.38 with w/b of 0.38. The selected mixes had relatively small rubber content (combined 20% CR and FR replacement) so as to enable the manufacturing of samples including representative volumes of both mineral and rubber aggregates in all samples. Average 7-day cube strength (three cubes per mix) for mixes D, A-0.35, A-0.38 and O was 40 MPa, 39.2 MPa, 37.9 MPa and 37.5 MPa, respectively, with a maximum standard deviation of 5%. The darker features in Figure 14a-d represent voids or rubber, the mineral aggregates show an intermediate grey colour, whereas the hydrated cement phase is represented by a continuous light grey, as pinpointed in Figure 14c. Bright spots scattered across the images are either tyre steel fibres (Figure 14c) or unhydrated/partially hydrated cement particles as observed at higher magnifications (500x) for mixes O and D (see Figure 14e-f).
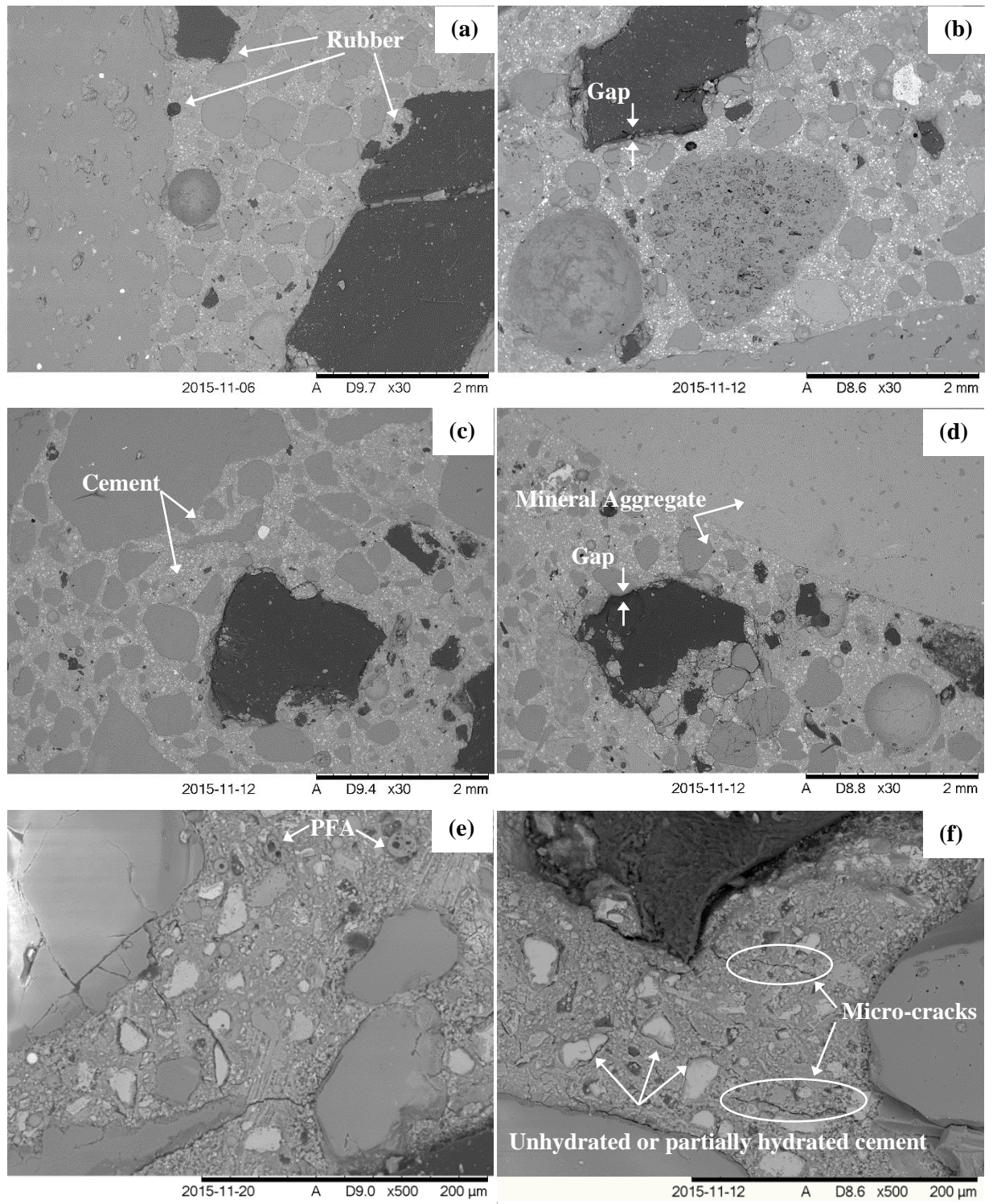
Figure 14. SEM images at 30x magnification: Mix D (a), mix O (b), mix A-0.35 (c) and mix A-0.38 (d) and at 500x magnification: Mix D (e) and mix O (f)

Whilst the rubber and mineral aggregates were randomly distributed over the concrete samples, large gaps (e.g. see Figure 14b) were evident between the rubber particles and the surrounding cement paste (notably in Mixes O and A-0.38). This effect could either be due to a) lack of bonding and limited cement hydration in the rubber-cement paste ITZ, b) rubber detachment during specimen preparation, or c) a combination of the two. A highly porous ITZ layer surrounded the rubber, exhibiting a slightly darker halo around the rubber particle (due to its lower density) (Figure 14f). Overall, the gaps between the rubber and the cement phase are smaller in samples extracted from mix D (Figure 14a) than in those extracted from mixes O and A-0.38 (Figure 14 b and d, respectively). This is due to the higher water content in mixes O and A-0.38, which, along with the rubber hydrophobicity, creates a film of air around the rubber, leading to reduced cement hydration, weaker bond and weaker ITZ in the rubber vicinity. Moreover, mixes O and A were weaker than mix D, thus promoting rubber detachment. The improved integration of the rubber particles in mix D emphasises the beneficial effect of mix optimisation with lower water content, as well as the filling effect of SF and PFA.

The images also reveal cracks across the Interfacial Transition Zone (ITZ) between the mineral aggregates and the cement paste and in the cement paste (Figure 14f). This cracking can be attributed to shrinkage of the cement paste and differential restrain provided by the aggregates. The weak ITZ phase between the cement and the aggregates is much thinner in mineral aggregates than in rubber particles (Figure 14f). This is in line with conclusions of previous research that found a 'double porosity' in the ITZ surrounding the rubber aggregates [38].

PFA particles (spherical shape) were observed in SEM images of samples from mix D (Figure 14e). This was validated using chemical analysis of mix D in this locality (at 1000x magnification, Figure 15a), which shows the combined presence of Silicon (Si), Aluminium (Al) and Oxygen (O), the main constituent elements of PFA. Chemical analysis of mixes D and O (Figure 15a-b) shows that no Zinc (Zn) was present on the rubber surface (or in the entire concrete sample). Zinc is often suspected to be a cause of rubber hydrophobicity [41].
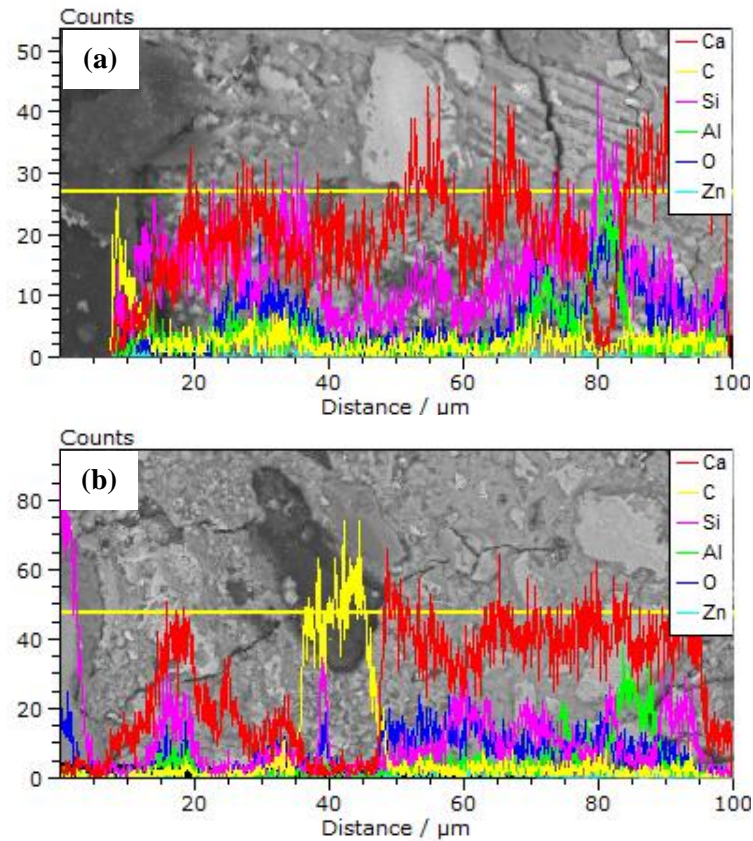
Figure 15. BSE elemental analysis for samples from mix D (a) and O (b) at 1000x magnification

The initial results from SEM observations indicate that the use of SF and PFA may have reduced the thickness of the gap between the rubber and the cement phase or the weak ITZ. Nevertheless, the influence of sample preparation must be evaluated and more images are needed from different parts of the sample to verify such result and to account for variability.

4 CONCLUSIONS

Based on the results presented in this article, the following conclusions are drawn:

Effects of rubber:

1. Higher rubber contents reduce concrete workability, hardened concrete density and compressive strength.

2. The concrete strength appears to be more influenced by the overall rubber volume rather than the type of rubber replacement (coarse or fine aggregate replacement). Nevertheless, RuC fresh properties were slightly inferior at high levels of fine aggregate replacement.

Mix optimisation:

1. Mix optimisation minimises the adverse effects of rubber on the concrete fresh and hardened mechanical properties. For instance, the replacement of 40% fine aggregates with rubber reduced the strength of the original mix (O) by 70%, whereas such reduction was only 49% in the optimised mix (D).

2. Optimised RuC mixes (D) enabled the use of high rubber contents (up to 60% total aggregate volume replacement) whilst maintaining an acceptable workability and a compressive strength of 7 MPa at 7 days.

3. Using SF and PFA to replace 20% of the cement mass increased the concrete flowability by 20% and the strength by 42%. SF and PFA had a filling effect (thus improving packing) and a pozzolanic reaction with the cement hydration products.

4. Pre-washing rubber with water or pre-coating with SF did not improve RuC performance.

Microstructure:

1. SEM analysis revealed a gap between rubber and the rubber-cement paste ITZ, particularly for larger rubber particles. The use of SF and PFA reduced this gap.

Acknowledgments

5 REFERENCES

[1] ETRA. The European Tyre Recycling Association. Available at: http://www.etra-eu.org [Last accessed: 10/06/2014].

[2] Council Regulation (EC) 31/1999 of 26 April 1999 on the landfill of waste [1999] OJ L182/1.

[3] Directive (EC) 98/2008 of the European Parliament and of the Council of 19 November 2008 on waste and replacing certain Directives [2008] OJ L312/3.

[4] Siddique R, Naik TR. Properties of concrete containing scrap-tire rubber–an overview. Waste Management. 2004;24(6):563-9.

[5] Najim K, Hall M. A review of the fresh/hardened properties and applications for plain-(PRC) and self-compacting rubberised concrete (SCRC). Construction and Building Materials. 2010;24(11):2043-51.

[6] Montella G, Calabrese A, Serino G. Mechanical characterization of a Tire Derived Material: Experiments, hyperelastic modeling and numerical validation. Construction and Building Materials. 2014;66:336-47.

[7] Atahan AO, Yücel AO. Crumb rubber in concrete: Static and dynamic evaluation. Construction and Building Materials. 2012;36:617-22.

[8] Toumi A, Nguyen T-H, Turatsinze A. Debonding of a thin rubberised and fibre-reinforced cement-based repairs: Analytical and experimental study. Materials & Design. 2013;49:90-5.

[9] Cheng Z, Shi Z. Vibration attenuation properties of periodic rubber concrete panels. Construction and Building Materials. 2014;50:257-65.

[10] Mohammed BS, Anwar Hossain KM, Eng Swee JT, Wong G, Abdullahi M. Properties of crumb rubber hollow concrete block. Journal of Cleaner Production. 2012;23(1):57-67.

[11] Al-Tayeb MM, Abu Bakar B, Ismail H, Akil HM. Effect of partial replacement of sand by recycled fine crumb rubber on the performance of hybrid rubberized-normal concrete under impact load: experiment and simulation. Journal of Cleaner Production. 2013;59:284-9.

[12] Mohammed BS. Structural behavior and m–k value of composite slab utilizing concrete containing crumb rubber. Construction and Building Materials. 2010;24(7):1214-21.

[13] Li G, Stubblefield MA, Garrick G, Eggers J, Abadie C, Huang B. Development of waste tire modified concrete. Cement and Concrete Research. 2004;34(12):2283-9.

[14] Toutanji HA. The use of rubber tire particles in concrete to replace mineral aggregates. Cement and Concrete Composites. 1996;18(2):135-9.

[15] Güneyisi E, Gesoğlu M, Özturan T. Properties of rubberized concretes containing silica fume. Cement and Concrete Research. 2004;34(12):2309-17.

[16] Khatib ZK, Bayomy FM. Rubberized Portland cement concrete. Journal of materials in civil engineering. 1999;11(3):206-13.

[17] Aiello MA, Leuzzi F. Waste tyre rubberized concrete: Properties at fresh and hardened state. Waste Management. 2010;30(8):1696-704.

[18] Dong Q, Huang B, Shu X. Rubber modified concrete improved by chemically active coating and silane coupling agent. Construction and Building Materials. 2013;48:116-23.

[19] Daniel DG. Factors influencing concrete workability. Significance of tests and properties of concrete and concrete making materials, Bridgeport. 2006:59-72.

[20] Turatsinze A, Garros M. On the modulus of elasticity and strain capacity of self-compacting concrete incorporating rubber aggregates. Resources, Conservation and Recycling. 2008;52(10):1209-15.

[21] Richardson AE, Coventry KA, Ward G. Freeze/thaw protection of concrete with optimum rubber crumb content. Journal of Cleaner Production. 2012;23(1):96-103.

[22] Neville A, Brooks J. Concrete Technology. Revised Edition-2001 Standards Update. Harlow. Pearson Education Limited; 1990.

[23] Güneyisi E, Gesoglu M, Naji N, İpek S. Evaluation of the rheological behavior of fresh self-compacting rubberized concrete by using the Herschel–Bulkley and modified Bingham models. Archives of Civil and Mechanical Engineering. 2016;16(1):9-19.

[24] Eldin NN, Senouci AB. Measurement and prediction of the strength of rubberized concrete. Cement and Concrete Composites. 1994;16(4):287-98.

[25] Batayneh MK, Marie I, Asi I. Promoting the use of crumb rubber concrete in developing countries. Waste Management. 2008;28(11):2171-6.

[26] Najim KB, Hall MR. Crumb rubber aggregate coatings/pre-treatments and their effects on interfacial bonding, air entrapment and fracture toughness in self-compacting rubberised concrete (SCRC). Materials and Structures. 2013;46(12):2029-43.

[27] Najim KB, Hall MR. Mechanical and dynamic properties of self-compacting crumb rubber modified concrete. Construction and Building materials. 2012;27(1):521-30.

[28] Ganjian E, Khorami M, Maghsoudi AA. Scrap-tyre-rubber replacement for aggregate and filler in concrete. Construction and Building Materials. 2009;23(5):1828-36.

[29] Sukontasukkul P, Chaikaew C. Properties of concrete pedestrian block mixed with crumb rubber. Construction and Building Materials. 2006;20(7):450-7.

[30] Bignozzi MC, Sandrolini F. Tyre rubber waste recycling in self-compacting concrete. Cement and concrete research. 2006;36(4):735-9.

[31] Da Silva FM, Barbosa LAG, Lintz RCC, Jacintho AEP. Investigation on the properties of concrete tactile paving blocks made with recycled tire rubber. Construction and Building Materials. 2015;91:71-9.

[32] Aliabdo AA, Elmoaty AEMA, AbdElbaset MM. Utilization of waste rubber in non-structural applications. Construction and Building Materials. 2015;91:195-207.

[33] Bing C, Ning L. Experimental research on properties of fresh and hardened rubberized concrete. Journal of Materials in Civil Engineering. 2013.

[34] Correia SL, Partala T, Loch FC, Segadães A. Factorial design used to model the compressive strength of mortars containing recycled rubber. Composite Structures. 2010;92(9):2047-51.

[35] Flores-Medina D, Medina NF, Hernández-Olivares F. Static mechanical properties of waste rests of recycled rubber and high quality recycled rubber from crumbed tyres used as aggregate in dry consistency concretes. Materials and Structures. 2014;47(7):1185-93.

[36] Ling T-C. Prediction of density and compressive strength for rubberized concrete blocks. Construction and Building Materials. 2011;25(11):4303-6.

[37] Gupta T, Chaudhary S, Sharma RK. Assessment of mechanical and durability properties of concrete containing waste rubber tire as fine aggregate. Construction and Building Materials. 2014;73:562-74.

[38] Turki M, Bretagne E, Rouis M, Quéneudec M. Microstructure, physical and mechanical properties of mortar–rubber aggregates mixtures. Construction and Building Materials. 2009;23(7):2715-22.

[39] Pelisser F, Zavarise N, Longo TA, Bernardin AM. Concrete made with recycled tire rubber: effect of alkaline activation and silica fume addition. Journal of Cleaner Production. 2011;19(6):757-63.

[40] Benazzouk A, Douzane O, Langlet T, Mezreb K, Roucoult JM, Quéneudec M. Physico-mechanical properties and water absorption of cement composite containing shredded rubber wastes. Cement and Concrete Composites. 2007;29(10):732-40.

[41] Youssf O, ElGawady MA, Mills JE, Ma X. An experimental investigation of crumb rubber concrete confined by fibre reinforced polymer tubes. Construction and Building Materials. 2014;53:522-32.

[42] Eldin NN, Senouci AB. Rubber-tire particles as concrete aggregate. Journal of Materials in Civil Engineering. 1993;5(4):478-96.

[43] Ganesan N, Raj B, Shashikala AP. Behavior of Self-Consolidating Rubberized Concrete Beam-Column Joints. ACI Materials Journal. 2013;110(6).

[44] Segre N, Monteiro PJM, Sposito G. Surface characterization of recycled tire rubber to be used in cement paste matrix. Journal of Colloid and Interface Science. 2002;248(2):521-3.

[45] Meddah A, Beddar M, Bali A. Use of shredded rubber tire aggregates for roller compacted concrete pavement. Journal of Cleaner Production. 2014;72:187-92.

[46] Raghavan D, Huynh H, Ferraris CF. Workability, mechanical properties, and chemical stability of a recycled tyre rubber-filled cementitious composite. Journal of Materials Science. 1998;33(7):1745-52.

[47] Huang B, Shu X, Cao J. A two-staged surface treatment to improve properties of rubber modified cement composites. Construction and Building Materials. 2013;40:270-4.

[48] Chou LH, Lin CN, Lu CK, Lee CH, Lee MT. Improving rubber concrete by waste organic sulfur compounds. Waste Management & Research. 2010;28(1):29-35.

[49] Chou LH, Yang CK, Lee MT, Shu CC. Effects of partial oxidation of crumb rubber on properties of rubberized mortar. Composites Part B: Engineering. 2010;41(8):613-6.

[50] Ossola G, Wojcik A. UV modification of tire rubber for use in cementitious composites. Cement and Concrete Composites. 2014;52:34-41.

[51] Li Z, Li F, Li J. Properties of concrete incorporating rubber tyre particles. Magazine of Concrete Research. 1998;50(4):297-304.

[52] Onuaguluchi O, Panesar DK. Hardened properties of concrete mixtures containing pre-coated crumb rubber and silica fume. Journal of Cleaner Production. 2014;82:125-31.

[53] Quiroga PN, Fowler DW. The effects of aggregates characteristics on the performance of Portland cement concrete. Research report. International Center for Aggregates Research, University of Texas at Austin; 2004.

[54] Ho AC, Turatsinze A, Hameed R, Vu DC. Effects of rubber aggregates from grinded used tyres on the concrete resistance to cracking. Journal of Cleaner Production. 2012;23(1):209-15.

[55] Ohemeng EA, Yalley PP-K. Models for predicting the density and compressive strength of rubberized concrete pavement blocks. Construction and Building Materials. 2013;47:656-61.

[56] Hernandez-Olivares F, Barluenga G, Bollati M, Witoszek B. Static and dynamic behaviour of recycled tyre rubber-filled concrete. Cement and Concrete Research. 2002;32(10):1587-96.

[57] Fung W, Kwan A, Wong H. Wet packing of crushed rock fine aggregate. Materials and structures. 2009;42(5):631-43.

[58] Sukontasukkul P. Use of crumb rubber to improve thermal and sound properties of pre-cast concrete panel. Construction and Building Materials. 2009;23(2):1084-92.

[59] Khaloo AR, Dehestani M, Rahmatabadi P. Mechanical properties of concrete containing a high volume of tire–rubber particles. Waste Management. 2008;28(12):2472-82.

[60] Holmes N, Browne A, Montague C. Acoustic properties of concrete panels with crumb rubber as a fine aggregate replacement. Construction and Building Materials. 2014;73:195-204.

[61] Reda Taha MM, El-Dieb AS, Abd El-Wahab MA, Abdel-Hameed ME. Mechanical, fracture, and microstructural investigations of rubber concrete. Journal of materials in civil engineering. 2008;20(10):640-9.

[62] Liu F, Zheng W, Li L, Feng W, Ning G. Mechanical and fatigue performance of rubber concrete. Construction and Building Materials. 2013;47:711-9.

[63] BSI 197-1:2011. Cement. Part 1: Composition, specifications and conformity criteria for common cements. 2011, BS EN 197 Part 1. London UK.

[64] Elkem Materials. Elkem Microsilica Grade 940 - Fibre Cement FC2-01 Products. Product Data Sheet. Available at https://www.elkem.com/silicon-materials/fibre-cement/microsilica-grade-940/ [Last accessed 20/01/2017].

[65] Ash Solutions Ltd. Fly Ash - BSEN 450 - 1 Class N Category B LOI Fly Ash. Product Information. Available at https://cms.esi.info/Media/documents/77639_1332234960909.pdf [Last accessed 20/01/2017].

[66] Sika Limited. Sika Viscoflow 1000. Product Data Sheet. Edition-21/05/2015; Identification no: 02 13 01 01 100 0 000853. Available at https://goo.gl/mMDfay [Last accessed 10/12/2015].

[67] Sika Limited. Sika Viscoflow 2000. Product Data Sheet. Edition-15/10/2014; Identification no: 02 13 01 01 100 0 001325. Available at https://goo.gl/kMfHcU [Last accessed 10/12/2015].

[68] ASTM Standard C136, 2006, "Standard Test Method for Sieve Analysis of Fine and Coarse Aggregates", ASTM International, West Conshohocken, PA, 2006, DOI:10.1520/C0136-06.

[69] ADRIA Abruzzo s.r.l. Available at: http://www.adria-abruzzo.it/ADRIA/index.html [Last accessed: 29/03/2016].

[70] BSI 1097-6: 2013. Tests for mechanical and physical properties of aggregates. Determination of particle density and water absorption. 2013, BS EN 1097 Part 6. London, UK.

[71] BSI 1097-3:1998. Tests for mechanical and physical properties of aggregates: Determination of loose bulk density and voids. 1998, BS EN 1097 Part 3. London, UK.

[72] BSI 933-3:2012. Tests for geometrical properties of aggregates. Determination of particle shape - Flakiness index. 2012, BS EN 933 Part 3. London, UK.

[73] BSI 12390-2:2009. Testing hardened concrete. Part 2: Making and curing specimens for strength tests. 2009, BS EN 12390 Part 2. London, UK.

[74] BSI 12390-3:2009. Testing hardened concrete. Part3: Compressive strength of test specimens. 2009, BS EN 12390 Part 3. London, UK.

[75] ASTM Standard C617/C617M - 12, "Standard Practice for Capping Cylindrical Concrete Specimens", ASTM International, West Conshohocken, PA, 2012, DOI:10.1520/C0617_C0617M-12.

[76] BSI 12350-2:2009. Testing fresh concrete. Part 2: Slump-test. 2009, BS EN 12350 Part 2. London, UK.

[77] BSI 12350-5:2009. Testing fresh concrete. Part 5: Flow table test. 2009, BS EN 12350 Part5. London, UK.

[78] ASTM Standard C1611/C1611M - 09b, "Standard Test Method for Slump Flow of Self-Consolidating Concrete", ASTM International, West Conshohocken, PA, 2009, DOI:10.1520/C1611_C1611M-09B.

[79] Institution BS. Eurocode 2: Design of Concrete Structures: Part 1-1: General Rules and Rules for Buildings: British Standards Institution; 2004.

[80] The Concrete Society. The role of water in concrete and its influence on properties - Concrete Society Discussion Document 2005 IX.

[81] Wong HH, Kwan AK. Packing density of cementitious materials: part 1—measurement using a wet packing method. Materials and Structures. 2008;41(4):689-701.

Chapter 3

Unconfined and FRP-confined rubberised concrete in axial compression

Raffoul S., Garcia, R., Escolano-Margarit, D., Guadagnini, M., Hajirasouliha, I. and Pilakoutas, K., (2016). Behaviour of unconfined and FRP-confined rubberised concrete in axial compression. Construction and Building Materials. 147, 388-97.

This article investigates the use of externally bonded Fibre Reinforced Polymer (FRP) jackets to develop a novel high-strength, highly-deformable FRP Confined Rubberised Concrete (CRuC). Sixty rubberised concrete (RuC) cylinders were tested in axial compression. The cylinders were produced using recycled tyre rubber to replace i) 0 to 100% fine or coarse aggregate volume or ii) a replacement of 40% or 60% of the total aggregate volume. Six cylinders of the latter mix were then confined with either two or three layers of Aramid FRP sheets. The results indicate that the use of high rubber contents in concrete lead to premature microcracking and lateral expansion, the latter of which can be used to activate the FRP confinement earlier and achieve higher confinement effectiveness. The CRuC cylinders reached compressive strengths of up to 75 MPa and unprecedented ultimate axial strains up to 5%, i.e. about fourteen times larger than those of normal concrete (0.35%). Such novel high-strength, highly-deformable CRuC is of great value to engineers and can be used for structural applications where large deformability is required.

1 INTRODUCTION

Worldwide tyre production is forecast to exceed 2.9 billion units per year by the end of 2017 [1] and over 300 million tyres reach their service life every year in the EU alone [2]. Whilst stringent EU directives control waste tyre disposal [3], waste tyres are still landfilled and can cause major public health risks and environmental issues. This has increased the incentive to generate innovative applications for the main components of scrap tyres (vulcanised rubber, steel wire and textile fibres) in the construction industry [4-6].

Vulcanised rubber used in tyre manufacturing has good strength and flexibility and an ability to maintain its volume under compressive stress. Over the last few years, extensive research has investigated the use of recycled tyre rubber as mineral aggregate replacement in concrete. The results from these studies indicate that, compared to normal concrete, rubberised concrete (RuC) has higher deformation capacity [7, 8] and vibration damping [9-11]. Conversely, RuC has lower compressive strength, tensile strength and stiffness [12-16]. The compressive strength of RuC with high rubber contents (replacement volumes >50-60%) can be up to 90% lower than that of normal concrete [12, 13, 17, 18]. Such low strength can be mainly attributed to the a) low stiffness and high Poisson's ratio of rubber, resulting in stress concentrations within the mix, b) hydrophobic nature of rubber, which causes weak rubber-cement matrix bonding, c) increased mix non-homogeneity, d) increased porosity and air content, and e) lower "mass stiffness" of RuC [14-16]. The inclusion of rubber in concrete also affects its mix fresh properties, leading to high segregation and bleeding, high air content, as well as low slump and workability [17, 19-21]. Whilst considerable amount of literature has been published on RuC, there is a general lack of consensus on the influence of rubber on the physical and mechanical properties of fresh and hardened concrete. Due to the insufficient understanding of the influence of rubber on the mechanical properties of concrete, to date RuC is mainly used in low-strength, non-structural applications such as concrete pedestrian blocks, traffic barriers or lightweight fills [18, 21-23].

More recently, limited research has examined the use of Fibre Reinforced Polymer (FRP) sheets to confine RuC specimens (containing low rubber contents) in an attempt to develop adequate axial strength and exploit the potential deformation capacity that RuC can offer [24-28]. Li et al. [25] tested confined rubberised concrete (CRuC) cylinders cast in prefabricated Glass FRP (GFRP) pipes. Whilst the GFRP CRuC specimens were up to 5.25 times stronger than the equivalent unconfined RuC specimens, relatively low compressive strengths of 16.3 to 22.9 MPa were achieved. Moreover, maximum axial strain values of only about 2.5% could be developed, which are similar to what can be achieved with GFRP confined cylinders made of conventional concrete [29]. Youssf et al. [24] tested CRuC cylinders cast in preformed Carbon FRP (CFRP) tubes. The compressive strength of these cylinders ranged from 61.7 MPa (for one CFRP layer) to 112.5 MPa (for three CFRP layers), thus being suitable for structural applications. However, the deformability potential from using rubber particles was not fully exploited, since the stress-strain behaviour of the CFRP CRuC cylinders [24] was similar to that of CFRP-confined cylinders with conventional concrete [29]. More recently, Duarte et al. [27] tested short RuC columns confined with cold formed steel tubes. Whilst the column ductility was increased by up to 50%, the capacity of the specimens was limited by the premature local buckling of the steel tubes. It should be noted that the studies discussed above only made use of low rubber contents, replacing about 30% of the fine aggregates [25], or 10% [24] and 15% [27] of the total aggregates, and provide evidence that the use of small volumes of rubber aggregate replacement has a minor effect on concrete deformability. The use of higher rubber contents has been previously associated with several material and technological issues and, only recently, work by the authors [30] has successfully addressed some of these challenges and enabled the development of a modified concrete with high rubber contents (>50%) suitable for the manufacture of highly deformable CRuC (axial strains >5%) elements for structural applications.

This article summarises the methodology implemented for the development of improved rubber modified concrete mixes and investigates experimentally the use of externally bonded FRP

confinement to exploit the deformation capacity of RuC and develop high-strength, highly-deformable FRP CRuC elements. The results presented in this article are part of the ongoing EU-funded project Anagennisi, which investigates the innovative reuse of all tyre components in concrete [31]. This work is expected to contribute towards the understanding of the mechanical behaviour of FRP CRuC and towards the development of a highly-deformable concrete for high-value structural applications.

2   EXPERIMENTAL PROGRAMME

The mechanical performance of RuC (with and without FRP confinement) was investigated experimentally using a total of 66 cylinders (100×200mm) cast from 15 different mixes. The main parameters investigated were the effect of rubber content, rubber type and the number of FRP layers on the stress-strain behaviour of RuC up to peak stress.

2.1   Materials

2.1.1   Concrete and rubber

All mixes were produced using CEM II-52.5 N Portland Limestone Cement, containing around 10-15% Limestone in compliance with BS EN 197-1 [32]. Two types of commercial high-range water reducing admixtures [33, 34] were used. The fine aggregates were medium grade river washed sand from Shardlow, Derbyshire (UK) with size: 0-5mm, specific gravity: 2.65, water absorption: 0.5%, and fineness modulus: 2.64. The coarse aggregates were round river washed gravel from Trent Valley (UK) with sizes: 5-10 and 10-20mm, specific gravity: 2.65, and water absorption: 1.24%.

To examine the influence of rubber type and content on the stress-strain behaviour of RuC, rubber particles were used to replace either a) fine aggregates (sand) by 0-100% by volume, b) coarse aggregates (gravel) by 0-100% by volume, or c) both fine and coarse aggregates by 40% and 60% by volume. The rubber particles were obtained from mechanical shredding of vehicular tyres and had a rough, jagged surface with traces of contamination from steel and

polymer fibres. The rubber particles (shown in Figure 1) were classified as follows: a) fine rubber particles (size 0-5mm) used as sand replacement, and b) coarse rubber particles (sizes 5-10mm and 10-20mm) used as gravel replacement. Figure 2 shows the particle size distribution of the rubber aggregates determined according to ASTM C136 [35]. Table 1 summarises the physical properties of rubber and mineral aggregates. The rubber particle density and water absorption, flakiness index and bulk density were obtained following Annex C of BS EN 1097-6 (lightweight aggregates) [36], BS EN 933-3 [37] and BS EN 1097-3 [38], respectively. It should be noted, however, that these tests could not be performed on the fine rubber particles (size 0-5mm) as these float in water and agglomerate due to surface tension and inter-particular forces.

Figure 1. Rubber particles used to replace sand (0-5mm) and gravel (5-10mm and 10-20mm)
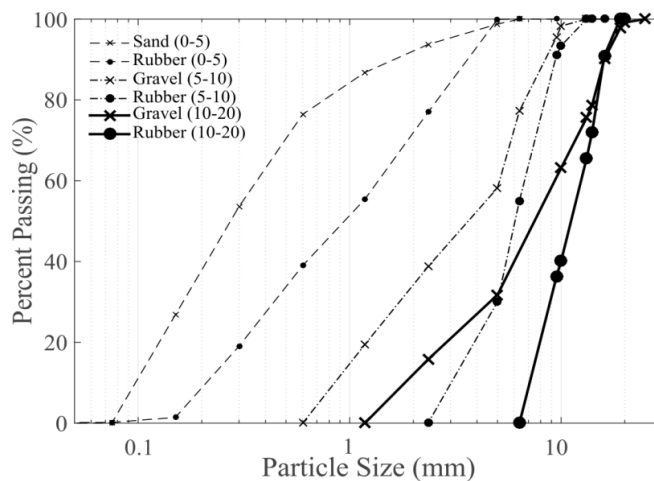
Figure 2. Sieve analysis of rubber and mineral aggregates

Table 1. Physical properties of rubber and mineral aggregates (adapted from Raffoul et al. [30])

Material (size in mm)	Apparent density (t/m^3)	Oven dry density (t/m^3)	SSD[a] density (t/m^3)	Water absorption (%)	Specific gravity	Bulk density (t/m^3)	Flakiness Index
Rubber (0-5)	0.80[b]	-	-	-	-	0.40-0.46	N/A
Rubber (5-10)	1.10-1.20	1.00-1.10	1.10-1.2	5.30-8.90	1.10	0.45	6.6-8.3
Rubber (10-20)	1.10	1.10	1.10	0.80-1.30	1.10	0.48	10.4-17.5
Sand (0-5)	2.65	2.62	2.63	0.50	2.65	1.78	N/A
Gravel (5-10)	2.69	2.60	2.63	1.24	2.65	1.51	7.1
Gravel (10-20)	2.69	2.60	2.63	1.24	2.65	1.58	9.7

[a]Saturated Surface Dry
[b]Average from literature (see [30])

Mix Design

Previous research by the authors [30] indicated that the inclusion of large volumes of rubber in concrete could lead to very unstable mixes with high levels of segregation and a lack of cohesion, accompanied with significant compressive strength reductions. To minimise such adverse effects, the authors investigated the various mix parameters that influence RuC and proposed an 'optimised' mix design [30] that results in a concrete with good fresh properties (homogeneity and cohesion) and enhanced compressive strength. For instance, when compared to a non-optimised mix with 100% fine rubber replacing sand, the 'optimised' mix was 2.6 times stronger (average strengths of 3.7 and 9.6 MPa, respectively). The 'optimised' mix proportions, used in this study, are presented in Table 2. The mix was designed to be highly

flowable with relatively high cement content and water to binder ratio (w/b=0.35). Rubber contents varied from 0 to 100% of the fine (F) or coarse (C) aggregate volume. A replacement of both fine and coarse mineral aggregates (F&C) was also examined so as to maximise the total volume of rubber in the mix. This comprised: i) a replacement of 40% fine aggregate and 40% coarse aggregate by volume (40F&C, i.e. 40% replacement of the total aggregate volume with rubber), or ii) a replacement of 60% fine aggregate and 60% coarse aggregate by volume (60F&C, i.e. 60% replacement of the total aggregate volume with rubber). Table 3 summarises the rubber and mineral aggregate proportions used for the RuC mixes in this study.

Table 2: Mix proportions for the optimised mix used in this study

Material	Quantity
CEM II – 52.5 MPa	340 kg/m^3
Silica Fume (SF)	42.5 kg/m^3
Pulverised Fuel Ash (PFA)	42.5 kg/m^3
Aggregates 0/5mm	820 kg/m^3
Aggregates 5/10mm	364 kg/m^3
Aggregates 10/20mm	637 kg/m^3
Water	150 l/m^3
Plasticiser (P)	2.5 l/m^3
Superplasticiser (SP)	5.1 l/m^3

Table 3. Proportions of rubber and mineral aggregate at different levels of replacement

Replacement Type	ID	Mass of rubber (kg/m^3) C	F	Mass of CA[a] (kg/m^3)	Mass of FA[a] (kg/m^3)
None	Plain	-	-	1001.0	820.0
	10F	-	24.8	1001.0	738.0
	20F	-	49.5	1001.0	656.0
Fine Rubber (F)	40F	-	99.0	1001.0	492.0
	60F	-	148.5	1001.0	328.0
	100F	-	247.6	1001.0	0.0
	10C	30.2	-	900.9	820.0
	20C	60.4	-	800.8	820.0
Coarse Rubber (C)	40C	120.9	-	600.6	820.0
	60C	181.3	-	400.4	820.0
	100C	302.2	-	0.0	820.0
Fine & Coarse	40F&C	120.9	99.0	600.6	492.0
Rubber (F&C)	60F&C	181.3	148.5	400.4	328.0

[a]CA = coarse aggregate, FA = fine aggregate

The concrete constituents were mixed as follows: 1) the aggregates (both mineral and rubber) were dry-mixed for 30 seconds (all mineral aggregates were Saturated Surface Dry (SSD), whereas the rubber particles were mixed dry and as-received), 2) half of the mixing water was added and mixed for another minute, 3) the mix was allowed to rest for three minutes, 4) the binder materials and the remaining mixing water were then added followed by a gradual addition of the admixtures, and 5) the concrete was then mixed for another three minutes. The cylinders were cast in two layers and vibrated on a vibrating table (15-20s per layer). After casting, the specimens were covered with plastic sheets and kept under standard laboratory conditions for 48hrs. They were then demoulded and stored in a mist room for another 25 days.

2.1.2 FRP confinement

In an effort to develop highly deformable RuC, six cylinders of mix 60F&C were confined with two or three layers of FRP sheets using a wet lay-up technique. Aramid FRP (AFRP) was selected as confining material as it combines good tensile strength and high ultimate elongation. The mean mechanical and physical properties of the unidirectional AFRP sheets, as provided by the manufacturer, were: tensile strength f_f=2400 MPa, modulus of elasticity E_f=116GPa, ultimate elongation of the fibres ε_{fu}=2.5%, and thickness of sheet t_f=0.2 mm. Before applying the AFRP confinement, the surface of the cylinders was brushed and cleaned to improve adherence. To avoid direct contact of the loading device platens with the AFRP confinement and prevent the axial load from being transferred directly to the FRP layers during the tests, the total height of the sheets was 180 mm, i.e. 10 mm at the cylinders' top and bottom were unconfined. The sheets were overlapped by a length of 100 mm with the AFRP fibres oriented perpendicular to the cylinders' axes. As such, the total length of the AFRP sheet needed to confine the 100x200mm cylinders was: i) 728mm for two layers and ii) 1042mm for three layers. Acetate sheets were then placed on the exposed surface of the AFRP to achieve a smooth resin layer finish, thus enabling the easy subsequent installation of foil-type strain gauges. These acetate sheets were removed after one day of resin curing.

2.2   Test setup and instrumentation

All cylinders were subjected to compressive load using a 3,000 kN capacity compressive machine connected to a data logger. To prevent possible concrete failure due to stress concentrations during testing, the top and bottom of all cylinders were confined using high-strength high-ductility post tensioned metal straps [39] of thickness 0.8 mm and width 13 mm (for unconfined RuC specimens) or 25 mm (for FRP CRuC specimens). Figure 3 shows the final setup during the test. The cylinders were tested monotonically in load control using a loading rate of 0.25 MPa/s up to failure. For cylinders with very high rubber contents (above 60% F or C replacement), a load rate of 0.1 MPa/s was used to capture the stress-strain behaviour at smaller time steps.
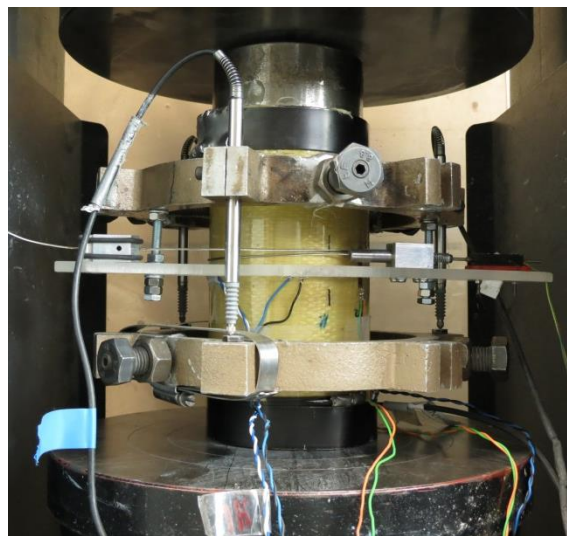
Figure 3. General view of test setup

The test rig was designed to measure local and global vertical and horizontal deformations. To measure local strains, 10 mm foil-type electrical resistance strain gauges were fixed on each cylinder at the locations shown schematically in Figure 4. Two vertical strain gauges (V1 and V2), located at the cylinders' mid-height (180° apart) were used to measure axial strains, whilst three horizontal strain gauges (H1 to H3) placed radially at 120° were used to monitor lateral strains. In the FRP CRuC cylinders, gauge H3 was located in the middle of the overlap of the

AFRP sheets. Global axial displacements were monitored using three LVDTs mounted radially at 120° on two steel rings (LVDTs 1 to 3 in Figure 4) located at the cylinders' mid-height. The steel rings were fixed to the cylinders using three clamp screws with a centre-to-centre distance of 100 mm. Global horizontal displacements (lateral expansion) were obtained using readings from a LVDT attached to a pre-tensioned circumferential wire around the mid-height of the cylinders (LVDT H).
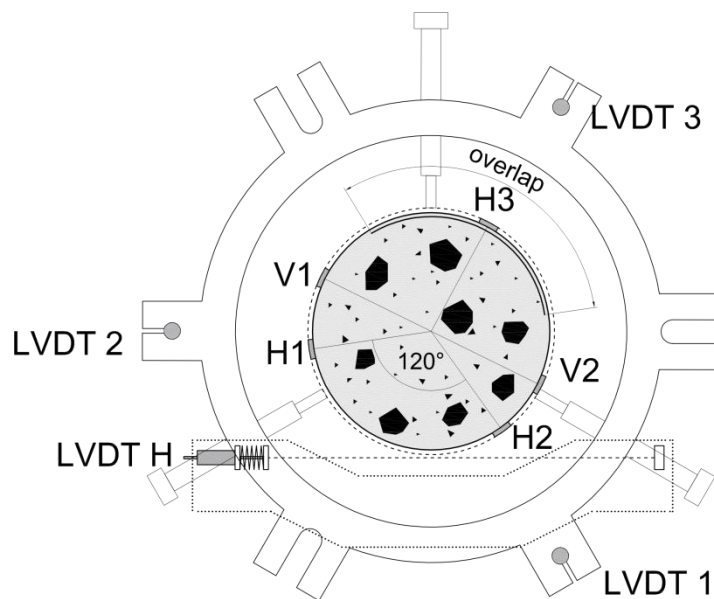
Figure 4. Typical instrumentation used to test the cylinders

3   RESULTS AND DISCUSSION: UNCONFINED RUC

Table 4 summarises the unconfined compressive strength (f_c), initial modulus of elasticity (E_c), absolute values of axial (ε_{cp}) and lateral (ε_{clp}) strains at f_c, as well as the axial strains at the limit of proportionality (LOP), which indicates the onset of microcracking, (ε_{cLOP}). The table also includes the ratio $\varepsilon_{cp}/\varepsilon_{cLOP}$ and the rubber content as a percentage of the total aggregate volume. The compressive strength (f_c) results listed in Table 4 were obtained from at least 4 cylinders per rubber content to account for strength variability, whereas stress-strain results, also discussed in following sections, were obtained for one cylinder per rubber content. The following sections discuss the results of this phase of the testing programme and summarise the

most significant observations. It should be noted that a few test data in Table 4 are not reported due to premature failure of the test setup/instrumentation.

Table 4. Results from unconfined RuC with different rubber contents

ID	Total aggregate replaced (%)	f_c (MPa)	ε_{cLOP} (με)	ε_{cp} (με)	ε_{clp} (με)	E_c (GPa)	$\varepsilon_{cp}/\varepsilon_{cLOP}$
Plain	0	61.7 ± 4.1	550	2180	885	39.4	3.96
10F	4.5	53.4 ± 2.1	560	1900	890	38.8	3.39
20F	9.0	43.2 ± 4.3	415	1840	1000	35.6	4.43
40F	18.0	32.0 ± 0.9	-[b]	-[b]	1745	-[b]	NA
60F	27.0	20.6 ± 1.0	-[b]	-[b]	1280	-[b]	NA
100F	45.0	9.6 ± 0.7	150	1140	1925	19.9	7.60
10C	5.5	45.9 ± 3.1	390	1830	695	38.7	4.69
20C	11.0	35.5 ± 6.4	310	1590	700	37.0	5.13
40C	22.0	25.3 ± 4.0	290	1670	-[b]	26.9	5.76
60C	33.0	15.8 ± 4.3	230	1430	3040	20.5	6.22
100C	55.0	8.7 ± 1.4	150	1080	1440[b]	14.0	7.20
40F&C	40.0	10.5 ± 0.0[a]	125	1320	3005	18.3	10.56
60F&C	60.0	7.1 ± 1.2	135	1420	3565	11.4	10.52

[a] Only two 40F&C RuC cylinders were tested

[b] Premature failure of test setup and/or instrumentation

3.1　Failure modes

All plain (0% rubber) and RuC cylinders with low rubber contents (10-20% F or C replacement) failed suddenly in an explosive manner. However, the failure of RuC cylinders with more than 40% coarse or fine rubber replacement was more gradual as the cylinders experienced a large amount of fine microcracks and bulging at the mid-height prior to failure (see Figure 5). This bulging can be attributed to significant lateral dilation produced by the rubber. Overall, the use of metal straps was successful at preventing local failures at the top and bottom of the cylinders.

Figure 5. Typical failure of 60F&C RuC cylinders

3.2 Stress-strain behaviour

Figures 6a-c show the 7-day axial compressive stress against axial and lateral strains obtained from cylinders with F, C and F&C rubber replacement, respectively. In Figures 6a-c, the axial strain is shown as positive, whereas the lateral strain is shown as negative. It should be noted that the axial strain results in Figure 6 were obtained using average global measurements from LVDTs and verified using data from strain gauges (V1 and V2 in Figure 4). Unfortunately, in the unconfined RuC specimens the circumferential wire often only started recording readings when relatively high lateral strains (above 500µε) were reached in the strain gauges. Consequently, Figure 6 and Table 4 show the average of the three horizontal gauges (H1-H3 in Figure 4). Note that due to issues in the instrumentation/test setup no axial strain measurements were recorded for 40F and 60F, whereas the lateral strain measurements of 40C were unreliable. Since one of the gauges measuring lateral strains failed at around 1100µε, the lateral strain of mix 100C is shown up to that point only.

A linear regression analysis was used to determine the LOP, i.e. the point where the axial stress-strain graph deviates from its initial linear behaviour. In the following sections, the stress and strains at LOP are used to compare cracking and volumetric behaviour of RuC and plain concrete specimens, and to examine the overall effect of rubber on concrete performance.
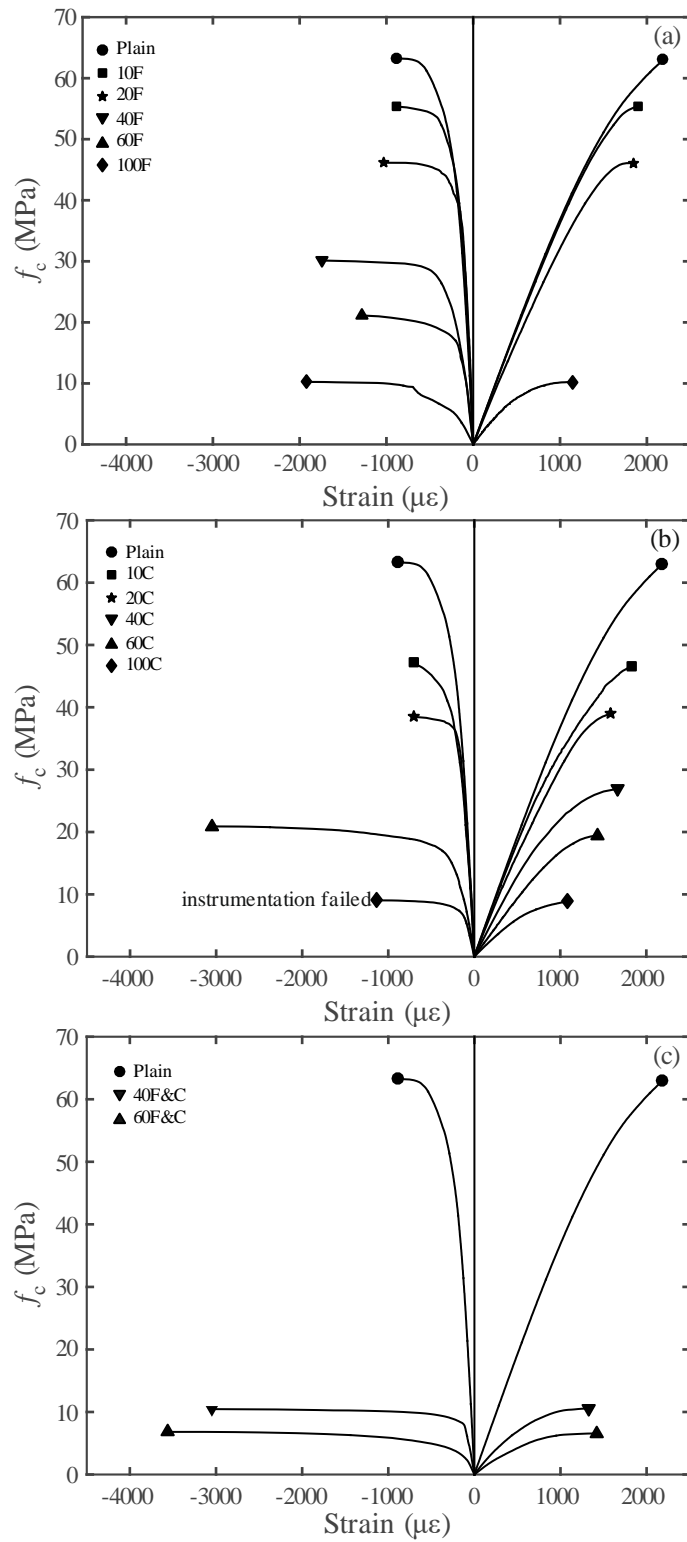
Figure 6. Uniaxial compressive stress-strain behaviour of unconfined RuC with a) fine rubber replacement (F), b) coarse rubber replacement (C), and c) combined replacement of fine and coarse rubber (F&C)

Figure 6a indicates that for relatively low fine rubber contents (i.e. 10F and 20F), the axial and lateral strains of RuC are similar to those of plain concrete. For instance, mixes 10F and 20F had 12% and 27% reduction in compressive strength, respectively, whereas their axial strains (ε_{cp} of 1900με and 1840με, respectively) and lateral strains (ε_{clp} of 890με and 1000με, respectively) at peak stress were similar to those of conventional concrete (see also Table 4). Conversely, more significant changes are observed in the RuC stress-strain behaviour at higher fine rubber contents (i.e. 40F, 60F and 100F), especially in terms of lateral strain behaviour. For instance, mix 100F experienced 118% increase in ε_{clp} and 48% reduction in ε_{cp} compared to the plain mix.

A similar trend was observed in mixes with coarse aggregate replacement (see Figure 6b and Table 4). In this case, all mixes experienced a reduction in ε_{cp} and an increase in ε_{clp} when compared to the plain mix (except for mixes 10C and 20C with lower ε_{clp}). Compared to the plain mix, ε_{cp} of mix 60C was reduced by 35% (1430με), whereas ε_{clp} increased by 245% (3040με). A larger reduction in axial strain was observed for 100C (50% reduction in ε_{cp} over the plain mix); however, ε_{clp} was not recorded due to excessive cracking at the cylinder's mid-height, which led to failure in the horizontal gauges (see Figure 6b).

The combined replacement of fine and coarse aggregates with rubber (mixes 40F&C and 60F&C, see Figure 6c and Table 4) changes significantly the constitutive behaviour of RuC when compared to mixes with only fine or coarse aggregate replacement. While mixes 40F&C and 100F had similar levels of total aggregate replacement (40% and 45% of the total aggregates replaced, respectively), ε_{clp} of mix 40F&C was 55% higher. Mix 60F&C exhibits the largest increase in lateral strain capacity (around 300% increase over the plain mix), reaching ε_{clp} of 3565με. The large lateral expansion in some mixes with high levels of C or F&C replacement (as opposed to F replacement) can be attributed to a higher local expansion of rubber particles, particularly if strain gauges happened to be placed near large coarse rubber

particles, but also due to the rubber's ability to hold the concrete together and maintain its integrity as lateral strains increase, as proven by previous research [4, 11, 17, 40].

Overall, the results in Figure 6 show that RuC cylinders with low rubber contents (<18% of the total aggregate volume) behave similarly to plain concrete and therefore have limited lateral expansion. This could explain why previous research on CRuC (all using rubber contents below 15% of the total aggregate volume [24, 25, 27]) showed that the concrete volumetric behaviour changed only marginally, compared to confined conventional concrete. Conversely, the observed axial and lateral strain behaviour of RuC with high rubber contents (>27% of the total aggregate volume) is heavily influenced by the low stiffness and high Poisson ratio of rubber. When a RuC cylinder is subjected to axial load, rubber tends to expand laterally more than the surrounding concrete. This results in tensile stress concentrations in the concrete around the rubber and in the premature formation of micro-cracks, thus leading to failure of RuC at lower peak axial strain when compared to conventional concrete. Premature micro-cracking and rubber expansion also increases the concrete overall volumetric expansion. This unique feature (and disadvantage) of RuC with high rubber contents can be used to activate the confining pressure of CRuC earlier than in confined conventional concrete.

Previous research by the authors [30] showed that the compressive strength of RuC mixes with similar percentages of total volume of fine or coarse aggregate replacement with rubber is similar. Based on this observation, Figures 7a, b, c and d compare the stress (f_c), modulus of elasticity (E_c), axial strain (ε_{cp}), and lateral strain (ε_{clp}) at peak stress, respectively, as a function of the total aggregate volume replaced with rubber. As expected, the results in Figure 7a confirm that regardless of the type of rubber replacement (C, F or F&C), the strength of RuC mixes reduces with increasing rubber content (up to 90% for mix 60F&C with the highest total aggregate replacement). However, the rate at which the compressive strength reduces is faster at lower rubber contents and seems to stabilise at total rubber contents above 40%, where rubber properties appear to dominate the compressive behaviour of RuC.
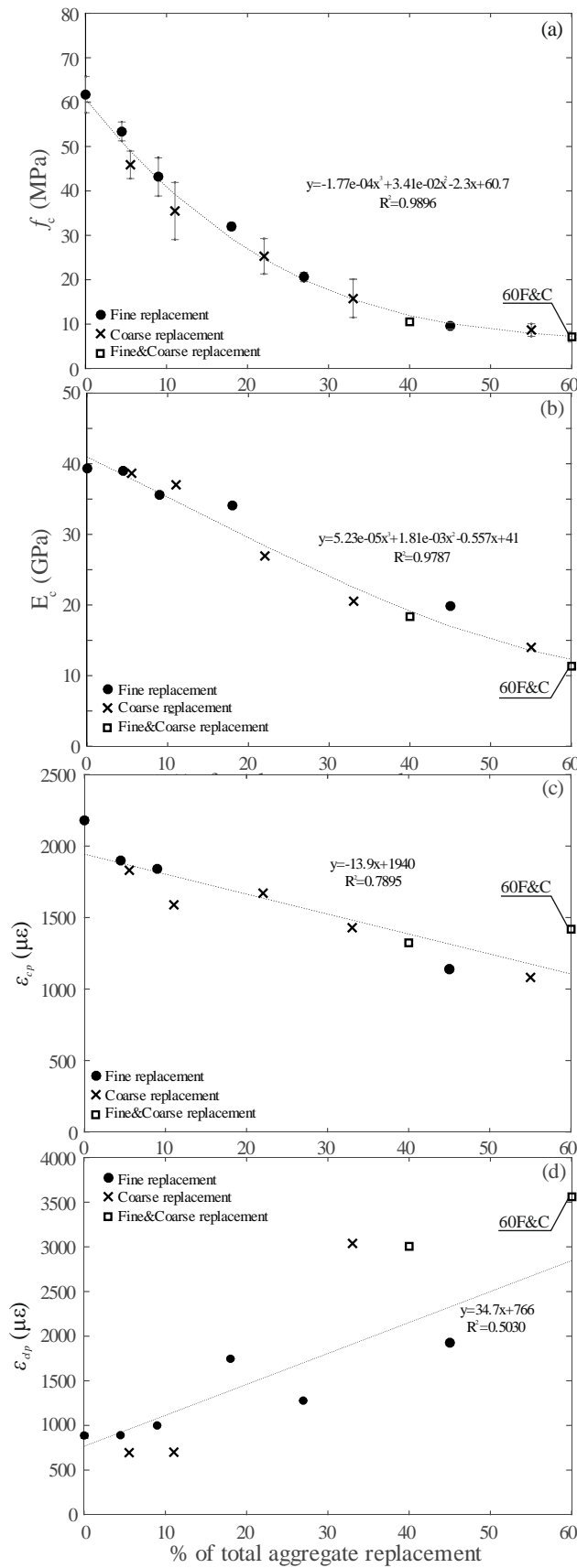
Figure 7. Variation in a) stress, b) modulus of elasticity, c) peak axial strain, and d) peak lateral strain as function of the percentage of total aggregate volume replaced with rubber

Figure 7b shows that E_c also reduces with increasing rubber content. Such reduction in stiffness can be attributed to the lower stiffness of rubber particles (compared to mineral aggregates) and to the higher air content, as confirmed by previous research [40]. However, E_c seems to be minimally affected by the type of rubber replacement (fine or coarse).

The data in Figure 7c and Table 4 indicate that the axial strain at peak stress (ε_{cp}) reduces with increasing rubber content. For mixes with high rubber contents (e.g. mix 100C), ε_{cp} was only 50% of the corresponding value for plain concrete (1080$\mu\varepsilon$ vs 2180$\mu\varepsilon$, see Table 4). This reduction in ε_{cp} was also accompanied by a reduction in axial strains at LOP (ε_{cLOP}). For instance, ε_{cLOP} reduced from 550$\mu\varepsilon$ in the plain mix to 150$\mu\varepsilon$ for mixes 100F and 100C, and to 135$\mu\varepsilon$ for mix 60F&C, respectively (see Table 4). This indicates that the onset of localised micro-cracking occurs at earlier stages when large volumes of rubber are added to concrete, thus leading to premature lateral expansion. Whilst both ε_{cp} and ε_{cLOP} reduced with increasing rubber contents, ε_{cLOP} reduced at a faster rate as evidenced by a consistently increasing $\varepsilon_{cp}/\varepsilon_{cLOP}$ ratio (see Table 4) with increasing rubber contents (e.g. 4.69 and 10.52 for 10C and 60F&C, respectively).

Although the data obtained from lateral strain gauges may have been affected by high heterogeneity of RuC and local phenomena (such as the high local expansion of large rubber particles), the results in Figure 7d and Table 4 show clearly that the lateral expansion ε_{clp} of RuC increases with the rubber contents, reaching values of more than 3500$\mu\varepsilon$ for mix 60F&C (i.e. 4 times the ε_{clp} of the plain mix).

Based on the above discussion, it is evident that the inclusion of high rubber contents in concrete leads to larger lateral expansion and premature cracking, which result in low compressive strengths, stiffness and peak axial strains. This effect of rubber content on RuC mechanical performance follows a clear trend (as illustrated in Figures 7a-d); nevertheless, due to high material heterogeneity and local effects, more work is required to develop accurate predictive models. Whilst the above-mentioned behaviour is highly detrimental for structural

unconfined concrete, the premature lateral expansion of RuC can be exploited to activate the (passive) confining pressure provided by FRP, which relies on concrete dilation. In an effort to fully utilise the maximum axial deformability potential of confined RuC, mix 60F&C (with the highest lateral strain capacity) was selected to develop a highly deformable FRP CRuC, as discussed in the following section.

4   RESULTS AND DISCUSSION: FRP-CONFINED RUC

Table 5 summarises the results of compression tests conducted on six AFRP CRuC cylinders (obtained from the same batch of concrete) in terms of: confined compressive strength (f_{cc}), absolute values of axial strain at LOP (ε_{ccLOP}), ultimate axial strain (ε_{ccu}), lateral strain at LOP (ε_{cclLOP}), ultimate lateral strain (ε_{cclu}), and initial modulus of elasticity (E_c). The confinement effectiveness (f_{cc}/f_c) and ductility ($\varepsilon_{ccu}/\varepsilon_{ccLOP}$) ratios are also included for comparison. In Table 5, the cylinders are identified according to the mix designation (60F&C), the number of confining AFRP layers (2L or 3L) and the specimen number. The following sections discuss the results of this phase of the testing programme and summarise the main experimental observations.

Table 5. Main results from AFRP CRuC cylinders

ID	# of layers	f_{cc} (MPa)	ε_{ccLOP} (µm)	ε_{ccu} (µm)	ε_{cclLOP} (µm)	ε_{cclu} (µm)	E_c (GPa)	f_{cc}/f_c	$\varepsilon_{ccu}/\varepsilon_{ccLOP}$
60F&C-2L-1	2	41.0*	1031	27860	640	15555	10.6	6.1	27
60F&C-2L-2	2	49.8	894	37390	523	19490	10.1	7.4	42
60F&C-2L-3	2	56.2	928	46610	381	20300	9.9	8.4	50
60F&C-3L-1	3	74.9	800	49730	302	16210	13.0	11.2	62
60F&C-3L-2	3	73.3	934	46650	293	16270	12.0	10.9	50
60F&C-3L-3	3	62.4*	1200	33450	207	14660	7.3	9.3	28

* Premature failure of test set-up or instrumentation.

4.1 Failure modes

All specimens failed in an explosive manner dominated by rupture of the AFRP jackets at the cylinders' mid-height (see typical failure in Figure 8). The horizontal strain gauges recorded strains in the range of 14660-20300με, i.e. between 70-96% of the theoretical ultimate strains of the AFRP fibres (21000με). Only minor damage was observed at the top or bottom of the cylinders, which indicates that the metal straps successfully prevented concrete crushing at these regions. Unfortunately, the straps of cylinders 60F&C-2L-1 and 60F&C-3L-3 failed prematurely and therefore these tests had to be halted.

Figure 8. Typical failure modes of AFRP CRuC cylinders

4.2 Stress-strain behaviour

The results in Table 5 indicate that the use of two (2L) or three (3L) AFRP layers enhanced the compressive strength of CRuC by an average of 7.3 and 10.1 times over RuC, respectively. Likewise, axial strains reached an average of 4.2% and 4.8% in CRuC (excluding cylinders with instrumentation failure) with 2L or 3L of AFRP confinement, respectively. Figure 9a shows the compressive stress vs axial strains (shown as positive) and lateral strains (shown as negative) for the 2L and 3L AFRP CRuC cylinders, as well as the corresponding average results.
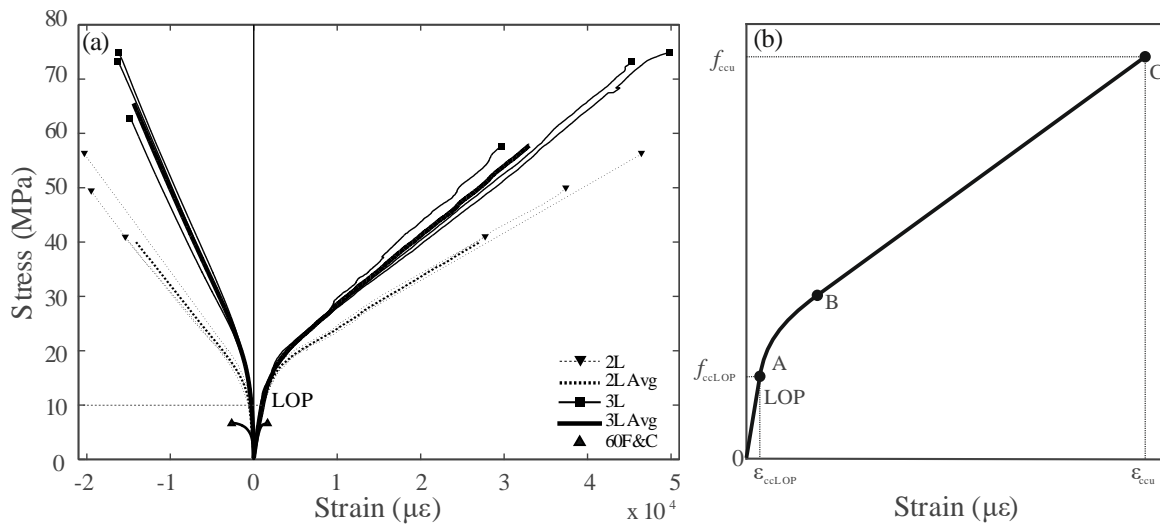
Figure 9. Stress-strain relations of a) tested CRuC cylinders and b) typical FRP-confined concrete

The results indicate that the curves of AFRP CRuC have a bilinear shape similar to that of regular FRP confined concrete [41] with two distinctive parts (see Figure 9b):

1) An initial linear elastic part controlled by the unconfined behaviour of RuC (point 0 to A), where the material reaches the LOP, followed by a transition zone (A to B).

2) A second linear part controlled by the lateral expansion of the AFRP jacket (B to C). The RuC is progressively crushing but it can sustain high axial as well as lateral deformations, the latter enhancing the effectiveness of the AFRP confining jackets.

It should be noted that, in Figure 9, the axial strains for the initial elastic part (0 to A) were taken as the average readings from the two vertical strain gauges (V1 and V2 in Figure 4). After point A (i.e. LOP), the measurements from the gauges deviate from those of the LVDTs due to localised bulging of the AFRP sheets in the vertical direction. Therefore, the axial strain measurements after the LOP were taken as the average values of the three vertical LVDTs. The horizontal strains in Figure 9 were taken as the average from the horizontal strain gauges H1 to H3.

Figure 9 indicates that the AFRP confinement delays the onset of cracking, which is evident by the increase in the elastic region 0-A in CRuC, when compared to the unconfined RuC with

identical rubber content (60F&C in Figure 9a). This is in agreement with observations reported in previous tests [25]. As shown in Figure 9a, the stress at LOP was on average 10 MPa, which is 1.5 times larger than the elastic stress for the unconfined 60F&C RuC, with a peak strength of 6.7 MPa (Figure 9a and Table 4). This can be attributed to the low axial stiffness and large lateral deformation capacity of the RuC mix 60F&C, which engaged the confinement even before the RuC starts cracking. Future research should examine how the amount and type of confinement delay the onset of cracking in different RuC mixes confined with FRP.

4.3 Volumetric strain

To provide further insight into the constitutive behaviour of AFRP CRuC, this section examines the volumetric strain (ε_{vol}) of the tested cylinders. Using the axial and lateral strains recorded during the tests, ε_{vol} can be calculated according to the following equation:

$$\varepsilon_{vol} = \varepsilon_a + 2\varepsilon_l \tag{1}$$

where ε_a is the axial strain (taken as negative for compression), and ε_l is the lateral strain (taken as positive for tension). As such, negative values of ε_{vol} indicate volumetric contraction of concrete, whereas positive values indicate volumetric expansion.

Figure 10 shows the axial stress vs volumetric strain of AFRP CRuC cylinders. Note that the results are the average of three specimens. It is shown that all AFRP CRuC cylinders contracted at the initial elastic stage, where the curves of CRuC cylinders with 2L or 3L of AFRP were similar. Conversely, after the LOP, specimens 2L experienced expansion, whereas specimens 3L carried on contracting (decrease in overall volume). This behaviour may be attributed to the (incompressible) nature of the rubber particles, which fill up the voids left by crushed/pulverised concrete. Figure 10 indicates that the volumetric behaviour of AFRP CRuC with 3 layers of AFRP is considerably different to that of RuC cylinders confined with 2 layers of AFRP. Whilst 2 AFRP layers led to RuC expansion after LOP, RuC cylinders confined with 3 AFRP layers did not expand. Nevertheless, further tests are necessary to confirm these results.

Current research is also investigating other aspects of FRP CRuC behaviour (e.g. shear and short/long term durability) in order to provide practical design guidelines. These results will be published in future papers.
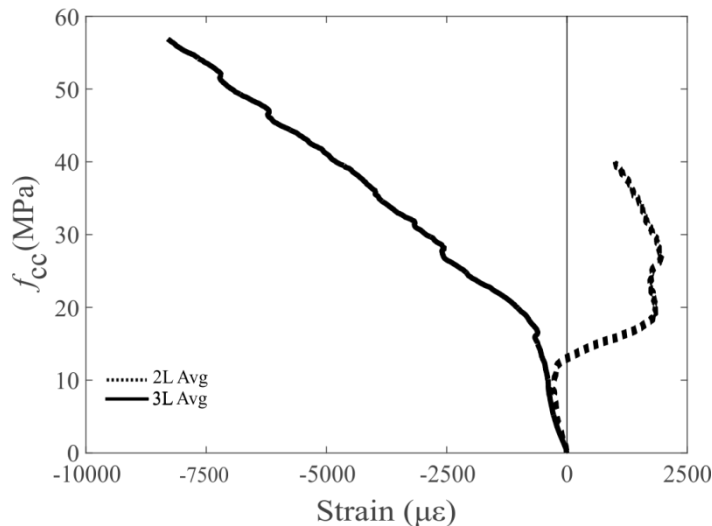
Figure 10. Axial stress-volumetric strain relationships of CRuC cylinders

5 CONCLUSIONS

This article investigates the use of externally bonded FRP jackets to develop a new high-strength, highly-deformable FRP CRuC for structural applications. Sixty RuC and six CRuC standard cylinders were tested in axial compression to evaluate the behaviour of unconfined and confined RuC. Based on the results of this study, the following conclusions can be drawn:

- The stress-strain behaviour of cylinders made with concrete with low rubber contents (less than 18% of the total aggregate volume) is similar to that of conventional concrete. However, even such modest replacement volumes led to large reductions in compressive strength (up to 40% for mix 20C with 11% aggregate replacement).

- Replacing aggregates with rubber also reduces the axial strain of the resulting concrete at peak stress. This effect was particularly evident for high rubber contents (>27% of the total aggregate volume). As rubber content was increased, the reduction in axial strains was accompanied by a premature onset of localised micro-cracking.

- The difference in compressive strength when comparing fine or coarse aggregate replacement with similar overall aggregate replacement is marginal. The combined replacement of coarse and fine aggregate is the best option to maximise rubber content and deformability potential, while achieving adequate workability.

- Replacing aggregates with rubber increases the lateral deformation capacity of RuC by up to 300% over the plain mix. Confining such RuC with two and three layers of AFRP increased the compressive strength by up to 10.1 times (f_{cc}=75 MPa) over the control mix. Moreover, average axial ultimate strains of up to 5% were achieved (i.e. 14 times more than conventional concrete). This indicates that CRuC is suitable for structural applications where high deformability is required.

- The lateral confinement modified the volumetric behaviour of CRuC. Specimens with 2 layers of AFRP had volumetric expansion after the LOP, whereas those with 3 layers of AFRP maintained volumetric contraction. This behaviour can be attributed to the incompressible nature of the rubber particles, which can fill the voids in concrete under heavy confinement, leading to overall contraction of the cylinders with 3 AFRP layers.

- Whilst the use of metal straps was successful at preventing local crushing of concrete at the top and bottom of the cylinders, premature failure was occasionally observed due to the failure of the metal straps (e.g. cylinders 60F&C-2L-1 and 60F&C-3L-3).

The results of this study confirm the feasibility of developing highly deformable AFRP CRuC with sufficient strength for structural applications. However, due to the limited experimental data, future research should verify the variability of results and possible size effects. Additional research is also needed to investigate the effect of the experimental setup, i.e. the confinement by the metal straps and the friction between the cylinder surface and the platens of the testing machine, on the potential distortion of the strain profile along the cylinder height. The presence of bending in the cylinder due to its uneven surfaces or surfaces that are not parallel to the platens of the testing machine also requires further investigation. To minimise such effects, a more reliable experimental setup, which uses accurately levelled aluminium caps at the top and

the bottom of the cylinder, was developed for the following tests (Chapters 4 and 5). Moreover, the use of more widely available confining materials such as Carbon FRP was also studied.

6   REFERENCES

[1] Business T. Global tire sales to grow 4.3% per year. Tire Business, 1/17/2014; 2014.

[2] ETRA. The European Tyre Recycling Association. Available at: http://www.etra-eu.org [Last accessed: 10/06/2014].

[3] Directive (EC) 98/2008 of the European Parliament and of the Council of 19 November 2008 on waste and replacing certain Directives [2008] OJ L312/3.

[4] Thomas BS, Gupta RC. A comprehensive review on the applications of waste tire rubber in cement concrete. Renewable and Sustainable Energy Reviews. 2016;54:1323-33.

[5] Sengul O. Mechanical behavior of concretes containing waste steel fibers recovered from scrap tires. Construction and Building Materials. 2016;122:649-58.

[6] Huang S-S, Angelakopoulos H, Pilakoutas K, Burgess I. REUSED TYRE POLYMER FIBRE FOR FIRE-SPALLING MITIGATION. Applications of Structural Fire Engineering. 2016.

[7] Goulias D, Ali A-H. Evaluation of rubber-filled concrete and correlation between destructive and nondestructive testing results. cement, concrete and aggregates. 1998;20(1):140-4.

[8] Son KS, Hajirasouliha I, Pilakoutas K. Strength and deformability of waste tyre rubber-filled reinforced concrete columns. Construction and Building Materials. 2011;25(1):218-26.

[9] Liu F, Zheng W, Li L, Feng W, Ning G. Mechanical and fatigue performance of rubber concrete. Construction and Building Materials. 2013;47:711-9.

[10] Xue J, Shinozuka M. Rubberized concrete: A green structural material with enhanced energy-dissipation capability. Construction and Building Materials. 2013;42:196-204.

[11] Najim KB, Hall MR. Mechanical and dynamic properties of self-compacting crumb rubber modified concrete. Construction and Building materials. 2012;27(1):521-30.

[12] Batayneh MK, Marie I, Asi I. Promoting the use of crumb rubber concrete in developing countries. Waste Management. 2008;28(11):2171-6.

[13] Khatib ZK, Bayomy FM. Rubberized Portland cement concrete. Journal of materials in civil engineering. 1999;11(3):206-13.

[14] Ganjian E, Khorami M, Maghsoudi AA. Scrap-tyre-rubber replacement for aggregate and filler in concrete. Construction and Building Materials. 2009;23(5):1828-36.

[15] Bignozzi MC, Sandrolini F. Tyre rubber waste recycling in self-compacting concrete. Cement and concrete research. 2006;36(4):735-9.

[16] Li G, Stubblefield MA, Garrick G, Eggers J, Abadie C, Huang B. Development of waste tire modified concrete. Cement and Concrete Research. 2004;34(12):2283-9.

[17] Toutanji HA. The use of rubber tire particles in concrete to replace mineral aggregates. Cement and Concrete Composites. 1996;18(2):135-9.

[18] Sukontasukkul P, Chaikaew C. Properties of concrete pedestrian block mixed with crumb rubber. Construction and Building Materials. 2006;20(7):450-7.

[19] Turatsinze A, Granju JL, Bonnet S. Positive synergy between steel-fibres and rubber aggregates: effect on the resistance of cement-based mortars to shrinkage cracking. Cement and concrete research. 2006;36(9):1692-7.

[20] Richardson AE, Coventry KA, Ward G. Freeze/thaw protection of concrete with optimum rubber crumb content. Journal of Cleaner Production. 2012;23(1):96-103.

[21] Pierce C, Blackwell M. Potential of scrap tire rubber as lightweight aggregate in flowable fill. Waste Management. 2003;23(3):197-208.

[22] Zhu H, Thong-On N, Zhang X. Adding crumb rubber into exterior wall materials. Waste management & research. 2002;20(5):407-13.

[23] Sukontasukkul P. Use of crumb rubber to improve thermal and sound properties of pre-cast concrete panel. Construction and Building Materials. 2009;23(2):1084-92.

[24] Youssf O, ElGawady MA, Mills JE, Ma X. An experimental investigation of crumb rubber concrete confined by fibre reinforced polymer tubes. Construction and Building Materials. 2014;53:522-32.

[25] Li G, Pang S-S, Ibekwe SI. FRP tube encased rubberized concrete cylinders. Materials and structures. 2011;44(1):233-43.

[26] Abendeh R, Ahmad HS, Hunaiti YM. Experimental studies on the behavior of concrete-filled steel tubes incorporating crumb rubber. Journal of Constructional Steel Research. 2016;122:251-60.

[27] Duarte A, Silva B, Silvestre N, de Brito J, Júlio E, Castro J. Experimental study on short rubberized concrete-filled steel tubes under cyclic loading. Composite Structures. 2015.

[28] Moustafa A, ElGawady MA. Strain Rate Effect on Properties of Rubberized Concrete Confined with Glass Fiber–Reinforced Polymers. Journal of Composites for Construction. 2016:04016014.

[29] Lam L, Teng J. Ultimate condition of fiber reinforced polymer-confined concrete. Journal of Composites for Construction. 2004;8(6):539-48.

[30] Raffoul S, Garcia R, Pilakoutas K, Guadagnini M, Medina NF. Optimisation of rubberised concrete with high rubber content: An experimental investigation. Construction and Building Materials. 2016;124:391-404.

[31] Innovative Use of all Tyre Components in Concrete, Anagennisi Project. 2014. Available at: http://www.anagennisi.org/.

[32] BSI 197-1:2011. Cement. Part 1: Composition, specifications and conformity criteria for common cements. 2011, BS EN 197 Part 1. London UK.

[33] Sika Limited. Sika Viscoflow 2000. Product Data Sheet. Edition-15/10/2014; Identification no: 02 13 01 01 100 0 001325. Available at https://goo.gl/kMfHcU [Last accessed 10/12/2015].

[34] Sika Limited. Sika Viscoflow 1000. Product Data Sheet. Edition-21/05/2015; Identification no: 02 13 01 01 100 0 000853. Available at https://goo.gl/mMDfay [Last accessed 10/12/2015].

[35] ASTM Standard C136, 2006, "Standard Test Method for Sieve Analysis of Fine and Coarse Aggregates", ASTM International, West Conshohocken, PA, 2006, DOI:10.1520/C0136-06.

[36] BSI 1097-6: 2013. Tests for mechanical and physical properties of aggregates. Determination of particle density and water absorption. 2013, BS EN 1097 Part 6. London, UK.

[37] BSI 933-3:2012. Tests for geometrical properties of aggregates. Determination of particle shape - Flakiness index. 2012, BS EN 933 Part 3. London, UK.

[38] BSI 1097-3:1998. Tests for mechanical and physical properties of aggregates: Determination of loose bulk density and voids. 1998, BS EN 1097 Part 3. London, UK.

[39] Garcia R, Pilakoutas K, Hajirasouliha I, Guadagnini M, Kyriakides N, Ciupala MA. Seismic retrofitting of RC buildings using CFRP and post-tensioned metal straps: shake table tests. Bull Earthquake Eng. 2015:1-27.

[40] Turatsinze A, Garros M. On the modulus of elasticity and strain capacity of self-compacting concrete incorporating rubber aggregates. Resources, Conservation and Recycling. 2008;52(10):1209-15.

[41] Teng J, Chen J-F, Smith ST, Lam L. FRP: strengthened RC structures. Frontiers in Physics. 2002;1.

Chapter 4

Constitutive model for passively confined rubberised concrete

This article develops an analysis-oriented stress-strain model for rubberized concrete (RuC) passively confined with FRP composites, utilizing highly instrumented experiments on 38 cylinders with high rubber contents (60% replacement of the total aggregate volume) tested under uniaxial compression. The parameters investigated include cylinder size (ϕ100x200mm or ϕ150x300mm), as well as amount (two, three, four or six layers) and type of external confinement (Carbon (CFRP) or Aramid FRP (AFRP)). FRP-confined rubberized concrete (FRP-CRuC) develops high compressive strengths of up to 100 MPa, and extremely high deformability (axial strains of up to 6%). It is shown that existing stress-strain models for FRP-confined concrete do not predict the behavior of such highly deformable FRP-CRuC. Based on the results, this study develops a new analysis-oriented model that predicts accurately the behavior of such concrete. This article contributes towards developing advanced constitutive models for analysis/design of sustainable high-value FRP-CRuC components that can develop high deformability.

1   INTRODUCTION

Modern design codes for reinforced concrete (RC) structures aim to ensure that plastic hinge zones forming at beams and columns can sustain large inelastic deformations. The deformation capacity of RC elements depends heavily on the compressive behavior of concrete and, specifically, on the capacity of concrete to develop large axial compressive strains (Paulay and Priestley 1992). Over the last 20 years, external FRP confinement has been widely used to increase the ultimate compressive strain of concrete cylinders (Mortazavi et al. 2003; Rousakis and Athanasios 2012; Spoelstra and Monti 1999) and deformability of columns (Garcia et al. 2014). However, the quasi-brittle nature of concrete somehow limits the potential deformation that such elements could achieve and special elements are used in regions of high deformation demand such as bearings, base isolation systems and coupling beams.

Rubber from end of life tires has good strength and flexibility and can maintain its volume under compressive stress. Consequently, extensive research has examined the use of recycled tire rubber to produce rubberized concrete (RuC) in an attempt to further enhance the deformation capacity of concrete (Bompa et al. 2017; Ganesan et al. 2013; Li et al. 2004; Toutanji 1996). However, the compressive strength of RuC reduces by up to 90% at high levels of rubber replacement (e.g. 100% sand replacement) (Batayneh et al. 2008), which makes RuC unsuitable for most structural applications. To recover the strength of RuC, recent studies have investigated the use of different types of confinement to produce confined rubberized concrete (CRuC). For example, Duarte et al. (2016) showed that rubberized concrete (rubber replacing 15% of the aggregate volume) cast in cold-formed steel tubes improved the ductility of columns by up to 50%. Nevertheless, compared to conventional concrete counterparts, the steel confinement around RuC columns was less effective and this was attributed to the lower dilation angle in RuC. Moreover, RuC columns were more prone to local buckling. Youssf et al. (2014) cast rubberized concrete (RuC) with a 10% rubber replacement of aggregate volume in preformed CFRP tubes. The results showed that the use of three CFRP confining layers led to a

cylinder compressive strength of 112.5 MPa, which is suitable for most structural applications. Similar results were reported by Li et al. (2011) from RuC (with 30% rubber replacing fine aggregate volume) cast in GFRP pipes, leading to an increase in compressive strength up to 5.25 times that of the unconfined rubberized concrete (RuC). While the above confinement led to some improvements in RuC strength, its influence on concrete deformability was limited when compared to conventional confined concrete (Lam and Teng 2004). This can be attributed to the relatively low amounts of rubber used in the aforementioned studies, which are insufficient to produce significant lateral dilation to activate the passive confinement pressure.

The inclusion of high volumes of recycled tire rubber in concrete is associated with various material and technology challenges, such as poor fresh properties (Flores-Medina et al. 2014; Güneyisi et al. 2004; Toutanji 1996) . Research by the authors (Raffoul et al. 2016) has shown that some of these drawbacks can be overcome by optimizing the concrete mix parameters, leading to the development of RuC with high rubber content (>50% total aggregate content) and good workability, homogeneity and cohesiveness. More recent research (Raffoul et al. 2017) demonstrated that the external confinement of such RuC with three layers of AFRP can lead to high strength (>75 MPa) and high deformability (axial strains >5%). This innovative FRC CRuC can be used for structural applications where high concrete deformability is required, e.g. plastic hinge zones or short columns. However, it is necessary to provide constitutive models suitable for the analysis and design of highly deformable elements. Using CRuC with high rubber contents, this article develops such a constitutive model for FRP CRuC.

This study begins with a description of the experimental program on 38 cylinders. Section 3 discusses the experimental results in terms of the effect of confining material and pressure on the stress-strain behavior. Based on the test results, Section 4 proposes a unified constitutive model to predict the stress-strain behavior of FRP CRuC. Concluding remarks of this study are given in Section 5. This article contributes towards the development of analysis/design models so that FRP CRuC can be used for the development of highly deformable elements. The results presented in this study are part of the FP7 EU-funded project Anagennisi which aims to develop

solutions to reuse all tire components in high value innovative concrete applications (Pilakoutas et al. 2015).

2   EXPERIMENTAL PROGRAM

A total of 38 RuC cylinders confined with FRP jackets were subjected to axial compression. The main parameters investigated include the type of FRP material (Carbon or Aramid FRP), confinement pressure (number of FRP layers) and cylinder size (ϕ100×200mm or ϕ150×300mm).

2.1 Materials

2.1.1 Concrete

All cylinders were cast with a concrete mix in which 60% of the fine and coarse aggregate volume was replaced with tire crumbs. Two batches were produced for this study. The selected mix was 'optimized' in a previous study (Raffoul et al. 2016) that minimized the adverse effects of large quantities of rubber on the fresh and hardened properties of RuC. The mix components for 1m^3 of RuC were: i) 340 kg of High strength Portland Limestone Cement CEM II–52.5 N (10-15% Limestone) conforming to (BS EN 197-1: 2011); ii) 42.5 kg of Silica Fume (SF) (Microsilica – Grade 940) and 42.5 kg of Pulverised Fuel Ash (PFA) (BSEN 450–1, Class N Category B LOI); iii) two commercially available admixtures: 2.5 liters of Plasticiser (P) and 5.1 liters of Super Plasticiser (SP) (polycarboxylate polymers conforming to BS EN 934-2:2009); iv) 400.4. kg of Coarse Aggregate (CA): round river washed gravel (Sizes: 5-10 mm and 10-20 mm; Specific gravity: 2.65; Absorption: 1.24%), v) 328 kg of Fine Aggregate (FA): medium grade river washed sand (Sizes: 0-5 mm; Specific gravity: 2.65; Absorption: 0.5%, Fineness modulus: 2.64); and vi) rubber particles recycled through mechanical shredding of car and truck tires: 148.5 kg of Fine Rubber (FR) (sizes: 0-5mm) and 181.3 kg of Coarse Rubber (CR) (sizes 5-10mm and 10-20mm). The water to binder ratio (w/b) was set to 0.35. The rubber particles were selected to replace mineral aggregates of similar sizes. The mass of the rubber replacement particles was obtained considering a relative density of 0.80. Table 1 presents

average results from uniaxial compressive tests on three ϕ100×200mm RuC control cylinders at 28 days.

Table 1. Mean mechanical properties of RuC at 28-days

Compressive strength (MPa)		Strain at peak strength (με)		Modulus of elasticity (GPa)	
Mean	SD	Mean	SD	Mean	SD
7.6	1.3	1350	200	10.3	1.8

2.1.2 Fiber reinforced polymer jacket

To enhance the compressive strength of the RuC described above, a series of ϕ100×200mm cylinders were externally confined with two, three or four layers of Carbon FRP (CFRP) or Aramid FRP (AFRP) sheets. The behavior of larger ϕ150×300mm RuC cylinders confined using three or six CFRP or AFRP layers was also investigated to assess possible size effect. The number of confining layers for the larger specimens was determined according to Equation (1) to ensure a confining pressure equivalent to that given by two and four layers on the ϕ100mm cylinders. Equation (1) assumes that a) a uniform confinement pressure was applied across the cylinder section (circular geometry), and b) the force in the FRP was equal to the force resisted by the concrete core.

$$f_l = \frac{2nt_f}{D} f_f \qquad (1)$$

where f_l is the confinement pressure, n is the number of FRP layers, t_f is the thickness of one layer of FRP sheet, f_f is the tensile strength of the FRP fibers and D is the cylinder diameter.

At least five small cylinders were tested for each type and number of FRP layers, while two large cylinders were tested per parameter.

The FRP jackets consisted of unidirectional Aramid or Carbon fabrics embedded in an epoxy matrix. The FRP jackets were applied using wet lay-up. The sheets were oriented perpendicular to the cylinder axis and overlapped by a length of 100 mm. Table 2 summarizes mean properties and corresponding standard deviation (SD) obtained from direct tensile tests on more than 30

FRP coupons (250 mm×15 mm×t_f). In this table, t_f is the dry fiber thickness; f_f is the tensile

strength; E_f is the modulus of elasticity; and ε_{fu} is the ultimate elongation of the FRP composite.

Table 2. Mechanical properties of FRP jackets based on direct tensile coupon tests

Fiber type	No. of layers	t_f (mm)	f_f (MPa)	$f_{f,\,AVG}$ (MPa)	E_f (GPa)	$E_{f,AVG}$ (MPa)	ε_{fu} (%)	$\varepsilon_{fu,AVG}$ (%)
Aramid	2L	0.40	2410	2430 (260*)	116	122 (16*)	2.08	2.06 (0.11*)
	3L	0.60	2705		140		1.94	
	4L	0.80	2180		110		2.16	
Carbon	2L	0.37	2040	2065 (80*)	242	225 (12*)	0.84	0.90 (0.07*)
	3L	0.56	2000		220		0.88	
	4L	0.74	2150		220		0.98	

*Standard Deviation

2.2 Experimental setup, instrumentation and load protocol

Fig. 1 shows the typical test setup and instrumentation used for the tests. All specimens were

subjected to axial compression using a servo controlled ESH Universal Testing Machine of

1,000 kN capacity. The top and bottom of the specimens were confined using aluminum caps to

avoid failure at the end zones of the cylinder due to stress concentrations (Kotsovos and

Newman 1981). Vertical strains were derived using vertical displacements. This was achieved

by fixing two parallel aluminum rings (placed 100 mm apart) around the cylinders (Fig. 1b).

The screws used to fix the aluminum rings were fitted with springs to allow lateral expansion of

the cylinders without adding further confinement. During the tests, three vertical lasers (L1 to

L3 in Fig. 2) mounted on the aluminum rings measured the shortening of the specimens at the

center of the cylinders. To determine horizontal strains, the horizontal expansion was measured

using a tensioned wire and a LVDT around the specimens' mid-height. Three horizontal (H) and

two vertical (V) gauges measured local strains along the mid-height of the FRP jacket at the

locations shown schematically in Fig. 2.
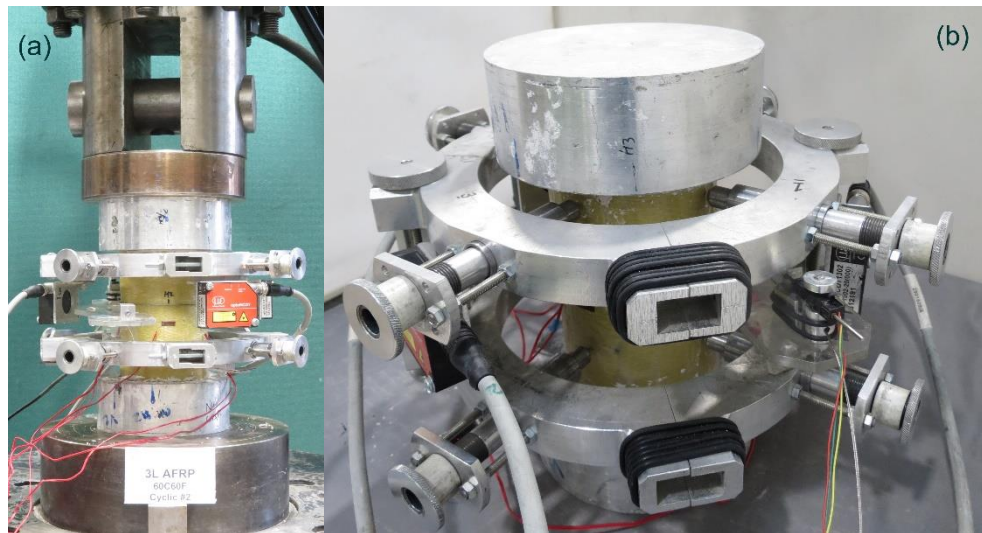
Figure 1. Typical test setup for compression tests on FRP CRuC cylinders
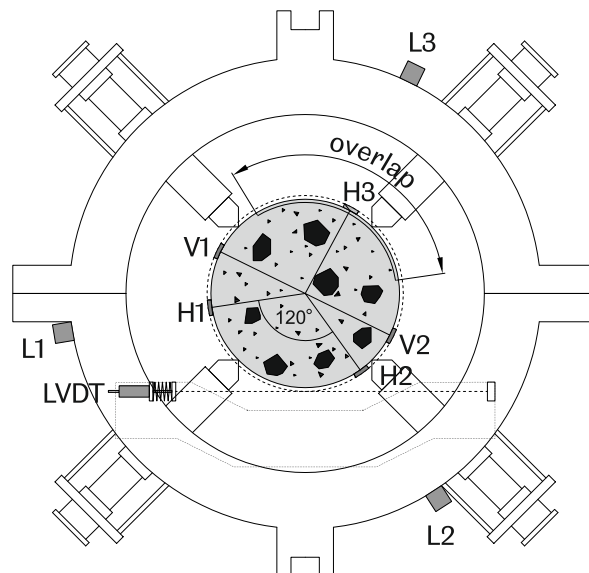
Figure 2. Schematic view of instrumentation

Two test protocols were applied: i) Monotonically increasing displacement at a rate of 0.5 mm/min up to cylinder failure, and ii) consecutive sets of five unloading/reloading load cycles at increasing stress levels (+10 MPa/set) up to cylinder failure. At least two nominally identical small cylinders were tested monotonically, whereas three were subjected to cyclic load for each thickness and type of FRP. All large cylinders were loaded monotonically, and at least two cylinders were tested for each parameter.

3   RESULTS AND DISCUSSION

Table 3 summarizes mean test results from the FRP CRuC specimens. The cylinders are identified according to the number of confining layers (2, 3, 4 or 6), confining material (A=AFRP or C=CFRP), loading type (M=monotonic or C=cyclic) and specimen number (1, 2 or 3). A letter (L) after the specimen number denotes the larger ϕ150×300mm cylinders. For example, 3A-M1-L stands for specimen #1 of a large cylinder subjected to monotonic load and wrapped with three AFRP layers. Table 3 includes mean values (Avg) and standard deviations (SD) of: ultimate compressive strength (f_{cc}), ultimate axial (ε_{cc}) and lateral (ε_{ccl}) strains, confinement effectiveness (f_{cc}/f_{co}), ductility ($\varepsilon_{cc}/\varepsilon_{co}$), critical stress ($f_{cr}$), as well as the axial strain, lateral strain and Poisson's ratio at f_{cr} (ε_{cr}, ε_{lcr}, and ν_{cr}, respectively). Table 3 also shows the confinement stiffness (K_j) provided to each cylinder, calculated using equation (2).

$$K_j = \frac{2nt_f}{D}E_f \qquad\qquad (2)$$

Fig. 3a provides a schematic presentation of the aforementioned parameters. The critical stress (f_{cr}) indicates the initiation of unstable crack propagation and concrete expansion, which activates the confining jacket leading to a significant change in the gradient of the curve, which depends on the FRP-jacket stiffness. The value of f_{cr} was defined as the inflection/pivot point of the CRuC secant modulus-stress relationship (E_{sec}-f_c) (Fig. 3b) at the minimum of its derivative function (dE_{sec}/df_c,) (Fig. 3c). This inflection point indicates a shift in the rate of stiffness degradation, which designates the activation of confinement pressure. Following careful examination of the results, f_{cr} was found to consistently occur when E_c drops to around 70% of the concrete initial stiffness E_{co} (Fig. 3b). f_{cc}/f_{co} and $\varepsilon_{cc}/\varepsilon_{co}$ were calculated as the ratio of the ultimate stress and strain of the CRuC to the average peak stress (6.8MPa-8.2MPa) and peak strain (1350με) of the unconfined RuC cylinders, respectively. The axial strains between 0-A were taken from the two vertical strain gauges V1 and V2, whereas the axial strains from A-C were derived from the lasers L1-L3. This was because, after f_{cr} (point A), excessive localized bulging on the FRP jacket led to spurious strain gauge readings. The horizontal strains were

obtained from average readings from the horizontal gauges H1-H3 and corroborated using LVDT measurements of the wire. The results in Table 3 are discussed in the following sections.
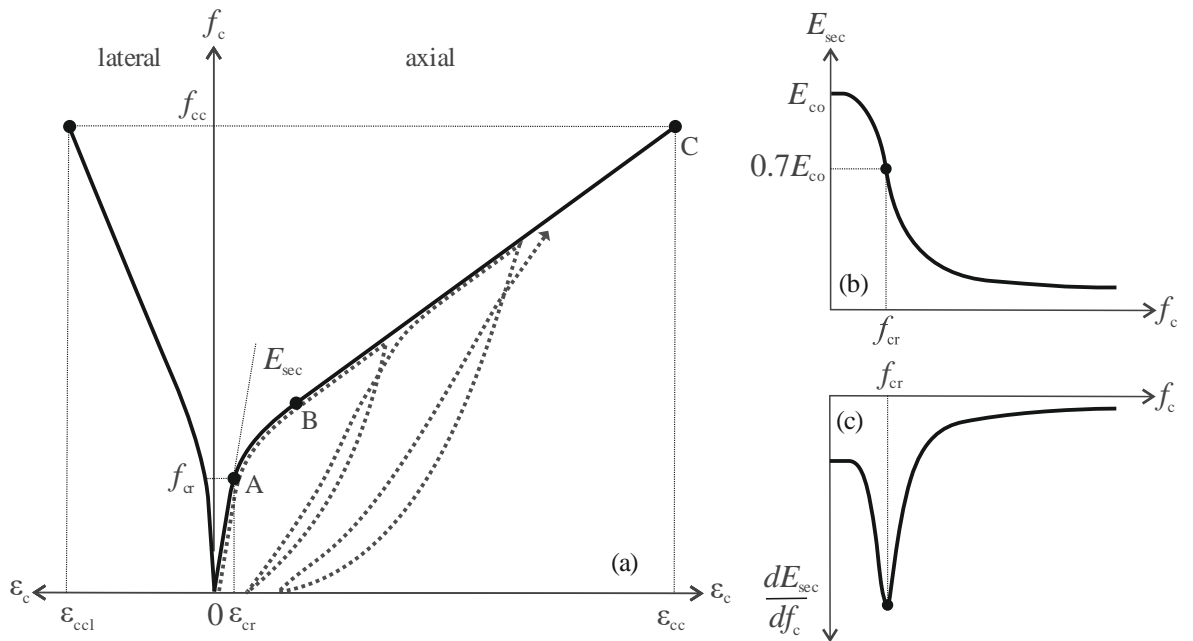
Figure 3. Schematic representation of a) the strain-stress performance of CRuC, b) the variation of E_c as function of stress, and c) its derivative function

Table 3. Main test results from cylinders

ID	K_j (MPa)	f_{cc} (MPa)	Avg (SD)	f_{cr} (MPa)	Avg (SD)	ε_{ccu} (%)	Avg (SD)	ε_{cr} (μm)	Avg (SD)	ε_{cclu} (%)	Avg (SD)	ε_{lcr} (μm)	Avg (SD)	v (GPa)	Avg (SD)	f_{cc}/f_c (Avg)	$\varepsilon_{ccu}/\varepsilon_{cp}$ (Avg)
2A-M1		39.9		8.1		3.78		1020		1.42		400		0.39			
2A-M2		44.6		8.7		4.60		1160		1.93		330		0.28			
2A-C1	976	39.5	40.1 (2.8)	11.7	10.7 (2.2)	4.16	3.90 (0.48)	2090	1580 (485)	1.51	1.55 (0.22)	665	665 (305)	0.32	0.36 (0.08)	5.9 (0.4)	28.9 (3.6)
2A-C2		39.6		12.9		3.40		2010		1.44		925		0.46			
2A-C3		37.0		12.1		3.58		1610		1.44		-		-			
3A-M1		73.5		12.8		4.97		1250		1.62		520		0.42			
3A-M2		66.2		11.2		5.51		1615		1.40		650		0.40			
3A-C1	1464	70.2	69.9 (2.6)	18.6	13.5 (3.1)	4.96	5.41 (0.45)	2730	1800 (555)	1.29	1.57 (0.24)	540	525 (80)	0.20	0.31 (0.09)	8.5 (0.3)	40.1 (3.4)
3A-C2		69.8		11.2		6.02		1825		1.90		490		0.27			
3A-C3		69.6		13.7		5.61		1590		1.62		425		0.27			
4A-M1		101.4		15.3		7.25		2720		1.80		645		0.24			
4A-M2		90.7		13.6		5.56		2370		1.39		700		0.30			
4A-C1	1952	89.8	92.5 (5.0)	11.6	13.9 (1.8)	5.49	6.05 (0.76)	1700	2010 (510)	1.61	1.63 (0.15)	445	580 (140)	0.26	0.30 (0.07)	11.3 (0.6)	44.8 (5.6)
4A-C2		90.1		13.0		6.36		1575		1.71		410		0.26			
4A-C3		90.3		16.1		5.58		1670		1.64		700		0.42			
3A-M1-L	976	36.1	36.3 (0.3)	9.9	9.8 (0.2)	3.42	3.33 (0.1)	1962	1550 (590)	1.46	1.43 (0.0)	620	525 (135)	0.32	0.35 (0.05)	5.3 (0.0)	24.7 (0.9)
3A-M2-L		36.5		9.6		3.24		1130		1.40		435		0.38			
6A-M1-L	1952	73.7	73.0 (1.1)	16.2	13.6 (3.7)	6.03	5.78 (0.3)	2650	2495 (220)	1.20#	1.53# (0.5)	725	685 (55)	0.27	0.28 (0.01)	10.7 (0.2)	42.9 (2.6)
6A-M2-L		72.2		11.0		5.54		2340		1.86		645		0.28			

Table 3. Main test results from cylinders (continued)

Specimen																	
2C-M1		33.6		11.2		2.69		1600		0.74		725		0.45			
2C-M2		29.8		11.4		1.73		1810		0.62		630		0.35			
2C-C1	1665	34.2	33.1 (2.4)	11.4	12.0 (1.0)	1.96	2.30 (0.47)	1590	2150 (695)	0.79	0.76 (0.10)	685	895 (305)	0.43	0.42 (0.07)	4.9 (0.4)	17.1 (3.4)
2C-C2		36.0		12.4		2.83		3160		0.90		1095		0.35			
2C-C3		31.7		13.6		2.30		2590		0.73		1330		0.51			
3C-M1		46.4		-		2.56		-		0.75		-		-			
3C-M2		51.2		16.0		2.63		2920		0.85		995		0.34			
3C-C1	2498	49.9	49.3 (2.0)	13.3	12.3 (3.2)	3.20	2.82 (0.65)	1930	2250 (685)	0.88	0.82 (0.20)	720	745 (320)	0.37	0.32 (0.07)	7.3 (0.3)	22.4 (3.9)
3C-C2		49.6		11.6		3.69		2695		1.09		965		0.36			
3C-C3		28.6#		8.4		2.00#		1445		0.58#		300		0.21			
4C-M1		63.7		15.4		4.07		2750		0.85		590		0.21			
4C-M2		61.6		15.4		3.24		2140		0.81		575		0.27			
4C-C1	3330	49.9	59.8 (6.3)	16.7	14.5 (1.9)	3.01	3.57 (0.56)	2354	2305 (270)	0.55	0.77 (0.19)	800	550 (175)	0.34	0.24 (0.07)	8.8 (0.9)	26.4 (4.1)
4C-C2		57.9		12.4		3.26		2055		0.61		340		0.17			
4C-C3		66.1		12.8		4.26		2223		1.02		440		0.20			
3C-M1-L	1665	29.6	30.2 (0.9)	11.4	12.1 (1.0)	1.96	2.05 (0.1)	-	-	0.48	0.58 (0.1)	795	735 (88)	-	-	4.4 (0.1)	15.2 (1.0)
3C-M2-L		30.8		12.8		2.15		2605		0.68		680		0.26			
6C-M1-L	3330	58.0	58.8 (1.2)	14.1	14.2 (0.2)	3.19	3.35 (0.2)	2130	2470 (480)	0.87	0.78 (0.1)	690	695 (10)	0.32	0.29 (0.05)	8.7 (0.2)	24.8 (1.7)
6C-M2-L		59.7		14.4		3.51		2810		0.70		705		0.25			

Premature failure of test set-up or instrumentation

3.1　Ultimate condition and failure mode

All FRP CRuC specimens failed abruptly by tensile rupture of the FRP jackets (see Fig. 4). In all cases, FRP rupture initiated at approximately the mid-height of the specimens. Overall, the recorded FRP strains at cylinder rupture (ε_{ccl}) were below the failure tensile strains measured in the FRP coupons (ε_{fu}) (see Table 2 and Table 3). For instance, ε_{ccl} in AFRP-confined cylinders was around 70-80% of ε_{fu} of the AFRP coupons, while ε_{ccl} in CFRP-confined cylinders was 65-95% of ε_{fu} of the CFRP coupons. Premature rupture is also reported in previous studies (Lam and Teng 2004; Matthys et al. 2006) and can be attributed to local effects (non-homogeneous concrete deformations) leading to stress concentrations in the FRP, as well as to the effect of jacket curvature, overlap length and fiber misalignment.
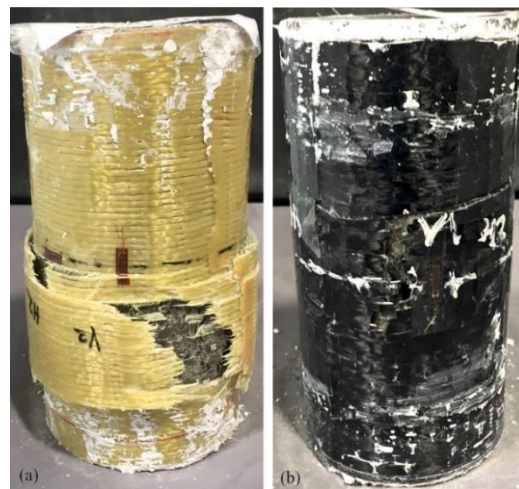
Figure 4. Typical failure modes for a) AFRP or b) CFRP CRuC

3.2　Stress-strain behavior

Fig. 5a-c and d-f compare the stress-strain behavior of AFRP CRuC and CFRP CRuC cylinders, respectively. The figures show individual stress-strain curves of monotonically loaded cylinders, the envelope of cyclically loaded cylinders (determined as shown in Fig. 3), as well as average curves for cylinders with similar FRP confinement. The direct comparison of monotonic and cyclic results is possible because the envelopes from cyclic tests typically follow the monotonic curves (Buyukozturk and Tseng 1984; Chang and Mander 1994; Lam et al. 2006; Osorio et al. 2013; Rousakis and Tepfers 2001).
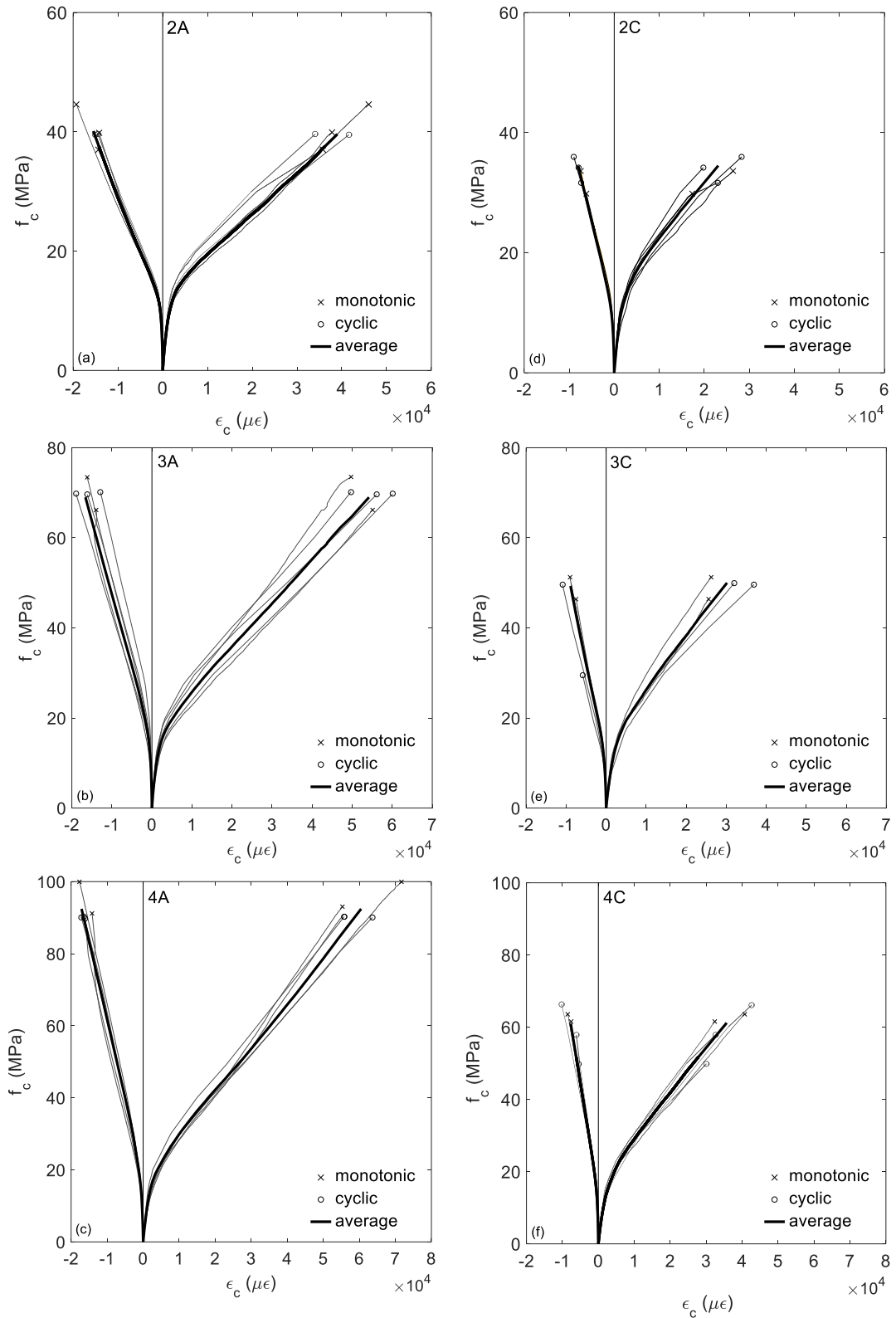
Figure 5. Behavior of AFRP CRuC (a, b and c) and CFRP CRuC (d, e and f)

The results in Fig. 5a-c and d-f show that the axial and lateral stress-strain curves (both monotonic and cyclic envelope) are similar, and that the curves vary within the acceptable

variability of the material. The data in Table 3 confirm that the ultimate stress and strain of specimens subjected to monotonic and cyclic load were similar. As expected, the stress-strain curves have an initial linear-elastic branch (controlled by the unconfined concrete behavior) until the critical stress f_{cr} (line 0-A in Fig. 3). This is followed by a transition curve (A-B in Fig. 3) and then a linear branch (B-C in Fig. 3) controlled by the expansion of the FRP, as discussed in a previous study by the authors (Raffoul et al. (2017)). Beyond f_{cr}, concrete cracking increases the cylinders' lateral expansion, thus activating the confinement progressively. As expected, higher confining pressure led to a steeper branch B-C.

The results in Table 3 indicate that an increase in confinement stiffness (K_j) delays concrete cracking, which resulted in higher average critical stresses (f_{cr}) and strains (ε_{cr}) for both AFRP and CFRP confinement. For example, at a confining stiffness of 975 MPa (2LA), the average f_{cr} and ε_{cr} were 10.7 MPa and 1580 µε, respectively, while at a jacket stiffness of 1950 MPa (4LA), these values increased to 13.9 MPa and 2010 µε, respectively. The effectiveness of FRP confinement on RuC is also confirmed by the ratios f_{cc}/f_{co} and $\varepsilon_{cc}/\varepsilon_{co}$. For RuC cylinders confined with four AFRP layers, f_{cc}/f_{co}=10 and $\varepsilon_{cc}/\varepsilon_{co}$=50. Comparatively, for conventional FRP-confined concrete with identical confining pressure, such values were only f_{cc}/f_{co}=4.2 and $\varepsilon_{cc}/\varepsilon_{co}$=18.5 (Jiang and Teng 2007; Lam and Teng 2003).

Table 3 also shows that the increase in f_{cr} due to increasing jacket stiffness was accompanied by a drop in lateral strain ε_{lcr} and, more notably, by lower Poisson's ratios (v_{cr}) at f_{cr}. For example, v_{cr} was approximately 0.42 for K_j=976 MPa (2LA) and it dropped to 0.30 for K_j=1952 MPa (4LA), indicating that the overall expansion was better controlled in the latter cylinder. Since the increase in Poisson's ratio can be used as an indicator of damage (Neville 1995), the above results indicate that increasing confinement stiffness delayed overall damage.

3.3 CFRP vs AFRP confinement

Fig. 6 compares the stress-strain behavior of AFRP and CFRP CRuC cylinders, normalized to the corresponding unconfined concrete strength (8.2 MPa and 6.8 MPa, respectively). Note that

these results are the average of the individual curves respectively shown in Fig. 5a-c and d-f. The data in Fig. 6 clearly indicate that for the same number of CFRP or AFRP layers, CFRP jackets provided higher confinement pressure, which in turn led to a stiffer response in both axial and lateral directions after f_{cr}. This is due to the much higher stiffness of a CFRP jacket when compared to an AFRP jacket with the same number of layers (see Table 3).
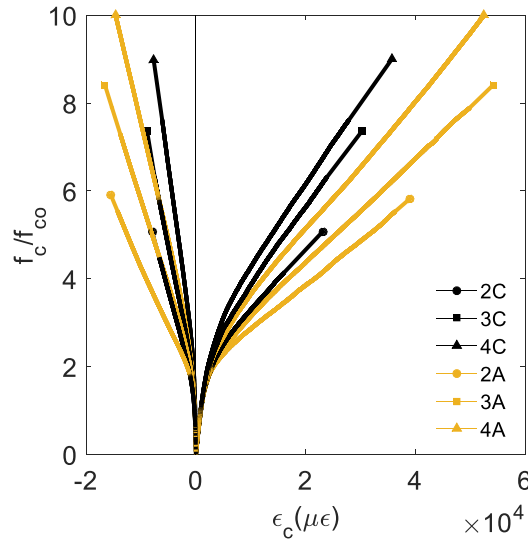
Figure 6. Average normalized stress-strain behavior of RuC cylinders confined with 2, 3 and 4 layers of CFRP or AFRP

The results in Table 3 also show that, in addition to the confining stiffness, the type of material also influenced the stress-strain behavior at f_{cr} and at the ultimate condition of CRuC. The rate of reduction in ν_{cr} and ε_{lcr} as a function of K_j was higher for AFRP CRuC cylinders than for CFRP CRuC cylinders. For example, for 3LA (K_j=1464 MPa), ν_{cr} was 0.31 and ε_{lcr} was 525με, whilst despite having a higher jacket stiffness, cylinders with 2LC (K_j=1665 MPa) exhibited higher Poisson's ratio (ν_{cr}=0.42) and higher lateral expansion (ε_{lcr}=895με) prior to f_{cr}. This indicates that the confining effect of AFRP activated earlier than in CFRP, thus limiting the RuC expansion more effectively in AFRP-confined cylinders. Similar results were observed for higher levels of CFRP confinement. For example, cylinders 3LC (K_j=2498 MPa) had higher ε_{lcr} and ν_{cr} (745με and 0.32, respectively) than cylinders 3LA (K_j=1464 MPa), even when the former had significantly higher jacket stiffness.

The effect of using different confining FRP material on concrete behavior has been previously discussed in the literature. Based on tests on conventional concrete cylinders confined with FRP, Dai et al. (2011), indicated that the efficiency factor (i.e. ratio of ε_{lcr} to ε_{fu}) is significantly higher for AFRP (around 0.93) than for CFRP (around 0.64). Ozbakkaloglu and Akin (2012) showed that conventional concrete confined with AFRP has significantly higher $\varepsilon_{cc}/\varepsilon_{co}$ than if confined with CFRP, despite the two composites having similar f_{cc}/f_{co}. Similar results were observed by Teng et al. (2009) when comparing GFRP to CFRP confined conventional concrete with identical confinement ratios. Despite the excellent performance of AFRP as confining material, existing studies on AFRP confined concrete are very limited (Dai et al. 2011; Ozbakkaloglu and Akin 2012) and even fewer studies compare the effectiveness of AFRP and CFRP confinement (Ozbakkaloglu and Akin 2012). Overall, the lower effectiveness of the CFRP compared to AFRP can be attributed to various reasons related to the physical and mechanical characteristics of the materials. These include: i) different initial pre-stress during the application of the fibers (due to the lower flexibility of the CFRP sheets), which leads to the CFRP sheet being less tightly wrapped around the cylinder and the presence of air voids; ii) higher stiffness in the CFRP, which can lead to higher axial load being transferred to the CFRP (transversely); and iii) minor misalignment of the fibers. Nonetheless, a rational explanation of why the performance of AFRP/CFRP sheets with identical stiffness differs in confinement applications differs, remains elusive.

3.4 Size effect

To investigate the effect of specimen size, Fig. 7a-b compare the stress-strain behavior of small (ϕ100×200mm) and large (ϕ150×300mm) cylinders with similar confining pressure. The data in Fig. 7 is normalized to the unconfined concrete strength, i.e. 8.2 MPa for the small cylinders confined with 2 or 4 layers of AFRP, and 6.8 MPa for all remaining cylinders cast from the same batch. The data in Fig. 7a-b show that the cylinder size has negligible effects on the effectiveness of the confinement at similar confining pressure, which is line with previous results reported in the literature (Cui and Sheikh 2010). For instance, the curves of the large

cylinders (3L) are similar to those of the small cylinders (2L) with identical confinement

pressure for both AFRP (Fig. 7a) and CFRP confinement (Fig. 7b).
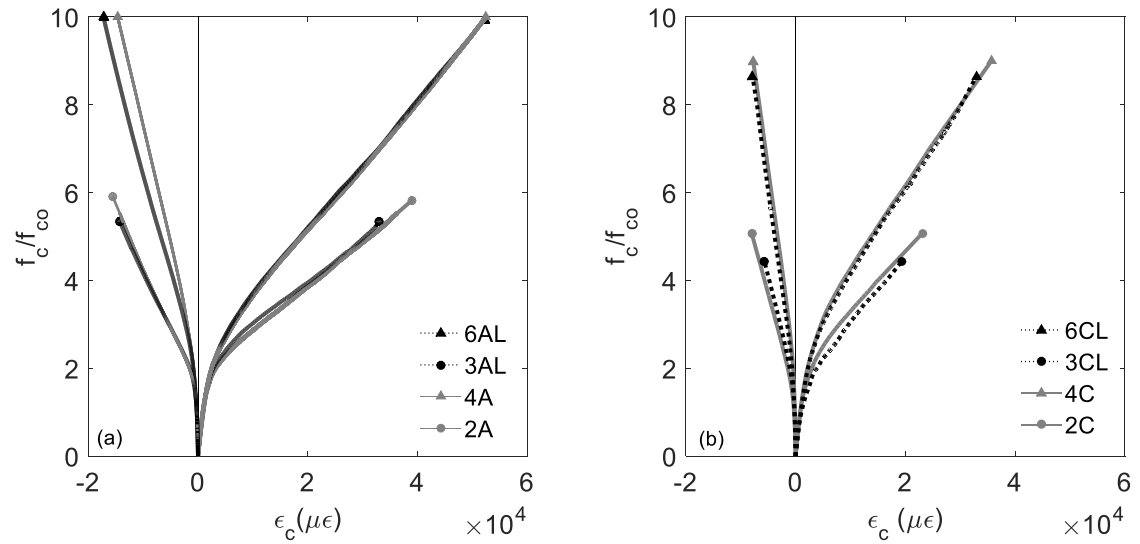
Figure 7. Average normalized stress-strain behavior of small and large cylinders confined with (a)

AFRP and (b) CFRP sheets

3.5 Volumetric behavior

To provide further insight into the mechanical behavior of FRP CRuC, Fig. 8 compares the

average axial stress of the tested cylinders and their corresponding volumetric strains (ε_{vol}),

which was calculated as:

$$\varepsilon_{vol} = 2\varepsilon_{lat} - \varepsilon_{ax} \qquad (3)$$

where ε_{lat} and ε_{ax} are the absolute lateral and axial strains measured during the tests,

respectively. In equation (3), negative ε_{vol} values denote volumetric contraction. ε_{vol} is

determined based on average stress-strain monotonic and cyclic curves of small (ϕ100×200mm)
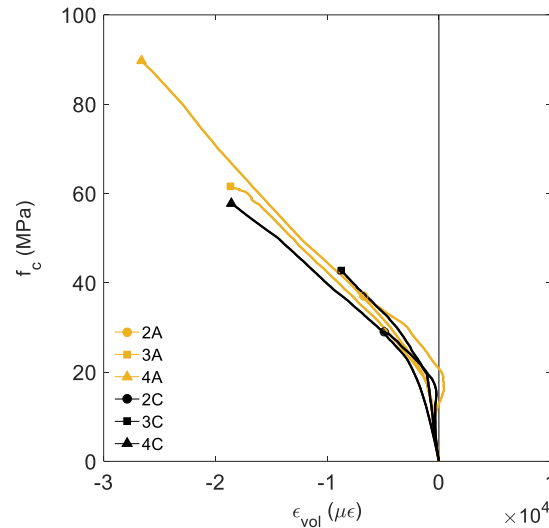
cylinders.

Figure 8. Average volumetric strains for small cylinders confined AFRP/CFRP

Fig. 8 indicates that the CRuC cylinders experienced volumetric contraction at the initial elastic stage. Such behavior is expected and similar to that observed in conventional FRP-confined concrete (Jiang and Teng 2007; Papastergiou 2010). However, the volume of the cylinders also continued to reduce at levels of applied stress exceeding f_{cr}. This behavior is considerably different from that observed in conventional FRP-confined concrete, which typically expands at stress levels beyond f_{cr} (Jiang and Teng 2007; Lam and Teng 2003; Papastergiou 2010). The different behavior may be attributed to the "fluidity" of rubber particles, which possibly filled up the voids left by crushed/pulverized concrete. It should be noted that this behavior was also observed in a previous experimental study by the authors (Raffoul et al. 2017).

The experimental results from previous sections indicate that, compared to conventional FRP-confined concrete, FRP CRuC presents unique mechanical characteristics that need to be considered for the development of constitutive models. These include: i) higher stress and strain enhancement ratios (i.e. f_{cc}/f_{co} and $\varepsilon_{cc}/\varepsilon_{co}$, respectively); ii) larger cracking strain, thus increased f_{cr}; and iii) continuous volumetric contraction up to failure. The following sections assess the accuracy of relevant existing models at predicting the ultimate condition of FRP CRuC. An active confinement model that predicts the stress-strain behavior of RuC confined with AFRP/CFRP sheets is then proposed.

4 MODELING OF FRP CRUC

4.1 Existing analytical models for FRP-confined concrete

Numerous studies have proposed design or analysis oriented models for conventional FRP-confined concrete. The latter models (Fardis and Khalili 1982; MC2010; Lam and Teng 2003; Miyauchi et al. 1999; Mortazavi 2003; Papastergiou 2010; Saadatmanesh et al. 1994; Jiang and Teng 2007; Toutanji 1999) are considered as more versatile as they a) can be modified to consider different confining materials, and b) can serve as the basis of simpler design-oriented models (Jiang and Teng 2007). To evaluate the accuracy of the above analysis-oriented models at predicting the ultimate strength and strain of FRP CRuC, Fig. 9 a and b compare the experimental results (Table 3) and model predictions of f_{cc}/f_{co}. In this figure, the amount of confinement is expressed as a mechanical volumetric confinement ratio ω_w (equation (4)) calculated using the ultimate lateral strains in the cylinders upon FRP rupture (ε_{ccl}), as proposed by Mortazavi (2003). Likewise, Fig. 10 a and b compare the experimental values to predictions of $\varepsilon_{cc}/\varepsilon_{co}$ as function of f_{cc}/f_{co}.

$$\omega_w = \frac{4nt_f}{D} \frac{E_f \varepsilon_{ccl}}{f_{co}} \qquad (4)$$

where all the variables are as defined before.
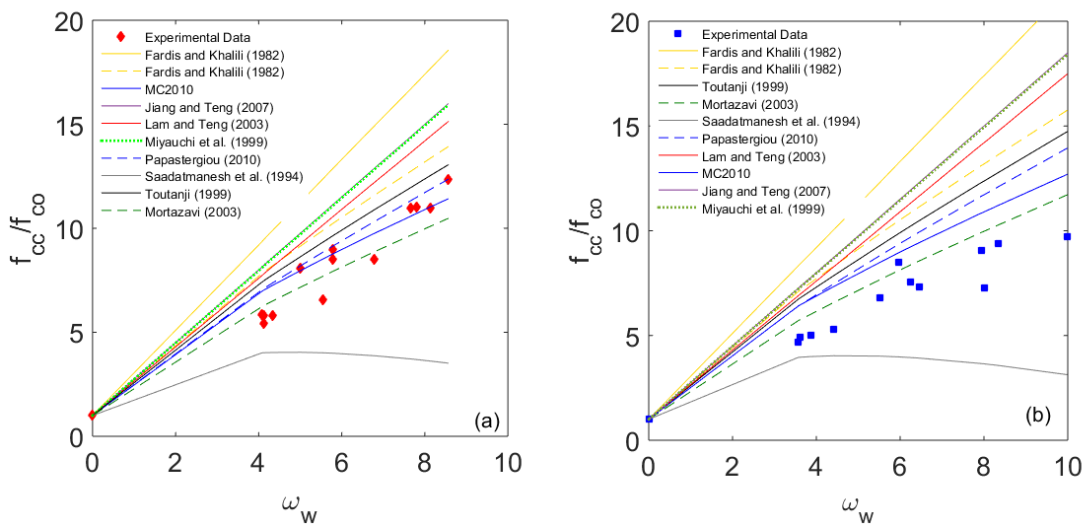
Figure 9. Experimental results and existing model predictions of f_{cc}/f_{co} for: a) AFRP and b) CFRP
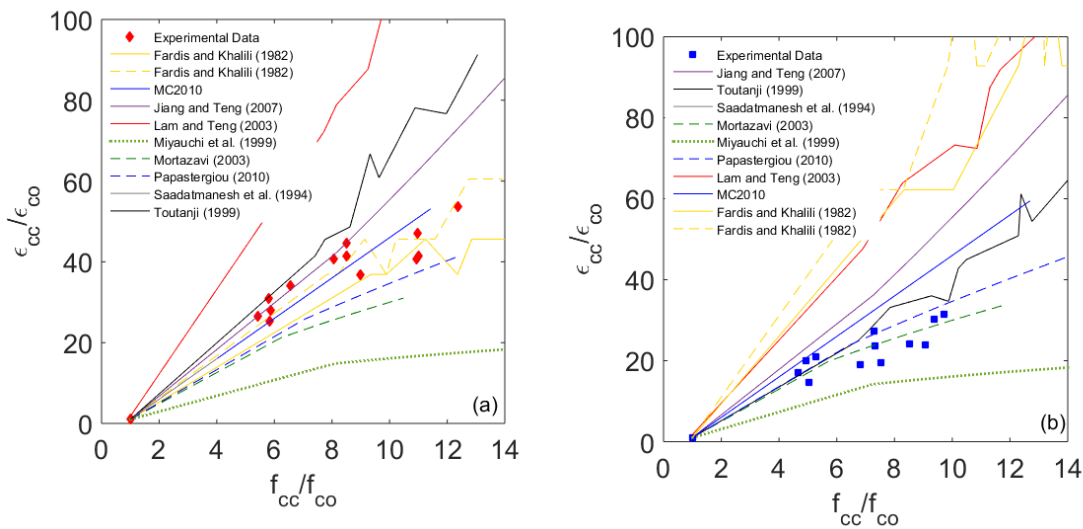
CRuC cylinders

Figure 10. Experimental results and existing model predictions of $\varepsilon_{cc}/\varepsilon_{co}$ for: a) AFRP and b) CFRP

CRuC cylinders

The results in Fig. 9 show that the models by Fardis and Khalili (1982), Lam and Teng (2003), Miyauchi et al. (1999) and Toutanji (1999) tend to overestimate the strength effectiveness of CRuC as a function of confinement ratio. This is especially evident for CFRP CRuC as can be seen in Fig. 9b. Conversely, Saadatmanesh et al. (1994) model underestimates f_{cc}/f_{co} for both AFRP and CFRP CRuC at all levels of confinement. It is also shown that Papastergiou (2010),

Mortazavi (2003) and MC2010 (2010) models predict satisfactorily the ratios f_{cc}/f_{co} only for heavy AFRP confinement (ω_w>4). Overall, none of the aforementioned models can predict satisfactorily the values of both f_{cc}/f_{co} and $\varepsilon_{cc}/\varepsilon_{co}$ for FRP CRuC.

4.2 Proposed model

Based on regression analyses of the experimental results, a new model for FRP CRuC is proposed in the following. The model is based on the active confinement model by Mander et al. (1988), and on a refined version of an incremental iterative procedure based on lateral-to-axial strain relationships proposed by Papastergiou (2010). Mander et al.'s (1988) model was originally developed for steel confined concrete and consists of a family of axial stress-strain curves at different values of constant lateral confinement pressure applied to the concrete core. The stress-strain curves can be determined using equations (5) to (7).

$$f_c = \frac{f_{cc,\omega}\, x r}{r - 1 + x^r} \tag{5}$$

where

$$x = \frac{\varepsilon_c}{\varepsilon_{cc,\omega}} \tag{6}$$

$$r = \frac{E_{co}}{E_{co} - E_{sec,\omega}} \tag{7}$$

where $f_{cc,\omega}$ and $\varepsilon_{cc,\omega}$ represent the ultimate compressive strength and corresponding strain of the actively confined concrete and $E_{sec,\omega}$ is the secant modulus ($f_{cc,\omega}/\varepsilon_{cc,\omega}$) for the corresponding confinement ratio (ω_{wi}).

The proposed analytical model assumes that at a given confinement ratio, concrete with either passive or active confinement exhibits similar axial stress and strain values (Jiang and Teng 2007; Papastergiou 2010). Accordingly, the axial stress for the FRP-confined cylinders at a given axial strain and confining pressure can be determined using the following iterative procedure:

1. An initial value of axial strain (ε_c) is imposed (for example, $\varepsilon_c = 500\mu\varepsilon$).

2. A small initial confining ratio is assumed ($\omega_{wi}=0.001$). The corresponding critical stress (f_{cr}), ultimate stress ($f_{cc,\omega}$) and ultimate strain ($\varepsilon_{cc,\omega}$) for the current ω_{wi} are calculated using equations (8), (11) and (12), respectively (see section below).

3. At the assumed confining pressure, the axial stress f_c is determined using the base active confinement model (equation (5)).

4. The lateral strain (ε_l) is calculated using equation (13) and the corresponding confinement ratio (ω_{wf}) is determined. If ω_{wf} coincides with the initial confinement ratio (ω_{wi}) applied in step 2, then f_c and ε_c (determined in steps 3 and 1, respectively) correspond to a point on the predicted stress-strain curve of the FRP-passively confined concrete. Otherwise, steps 2 to 4 are repeated using the updated confinement ratio (ω_{wf}) until the two ratios converge.

5. The above steps are then repeated with an incremental increase in ε_c to generate the full stress-strain curve for FRP CRuC. The incremental process ends when the lateral failure strain (ε_{ccl}) of the FRP confinement is reached (refer to values in Table 3).

A reliable characterization of lateral-to-axial strain relationships, $f_{cc,\omega}$, $\varepsilon_{cc,\omega}$ and f_{cr} is key in developing a model that can accurately capture the observed experimental behavior of CRuC confined with different amounts of FRP. The following sections provide a brief description of the procedure used to determine such parameters.

4.2.1   Axial stress and strain at peak stress

To capture the elastic behavior and the increase in f_{cr} with increasing jacket stiffness, this model uses f_{cr} (as opposed to f_{co} as used in Jiang and Teng (2007), Papastergiou (2010) and Toutanji (1999)) to determine the strength and strain enhancement (f_{cc}/f_{cr} and $\varepsilon_{cc}/\varepsilon_{cr}$, respectively) at different confining levels. Based on calibration with test data, the variation in f_{cr} as a function of f_{co} and normalized confinement stiffness K_{jn} was determined using equation (8), whereas ε_{cr} was determined as function of K_{jn} as shown in equation (9).

$$f_{cr} = f_{co}\left(-6.5x10^{-6}K_{jn}^2 + 5.8x10^{-3}K_{jn} + 0.8\right) \tag{8}$$

$$\varepsilon_{cr} = \varepsilon_{co}\left(-5.2x10^{-9}K_{jn}^2 + 5.2x10^{-6}K_{jn} + 0.0011\right) \tag{9}$$

where K_{jn} is determined as follows:

$$K_{jn} = \beta\frac{2nt_f}{D}\frac{E_f}{f_{co}} \tag{10}$$

where β is an effectiveness factor (calibrated with test data) that accounts for the effect of the type of confining material on the critical and ultimate stress-strain behavior of CRuC (described in section "CFRP vs. AFRP confinement"). Based on the experimental data, β was found to be 0.75 for CFRP and 1.0 for AFRP confined cylinders, thus indicating a 25% reduction in the effectiveness of the CFRP compared to AFRP with identical confining stiffness.

A regression analysis was used to capture the strength and strain enhancement ratios (i.e. $f_{cc,\omega}/f_{cr}$ and $\varepsilon_{cc,\omega}/\varepsilon_{cr}$) at different confining pressures. The ultimate compressive strength ($f_{cc,\omega}$) at each AFRP/CFRP confining ratio can be calculated using equation (11).

$$f_{cc,\omega} = f_{cr}(1.06\beta\omega_{wi} + 1.25) \tag{11}$$

The ultimate strain at peak stress ($\varepsilon_{cc,\omega}$) may be predicted for AFRP and CFRP using equation (12).

$$\varepsilon_{cc,\omega} = \varepsilon_{cr}\left(4.7\left(\frac{f_{cc,\omega}}{f_{cr}} - 1.25\right)^{1.2} + 1.5\right) \tag{12}$$

4.2.2 Lateral to axial stress-strain relations

The following general equation (13) by Papastergiou (2010) is proposed to determine the lateral strain of the FPR jacket:

$$\varepsilon_l = \left(\frac{1}{b}\left(\frac{E_{co}\varepsilon_c}{f_c} - 1\right)^a + v\right)\frac{f_c}{E_{co}} \tag{13}$$

where *a* and *b* are empirically calibrated factors, and *v* is the concrete (initial) Poisson ratio.

The value of ε_l has a significant influence on the gradient of the linear part of the stress-strain relationship (slope of line B-C in Fig. 3) and it also controls the convergence of the model. Based on single and multiple objective genetic algorithm optimization (Chipperfield and Fleming 1995), the optimal combination of *a* and *b* to fit the experimental data of the average plots for all levels of AFRP/CFRP confinement was obtained. The optimization function criterion was to minimize the error between the experimental and predicted curves in terms of the area under the curves as well as the ultimate conditions. While a constant value of *a*=1 was found suitable for all of the tested configurations, equation (14) was developed to describe the variation of *b* with K_{jn} and account for the effect of multiple confining layers and different FRP material.

$$b = 2.15 + 0.0045K_{jn} \tag{14}$$

4.3   Model predictions

Fig. 11 a and b compare the curves predicted by the proposed model and the average experimental results for AFRP and CFRP CRuC cylinders, respectively. The results indicate that, in general, the model predicts well the average initial stiffness, critical stress and strain, gradient of the curve and the ultimate stress and strain values of the tested cylinders.
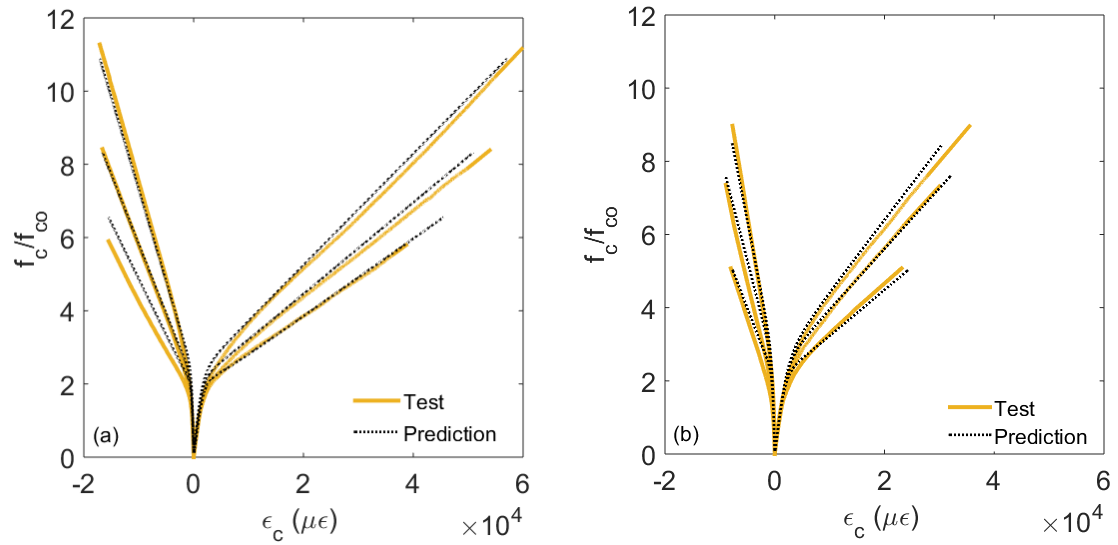
Figure 11. Experimental stress-strain curves and model predictions for a) AFRP and b) CFRP CRuC

Fig. 12 a and b compare the test results and the predictions of the main curve parameters (ultimate conditions f_{cc}/f_{cr} and $\varepsilon_{cc}/\varepsilon_{cr}$, respectively). Fig. 12a-b include data from individual cylinders as well as the average data used to calibrate the predictive model equations in the previous section. It must be noted that the model overestimates f_{cc}/f_{cr} and $\varepsilon_{cc}/\varepsilon_{cr}$ for CRuC with light AFRP confinement (2LA), while it underestimates these values for heavy CFRP confinement (4LC). This slight discrepancy is attributed to the difficulty of achieving a unified model with a regression that fits perfectly all levels of confinement. An accurate prediction of the ultimate conditions (f_{cc} and ε_{cc}) requires a simultaneously accurate prediction of the stress and strain at peak (f_{cr} and ε_{cr}), which is difficult to achieve. Overall, however, the predictions of ultimate conditions are within the expected variability of the individual test data (see Fig. 12 and Table 3), with an average standard deviation smaller than 5%.
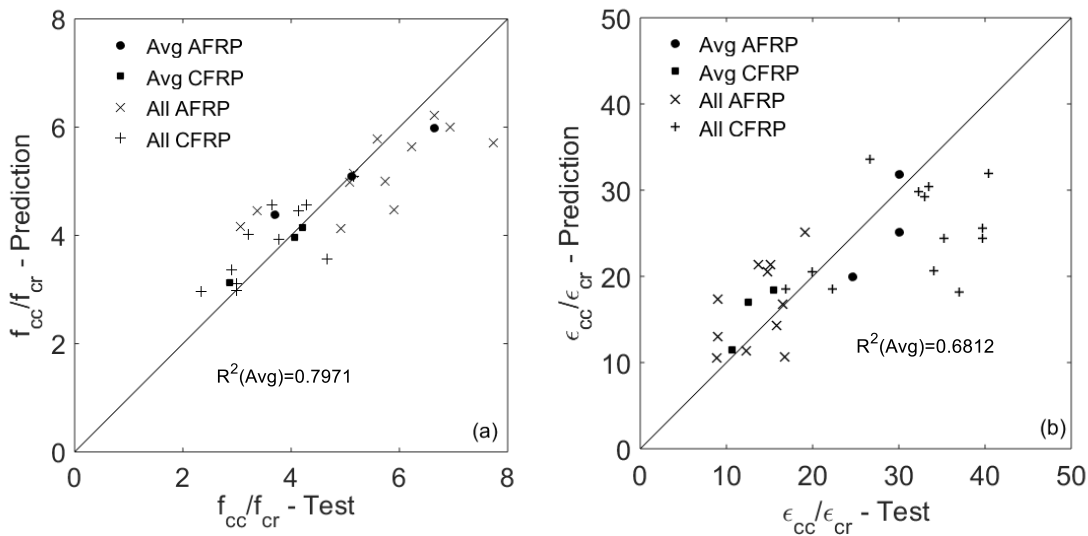
Figure 12. Performance of proposed model in predicting strength (a) and strain (b) enhancement ratios for AFRP and CFRP CRuC.

It should be noted that the proposed model is only applicable for high rubber contents as those used in this study (60% aggregate volume replacement). To date, research on CRuC with high rubber contents is not available in the literature, and therefore further research is necessary to validate the accuracy of the model using other experimental datasets. Future research should also extend the applicability of the proposed model to Glass FRP. The lower effectiveness observed in CFRP CRuC also requires further investigation. Experimental and analytical work on the cyclic behavior of highly-deformable structural elements made with FRP CRuC has also been conducted by the authors and will be reported in future publications.

5   CONCLUSIONS

This article proposes a new analysis-oriented stress-strain model for rubberized concrete (RuC) confined with FRP composites. The model is based on monotonic and cyclic test results from RuC cylinders confined externally with 2, 3, 4 or 6 layers of AFRP or CFRP sheets. Based on the results of this study, the following conclusions can be drawn:

1) FRP-confined RuC (FRP CRuC) made with high rubber volumes (>60% of aggregate replacement) can develop high compressive strength (up to 100 MPa) and very high

deformations (axial strains of 6%). This innovative concrete can be used to build strong and highly deformable RC components for structural applications.

2) The confining effect of FRP activates earlier in FRP CRuC than in conventional FRP-confined concrete, which in turn leads to enhanced strengths and strains in FRP CRuC (enhancement ratios of 11 and 45, respectively). The better effectiveness of the confinement can be attributed to the large lateral expansion of the RuC used in this study, which activates the FRP early.

3) The test results confirm that, unlike conventional FRP-confined concrete, the volume of the FRP CRuC cylinders tested in this study undergoes continuous contraction. An increase in the stress at cracking (f_{cr}) was also observed. Such behavior needs to be considered in the development of constitutive relations of CRuC.

4) The use of CFRP confining sheets led to lower strengths and strain effectiveness when compared to AFRP sheets with identical confining jacket stiffness. Future research should investigate the reasons behind this behavior.

5) Existing stress-strain models for conventional FRP-confined concrete cannot predict the behavior of the tested FRP CRuC cylinders. The new analysis-oriented model proposed in this study predicts well the stress-strain relationships of both AFRP and CFRP CRuC (average standard deviation for predictions of the ultimate conditions <5%). However, future research should validate the accuracy of this model using other experimental datasets and different types of FRP (e.g. glass or basalt FRP sheets).

6   REFERENCES

Batayneh, M. K., Marie, I., and Asi, I. (2008). "Promoting the use of crumb rubber concrete in developing countries." *Waste Management*, 28(11), 2171–2176.

Bompa, D. V., Elghazouli, A. Y., Xu, B., Stafford, P. J., and Ruiz-Teran, A. M. (2017). "Experimental assessment and constitutive modelling of rubberised concrete materials."

Construction and Building Materials, 137, 246–260.

Buyukozturk, O., and Tseng, T. (1984). "Concrete in Biaxial Cyclic Compression." *Journal of Structural Engineering*, 110(3), 461–476.

Chang, G. a, and Mander, J. B. (1994). "Seismic Energy Based Fatigue Damage Analysis of Bridge Columns : Part 1 - Evaluation of Seismic Capacity by." *NCEER Technical Report No. NCEER-94-0006; State University of New York, Buffalo, New York.*

Chipperfield, A. J., and Fleming, P. J. (1995). "The MATLAB genetic algorithm toolbox." IET.

Cui, C., and Sheikh, S. A. (2010). "Experimental study of normal-and high-strength concrete confined with fiber-reinforced polymers." *Journal of Composites for Construction*, American Society of Civil Engineers, 14(5), 553–561.

Dai, J., Bai, Y., and Teng, J. (2011). "Behavior and modeling of concrete confined with FRP composites of large deformability." *Journal of Composites for Construction*, 15(December 2011), 963–974.

Duarte, A. P. C., Silva, B. A., Silvestre, N., de Brito, J., Júlio, E., and Castro, J. M. (2016). "Tests and design of short steel tubes filled with rubberised concrete." *Engineering Structures*, 112, 274–286.

EN, B. S. (2011). "197-1: 2011." *Cement, Composition, Specifications and Conformity Criteria for Common Cements. London, England: British Standard Institution (BSI).*

Fardis, M. N., and Khalili, H. H. (1982). "FRP-encased concrete as a structural material." *Magazine of concrete Research*, 34(121), 191–202.

fib Model Code (Fédération internationale du béton). (2010). Model Code for Concrete Structures 2010. *Berlin, Germany*.

Flores-Medina, D., Medina, N. F., and Hernández-Olivares, F. (2014). "Static mechanical properties of waste rests of recycled rubber and high quality recycled rubber from crumbed tyres used as aggregate in dry consistency concretes." *Materials and structures*, 47(7), 1185–1193.

Ganesan, N., Raj, B., and Shashikala, A. P. (2013). "Behavior of Self-Consolidating Rubberized Concrete Beam-Column Joints." *ACI Materials Journal*, 110(6), 697–704.

Garcia, R., Jemaa, Y., Helal, Y., Guadagnini, M., and Pilakoutas, K. (2014). "Seismic Strengthening of Severely Damaged Beam-Column RC Joints Using CFRP." *Journal of Composites for Construction*, 18(2), 4013048.

Güneyisi, E., Gesoğlu, M., and Özturan, T. (2004). "Properties of rubberized concretes containing silica fume." *Cement and Concrete Research*, 34(12), 2309–2317.

Jiang, T., and Teng, J. G. (2007). "Analysis-oriented stress–strain models for FRP–confined concrete." *Engineering Structures*, Elsevier, 29(11), 2968–2986.

Kotsovos, M. D., and Newman, J. B. (1981). "Effect of boundary conditions upon the behaviour of concrete under concentrations of load." *Magazine of Concrete Research*, 33(116), 161–170.

Lam, L., and Teng, J. G. (2003). "Design-oriented stress–strain model for FRP-confined concrete." *Construction and building materials*, Elsevier, 17(6), 471–489.

Lam, L., and Teng, J. G. (2004). "Ultimate condition of fiber reinforced polymer-confined concrete." *Journal of Composites for Construction*, American Society of Civil Engineers, 8(6), 539–548.

Lam, L., Teng, J. G., Cheung, C. H., and Xiao, Y. (2006). "FRP-confined concrete under axial cyclic compression." *Cement and Concrete composites*, Elsevier, 28(10), 949–958.

Li, G., Pang, S.-S., and Ibekwe, S. I. (2011). "FRP tube encased rubberized concrete cylinders." *Materials and structures*, 44(1), 233–243.

Li, G., Stubblefield, M. A., Garrick, G., Eggers, J., Abadie, C., and Huang, B. (2004). "Development of waste tire modified concrete." *Cement and Concrete Research*, 34(12), 2283–2289.

Mander, J. B., Priestley, M. J. N., and Park, R. (1988). "Theoretical stress-strain model for confined concrete." *Journal of structural engineering*, 114(8), 1804–1826.

Matthys, S., Toutanji, H., and Taerwe, L. (2006). "Stress – Strain Behavior of Large-Scale Circular Columns Confined with FRP Composites." *Journal of Structural Engineering*, 132(1), 123–133.

Miyauchi, K., Inoue, S., Kuroda, T., and Kobayashi, A. (1999). "Strengthening effects with carbon fiber sheet for concrete column." *Proc Jpn Concr Inst*, 21(3), 1453–1458.

Mortazavi, A.A. (2003). Repair/stregthening of RC columns with FRP. PhD Thesis, University of Sheffield.

Mortazavi, A. A., Pilakoutas, K., and Son, K. S. (2003). "RC column strengthening by lateral pre-tensioning of FRP." *Construction and Building Materials*.

Neville, A. M. (1995). "Properties of Concrete." Pearson Education Limited, Essex, England.

Osorio, E., Bairán, J. M., and Marí, A. R. (2013). "Lateral behavior of concrete under uniaxial compressive cyclic loading." *Materials and Structures*, 46(5), 709–724.

Ozbakkaloglu, T., and Akin, E. (2012). "Behavior of FRP-Confined Normal- and High-Strength Concrete under Cyclic Axial Compression." *Journal of Composites for Construction*,

American Society of Civil Engineers, 16(4), 451–463.

Papastergiou, P. (2010). "A confinement model for concrete wrapped or pretensioned with FRP. PhD Thesis." University of Sheffield.

Paulay, T., and Priestley, M. J. N. (1992). *Seismic Design Of Reinforced Concrete And Masonry Buildings*. John Wiley & Sons, Inc.

Pilakoutas, K., Raffoul, S., Papastergiou, P., Garcia, R., Guadagnini, M., and Hajirasouliha, I. (2015). "A STUDY OF THE REUSE OF ALL TYRE COMPONENTS IN CONCRETE: THE ANAGENNISI PROJECT." *International conference on sustainable structural concrete*, La Plata, Argentina, Argentina.

Raffoul, S., Garcia, R., Escolano-Margarit, D., Guadagnini, M., Hajirasouliha, I., and Pilakoutas, K. (2017). "Behaviour of unconfined and FRP-confined rubberised concrete in axial compression." *Construction and Building Materials*, 147, 388–397.

Raffoul, S., Garcia, R., Pilakoutas, K., Guadagnini, M., and Medina, N. F. (2016). "Optimisation of rubberised concrete with high rubber content: An experimental investigation." *Construction and Building Materials*, 124.

Rousakis, T. C., and Athanasios, K. I. (2012). "Adequately FRP confined reinforced concrete columns under axial compressive monotonic or cyclic loading." *Materials and structures*, 45, 957–975.

Rousakis, T., and Tepfers, R. (2001). "Experimental investigation of concrete cylinders confined by carbon FRP sheets, under monotonic and cyclic axial compressive load." *Research Rep*, 44, 1–87.

Saadatmanesh, H., Ehsani, M. R., and Li, M.-W. W. (1994). "Strength and ductility of concrete columns externally reinforced with fiber composite straps." *ACI Structural journal*, 91(4), 434–447.

Saadatmanesh, H., Ehsani, M. R., and Li, M. W. (n.d.). "Strength and Ductility of Concrete Columns Externally Reinforced with Fiber Composite Straps." *ACI Structural Journal ACI Structural Journal ACI Structural Journal*, 91(4).

Spoelstra, M. R., and Monti, G. (1999). "FRP-confined concrete model." *Journal of composites for construction*, American Society of Civil Engineers, 3(3), 143–150.

Teng, J. G., Huang, Y. L., Lam, ; L, Ye, L. P., Lam, L., Ye, L. P., Lam, ; L, and Ye, L. P. (2007). "Theoretical model for fiber-reinforced polymer-confined concrete." *Journal of composites for construction*, American Society of Civil Engineers, 11(2), 201–210.

Teng, J. G., Jiang, T., Lam, L., and Luo, Y. Z. (2009). "Refinement of a design-oriented stress–

strain model for FRP-confined concrete." *Journal of Composites for Construction*, American Society of Civil Engineers, 13(4), 269–278.

Toutanji, H. A. (1996). "The use of rubber tire particles in concrete to replace mineral aggregates." *Cement and Concrete Composites*, 18(2), 135–139.

Toutanji, H. A. (1999). "Stress-strain characteristics of concrete columns externally confined with advanced fiber composite sheets." *ACI materials journal*, American Concrete Institute, 96(3), 397–404.

Youssf, O., ElGawady, M. A., Mills, J. E., and Ma, X. (2014). "An experimental investigation of crumb rubber concrete confined by fibre reinforced polymer tubes." *Construction and Building Materials*, 53, 522–532.

Chapter 5

Cyclic behaviour of FRP-confined rubberised concrete cylinders

This article develops a constitutive model to predict the cyclic behaviour of rubberised concrete cylinders confined with fibre reinforced polymer sheets (FRP). In total, 30 cylinders were cast with rubberised concrete having 60% of the total aggregate volume replaced with recycled tyre rubber. The influence of the type of confining material (Carbon or Aramid FRP), number of layers (2, 3 or 4) and type of load (monotonic or cyclic) was investigated. The results indicate that the load history did not have a significant effect on the stress-strain envelope of FRP-confined rubberised concrete. The proposed constitutive model predicts accurately the unloading/reloading cycles and it can be used for design/analysis of highly-deformable components made of FRP-confined rubberised concrete. This article contributes toward developing advanced constitutive models so as to promote the use of FRP-confined rubberised concrete in the construction industry.

1   INTRODUCTION

In recent years, numerous studies have examined the use of waste tire rubber as replacement of mineral aggregates in order to produce new concrete composites. Rubber in concrete can develop high ductility [1–3], particularly when large volumes of rubber are used [4,5]. Nevertheless, the inclusion of high volumes of recycled rubber in concrete leads to poor fresh properties [6–8], and lower compressive strength and stiffness [7,9], when compared to conventional concrete. Research by the authors [10] has shown that the fresh properties of rubberised concrete (RuC) can be improved by optimizing the concrete mix parameters, leading to the development of RuC with high rubber content (>50% total aggregate content) and good workability, homogeneity and cohesiveness. Nevertheless, significant reductions in strength were still experienced at high rubber contents [10]. This, to date, has limited the use of rubber in concrete to low rubber contents [8,11].

Recent research has shown that, the use of externally bonded Fibre Reinforced Polymer (FRP) or steel confinement successfully addresses some of these challenges and allows the development of adequate strength in confined rubberised concrete (CRuC) [12–16]. For example, Youssf et. al [13] reports that a compressive strength of 112.5 MPa can be achieved by casting RuC cylinders with 20% rubber replacing the sand volume in preformed CFRP tubes (three layers). Whilst the above use of confinement led to some improvements in RuC strength, it had limited influence on the concrete deformability with maximum strains (1.8%) that are comparable to or even lower than strains that can be achieved using conventional confined concrete [17]. Research by Duarte et al. [15] reported 50% increase in column ductility by confining concrete RuC with cold-form steel tubes. However, it was found that the RuC columns were less effectively confined than conventional concrete, due to the former's lower dilation angle. These results can be attributed to the relatively low rubber contents used (20% rubber replacing sand volume [13] or 15% rubber replacing total aggregate volume [15]), which did not fully exploit the large lateral expansion capacity of the rubber. More recently, it has been proved that the use of AFRP jackets to confine

high-rubber content RuC (60% total aggregate replacement) leads to compressive strengths >70 MPa while achieving high deformability in concrete with axial strains of around 5% [18]. This novel concrete can be used in numerous structural applications, such as plastic hinge zones or base isolation systems in seismic zones. A practical design-oriented model was also recently proposed to predict the monotonic stress-strain behaviour of FRP CRuC [19], but such model needs to be extended to consider cyclic load. This model is necessary for the design of FRP CRuC components that can develop large deformability.

This article examines experimentally the performance of FRP CRuC cylinders with high rubber contents (60% of the total aggregate volume) subjected to compression. Section 2 of this article presents an experimental programme that aims to identify the parameters that govern the cyclic strain-strain behaviour of FRP CRuC. Section 3 discusses the main experimental results. Based on the experimental results, Section 4 presents a new design-oriented cyclic model that predicts accurately the cyclic performance of FRP CRuC. Conclusions are drawn in Section 5 of this article. This study is part of the FP7 EU-funded project Anagennisi, which aims to develop high-value uses for all tyre components in concrete [20].

2   EXPERIMENTAL PROGRAMME

2.1   Test specimens

A total of 30 rubberised concrete (RuC) cylinders (100mm diameter x 200mm height) were confined with externally bonded FRP jackets and tested in uniaxial compression. The main variables studied were: i) the confining material (AFRP or CFRP); ii) the confinement ratio given by two, three of four layers of FRP and iii) the load pattern (cyclic or monotonic loading).

2.2   Concrete

The concrete was cast using a RuC mix optimised in a previous study [10] as part of a comprehensive investigation on the fresh and mechanical properties of RuC. The selected mix had high rubber content replacing 60% of the fine and coarse mineral aggregates by volume. This

high rubber content was selected based on a previous study by the authors, where the high amount of rubber led to high lateral expansion, leading to significantly high confinement effectiveness and ductility [21]. The concrete mix proportions for 1 m^3 were: i) 340 kg of Portland Limestone Cement with 10-15% limestone content (CEMII-52.5N); ii) 42.5 kg of silica fume; iii) 42.5 kg of pulverised fuel ash; iv) 149 litres of water (water to binder ratio of 0.35); v) 2.5 and 5.1 litres of water reducing admixtures (plasticizers and superplasticizers, respectively); vi) 400.4 kg of round river washed gravel (coarse aggregates, sizes 5-20mm) and 328 kg of medium grade river washed sand (fine aggregates, sizes 0-5mm); vii) 181.3 kg of coarse rubber (sizes 5-10mm) and 148.5 kg of fine rubber (sizes 0-5mm). Specific details on the concrete mix constituents and concrete mixing procedure can be found in [10]. The 28-day mechanical properties of three unconfined RuC cylinders subject to uniaxial compression are: Compressive strength (f_{co}): 7.6 MPa (stdev=1.3); Strain at peak stress (ε_{co}): 1350$\mu\varepsilon$ (stdev=200$\mu\varepsilon$); Modulus of elasticity (E_{co}): 10.3 GPa (stdev=1.8 GPa).

2.3　Fibre reinforced polymer sheets

The FRP composite consisted of a unidirectional fabric made of Aramid or Carbon fibres embedded in an epoxy matrix. The RuC cylinders were wrapped with the AFRP or CFRP jackets using a wet lay-up technique, in which the fibres were oriented perpendicular to the cylinder axis and overlapped by a length of 100 mm. The mean properties of the FRP composite, determined based on standardised uniaxial direct tensile tests on 30 FRP coupons (250x15xt_f) are presented in Table 1; where f_f is the tensile strength of the coupon, E_f is its modulus of elasticity, ε_{fu} is its ultimate tensile strain capacity and t_f is the dry fibre thickness of 1 layer of AFRP/CFRP.

Table 1. FRP dry fibre properties

Fibre type	f_f (MPa)	E_f (GPa)	ε_{fu} (%)	$t_f^{\#}$ (mm)
Carbon	2065 (80[*])	225 (12[*])	0.9 (0.07[*])	0.185
Aramid	2430 (260[*])	122 (16[*])	2.06 (0.11[*])	0.2

[#] tf – dry fibre thickness of 1 layer
[*] Standard deviation

2.4   Experimental setup and load protocol

The cylinders were tested in uniaxial compression using a servo-controlled Universal Testing Machine with a capacity of 3,000 kN up to failure. All cylinders were confined at the top and bottom using aluminium caps to limit stress concentrations and prevent failure at the specimens' end zones (Figure 1). Throughout the tests, axial and lateral strain measurements were obtained from cylinders both locally and globally. Figure 2 shows a diagram of the setup and the instrumentation during the test. Three horizontal (H) and two vertical (V) strain gauges measured the local jacket strains at the specimens' mid-height. Gauge H3 was placed on the centre of the overlap whilst H1 and H2 were set apart at a 120° angle (see Figure 2). The vertical strain gauges were spaced 180° apart. To measure the axial global deformation at the central region of the cylinder, two aluminium rings spaced 100mm apart were fixed using clamp screws. The screws were fitted with springs to enable the free lateral expansion of the cylinder. Three lasers (L), set apart at 120° angle, were mounted on the ring to measure the global relative displacement between the rings. The horizontal displacements were obtained using a tensioned wire around the specimens at middle height. The wire was attached to a potentiometer, which measured its displacement upon lateral expansion due to axial loading.

The cylinders were loaded using either: i) monotonic loading, in which the load was increased continuously under displacement control with a loading rate of 0.5mm/min, or ii) cyclic loading, which consists of sets of five unloading/reloading cycles at each prescribed stress level (increasing by 10MPa) at loading rate of 0.5mm/min for the first set of cycles, after which the rate was increased to 2mm/min. For each parameter (i.e. confining material and lateral pressure), two nominally identical cylinders were tested using monotonic load, while three were tested using cyclic load.
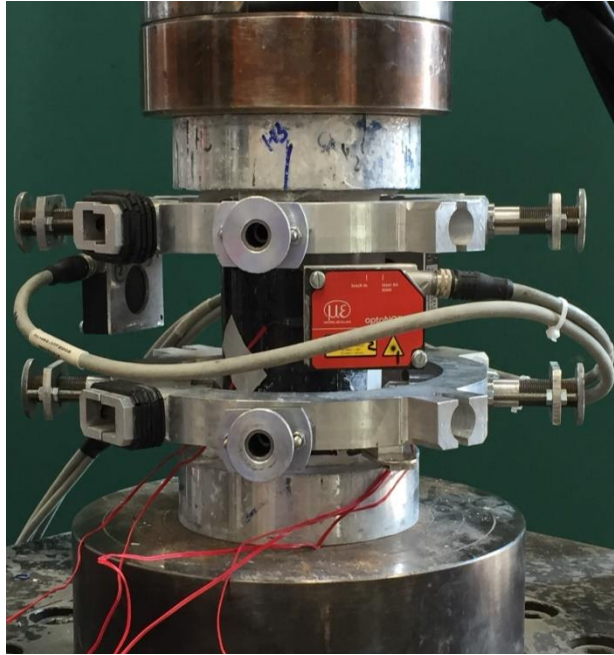
Figure 1. Typical experimental set-up for CRuC cylinders
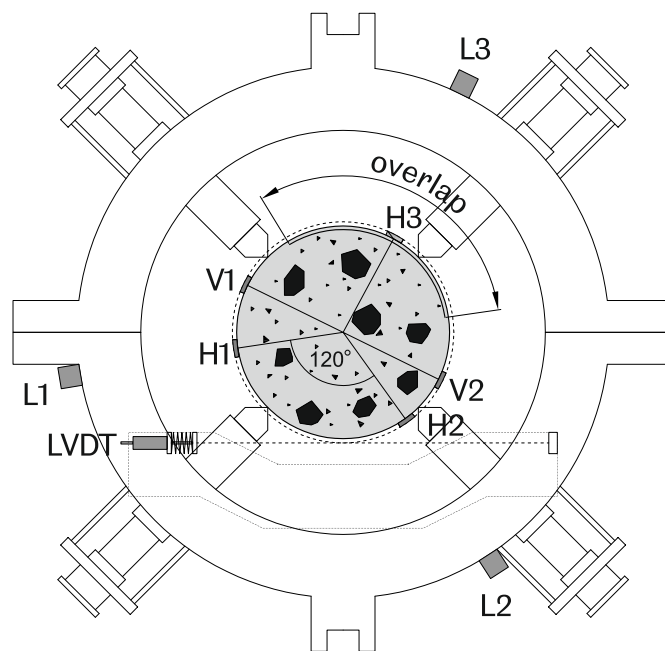
Figure 2. Instrumentation

3   RESULTS AND DISCUSSION

Table 2 summarises the following results from the tested cylinders: normalised jacket stiffness (K_{jn}, see equation (3), section 4.1), ultimate compressive strength (f_{cc}), ultimate axial and lateral strains (ε_{cc} and ε_{cl}, respectively), critical stress and strain (f_{cr} and ε_{cr}, respectively), the initial modulus of elasticity ($E_{c,0}$) as well as confinement effectiveness and ductility (f_{cc}/f_{co} and $\varepsilon_{cc}/\varepsilon_{co}$), the latter of which was considered as the ratio of the ultimate stress and axial strain to the peak stress (f_{co}) and corresponding axial strain (ε_{co}) of the unconfined RuC, respectively. The cylinders are identified according to the number of confining layers (2, 3, or 4), the type of confining material (A for AFRP or C for CFRP), the load protocol (M for monotonic and C for cyclic) and the specimen number in the aforementioned order. For example, specimen number 2 with 3 layers of AFRP confinement subject to cyclic loading is expressed as follows: 3A-C2.

Table 2. Main results from tested cylinders

ID	K_{jn}	f_{cc} (MPa)	Avg (SD)	ε_{cc} (%)	Avg (SD)	ε_{ccl} (%)	Avg (SD)	f_{cr} (MPa)	ε_{cr} (%)	f_0 (MPa)	Avg (SD)	$E_{c,0}$ (GPa)	Avg (SD)
2LA-M1		39.9	42.3 (3.4)	3.78	4.19 (0.6)	1.42	1.68 (0.4)	8.1	0.102	11.5	11.5 (0.0)	11.4	11.1 (0.5)
2LA-M2		44.6		4.60		1.93		8.7	0.116	11.5		10.7	
2LA-C1	119.0	39.5		4.16		1.51		11.7	0.209	13.3	13.2 (0.2)	8	9.3 (1.4)
2LA-C2		39.6	38.7 (1.5)	3.40	3.71 (0.4)	1.44	1.46 (0.0)	12.9	0.201	13.1		9.2	
2LA-C3		37.0		3.58		1.44		12.1	0.162	13.4		10.7	
3LA-M1		73.5	69.9 (5.2)	4.97	5.24 (0.4)	1.62	1.51 (0.2)	12.8	0.125	11.6	11.9 (0.4)	14.6	13.6 (1.5)
3LA-M2		66.2		5.51		1.40		11.2	0.162	12.2		12.5	
3LA-C1	178.5	70.2		4.96		1.29		18.6	0.273	12.7		15	
3LA-C2		69.8	69.9 (0.3)	6.02	5.53 (0.5)	1.90	1.60 (0.3)	11.2	0.183	11.9	12.7 (0.7)	10	12.4 (2.5)
3LA-C3		69.6		5.61		1.62		13.7	0.159	13.3		12.3	
4LA-M1		101.4	96.1 (7.5)	7.25	6.4 (1.2)	1.80	1.60 (0.3)	15.3	0.272	15.7	14.6 (1.6)	8	8.4 (0.6)
4LA-M2	238.1	90.7		5.56		1.39		13.6	0.237	13.5		8.8	
4LA-C1		89.8		5.49		1.61		11.6	0.170	19.6		7.8	
4LA-C2		90.1	90.04 (0.2)	6.36	5.81 (0.5)	1.71	1.65 (0.1)	13.0	0.158	15.5	18.5 (2.7)	11.8	11.1 (3.1)
4LA-C3		90.3		5.58		1.64		16.1	0.167	20.5		13.8	

Table 2. Main results from tested cylinders (continued)

Specimen														
2LC-M1		33.6		2.69		0.74		11.2	0.160	16.4		9.8	
2LC-M2		29.8	31.7 (2.7)	1.73	2.21 (0.7)	0.62	0.68 (0.1)	11.4	0.181	16.5	16.4 (0.1)	11.0	10.4 (0.9)
2LC-C1	183.6	34.2		1.96		0.79		11.4	0.159	15.8		10.2	
2LC-C2		36.0	33.9 (2.2)	2.83	2.37 (0.4)	0.90	0.81 (0.1)	12.4	0.316	17.2	15.9 (1.4)	6.8	8.2 (1.8)
2LC-C3		31.7		2.30		0.73		13.6	0.259	14.5		7.5	
3LC-M1		46.4		2.56		0.75		-	-	-		6.2	
3LC-M2		51.2	48.8 (3.4)	2.63	2.60 (0.1)	0.85	0.80 (0.1)	16.0	0.292	17.3	17.3	7.8	7.0 (1.1)
3LC-C1	275.5	49.9		3.20		0.88		13.3	0.193	16.7		9.8	
3LC-C2		49.6	42.7 (12.3)	3.69	2.96 (0.9)	1.09	0.84 (0.3)	11.6	0.270	17.5	18.3 (2.2)	9.4	9.2 (0.7)
3LC-C3		28.6		2.00		0.55		8.4	0.145	20.8		8.5	
4LC-M1		63.7		4.07		0.85		15.4	0.275	16.7		8.0	
4LC-M2		61.6	62.7 (1.5)	3.24	3.66 (0.6)	0.81	0.83 (0.0)	15.4	0.214	15.3	16.0 (1.0)	11.2	9.6 (2.3)
4LC-C1	367.3	49.9		3.01		0.55		16.7	0.235	18.3		10.2	
4LC-C2		57.9	58.0 (8.1)	3.26	3.51 (0.7)	0.61	0.73 (0.3)	12.4	0.206	18.0	17.8 (0.6)	8.6	9.1 (1.0)
4LC-C3		66.1		4.26		1.02		12.8	0.213	17.2		8.4	

3.1 Ultimate condition and failure mode

All specimens failed suddenly by rupture of the FRP jackets as the maximum lateral strain capacity of the FRP composite was reached (Figure 3). The results in Table 2 indicate that the loading history did not have a significant influence on the failure strain, as the ultimate strains of cylinders subjected to monotonic and cyclic load protocols were similar and fell within the standard deviation of the material.
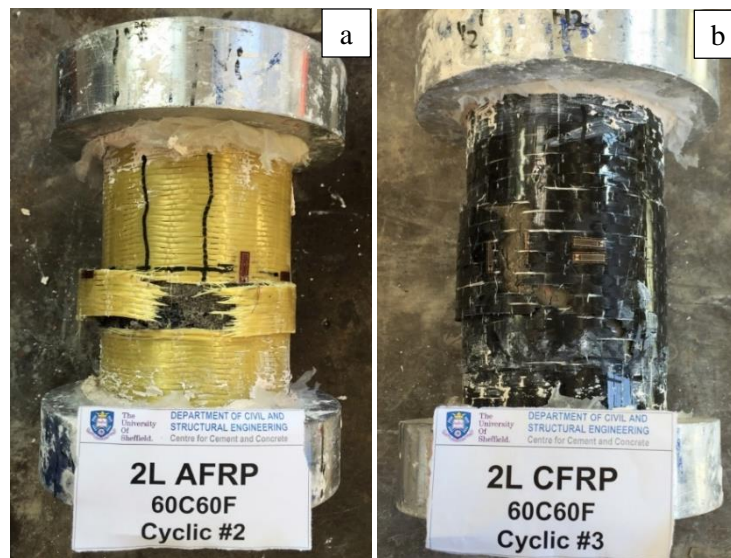
Figure 3. Failure Modes

The results also indicate that ε_{cl} was lower than average ultimate strains achieved from direct tensile (coupon) tests (ε_{fu}), presented in Table 1. The AFRP CRuC cylinders failed at ε_{cl} values around 70-80% of ε_{fu}. Similarly, CFRP CRuC cylinders failed at ε_{cl} values between 65-95% that of the corresponding coupon ε_{fu}. This is consistent with results from previous research [22,23] and may be attributed to i) localised stress concentrations, induced by non-homogeneous deformations in the concrete or strain distribution in the FRP, ii) FRP jacket curvature, iii) lap splice length, iv) axial loading of the FRP jacket and v) slight misalignment of the fibres.

3.2 Cyclic and envelope curves

Figure 4a–d presents a typical hysteretic stress-strain curve as well as the average monotonic and cyclic envelope curves of cylinders confined with two, three or four layers of AFRP or CFRP

sheets. The average monotonic and envelope curves were acquired by averaging the two monotonic and three envelope curves, respectively, for each level and type of confinement. The envelope curves were obtained by connecting the unloading points for the initial cycle of each set of loading sequence and therefore, it represents the upper bound of the stress-strain behaviour of the concrete subject to the above mentioned loading conditions. Axial (compressive) strains are indicated as positive whilst lateral (hoop tensile) strains are indicated as negative. The reported axial strains are the average vertical strain gauge readings up to the critical stress, after which the measurements were obtained from average readings from the three lasers. This was due to excessive localised bulging at the mid-height of the cylinder after the critical point, which led to spurious gauge results compared to the global measurements of the lasers. Horizontal strains are the average readings from the three horizontal gauges.

Both monotonic and envelope curves of FRP CRuC were characterised by an initial slope ($E_{c,0}$) controlled by the elastic unconfined behaviour of RuC, until the critical point (ε_{cr}, f_{cr}) is reached. This is followed by a non-linear transition zone and a second linear portion of the curve, with gradient ($E_{c,f}$) that is influenced by the axial stiffness of the confining jacket. At this stage the RuC is progressively crushing and continuously increasing the lateral expansion in the jacket.

As shown in Figure 4, the average monotonic stress-strain and cyclic envelope curves are similar up to failure, thus indicating that the loading history had a minor influence the overall envelope stress-strain behaviour of CRuC subject to cyclic loading. A similar behaviour has been reported for FRP or steel confined concrete [24–27], where the monotonic stress-strain curve has been often used as an approximation of the envelope cyclic behaviour. It should be noted that while some of these studies report lower ultimate failure strain in monotonically than cyclically loaded cylinders [26], this effect was not observed in this study, where CRuC subject to cyclic loading exhibited comparable failure stress and strains, when compared to identically confined cylinders loaded monotonically.
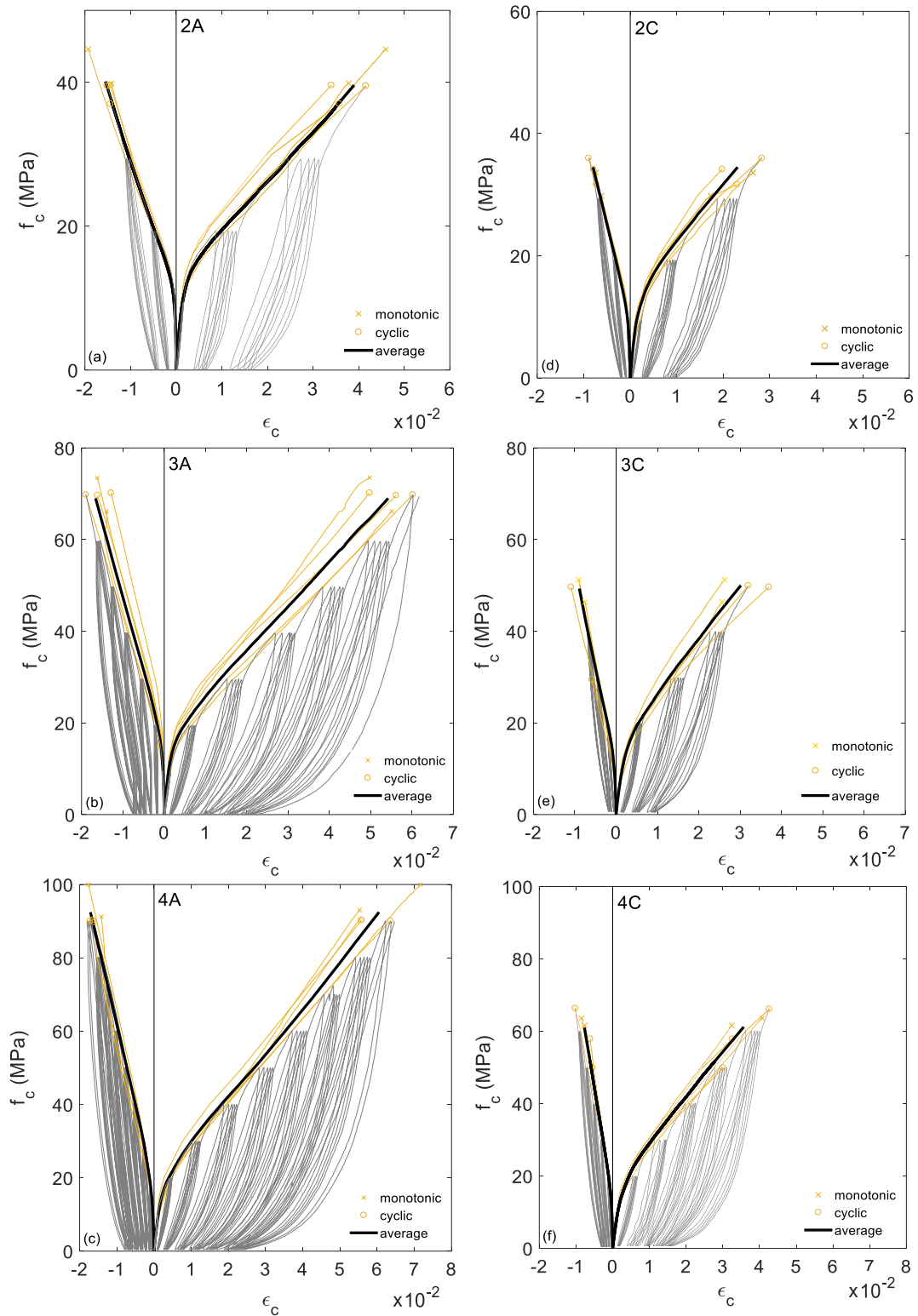
Figure 4. Stress-strain curves including average cyclic envelope and monotonic curves a) 2LA, b) 2LC, c) 3LA, d) 3LC, e) 4LA and f) 4LC

4   CYCLIC MODEL

The shape of the monotonic and envelope curves of FRP-confined conventional concrete has been extensively investigated and several models exist to predict the shape of these curves for FRP-confined conventional concrete [26,28,29]. Nonetheless, such models cannot predict the behaviour of CRuC due to its significantly higher strength and strain enhancement ratios, as well as delayed cracking when compared to conventional confined concrete [12,18]. Furthermore, no research can be found on the parameters of uniaxial cyclic loading of CRuC and therefore a new cyclic model is necessary for the accurate modelling of CRuC structural elements in cyclic conditions. Figure 5 illustrates the key parameters that define the typical stress-strain cyclic response of CRuC cylinders. The plot depicts a stress-strain curve with a continuously increasing envelope. The cylinder is subjected to unloading then reloading at a point after the critical point of the cylinder (ε_{cr}, f_{cr}) at the initiation of unstable cracking.
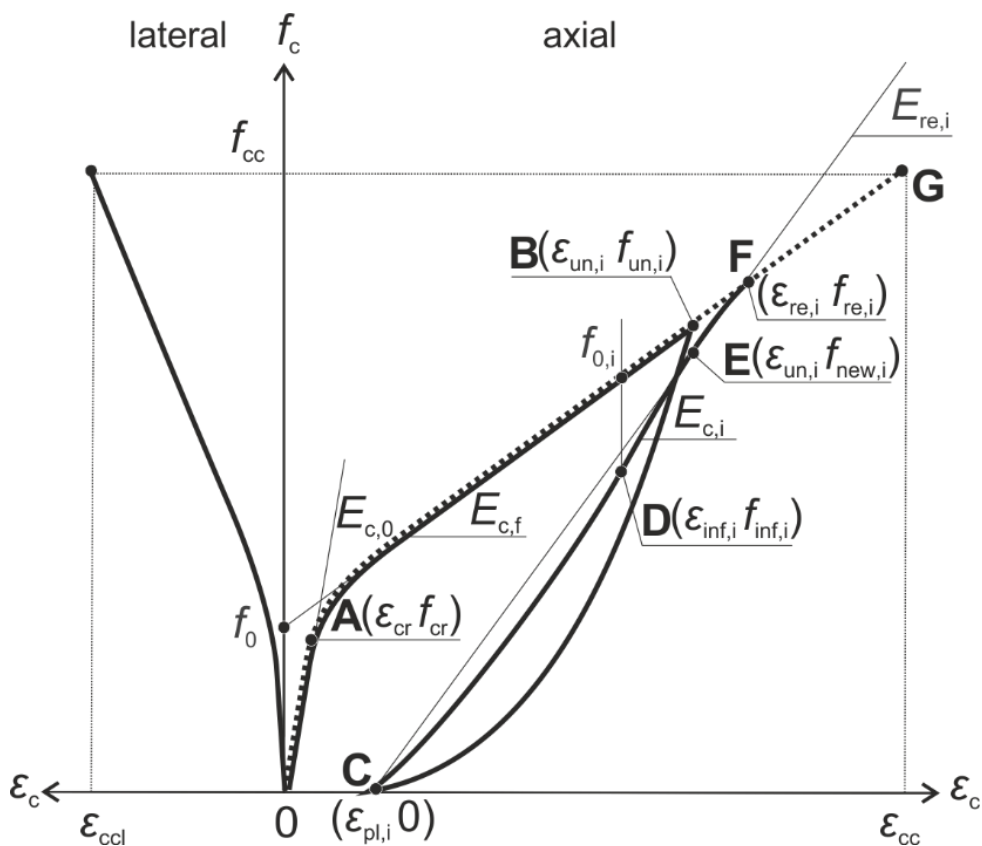
Figure 5. Key parameters for the cyclic behaviour of CRuC

As shown in Figure 5, the cyclic stress-strain behaviour of FRP CRuC can be divided into an envelope (0-G), an unloading curve (B-C) and a reloading curve (C-F). These components are shaped by the following parameters: initial modulus of elasticity ($E_{c,0}$), slope of the second gradient of the curve ($E_{c,f}$), intercept of the second linear branch of the curve with the y-axis (f_0), critical point A(ε_{cr}, f_{cr}), ultimate stress (f_{cc}) and strain (ε_{cc}) values, as well as the plastic residual strain ($\varepsilon_{pl,i}$), reloading secant modulus ($E_{re,i}$), stress at previous unloading ($f_{new,i}$), the intersection of reloading curve with the envelope F($\varepsilon_{re,i}$, $f_{re,i}$), for each unloading point E($\varepsilon_{un,i}$, $f_{un,i}$). Parameters of the reloading curve including the inflection point D($\varepsilon_{inf,i}$, $f_{inf,i}$), slope ($E_{c,i}$), and ($f_{0,i}$) at the intersection of the vertical ($\varepsilon_{inf,i}$, $f_{inf,i}$) with the envelope curve, for each unloading point, are also shown in Figure 5 and discussed in the section *Reloading part 2: softening curve*. The following sections analyse in detail the above parameters, and provide equations to predict their values, leading to the development of a model that can predict the stress-strain characteristics of cyclically loaded CRuC cylinders.

4.1   Ultimate stress-strain and envelope prediction

The experimental results in Table 2 were used to calibrate predictive equations to estimate the stress and strain values of CRuC with the different confining parameters.

Previous research has shown that the high lateral expansion in RuC activates the confinement from the jacket more promptly [12,19]. Depending on the jacket confining stiffness, this effect delays the initiation of cracking in the CRuC, leading to higher stress and strain enhancement ratios, when compared to FRP-confined conventional concrete. The results in this experiment show that the critical point (ε_{cr}, f_{cr}), determined as the point of change in the gradient of the curve upon the activation of the confinement pressure, increases with increasing normalised jacket stiffness (K_{jn}, see equation (3)). Following a thorough analysis of the experimental results (see Chapter 4 section 4.2.1), it was found that f_{cr} and ε_{cr} can be calculated as function of K_{jn} using equations (1) and (2), respectively.

$$f_{cr} = f_{co}(-6.5x10^{-6}K_{jn}^2 + 5.8x10^{-3}K_{jn} + 0.8) \tag{1}$$

$$\varepsilon_{cr} = \varepsilon_{co}(-5.2x10^{-9}K_{jn}^2 + 5.2x10^{-6}K_{jn} + 0.0011) \tag{2}$$

where

$$K_{jn} = \beta\frac{2nt_f}{D}\frac{E_f}{f_{co}} \tag{3}$$

The ultimate stress (f_{cc}) and the confinement ratio for AFRP and CFRP CRuC can be predicted by equations (4) and (5), respectively, whereas the variation in ultimate strain as function of strength enhancement ratio is given by equation (6) (see derivations in Chapter 4).

$$f_{cc} = f_{cr}(1.06\omega_w + 1.25) \tag{4}$$

$$\omega_w = \beta\frac{4nt_f}{D}\frac{E_f \varepsilon_{ccl}}{f_{cr}} \tag{5}$$

$$\varepsilon_{cc} = \varepsilon_{cr}(4.7\left(\frac{f_{cc}}{f_{cr}} - 1.25\right)^{1.2} + 1.5) \tag{6}$$

Equation (3) and (5) include an effectiveness factor (β) to account for the lower effectiveness of the CFRP confining effect relative to its jacket stiffness, compared to AFRP. Whilst this effect has been previously reported in the literature [26,30,31], the different effectiveness of CFRP and AFRP has not been explained. Based on regression analysis of the experimental data, β was found to be 0.75 for CFRP CRuC and 1.0 for AFRP CRuC.

Figure 6 shows f_{cc}/f_{cr} for AFRP and CFRP CRuC as function ω_w with or without considering β. It can be observed that at a selected ω_w (without β), the CFRP CRuC cylinders have a lower strength enhancement ratio than AFRP CRuC cylinders with similar ω_w, thus suggesting that the CFRP CRuC specimens were less effectively confined.
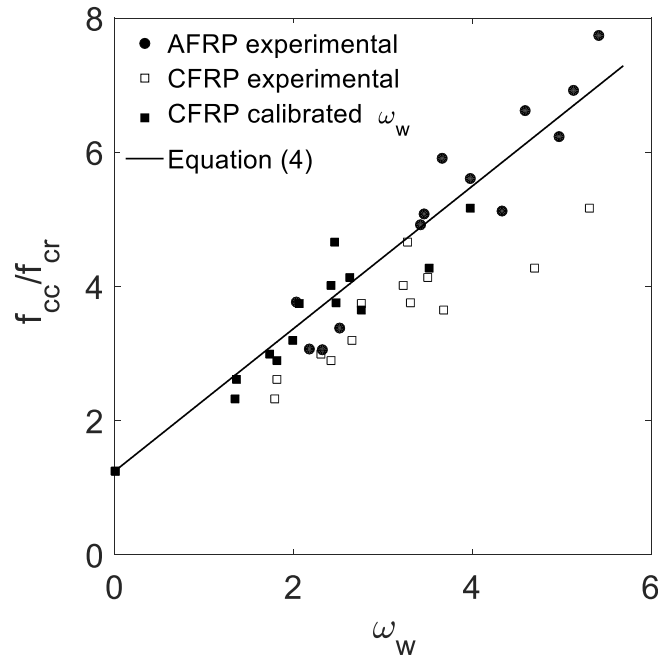
Figure 6. *f_{cc}/f_{cr}* **as function of ω_w with or without the effectiveness factor (β) for AFRP and CFRP**

CRuC

The envelope stress-strain model builds on the bi-linear stress-strain response proposed by

Samaan et al. [32] (also used by Shao et al. [28]), but it accounts for the different $E_{c,0}$, $E_{c,f}$, f_{cc}, ε_{cc},

and f_0. The envelope model comprises an initial modulus of elasticity, a curved transition zone

and a second linear slope, where n_0 is a shape parameter that defines the curvature of the transition

zone and f_0 is the intercept of the second linear branch of the curve with the y-axis (see Figure 5).

The stress-strain response is defined using equation (7).

$$f_c = \frac{(E_{c,0} - E_{c,f})\varepsilon_c}{\left[1 + \left(\frac{(E_{c,0} - E_{c,f})\varepsilon_c}{f_0}\right)^{n_0}\right]^{1/n_0}} + E_{c,f}\varepsilon_c \tag{7}$$

Similar to the work by Shao et al. [28], n_0 was found to be 1.5. Table 2 provides experimental

values for f_0. In the case of CRuC, f_0 was found to be larger than that of conventional confined

concrete due to the higher effectiveness and prompt activation of the FRP, as reported in previous

studies [12,21]. A regression analysis of the experimental data was used to calibrate $E_{c,f}$ and f_0,

which can be determined as a function of the normalized confining stiffness (K_{jn}), as shown in equations (8) and (9), respectively.

$$E_{c,f} = -0.0095(K_{jn})^2 + 6.85(K_{jn}) \tag{8}$$

$$f_0 = f_{co}(-7.35 * 10^{-6}(K_{jn})^2 + 6.9 * 10^{-3}(K_{jn}) + 1) \tag{9}$$

Figure 7 compares average stress-strain curves obtained from the experimental data of individual cylinders subject to monotonic or cyclic loading (see cylinders in Table 2) to the predictions of the stress-strain behaviour of CRuC using equations (1)-(9). The results indicate that the model predicts accurately all the characteristics of the stress-strain curves, although it slightly underestimates the average performance of cylinders confined with four layers of AFRP. This slight inconsistency is due to the difficulty of capturing the variability in the data obtained from cylinders confined with both AFRP/CFRP at different levels of confinement. Nevertheless, overall, the predictions are well within the observed variability of CRuC.
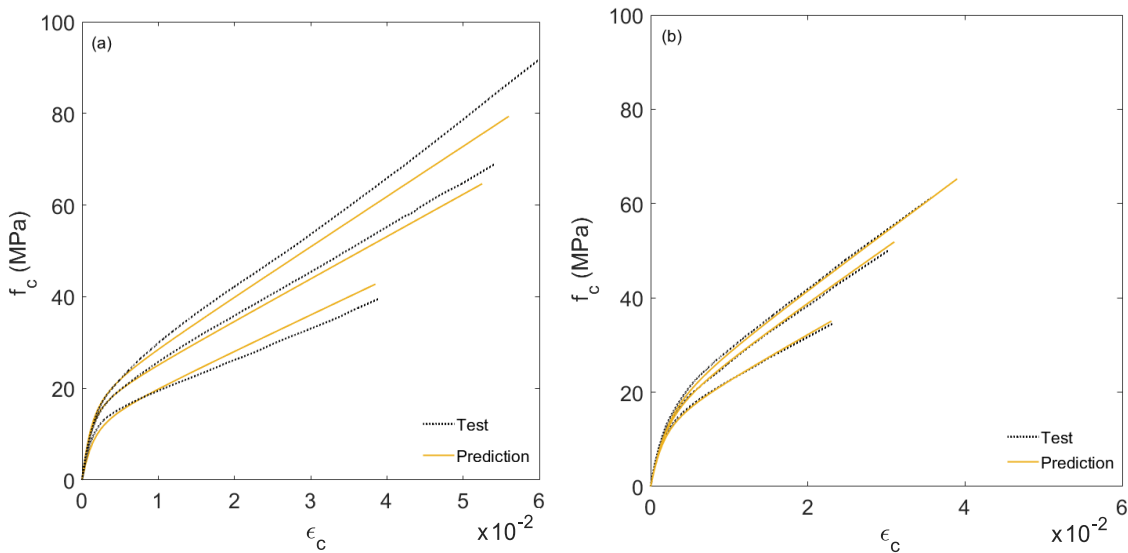
Figure 7. Predictions vs. experimental envelope curve for (a) AFRP and (b) CFRP CRuC cylinders

4.2 Plastic, Unloading and Reloading Strains

Figure 8 shows the relationship between the unloading strain ($\varepsilon_{un,i}$) and the plastic strain ($\varepsilon_{pl,i}$), for CRuC specimens subjected to cyclic loading. As expected, the concrete demonstrates an increase

in both $\varepsilon_{pl,i}$ and $\varepsilon_{un,i}$ with increasing load cycles applied on the cylinders. This is due to an increased damage in the concrete and packing of the material upon the successive loading and unloading. It is also observed that the variation in $\varepsilon_{pl,i}$ as function of $\varepsilon_{un,i}$ was not influenced by the type of confining material or the number of confining layers, since $\varepsilon_{pl,i}$ vs. $\varepsilon_{un,i}$ coincide for all levels of AFRP/CFRP confinement. This agrees with previous research that reported a linear relationship between $\varepsilon_{pl,i}$ and $\varepsilon_{un,i}$ and that found no significant influence of the unconfined concrete strength or confinement pressure on $\varepsilon_{pl,i}$ [25–27]. Based on the data in Figure 8, the variation in $\varepsilon_{pl,i}$ as function of $\varepsilon_{un,i}$ after concrete cracking (for $\varepsilon_{un,i} > \varepsilon_{cr}$), can be predicted using the linear relationship shown in equation (10).

$$\varepsilon_{pl,i} = 4 * \left(0.095\varepsilon_{un,i} - 0.0001\right), \qquad for\ \varepsilon_{un,i} > \varepsilon_{cr} \tag{10}$$
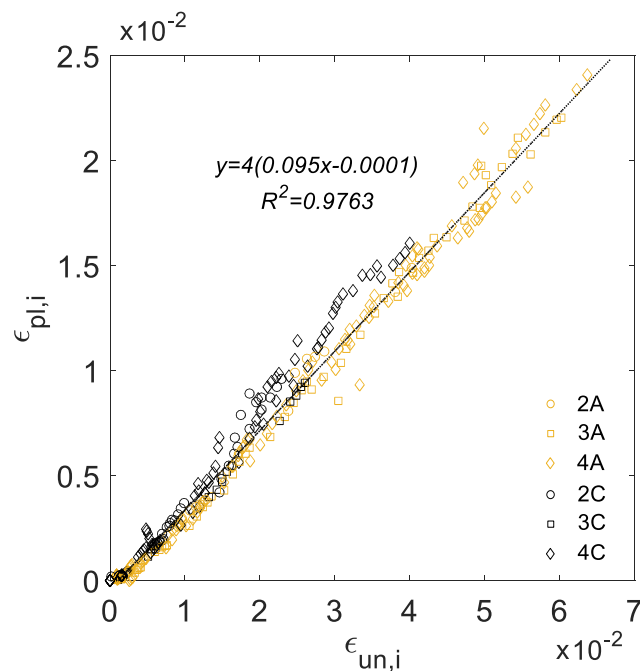
Figure 8. Plastic and unloading strains

Figure 9 presents the relationship between the reloading strain ($\varepsilon_{re,i}$) as function of $\varepsilon_{un,i}$, where $\varepsilon_{re,i}$ was determined as the intersection of the reloading curve of the fifth (final) cycle in each set of cycles with the envelope curve. The experimental data indicates that $\varepsilon_{re,i}$ also increases linearly when compared to with $\varepsilon_{un,i}$ of the designated cycle. Based on this data, $\varepsilon_{re,i}$ can be predicted for

$\varepsilon_{un,i}>\varepsilon_{cr}$ using equation (11). The estimated value of $\varepsilon_{re,i}$ can then be used to determine the reloading stress ($f_{re,i}$) using the envelope response in equation (7).

$$\varepsilon_{re,i} = 1.06\varepsilon_{un,i} + 0.002, \qquad for \; \varepsilon_{un,i} > \varepsilon_{cr} \qquad (11)$$
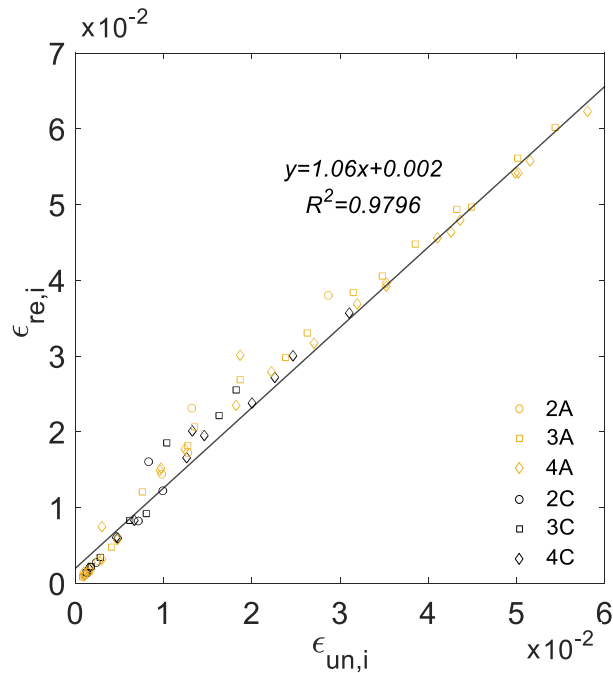
Figure 9. Reloading and unloading strains

4.3 Unloading path

The unloading path was defined by: 1) the unloading strain and stress on the envelope curve, i.e. point ($\varepsilon_{un,i}$, $f_{un,i}$) in Figure 5, and 2) the residual plastic strain ($\varepsilon_{pl,i}$) upon fully unloading the cylinder to zero stress, i.e. point ($\varepsilon_{pl,i}$, 0). Typical unloading curves for cylinders confined with 2 or 4 layers of CFRP/AFRP are shown in Figure 10. With the exception of the initial unloading cycles (prior to the critical stress), all unloading curves of CRuC are non-linear and have higher curvature with increasing unloading strains. Whilst the jacket stiffness does not affect the curvature of the unloading path, the value of $\varepsilon_{un,i}$ (or the maximum strain range) achieved in the cylinder has an effect on the unloading curve. For example, at the 3rd unloading cycle, cylinders with 2 layers of AFRP confinement or 4 layers of AFRP/CFRP confinement show similar unloading path curvature; despite having different $f_{un,i}$ and significantly different confining

stiffness (see K_{jn} in Table 2). These results are consistent with previous research that reports a

non-linear unloading path, which changes its degree of non-linearity as $\varepsilon_{un,i}$ increases [29].
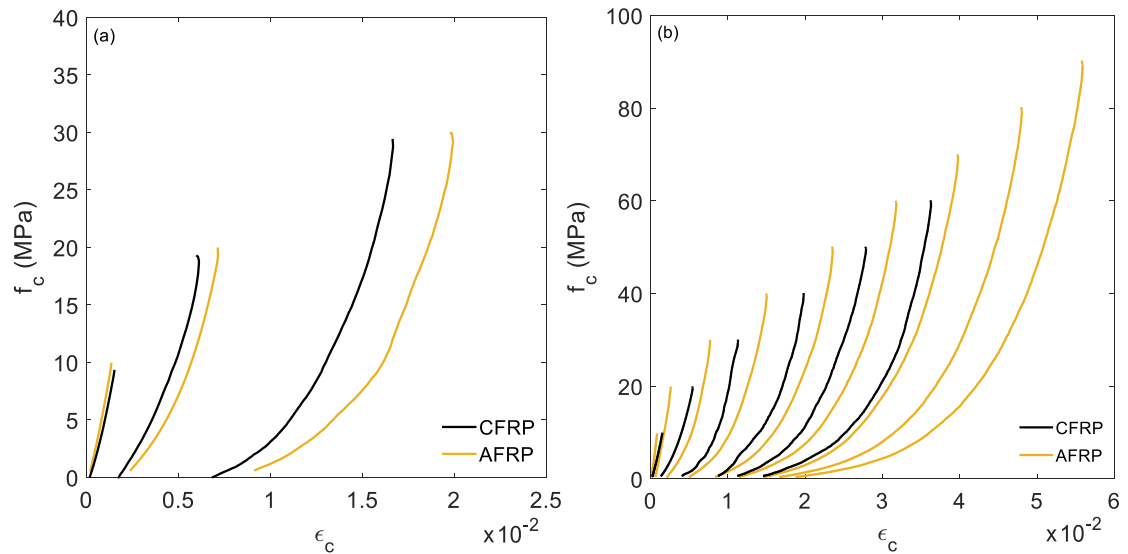
Figure 10. Typical unloading curves for cylinders confined with 2 layers (a) or 4 layers (b) of

AFRP/CFRP

Previous research has used $\varepsilon_{un,i}$ to reflect the degree of damage due to unloading and reloading

cycles [33]. Sima et al. [33] report that the characteristics of unloading and reloading curves

vary with the accumulation of non-recoverable damage in the concrete. For this reason, existing

cyclic models for unconfined and steel-confined concrete could not predict the unloading

behaviour of FRP-confined conventional concrete, due to their inability of capturing the

appropriate damage mechanisms at higher strain values, as reported by Lam and Teng [29]. The

presence of rubber particles, in combination with the large strains that can be developed in

CRuC specimens (>5% [21]) further affects the ways in which the damage accumulates and

cannot be appropriately captured by conventional models.

To generate the unloading curve for each cycle, the model by Shao et al. [28] was calibrated to

the CRuC experimental test data. A polynomial curve (equation (12)) was used to model the

unloading branch of the stress-strain curve.

$$f_c = \frac{(1-x)^m}{(1+kx)^{n_{un,i}}} f_{un,i} \tag{12}$$

where

$$x = \frac{\varepsilon_c - \varepsilon_{un,i}}{\varepsilon_{pl,i} - \varepsilon_{un,i}} \tag{13}$$

and $n_{un,i}$, m and k are empirically calibrated shape parameters.

Using the dataset of this article, a single objective genetic algorithm was used (using the MATLAB® genetic algorithm toolbox [34]) to find the optimal values of $n_{un,i}$, m and k for each set of loading/unloading curves, targeting the minimum difference in area under the curve for the experimental and predicted curves. Based on this analysis it was found that a value of 1 was suitable for *m* and *k*. To account for the effect of the increasing cyclic stress level on the curvature of the unloading curve, $n_{un,i}$ was set to vary with the change in the envelope $\varepsilon_{un,i}$, as shown in equation (14).

$$n_{un,i} = 16(\varepsilon_{un,i})^{0.5} \tag{14}$$

Based on the above equations, the increase in concrete damage (as evidenced by higher $\varepsilon_{un,i}$), leads to a higher value of $n_{un,i}$, which ultimately leads to higher curvature in the unloading curve as evident from equation (12). The unloading curves predicted using equation (12) and the estimated $\varepsilon_{pl,i}$ and $n_{un,i}$ values (equations (10) and (14), respectively) show close correlation with the experimental data, as shown in Figure 11 a and b, for cylinders confined with four layers of AFRP or CFRP respectively.
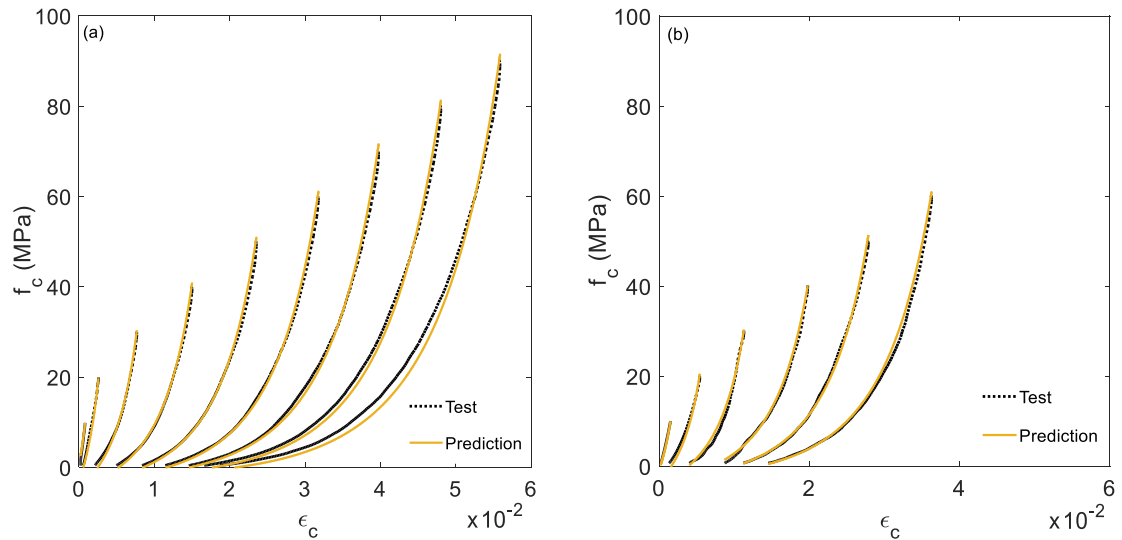
Figure 11. Predictions of unloading curves for RuC specimens confined with four layers of a) AFRP and b) CFRP

4.4   Cyclic stress and stiffness degradation

Figure 12 presents the cyclic stress degradation for RuC cylinders confined with AFRP or CFRP. Such degradation is determined as the ratio of the new stress ($f_{new,i}$) in the reloading curve achieved at the preceding unloading strain ($\varepsilon_{un,i}$) to the preceding unloading stress ($f_{un,i}$) (see Figure 5). For each designated set of cycles, this data was acquired by comparing $f_{new,i}$ of the first loading cycle to $f_{un,i}$ of the last unloading cycle in the preceding set of cycles. For example, the first value of stress degradation in Figure 12 corresponds to $f_{un,i}$ of the final (fifth) unloading cycle of the loading sequence (unloading/reloading) up to 10 MPa and $f_{new,i}$ of the first loading cycle of the subsequent set of cycles (loading to 20 MPa).
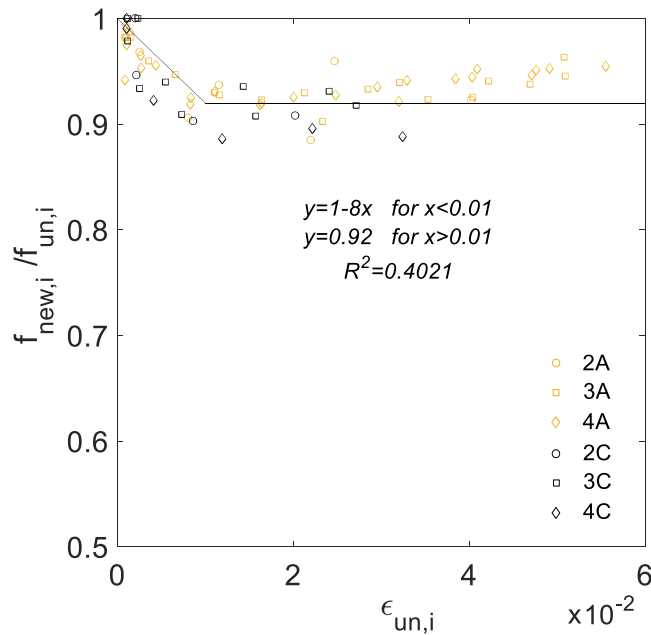
Figure 12. Degradation in stress ($f_{new,i}/f_{un,i}$) of cyclically loaded CRuC cylinders

Figure 12 shows that the number of confining layers or type of confining material does not have

a significant influence on the cylinder cyclic strength degradation. A similar trend was observed

for average data from cylinders confined with two, three or four layers of AFRP or CFRP

sheets. Based on the trends in Figure 12, the variation in $f_{new,i}/f_{un,i}$ with $\varepsilon_{un,i}$ is characterised by :

i) A rapid degradation in strength observed following initial load cycles ($\varepsilon_{un,i}$ up to 0.01), ii) the

curve reaches a plateau at a mean strength degradation of 92%, after which no further decrease

in $f_{new,i}/f_{un,i}$ is observed for increasing $\varepsilon_{un,i}$, and iii) a slight increase in $f_{new,i}/f_{un,i}$ in some

specimens was observed at very large unloading strains ($\varepsilon_{un,i}>0.03$). This can be attributed to i)

the increased material packing upon excessive cycling, which improves the bearing capacity of

confined concrete and ii) the properties of the rubber particles, which control the composite

behaviour after most concrete has crushed. Unlike conventional mineral aggregates, rubber

particles do not undergo significant cyclic damage [36]. On average, the overall degradation in

$f_{new,i}/f_{un,i}$ was less than 10%, whereas the increase in $f_{new,i}/f_{un,i}$ at exceptionally high unloading

strains (e.g. $\varepsilon_{un,i}=0.06$) was less than 4% compared to the value at plateau.

Similar to the research by Lam and Teng [29] and Yu et al. [37], it was found that two values can be reasonably assumed for the degradation in stress at subsequent cycles based on the level of damage (reflected by $\varepsilon_{un,i}$) achieved in the specimens. Hence, $f_{new,i}/f_{un,i}$ can be determined accordingly:

$$\frac{f_{new,i}}{f_{un,i}} \begin{cases} 1 - 8(\varepsilon_{un,i}) & for\ \varepsilon_{un,i} < 0.01 \\ 0.92 & for\ \varepsilon_{un,i} > 0.01 \end{cases} \tag{15}$$

Figure 13 presents the stiffness degradation for AFRP and CFRP CRuC for the first reloading curve of each load level as function of the increase in $\varepsilon_{un,i}$. The stiffness of each reloading curve is determined as the slope ($E_{re,i}$) of the secant connecting the point of complete unloading ($\varepsilon_{pl,i},0$) to the point ($\varepsilon_{un,i}, f_{new,i}$) on the succeeding reloading curve (see Figure 5).
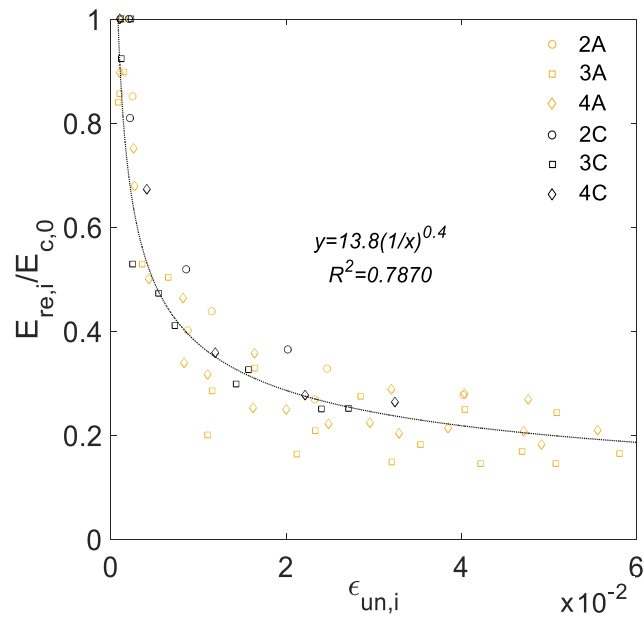
Figure 13. Stiffness degradation in cyclically loaded CRuC cylinders

The results indicate a significant stiffness degradation as the damage increases in the initial load cycles up to $\varepsilon_{un,i} = 0.01$, after which the degradation stabilises at around 20% the initial stiffness of the cylinder ($E_{c,0}$). The type and number of FRP layers did not have a noticeable influence on the stiffness degradation, which was mainly an influence of the level of axial strain achieved in

the cylinders ($\varepsilon_{un,i}$). Based on the data in Figure 13, the stiffness degradation for the initial cycle of each load level can be determined using:

$$E_{re,i} = 13.8 E_{c,0} \left(\frac{1}{\varepsilon_{un,i}} \right)^{0.4} \tag{16}$$

4.5 Reloading curve

The reloading path was attained by reloading from ($\varepsilon_{pl,i}$, 0) up to the stress level of the loading pattern (described in the *Experimental Programme* section). Due to the stress and stiffness degradation following each loading cycle, a lower stress ($f_{new,i}$) is achieved in the reloading curve at the initial unloading strain ($\varepsilon_{un,i}$). The intersection of the reloading curve with the envelope is denoted by ($\varepsilon_{re,i}$, $f_{re,i}$), as indicated in Figure 5. A linear relationship has been shown to adequately model the reloading curves of conventional FRP-confined concrete [33,38],. Nevertheless, reloading curves of CRuC are highly non-linear, particularly at higher stress levels (refer to Figure 4) and therefore conventional models cannot be used. This is attributed to the significantly large axial strains and the damage accumulated in CRuC, as previously described in the *Unloading Path* section.

The CRuC reloading curves are characterised by a double curvature comprising a soft initial part (pinching), which stiffens as the curve approaches the former unloading strain, followed by softening as the curves approaches the designated stress level at a higher strain the previous unloading strain ($\varepsilon_c > \varepsilon_{un,i}$). This pinching behaviour is more evident as the unloading strain increases. The soft behaviour in the initial part of the reloading curve can be attributed to the closure of cracks (which increase at higher strain levels [28]), and to the mechanical properties of the rubber particles, which compressive stress-strain curve is characterised by an initial hardening [36].

To accurately model the shape of the reloading curve, the inflection point ($\varepsilon_{inf,i}$, $f_{inf,i}$) at the change in gradient from strain hardening to softening was identified by determining the

maximum of the derivative function ($df_c/d\varepsilon_c$) of the reloading curve stress-strain relationship. It was found that for all reloading curves, the inflection point in the reloading curve was linearly increasing with $\varepsilon_{un,i}$, as shown in Figure 14 a and b.
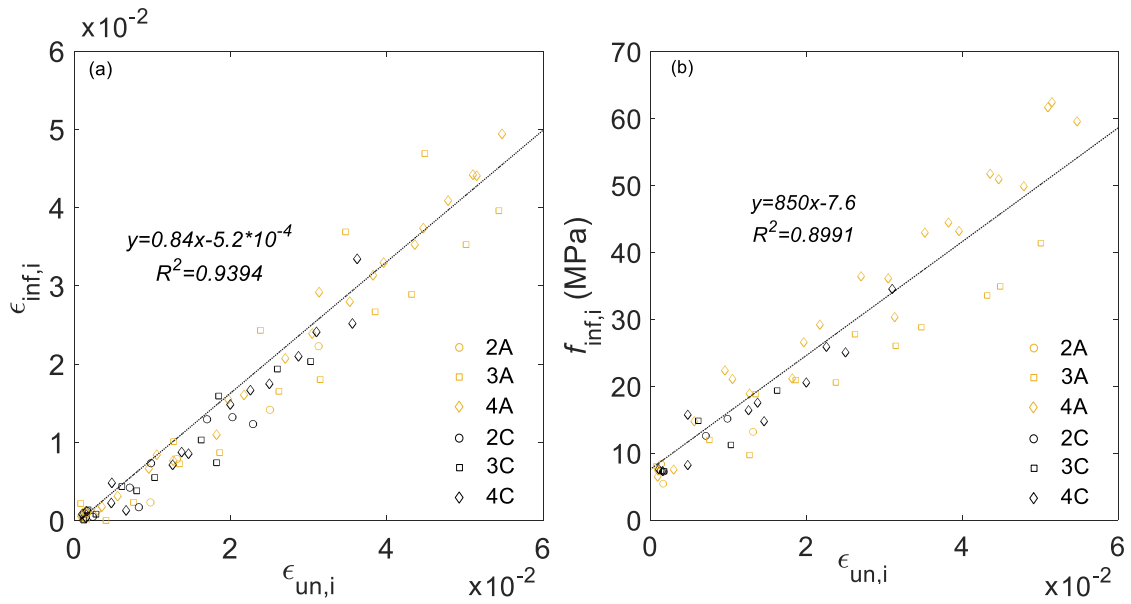
Figure 14. Inflection strain (a) and stress (b) as function of $\varepsilon_{un,i}$

Based on the above data, the coordinates of the inflection point ($\varepsilon_{inf,i}$, $f_{inf,i}$), can be calculated using:

$$\varepsilon_{inf,i} = 0.84\varepsilon_{un,i} - 5.2\text{x}10^{-4}, \qquad for \ \varepsilon_{un,i} > \varepsilon_{cr} \qquad (17)$$

$$f_{inf,i} = 850\varepsilon_{un,i} + 7.6, \qquad for \ \varepsilon_{un,i} > \varepsilon_{cr} \qquad (18)$$

This article uses two non-linear curves to represent the hardening curve, limited by ($\varepsilon_{inf,i}$, $f_{inf,i}$), then the softening curve of CRuC reloading up to its intersection with the envelope ($\varepsilon_{re,i}$, $f_{re,i}$).

4.5.1 Reloading part 1: Hardening curve

To generate the first portion of the reloading curve, the polynomial curve by Shao et al. [28], was also used with the maximum stress (f_c) and boundary conditions (for x) modified to predict the curve up to ($\varepsilon_{inf,i}$, $f_{inf,i}$) as shown in equations (19) and (20), respectively.

$$f_c = \frac{(1-x)^m}{(1+kx)^{n_{re,i}}} f_{inf,i} \tag{19}$$

$$x = \frac{\varepsilon_c - \varepsilon_{inf,i}}{\varepsilon_{pl,i} - \varepsilon_{inf,i}} \tag{20}$$

The shape parameters (m, $n_{re,i}$ and k) were calibrated empirically using the first part of the reloading curves from the tested specimens up to ($\varepsilon_{inf,i}$, $f_{inf,i}$). This was achieved using a single objective genetic algorithm, as described in the "*Unloading path*" section.

Based on this analysis, both m and k were found to be 1, whereas $n_{re,i}$ was set to vary with the change in the envelope $\varepsilon_{un,i}$, as shown in equation (21).

$$n_{re,i} = 55\left(\varepsilon_{un,i}\right)^{1.3} \tag{21}$$

4.5.2 Reloading part 2: Softening curve

A regression analysis was implemented to determine the intersection of the reloading curve with the envelope ($\varepsilon_{re,i}$, $f_{re,i}$). The second part of the curve is determined using the same parabolic function that was used to determine the envelope curve (see equation (7)), but with updated parameters to suit each cycle. For convenience, the stress-strain response for the softening part of the reloading curve is reported below:

$$f_c = \frac{\left(E_{c,i} - E_{c,f}\right)\varepsilon_c}{\left[1 + \left(\frac{\left(E_{c,i} - E_{c,f}\right)\varepsilon_c}{f_{0,i}}\right)^{n_{0,i}}\right]^{1/n_{0,i}}} + E_{c,f}\varepsilon_c \tag{22}$$

In this instance, $E_{c,i}$ represents the initial modulus of elasticity of the softening part of the reloading curve estimated by the slope or derivative ($df_c/d\varepsilon_c$) of the hardening curve (part 1) at point ($\varepsilon_{inf,i}$, $f_{inf,i}$), shown in equation (23); $f_{0,i}$, is the intersecting point of the vertical at ($\varepsilon_{inf,i}$, $f_{inf,i}$)

with the envelope curve; and $n_{0,i}$ the curvature of the transition zone between $(\varepsilon_{un,i}, f_{new,i})$ and $(\varepsilon_{re,i}, f_{re,i})$. $E_{c,f}$, which denotes the slope of the linear portion of the envelope curve, can be determined as function of the confining stiffness using equation (8).

$$E_{c,i} = \frac{1 + n_{re,i}}{\varepsilon_{inf,i} - \varepsilon_{pl,i}} f_{inf,i} \qquad (23)$$

Based on the regression of the experimental data, $f_{0,i}$ and $n_{0,i}$ can be estimated as function of $\varepsilon_{un,i}$ using equations (24) and (25).

$$f_{0,i} = 0.25 K_{jn} . \varepsilon_{un,i} + 8.1 \qquad (24)$$

$$n_{0,i} = 2132 (\varepsilon_{un,i})^2 - 255 \varepsilon_{un,i} + 8.5 \qquad (25)$$

Whilst the increase in $\varepsilon_{un,i}$ led to an increased curvature (controlled by an increase in $n_{re,i}$) in the slope of the initial (hardening) part of the curve, the softening part of the reloading curve was found to be less linear for higher axial strain levels. This is taken into account by using the variable $n_{0,i}$, which is set to develop a lower curvature at higher unloading strains, as shown in equation (25).

Figure 15 a and b compare the experimental data and the predictions of the model for the two portions of the reloading curves for cylinders confined with 4 layers of AFRP or CFRP, respectively. The predictions in this figure were calculated according to equations 17-25.
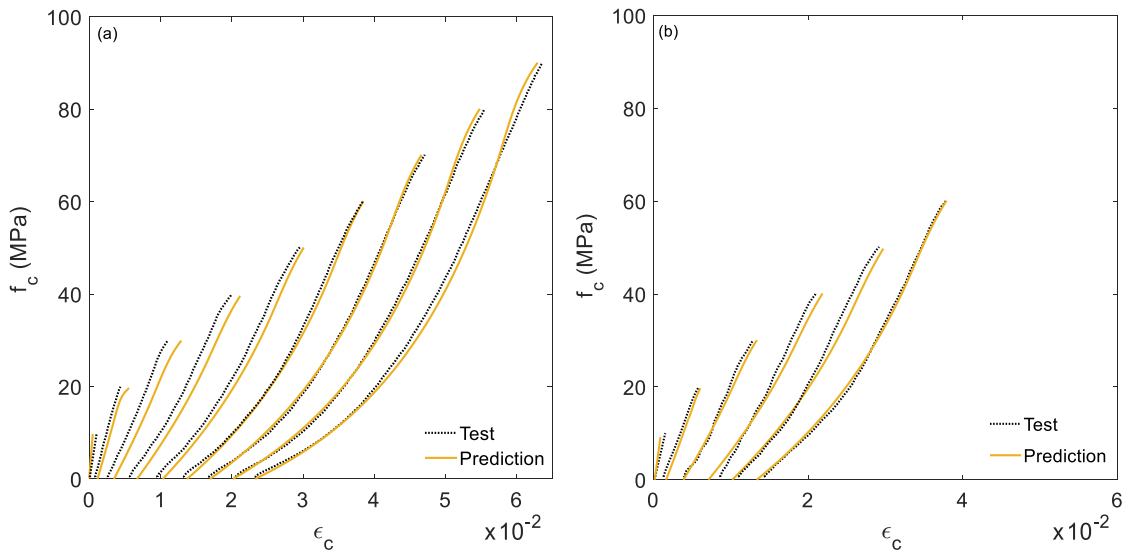
Figure 15. Predictions of reloading curves for RuC specimens confined with four layers of a) AFRP and b) CFRP

5 MODEL PREDICTIONS

Figure 16 a and b show the predicted response of the cyclically loaded RuC cylinder confined with 4 layers of AFRP or CFRP, respectively. The above response was assembled by implementing equations (1-25) to generate the loading, unloading and reloading cycles sequentially. The different cycles were simulated following the same protocols as in the experimental tests.
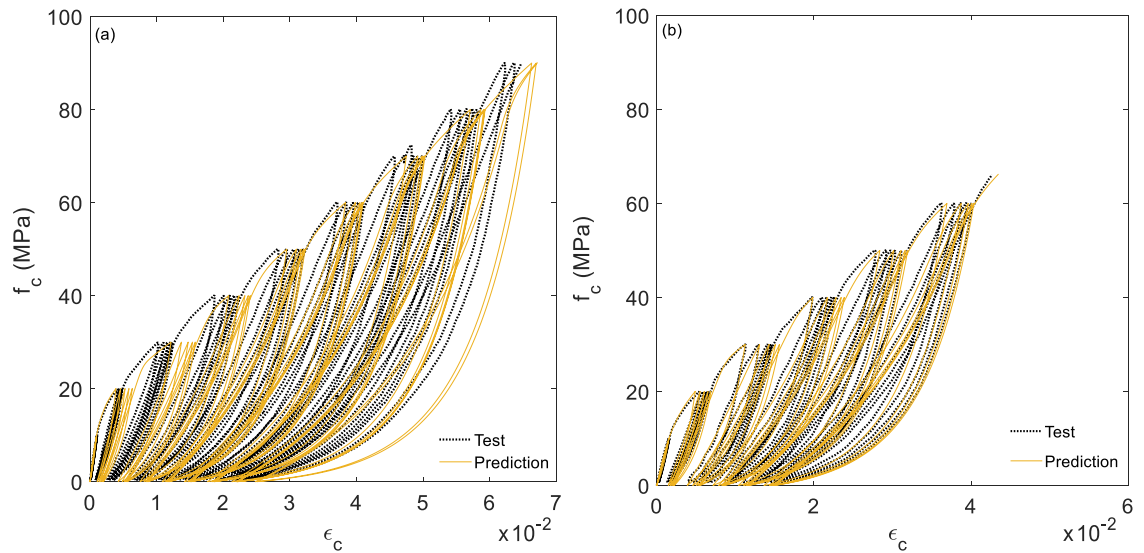
Figure 16. Predictions of cyclic behaviour of RuC specimens confined with four layers of AFRP (a) or CFRP (b)

The results indicate that, in general, the model can accurately predict the majority of loading and unloading cycles of CRuC cylinders confined with four layers of AFRP or CFRP. The slight discrepancy between the experimental and predicted curves (mainly observed in CRuC confined with 4 layers of AFRP) can be attributed to the difficulty of capturing the variability in the data obtained from AFRP and CFRP CRuC cylinders with different levels of confinement. Nevertheless, overall, the predictions fall within the observed variability of CRuC.

It should be noted that the proposed model is only applicable for FRP CRuC with particularly high rubber contents (i.e. replacing 60% of the total aggregate content). Future research is still needed to validate the model against other experimental data for CRuC with similar rubber contents, once these become available. The suitability of using this model to predict the behaviour of CRuC with lower rubber contents, different AFRP/CFRP strengthening systems and other confining materials (e.g. Glass and/or Basalt FRP) must also be investigated. Further work is also needed to validate the ability of the model to capture the behaviour of CRuC subjected to a high number of load cycles as well as the effect of partial unloading/loading. Finally, it will be useful to compare the performance of cyclically loaded CRuC (e.g. the strength and stiffness degradation

or energy dissipation per cycle) to that of FRP-confined conventional concrete subject to cyclic loading, to further evaluate the influence of rubber on confined concrete cyclic performance.

6   CONCLUSIONS

This paper presented results from uniaxial compressive tests on CRuC cylinders with high volumes of tyre rubber (60% total aggregate replacement). Parameters investigated included: i) type of confining material (AFRP or CFRP sheets), ii) number of FRP layers (2, 3, or 4 layers), and iii) load pattern (monotonic or cyclic). The key parameters that control the cyclic behaviour of CRuC were investigated and a design-oriented model was proposed for monotonically or cyclically loaded deformable elements made with FRP-CRuC.

From the test results and analysis presented, the following conclusions can be drawn:

1) The envelope stress-strain curves of cyclically loaded CRuC cylinders were similar to the stress-strain behaviour of monotonically loaded cylinders. The loading history did not significantly influence f_{cc} or ε_{cc} values achieved in monotonically/cyclically loaded specimens as all cylinders failed by rupture in the FRP sheets. The predictive equations for the strength and strain effectiveness of monotonically loaded CRuC can be applied to predict the envelope curve of cyclically loaded CRuC cylinders.

2) The variation in $\varepsilon_{pl,i}$ as function of $\varepsilon_{un,i}$ was found to be linear. This relationship is similar to that observed in conventional FRP-confined concrete.

3) Overall the strength degradation was minor (less than 10%), characterised by a sharp initial degradation for $\varepsilon_{un,i}$ up to 0.01, followed by a plateau. A significant degradation in stiffness is observed up to $\varepsilon_{un,i} = 0.01$, after which the stiffness degradation stabilises at around 20% of the initial stiffness of the cylinder ($E_{c,0}$).

4) The number of FRP confining layers did not significantly influence the parameters of the unloading/reloading curves such as the strength/stiffness degradation or the relationships

of $\varepsilon_{pl,i}$, $\varepsilon_{re,i}$ or $\varepsilon_{inf,i}$ with ε_{un}, which were found to follow similar trend-lines for all confining layers.

5) The unloading curve has a non-linear shape, which increases in curvature at higher $\varepsilon_{un,i}$. This was accurately captured by modifying the parameter ($n_{un,i}$) in the predictive equation by Shao et al. [28].

6) The reloading curve is characterised by a double curvature shape characterised by an initial hardening followed by softening as the curve approaches the preceding unloading strain ($\varepsilon_{un,i}$). The initial (hardening) of the curve was predicted using a similar parabolic function to that used to predict the unloading curve but with a modified parameter ($n_{re,i}$). To maintain continuity between the two parts of the reloading curve, the slope of the predicted hardening curve at the inflection point ($E_{c,i}$) was then used to predict the second (softening) part of the curve using another parabolic function (see equation (22)).

7) The cyclic model predicts with reasonable accuracy the behaviour of AFRP/CFRP CRuC.

7   REFERENCES

[1]   M. Ismail, A. Hassan, Ductility and Cracking Behavior of Reinforced Self-Consolidating Rubberized Concrete Beams, J. Mater. Civ. Eng. (2016) 4016174. doi:10.1061/(ASCE)MT.1943-5533.0001699.

[2]   A.C. Ho, A. Turatsinze, R. Hameed, D.C. Vu, Effects of rubber aggregates from grinded used tyres on the concrete resistance to cracking, J. Clean. Prod. 23 (2012) 209–215.

[3]   K.S. Son, I. Hajirasouliha, K. Pilakoutas, Strength and deformability of waste tyre rubber-filled reinforced concrete columns, Constr. Build. Mater. 25 (2011) 218–226.

[4]   L. Zheng, X.S. Huo, Y. Yuan, Strength, modulus of elasticity, and brittleness index of

rubberized concrete, J. Mater. Civ. Eng. 20 (2008) 692–699.

[5]   A. Benazzouk, O. Douzane, T. Langlet, K. Mezreb, J.M. Roucoult, M. Quéneudec, Physico-mechanical properties and water absorption of cement composite containing shredded rubber wastes, Cem. Concr. Compos. 29 (2007) 732–740.

[6]   D. Flores-Medina, N.F. Medina, F. Hernández-Olivares, Static mechanical properties of waste rests of recycled rubber and high quality recycled rubber from crumbed tyres used as aggregate in dry consistency concretes, Mater. Struct. 47 (2014) 1185–1193.

[7]   H.A. Toutanji, The use of rubber tire particles in concrete to replace mineral aggregates, Cem. Concr. Compos. 18 (1996) 135–139.

[8]   E. Güneyisi, M. Gesoğlu, T. Özturan, Properties of rubberized concretes containing silica fume, Cem. Concr. Res. 34 (2004) 2309–2317.

[9]   N.N. Eldin, A.B. Senouci, Measurement and prediction of the strength of rubberized concrete, Cem. Concr. Compos. 16 (1994) 287–298.

[10]   S. Raffoul, R. Garcia, K. Pilakoutas, M. Guadagnini, N.F. Medina, Optimisation of rubberised concrete with high rubber content: An experimental investigation, Constr. Build. Mater. 124 (2016). doi:10.1016/j.conbuildmat.2016.07.054.

[11]   Z.K. Khatib, F.M. Bayomy, Rubberized Portland cement concrete, J. Mater. Civ. Eng. 11 (1999) 206–213.

[12]   G. Li, S.-S. Pang, S.I. Ibekwe, FRP tube encased rubberized concrete cylinders, Mater. Struct. 44 (2011) 233–243.

[13]   O. Youssf, M.A. ElGawady, J.E. Mills, X. Ma, An experimental investigation of crumb rubber concrete confined by fibre reinforced polymer tubes, Constr. Build. Mater. 53 (2014) 522–532.

[14]   A.P.C. Duarte, B.A. Silva, N. Silvestre, J. de Brito, E. Júlio, J.M. Castro, Experimental study on short rubberized concrete-filled steel tubes under cyclic loading, Compos. Struct. (2015).

[15]   A.P.C. Duarte, B.A. Silva, N. Silvestre, J. de Brito, E. Júlio, J.M. Castro, Tests and design of short steel tubes filled with rubberised concrete, Eng. Struct. 112 (2016) 274–286.

[16]   A. Moustafa, M.A. ElGawady, Strain Rate Effect on Properties of Rubberized Concrete

Confined with Glass Fiber–Reinforced Polymers, J. Compos. Constr. (2016) 4016014.

[17]   L. Lam, J.G. Teng, Design-oriented stress–strain model for FRP-confined concrete, Constr. Build. Mater. 17 (2003) 471–489.

[18]   S. Raffoul, R. Garcia, D. Escolano-Margarit, M. Guadagnini, I. Hajirasouliha, K. Pilakoutas, Behaviour of unconfined and FRP-confined rubberised concrete in axial compression, Constr. Build. Mater. 147 (2017) 388–397. doi:10.1016/j.conbuildmat.2017.04.175.

[19]   S. Raffoul, D. Escolano-Margarit, R. Garcia, M. Guadagnini, K. Pilakoutas, Constitutive model for passively confined rubberized concrete, Submitt. to J. Compos. Constr. (2017).

[20]   K. Pilakoutas, S. Raffoul, P. Papastergiou, R. Garcia, M. Guadagnini, I. Hajirasouliha, A STUDY OF THE REUSE OF ALL TYRE COMPONENTS IN CONCRETE: THE ANAGENNISI PROJECT, in: Int. Conf. Sustain. Struct. Concr., La Plata, Argentina, Argentina, 2015.

[21]   S. Raffoul, R. Garcia, D. Escolano-Margarit, M. Guadagnini, I. Hajirasouliha, K. Pilakoutas, Behaviour of unconfined and FRP-confined rubberised concrete in axial compression, Constr. Build. Mater. 147 (2017) 388–397. doi:10.1016/j.conbuildmat.2017.04.175.

[22]   S. Matthys, H. Toutanji, L. Taerwe, Stress – Strain Behavior of Large-Scale Circular Columns Confined with FRP Composites, J. Struct. Eng. 132 (2006) 123–133. doi:10.1061/(ASCE)0733-9445(2006)132:1(123).

[23]   L. Lam, J.G. Teng, Ultimate condition of fiber reinforced polymer-confined concrete, J. Compos. Constr. 8 (2004) 539–548.

[24]   J.B. Mander, M.J.N. Priestley, R.Park, Theoretical Stress Strain Model for Confined Concrete, J. Struct. Eng. 114 (1988) 1804–1825. doi:10.1061/(ASCE)0733-9445(1988)114:8(1804).

[25]   R. Abbasnia, H. Ziaadiny, Behavior of concrete prisms confined with FRP composites under axial cyclic compression, Eng. Struct. 32 (2010) 648–655. doi:10.1016/j.engstruct.2009.11.011.

[26]   T. Ozbakkaloglu, E. Akin, Behavior of FRP-Confined Normal- and High-Strength Concrete under Cyclic Axial Compression, J. Compos. Constr. 16 (2012) 451–463.

doi:10.1061/(ASCE)CC.1943-5614.0000273.

[27]   L. Lam, J.G. Teng, C.H. Cheung, Y. Xiao, FRP-confined concrete under axial cyclic compression, Cem. Concr. Compos. 28 (2006) 949–958.

[28]   Y. Shao, Z. Zhu, A. Mirmiran, Cyclic modeling of FRP-confined concrete with improved ductility, Cem. Concr. Compos. 28 (2006) 959–968. doi:10.1016/j.cemconcomp.2006.07.009.

[29]   L. Lam, J.G. Teng, Stress-strain model for FRP-confined concrete under cyclic axial compression, Eng. Struct. 31 (2009) 308–321. doi:10.1016/j.engstruct.2008.08.014.

[30]   J. Dai, Y. Bai, J. Teng, Behavior and modeling of concrete confined with FRP composites of large deformability, J. Compos. Constr. 15 (2011) 963–974. doi:10.1061/(ASCE)CC.1943-5614.0000230.

[31]   J.G. Teng, T. Jiang, L. Lam, Y.Z. Luo, Refinement of a design-oriented stress–strain model for FRP-confined concrete, J. Compos. Constr. 13 (2009) 269–278.

[32]   B. Michel Samaan, A. Mirmiran, M. Shahawy, MODEL OF CONCRETE CONFINED BY FIBER COMPOSITES, (n.d.).

[33]   J.F. Sima, P. Roca, C. Molins, Cyclic constitutive model for concrete, Eng. Struct. 30 (2008) 695–706. doi:10.1016/j.engstruct.2007.05.005.

[34]   A.J. Chipperfield, P.J. Fleming, The MATLAB genetic algorithm toolbox, (1995).

[35]   J.B. Mander, M.J.N. Priestley, R. Park, Theoretical stress-strain model for confined concrete, J. Struct. Eng. 114 (1988) 1804–1826.

[36]   P.K. Freakley, A.R. Payne, Theory and practice of engineering with rubber, Applied Science Publishers London, 1978.

[37]   T. Yu, B. Zhang, J.G. Teng, Unified cyclic stress–strain model for normal and high strength concrete confined with FRP, Eng. Struct. 102 (2015) 189–201.

[38]   D. Palermo, F.J. Vecchio, Compression Field Modeling of reinforced concrete subjected to reverse loading: Verification, ACI Struct. J. 101 (2004) 155–164. doi:10.14359/12803.

Chapter 6

Summary, conclusions and recommendations for future research

6.1   SUMMARY AND CONCLUSIONS

The aim of this research was to advance the understanding of the behaviour of RuC with or without external FRP-confinement and to develop constitutive models that can be implemented in FEA software and in design guidelines to enable the use of CRuC in high-strength, high deformability structural applications.

This aim was achieved through extensive experimental and analytical work on the fresh and hardened mechanical properties of RuC and on the stress-strain behaviour of RuC externally confined with FRP under monotonic and cyclic loading.

This chapter summarises the main conclusions from this thesis and recommends future research in the field. All of the research objectives set out in Chapter 1 were achieved.

6.1.1 Optimisation of RuC

More than 40 rubberised concrete mixes were examined to develop an understanding of the effect of rubber and other mix parameters on RuC fresh properties and short-term compressive behaviour. The following conclusions are drawn:

Effect of rubber replacement type and content

- ❖ The incorporation of high rubber contents in concrete leads to reduced concrete workability and a lower hardened density and compressive strength.

- ❖ The type of rubber replacement (fine or coarse aggregate replacement) did not significantly affect the strength of RuC. The strength appears to be merely influenced by the total volume of rubber incorporated as an aggregate replacement in the mix.

- ❖ The replacement of high levels of fine aggregate with rubber leads to slightly inferior workability, compared to a similar volume of coarse aggregate replacement.

- ❖ The combined replacement of fine and coarse aggregates was deemed most suitable to achieve high rubber contents in the mix with minor effect on the concrete workability.

Effect of mix optimisation

❖ The optimisation of the concrete mix parameters mitigates the detrimental effects of rubber on some concrete fresh and mechanical properties.

❖ Whilst the majority of RuC mixes (with or without optimised parameters) had suitable slump and flowability for casting purposes, it is difficult to achieve highly flowable mixes without the risk of compromising concrete cohesion. Mixes without optimised parameters often experienced segregation, a lack of cohesion and bleeding. This is mainly due to the relatively low density of rubber and its hydrophobic nature, concrete porosity and lack of appropriate particle grading.

❖ Optimising RuC enabled the use of high rubber contents in the concrete mix (replacing up to 60% of the total aggregate volume) while achieving adequate workability and a strength of around 7 MPa at 7 days.

❖ The use of silica fume and pulverised fuel ash as a replacement of 20% of the cement mass improved fresh concrete flow by 20% and its compressive strength by 42%. This is due to their filling effect, which improved the packing of the concrete constituents as well as their pozzolanic reaction with the cement hydration products.

❖ Pre-washing the rubber with water or pre-coating with silica fume did not significantly change RuC performance.

❖ SEM imaging of RuC sample reveals a gap between the rubber and the rubber cement paste interphase transition zone (ITZ). This effect was more evident in the vicinity of larger rubber particles. The gap was less pronounced in the presence of silica fume and pulverised fuel ash (as observed in the optimised mix).

6.1.2 Unconfined and FRP-confined RuC

Sixty unconfined and six FRP-confined RuC cylinders cast using the optimised mix were tested in uniaxial compression to examine their stress-strain behaviour.

Unconfined RuC

❖ RuC with low rubber content (<18% of the total aggregate volume) exhibits similar strain behaviour to that of conventional concrete. Nevertheless, even such small rubber contents lead to undesirable reductions in strength. For example, a modest 20% replacement of the coarse aggregate volume with rubber reduced the RuC strength by 40%.

❖ The stress-strain behaviour of RuC is modified more significantly for high rubber contents (>27% of the total aggregate). At this replacement level, a significant reduction in axial strains and increase in the lateral strains at peak were observed, as well as an earlier initiation of micro-cracking.

❖ The rate of reduction in strength is faster at low rubber contents, and appears to stabilise at rubber contents >40% of the total aggregate volume.

❖ The strength reduction in RuC is a function of the total aggregate volume replaced with rubber.

❖ The use of high rubber contents leads to a considerable increase in the concrete lateral dilation. For mixes with 60% total aggregate volume replacement, the lateral strains increased by up to 300% (around 3500με), when compared to a control mix.

❖ Whilst the abovementioned high lateral strains are unfavourable in unconfined RuC, they can be utilised to activate early the FRP (passive) confining pressure, which is influenced by the concrete lateral expansion.

Confined RuC

❖ The confinement of RuC with high rubber contents (60% total aggregate replacement with rubber) using three layers of AFRP leads to strength effectiveness of 10.1 (compressive strength=75 MPa) and ultimate axial strain capacity of 5%, i.e. around 14 times the axial strain capacity of conventional concrete.

❖ Rubber inclusions significantly influence the volumetric behaviour of CRuC. Specimens with two layers of AFRP experienced some expansion. However, the use of three layers of AFRP confinement leads to continuous volumetric contraction. This may be attributed to the flowable nature of the rubber, which can fill the voids in heavily confined concrete.

❖ The majority of specimens failed by rupture in the FRP, nevertheless, premature failure was occasionally observed due to the failure of the metal straps at the top or bottom of the cylinders.

6.1.3 Monotonic behaviour of CRuC

A total of 38 AFRP and CFRP CRuC specimens were tested under monotonic and cyclic loading to investigate the effect of the type and amount of confinement, as well as cylinder size on their stress-strain performance. A constitutive model was developed.

Experimental observations

❖ The use of four layers of AFRP to confine RuC with high rubber volumes leads to compressive strength of 100 MPa and very high axial deformations (>6%). Such properties are suitable for many structural applications where high deformability is required.

❖ The confinement of the top and bottom of the cylinders using aluminium caps is more reliable, compared to the metal straps used in Chapter 3. The caps were also successful

in reducing bending during the axial loading of the cylinders due to poor quality surfaces. All specimens failed by rupture in the FRP.

❖ Axial strains from vertical strain gauge readings and global (laser) measurements were comparable up to the initiation of unstable cracking in the cylinders. After cracking the strain gauges led to spurious results due to excessive localised bulging at specimen mid-height.

❖ RuC activates the confinement earlier, when compared to conventional FRP-confined concrete, thus leading to a delay in critical stress as well as high strength and strain enhancement ratios (11 and 45, respectively, for cylinders confined with 4 layers AFRP).

❖ CFRP CRuC exhibits inferior performance (lower stress and strain enhancement ratios), compared to AFRP CRuC with identical confining stiffness.

❖ No significant size effect was observed when comparing the stress-strain behaviour of small (φ100×200mm) and large (φ150×300mm) cylinders with similar confining pressure.

Constitutive model

❖ Based on comparisons between test data, existing stress-strain models for conventional FRP-confined concrete cannot predict the behaviour of CRuC.

❖ A new analytical model was developed based on an active confinement model by Mander, Priestley and R.Park (1988) and a refined iterative procedure (previously proposed by Papastergiou (2010)) to predict both lateral and axial stress-strain curves simultaneously.

❖ The analytical model provides good predictions of the experimental results for both AFRP and CFRP CRuC cylinders. The average standard deviation of predictions of

ultimate stress and strain was less than 5%, which falls within the expected variability of concrete.

❖ The model slightly overestimates the strength and strain enhancement ratios (f_{cc}/f_{cr} and $\varepsilon_{cc}/\varepsilon_{cr}$, respectively) for lightly confined cylinders (two layers AFRP) and slightly overestimates them for heavily confined cylinders (four layers CFRP). This is due to the difficulty of finding unique relations for f_{cr}, ε_{cr}, f_{cc}/f_{cr} and $\varepsilon_{cc}/\varepsilon_{cr}$ that can provide accurate predictions at all levels of confinement.

❖ A reduction factor (β) has been implemented in the model predictions to account for the lower effectiveness observed in CFRP CRuC compared to AFRP CRuC with identical confining stiffness.

6.1.4 Cyclic behaviour of RuC

The key parameters that govern the cyclic behaviour of CRuC were investigated and were used to develop a new constitutive model to predict the behaviour of FRP CRuC subjected to cyclic load.

Experimental observations

❖ The stress-strain behaviour of monotonically loaded cylinders was similar to the envelope curve of cyclically loaded cylinders.

❖ The load history (cyclic/monotonic) did not have a significant influence on the ultimate stress and strain values achieved in the AFRP/CFRP CRuC cylinders. All cylinders failed abruptly by rupture in the FRP sheets. Hence, predictive equations for strength and strain effectiveness previously developed for monotonically loaded cylinders can be applied for the cyclic loaded cylinders.

❖ Similar to cyclically loaded FRP-confined conventional concrete, the variation in the plastic strain ($\varepsilon_{pl,i}$) as function of unloading strain ($\varepsilon_{un,i}$) in cyclically loaded CRuC follow a linear trend.

❖ The variation in the reloading strains ($\varepsilon_{re,i}$) as function of $\varepsilon_{un,i}$ can be approximated with a linear relationship.

❖ The unloading path of CRuC is characterised by a non-linear shape. This non-linearity increases significantly at high $\varepsilon_{un,i}$.

❖ Overall, strength degradation due to cyclic loading is minor (less than 10%). A sharp degradation in strength is observed initially (for $0<\varepsilon_{un,i}<10,000\mu\varepsilon$), followed by a plateau.

❖ A significant degradation in stiffness (around 70% reduction) occurs up to $\varepsilon_{un,i}=10,000\mu\varepsilon$ after which the stiffness stabilises at around 80% of the concrete initial stiffness.

❖ The reloading curve is characterised by a double curvature shape including a hardening initial part followed by softening as the curve approaches the previous $\varepsilon_{un,i}$. The relationship between the inflection point ($\varepsilon_{inf,i}, f_{inf,i}$) and $\varepsilon_{un,i}$ of all cycles was linear.

❖ The number of confining layers or the type of confinement did not have a significant influence on the main parameters governing the shape of the unloading/reloading curves, such as $\varepsilon_{pl,i}$, $\varepsilon_{re,i}$ or $\varepsilon_{inf,i}$, the unloading/reloading curvature, or the strength and stiffness degradation. It was found that these parameters were mainly influenced by level of axial strain achieved in the cylinder at unloading ($\varepsilon_{un,i}$).

Constitutive model

❖ A new bi-linear design-oriented model based on the model by Shao, Zhu and Mirmiran (2006) was calibrated to accurately predict the entire envelope stress-strain response of the CRuC cylinder.

❖ The unloading curve was accurately predicted using the polynomial curve by Shao, Zhu and Mirmiran (2006). An additional parameter was used to account for the increase in curvature at high levels of axial strains in the concrete.

❖ The reloading curve was modelled using two discrete parabolic functions to predict the hardening and softening parts of the curve.

❖ The cyclic model provides accurate predictions of the behaviour of cyclically loaded RuC cylinders with high rubber contents confined with ARRP/CFRP sheets.

6.2   RECOMMENDATIONS FOR FUTURE RESEARCH

This section presents recommendations for future research related to this study.

6.2.1   On the fresh properties of RuC

❖ The gaps observed in SEM imaging of RuC samples can be due to the lack of bond between rubber and concrete, but also to specimen preparation that may have caused rubber detachment. Future research should investigate other less invasive techniques to examine the bond at the interphase between the rubber and the cement paste (e.g. X-ray tomography).

❖ Further investigation is needed to examine rubber distribution throughout cylinders with different sizes and the influence of handling, casting and vibration techniques.

❖ The influence of rubber characteristics including rubber extraction techniques (e.g. mechanical shredding or cryogenic grinding), their contamination, and their shape and surface parameters on the fresh concrete and mechanical performance (such as bond and interlock with other mix constituents) should be examined.

❖ Practical onsite issues such as the easiness of casting and pumpability at heights should be further investigated. Additional tests such as the two-point test (Tattersall test) can be used for further insight.

6.2.2 On the stress-strain behaviour of RuC

❖ Due to the large amount of parameters investigated, a limited number of specimens were tested per parameter. Additional experiments are needed to investigate more thoroughly some of the results (e.g. variability).

❖ It is useful to develop a model that can predict the strength of RuC with different rubber contents as function of the influencing mix parameters. Existing models only account for the rubber content and size (Bompa *et al.,* 2017), and water to binder ratio (Correia *et al.,* 2010). However, based on the results of this study, it is evident that the strength of RuC is influenced by several other parameters (e.g. packing, admixture content, coarse and fine aggregate content and binder material).

❖ Different combinations of fine and coarse rubber replacement (e.g. 80% coarse aggregate and 20% fine aggregate) and other intermediate rubber contents should be investigated.

❖ The test setup and instrumentation used to test FRP CRuC cylinders need to be improved. For instance, in the unconfined RuC in this research, the circumferential wire only provided measurements until high lateral strains ($>500\mu\varepsilon$) were achieved in the cylinder. Hence, average strains from the three horizontal strain gauges were often used. The measurements from these gauges can be affected by local phenomena (e.g. if located near a large rubber aggregate as opposed to a coarse mineral aggregate) and cracking in the specimens, as reflected in large scatter in Fig.7 of Chapter 3. A potential solution for measuring lateral strains in future tests would be the use of 3D volumetric digital image correlation.

❖ The potential of using rubber chemical pre-treatments that can meaningfully improve rubber-cement paste bonding without comprising RuC durability requires further investigation.

6.2.3 On the confinement of RuC

General

❖ This research proved that very high deformability and strength can be achieved in CRuC. Nevertheless, such high deformability might not be required for all structural applications. Future research should assess the effectiveness of confining RuC with intermediate rubber contents (e.g. 40% total aggregate replacement) on the CRuC deformability and strength.

❖ It is useful to compare the stress-strain behaviour of CRuC to the behaviour of confined conventional concrete with similar unconfined concrete compressive strength when/if such experimental database is available.

❖ The lower effectiveness of CFRP CRuC when compared to AFRP CRuC with identical confining stiffness requires further investigation. Some areas that can be investigated include the influence of: i) the higher transversal stiffness of CFRP sheets, which can lead to higher axial load being transferred laterally, ii) the Poisson's ratio of the materials, leading to additional lateral strains, iii) the level of pre-stress applied during application and iv) strains along the overlap and the concrete face.

❖ Future research should investigate the use of other widely available confining materials such as glass or basalt FRP.

❖ Size effect (the scaling of confinement) for larger cylinders at structural scale can be investigated.

Cyclic loading

❖ Investigate the effect of subsequent load cycles within each set of cycles on the strength and stiffness degradation.

❖ Only limited research has verified experimentally and analytically the effectiveness of CRuC at enhancing deformability of structural elements (Escolano-Margarit *et al.*,

2017; Duarte *et al.,* 2016). Further research is necessary to show the potential of the new concrete in structural applications (e.g. current base isolation systems or bridge bearings).

6.2.4 On the constitutive modelling of CRuC

General

❖ CRuC with high rubber contents had not been tested before this study. Therefore, the new proposed models need to be validated against other experimental databases when/if available.

❖ The new proposed models are only applicable for CRuC mixes with particularly high rubber contents as those used in this study (60% total aggregate replacement). Future research should evaluate the applicability of these models to other rubber contents.

❖ Additional data would be useful to improve f_{cc}/f_{cr} and $\varepsilon_{cc}/\varepsilon_{cr}$ predictions for lightly confined and heavily confined CRuC cylinders.

Monotonic loading

❖ The analytical confinement model in this study was based on the active confinement model by Mander, Priestley and R.Park (1988), which was developed for conventional concrete. Further research should evaluate the use of active confinement models based on tri-axial testing of RuC with high rubber contents.

Cyclic loading

❖ Examine the ability of the model to capture the performance of CRuC with higher number of cycles (e.g. cyclic fatigue) as well as CRuC with partial unloading/reloading.

6.2.5 Other issues

Research on rubberised concrete is fairly recent and therefore many outstanding issues (not directly related to this study) require further investigation. Currently, the research on high rubber content RuC is extremely limited. The influence of high rubber contents on the durability of RuC, its thermal and acoustic behaviour, its performance in fire as well as other aspects of its mechanical behaviour such as shear and flexure need further investigation. Additionally, the effect of using external confinement on these properties and the required protection for the FRP material (e.g. to improve its durability and performance in fire) must also be investigated. The Life cycle assessment (LCA) and life cycle cost analysis (LCCA) of CRuC are also necessary.

6.3   REFERENCES

Bompa, D. V., Elghazouli, A. Y., Xu, B., Stafford, P. J. and Ruiz-Teran, A.M., (2017). Experimental assessment and constitutive modelling of rubberised concrete materials. *Construction and Building Materials*. **137**, 246-260.

Correia, S. L., Partala, T., Loch, F. C. and Segadães, A. M., (2010). Factorial design used to model the compressive strength of mortars containing recycled rubber. *Composite Structures*. **92**(9), 2047-2051.

Duarte, A. P. C., Silva, B. A., Silvestre, N., de Brito, J., Julio, E. and Castro, J. M., (2016). Tests and design of short steel tubes filled with rubberised concrete. *Engineering Structures*. **112**, 274-286.

Escolano-Margarit, D., Garcia, R., Raffoul, S., Di Benedetti, M., Hajirasouliha, I., Guadagnini, M. and Pilakoutas, K., (2017). Seismic performance evalutaion of couples walls using innovative highly deformable coupling beams. *In the 16th World Conference of Earthquake Engineering (16WCEE).* Santiago, Chile, 2017.

Mander, J. B., Priestley, M. J. N. and Park, R., (1988). Theoretical Stress Strain Model for Confined Concrete. *Journal of Structural Engineering*. **114**(8), 1804–1825.

Papastergiou, P., (2010). *A confinement model for concrete wrapped or pretensioned with FRP.* Ph.D. thesis, University of Sheffield.

Shao, Y., Zhu, Z. and Mirmiran, A., (2006). Cyclic modeling of FRP-confined concrete with improved ductility. *Cement and Concrete Composites*. **28,** 959–968.

Appendices

Appendix A. Characteristics of Rubber

This section presents additional literature on the properties of rubber and includes excerpts from deliverable 1.1 previously prepared by the author for the Anagennisi project.

A.1 RUBBER TYRE COMPOSITION

In general, rubber used in the tyre industry is composed of vulcanised natural rubber (NR, cis-1,4-polyisoprene (Beurrot-Borgarino *et al.*, 2013)) and synthetic rubbers (often vulcanised) such as styrene-butadiene rubber (SBR), synthetic cis-polyisoprene, ethylene-propylene, polybutadiene and/or butyl rubber (a copolymer of Isoprene and Isobutylene), which are blended for optimum mechanical properties (Freakley and Payne, 1978; Sienkiewicz *et al.*, 2012).

Reinforcing fillers such as amorphous silica and carbon black are dispersed within the rubber using rotating high-energy shearing blades. Using various chemicals, cross-links are formed among the compound materials (Freakley and Payne, 1978; ETRma, 2010). The fillers increase the rubber tensile strength, stiffness and deformation capacity prior to failure and improve its abrasion. Fillers also enhance the tear and rupture resistance of tyres, as well as their capacity to grip and transmit forces, thus enhancing the tyre safety (Leblanc, 2002; Fröhlich, Niedermeier and Luginsland, 2005; ETRma, 2010). Additionally, amorphous silica in tyres decreases the

negative environmental impact of the vehicles by reducing their fuel consumption (ETRma, 2010). Following the addition of fillers, the rubber is poured in moulds and vulcanisation is initiated (refer to section 2.2) (Freakley and Payne, 1978).

Rubber obtained from scrap tyres is usually contaminated with other tyre components including metal, textile, sulphur, zinc oxide and other additives. Tables A.1 and A.2 summarise the composition of typical tyres.

Table A.1 Tyre composition in the EU according to ETRA (©2014)

Composition by weight of car and truck tyres in the EU		
Material	**Car/utility %**	**Truck/Lorry %**
Rubber/Elastomers[a]	48	45
Carbon black + silica[b]	22	22
Metal	15	25
Textile	5	—
Zinc oxide	1	2
Sulphur	1	1
Additives	8	5

[a]Truck tyres contain proportionately more natural rubber in comparison to synthetic rubber than do car tyres.
[b]Different varieties of carbon black are used for different purposes and may appear in other categories of material

Table A.2 Typical proportions of synthetic and natural rubber in different types of tyres (as a percentage of total tyre weight) in Europe and USA (Sienkiewicz *et al.*, 2012)

Type of tyre	Synthetic Rubber	Natural Rubber
Passenger tyre (in Europe)	15%	22%
Passenger tyre (in USA)	27%	14%
Truck tyre (in Europe)	23%	30%
Truck tyre (in USA)	14%	27%

A.2   MOLECULAR STRUCTURE

Raw natural rubber (as found in the sap of the Hevea Brasiliensis tree) is mainly a hydrocarbon $(C_5H_8)_n$, or a polymer of isoprene (C_5H_8), formed with long polymer chains that slide and move independently. This movement results in a highly plastic behaviour or a 'permanent set' when exposed to loading (Figure A.2a) (Moore, 1950; Treloar, 1975; Freakley and Payne, 1978). The material is excessively viscous at high temperatures and is brittle and inflexible at low temperatures (due to prompt crystallisation). Therefore, the use of raw natural rubber is limited (Moore, 1950).

In 1839, Goodyear developed the vulcanisation process (Moore, 1950; Treloar, 1973), which uses sulphur, heat and pressure to transform raw rubber into a highly elastic and superior material, triggering the growth of rubber trade. During vulcanisation, random cross-links form within the long-chain molecule or between two individual molecules to form a 3-D chain network (Figure A.2b). These cross-links have low-intermolecular forces and can rotate freely, thus causing the rubber to be highly elastic and with a lower inclination to crystallise than natural unvulcanised rubber (Treloar, 1973; Freakley and Payne, 1978). Upon stretching, the molecules align into an orientation which requires more work than the random orientation of the molecules. In other words, the molecules have a higher tendency to spring back to their original, more 'probable' random contracted form once unloading occurs as described by Meyer (reported in (Treloar, 1973). This rotational freedom is subject to the amount of sulphur added during vulcanisation and becomes limited at high sulphur quantities, which could transform rubber into a hard 'ebonite' (Moore, 1950).
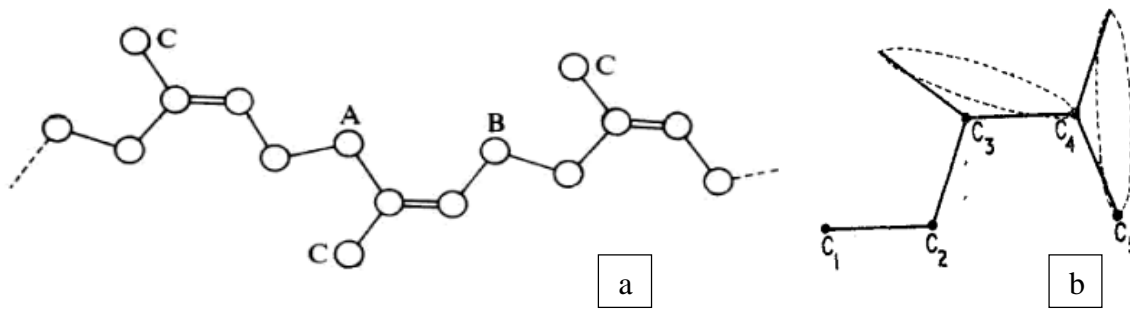
Figure A.1 Molecular structure of Hevea rubber (a) (Treloar, 1975) and rubber with a bond

rotational capacity (b) (Treloar, 1973) (A-B: isoprene unit, C=methyl group)

From a thermodynamic point of view, the elasticity of an ideal rubber is comparable to that of volume elasticity of an ideal gas ('kinetic theory') (Treloar, 1973; Tabor, 1994). For instance, unlike most crystalline solids, the high capacity of rubber to extend is due to decreases in its entropy, which is achieved through the reduction in the 'disorder' or a restriction in the configurations that could be adopted by the rubber molecule bonds and the straightening of the chain links (Moore, 1950; Treloar, 1973; Tabor, 1994). Only a small fraction of the rubber elasticity is related to an increase in its internal energy (Treloar, 1973) or intermolecular forces (Tabor, 1994).

A.3   MECHANICAL PROPERTIES

A.3.1 Stress-strain behaviour

The mechanical properties of rubber are dominated by a non-linear and highly elastic behaviour that is attributed to the rubber molecular structure (refer to section A.2). A typical stress-strain curve of natural vulcanised rubber is shown in Figure A.3. The strain behaviour of rubber, particularly when in tension, is influenced by the finite stretching capacity of the molecular chains and, at higher elongations, by tension stiffening resulting from rubber crystallisation. These influencing factors (described in (Treloar, 1973)) cause a deviation between theoretical and experimental stress-strain curves in the literature at high strain levels exceeding 100%.

Crystallisation, which is manifested in vulcanised natural rubber and in some synthetic rubbers, occurs at either high strain levels or after lengthy exposure to low temperatures (Treloar, 1973). It causes significant increases in the rubber density, elastic modulus and tensile strength (Beurrot-Borgarino *et al.*, 2013). According to Goppel and Arlman (1949), at a low rate of stretching, crystallisation occurs at a strain of about 200% and increases with an increase in strain. The onset of crystallisation is influenced by the amount of applied strain, strain rate, temperature and load duration (Beurrot-Borgarino *et al.*, 2013). The increase in crystalline material in vulcanised rubber as function of the tensile strain is shown in Figure A.4. Further literature on the crystallisation of rubber particles may be found in references (Bekkedahl and Wood, 1941; Goppel and Arlman, 1949; Moore, 1950; Poompradub *et al.*, 2005; Beurrot-Borgarino *et al.*, 2013).
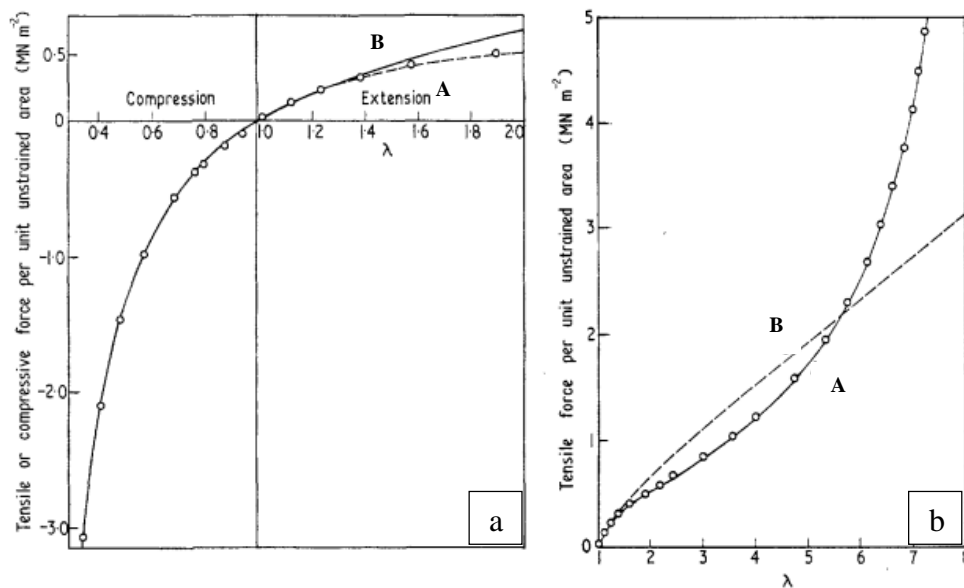
Figure A.2 Uniaxial compression (a) and extension (a and b) of rubber derived experimentally and theoretically. A=Experimental; B=theoretical (Treloar, 1975)
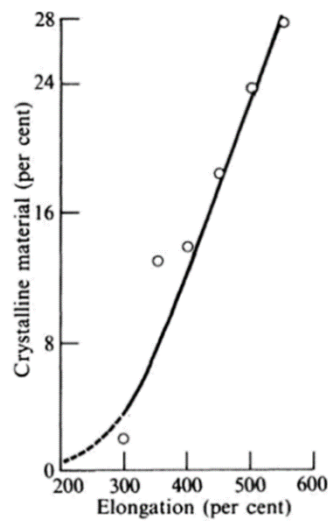
Figure A.3 The amount of crystalline material in a vulcanised rubber particles as function of its elongation (Treloar, 1975)

A.3.2 Elastic moduli and strength

It is generally accepted that the stiffness of rubber particles is very low despite the presence of reinforcing fillers. According to Tabor (1994), the Young's Modulus of rubber (E) is in the range of a few MPa, which is extremely low compared to values of 50 -70 GPa for conventional mineral aggregates. Other authors report that "compact" and "expanded" rubber aggregates from non-tyre automotive waste rubber has E values of 68 and 12 MPa, respectively (Benazzouk, Douzane and Quéneudec, 2004). Unlike most solids, E of rubber increases with an increase in the particle temperature or due to crystallization (Tabor, 1994). This may be attributed to the damaging effect of high temperatures on the rubber molecules' 3-D crosslinks (Scaffaro *et al.*, 2005). Alternatively, strain crystallization could cause stress relaxation or a reduction in the rubber's stiffness (Poompradub *et al.*, 2005). To the best of the author's knowledge, values for E of tyre rubber, in particular, are not available in the literature. However, it is anticipated that this value will vary between different types of tyres, the levels of rubber contamination (with steel/textile fibres), the proportions of synthetic and natural rubbers in the composite, and the load and environmental exposure history of the tyres.

The bulk modulus (K) and Poisson's ratio (*v*) of rubber are reported to be approximately 2400-2500 MPa (Tabor, 1994; Zimmermann and Stommel, 2013) and 0.5 (Zimmermann and Stommel, 2013), respectively. The high value of the bulk modulus of the rubber is an indication of the rubber's high resistance to compressive deformation or, in other words, of its incompressibility (Beurrot-Borgarino *et al.*, 2013; Zimmermann and Stommel, 2013).

Based on the theory of elasticity, under a compressive axial load (σ_x), a rubber particle is likely to contract axially (ε_x) and expand laterally (ε_y and ε_z) in accordance with Equation (A.1) (Timoshenko, Timoshenko and Goodier, 1951).

$$\varepsilon_x = \frac{\sigma_x}{E} \qquad \varepsilon_y = -v\frac{\sigma_x}{E} \qquad \varepsilon_z = -v\frac{\sigma_x}{E} \qquad (A.1)$$

Assuming that the material is perfectly isotropic and will expand similarly in all directions ($\varepsilon_y = \varepsilon_z = \varepsilon_L$), the volumetric ratio (ε_v) may be described by equation 2. By substituting equation (1) in equation (A.2) and assuming a rubber *v*=0.5, the volumetric ratio is 0, thus indicating that the material would maintain a constant volume under loading (equation (A.3).

$$\varepsilon_v = \varepsilon_x + 2\varepsilon_L \qquad (A.2)$$

$$\varepsilon_v = \frac{\sigma_x}{E} - (0.5)(2)\frac{\sigma_x}{E} \qquad (A.3)$$

Tabor (1994) indicates that the elastic properties of rubber, including the Young's (E), bulk (K) and shear moduli (n) are not interconnected. As shown in A.2, the Young's and shear moduli of rubber are more influenced by its entropy changes rather than its intermolecular forces. The bulk modulus, on the other hand, is associated with the rubber intermolecular forces. It is therefore reported that allocating a value for the Poisson's ratio to relate the independent elastic moduli of rubber is inappropriate (Tabor, 1994).

In a study by Goppel and Arlman (1949), the tensile strength of tyre rubber is reported to be in the range of 28 MPa. The compressive behaviour of rubber particles is generally characterised through its compressive set, according to the ASTM D395-03 (2008), which measures the ability of rubber to maintain its elastic behaviour after a long exposure to compression.

A.3.3 Fatigue and energy absorption

Due to its unique properties, rubber absorbs significant amounts of energy when deformed by an applied force and releases a large amount of this energy when such force is removed (Freakley and Payne, 1978). Rubber particles show various levels of hysteresis. Under tensile loading, the extension of rubber follows a stress-strain path that is different to that of its retraction upon removal of the applied load, dissipating energy in the form of heat (Freakley and Payne, 1978). This hysteretic behaviour is time dependent, occurs at excessive deformations and is influenced by rubber crystallisation (Freakley and Payne, 1978). It has been reported that the addition of carbon black as reinforcing material in the rubber reduces the 'resilience' of the rubber particle (Moore, 1950; Bijarimi, Zulkafli and Beg, 2010) and induces higher hysteretic losses and heat generation upon cyclic loading. This effect appears to be influenced by the size of rubber particles and is higher for finer rubber particles (Moore, 1950).

When exposed to cyclic tensile loading at high stress levels (Legorju-Jago and Bathias, 2002), vulcanised natural rubber with the capacity to crystallise had a higher fatigue resistance than amorphous, non-crystallising synthetic rubbers (Styrene Butyl Rubber). Alternatively, the fatigue and crack growth in the vulcanised rubber increases in the presence of Oxygen (when stretched) or at high temperatures, since it causes its chemical degradation and reduces the chances of crystallisation, which is favourable for fatigue resistance (Freakley and Payne, 1978; Legorju-Jago and Bathias, 2002).

When subject to cyclic loading, a significant tension softening behaviour and alteration in the stress-strain response of the rubber becomes apparent. The softening behaviour is more

prominent in cycles where the highest maximum strains acquired in preceding loads are exceeded, as shown in Figure 5. It has been reported that the highest amount of softening occurs in the first 10 cycles as a result of permanent breaking of some of the bonds within the compound (Mars and Fatemi, 2006). According to Mullin (Mars and Fatemi, 2006; Cantournet, Desmorat and Besson, 2009; Diani, Fayolle and Gilormini, 2009), the initial stress-strain curve obtained from a rubber particle cannot be reproduced and that several load cycles are needed to achieve a more appropriate stress-strain curve. Description of this behaviour, known as the Mullin's effect, is provided in several papers. (Mullins, 1969; Mars and Fatemi, 2006; Cantournet, Desmorat and Besson, 2009; Diani, Fayolle and Gilormini, 2009).
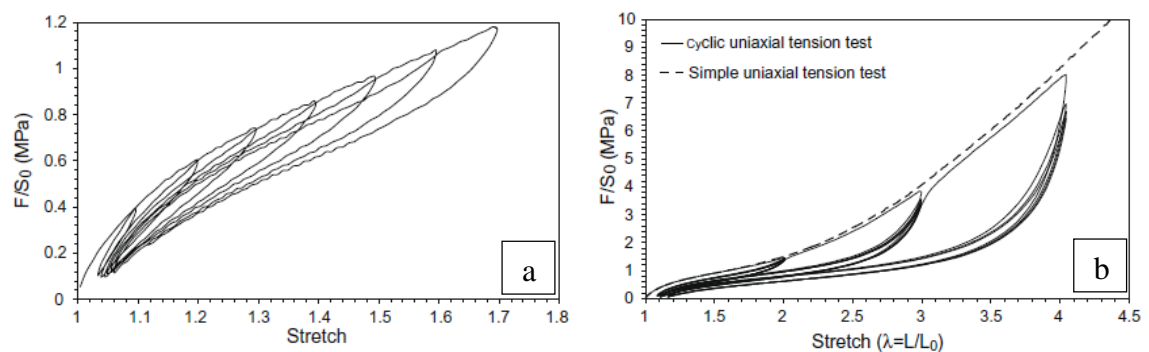
Figure A.4 Stress-strain behaviour of a Carbon-filled SBR particle subject to cyclic tensile loading at moderate deformations (a) and both cyclic and uniaxial tensile loading at high deformations (b) (Diani, Fayolle and Gilormini, 2009)

A.4   PHYSICAL PROPERTIES

The specific density of rubber varies in the literature between 0.5 (Atahan and Yücel, 2012) and 1.3 (Ganjian, Khorami and Maghsoudi, 2009; Ho *et al.*, 2012). In tyre rubber, this density is subject to the type of tyre (truck tyre or car tyre, among others) and rubber contamination with steel/textile materials.

Tyre rubber is characterised by a high friction coefficient and a hydrophobicity (a water repellent behaviour) that is increased in the presence of silicon (Si) applied to the tyre surface to

extend its life and zinc stearate, a rubber additive approximately 1-2% of the tyre weight (Table A.1) that often migrates to the surface (Freakley and Payne, 1978; Segre, Monteiro and Sposito, 2002; Richardson, Coventry and Ward, 2012). This hydrophobicity has been attributed to the non-polar nature (Sukontasukkul and Tiamlom, 2012) and texture (Mavridou and Oikonomou, 2011) of the rubber particles. Despite this hydrophobicity, it has been reported that wetting rubber particles with water can lubricate their surface and reduce the friction (Freakley and Payne, 1978).

When exposed to hydrocarbon solvents or organic liquids (such as petrol, benzene, and mineral lubricating oils), both natural and synthetic rubbers, tend to swell and gradually lose their strength. Some synthetic polymers have been engineered to avoid this problem (Freakley and Payne, 1978). This swelling is caused by the similarity in chemical and molecular constitutions of the two materials and the diffusivity of their molecules (Treloar, 1973). Rubber particles are also characterised by a poor heat and electrical conductivity, which makes them ideal for insulating purposes (Freakley and Payne, 1978).

A.5   TYRE RUBBER TYPES AND RETRIEVAL PROCESSES

The two main technologies employed to retrieve rubber products from scrap tyres include the cryogenic and ambient (mechanical) grinding processes. These practices have a slight influence on the characteristics of the retrieved rubber in terms of surface characteristics, particle sizes and the presence of steel and fabric.

The mechanical process consists of a series of stages before the final product is obtained. Initially, the tyre products are shredded into chips. Using a granulator, the tyre chips are then reduced in size into smaller chips followed by crumbs (or granules). Steel fibres and polymer fabric are removed by magnetic separation and air gusts, respectively. Finer rubber particles

may be achieved either through a secondary granulator or a high shear rotatory mill also known as the micro-mill (refer to Siddique and Naik (2004) for more details).

In the cryogenic process, the shredded tyres are frozen and embrittled, typically using liquid Nitrogen. Then they are shattered using an impact force and the steel and fabrics are easily removed (Shu and Huang, 2013).

It must be noted that most of the existing literature on rubberised concrete involves mechanically ground rubber. This may be attributed to the lower cost of ambient grinding and also to the rougher surface of the resulting rubber, which is more convenient for applications in the construction industry.

The rubber particles are classified in the literature according to size as follows:

- Rubber chips: normally used to replace coarse aggregates, rubber chips or shreds are normally produced through primary and secondary shredding processes to attain particle sizes of 13-76mm that are similar to the replaced aggregates (Siddique and Naik, 2004; Ganjian, Khorami and Maghsoudi, 2009).

- Rubber crumbs: are often used to replace sand fractions in rubberised concrete. Their sizes normally range between 0.425 and 4.75 mm (Ganjian, Khorami and Maghsoudi, 2009; Najim and Hall, 2010).

- Rubber powder: also known as ground rubber is normally a term for rubber particles with sizes finer than the rubber crumbs (i.e. less than 0.425mm) (Ganjian, Khorami and Maghsoudi, 2009; Najim and Hall, 2010).

- Rubber fibres: are rubber pieces cut in the shape of fibres. These particles are characterised with high length to width ratios and normally average a length of 12.5 mm (Najim and Hall, 2010).

A.6   SUMMARY

Research on the properties of tyre rubber is very limited. To the best of the author's knowledge, no proper characterisation of the mechanical properties of tyre rubber (i.e. stress-strain data, elastic moduli, fatigue and dynamic behaviour) exist in the literature. This may be due to the diversity in rubber composition (synthetic and natural) between the different types of tyres (i.e. truck tyres, car tyres, wet-weather tyres, all-terrain tyres and re-treads) and the various industries and technologies utilised in the process, which hinders a proper evaluation of the tyre rubber properties.

Sections (A.1-A.3) mainly focus on the properties of natural vulcanised rubber and synthetic cis-polyisoprene, formed using petroleum by-products to match the properties of natural rubber. Together, these components form a portion of the rubber in tyres (Table A.2). Other synthetic rubbers used in tyre products may have slightly different characteristics to those of natural rubber. Different levels of hysteresis, crystallisation (some synthetic rubbers do not crystallize), elasticity, heat build-up and gas permeability have been reported. A broad account of the differences between various rubber products, described by Freakley and Payne (1978), is shown below:

- Styrene-butadiene rubber (SBR): similar to natural rubber but slightly inferior. Additives are used to improve its behaviour. SBR is characterised with a high wear and abrasion resistance and enhanced ageing but also a higher heat-build up.

- Butyl rubber (IIR): Also known as isobutene-isoprene, butyl rubber has slightly inferior properties that NR including lower tensile properties and high hysteresis, both of which are improved during high temperature processing in the presence of additives. It is mainly used for its excellent impermeability and is also known for its high resistance to ozone attack, heat chemical deterioration and abrasion.

- Ethylene propylene rubbers: Also known as EPM and EPDM, which comprise of peroxide cross-linking and an extra monomer for sulphur cross-linking, respectively. This rubber is relatively expensive and is rarely used despite its good properties and excellent resistance to ozone.

A.3.7 References

ASTM. (2008). *Standard test methods for rubber property-compression set* D395-03. West Conshohoken, P.A.: ASTM international

Atahan, A. O. and Yücel, A. O., (2012). Crumb rubber in concrete: Static and dynamic evaluation. *Construction and Building Materials*. **36,** 617–622.

Bekkedahl, N. and Wood, L. A., (1941). Crystallization of vulcanized rubber. *Rubber Chemistry and Technology*. **14**(2), 347–355.

Benazzouk, A., Douzane, O. and Quéneudec, M., (2004). Transport of fluids in cement–rubber composites. *Cement and Concrete Composites*, **26**(1), 21–29.

Beurrot-Borgarino, S., Huneau, B., Verron, E. and Rublon, P., (2013). Strain-induced crystallization of carbon black-filled natural rubber during fatigue measured by in situ synchrotron X-ray diffraction. *International Journal of Fatigue*, **47**, 1–7.

Bijarimi, M., Zulkafli, H. and Beg, M. D. H., (2010). Mechanical Properties of Industrial Tyre Rubber Compounds. *Journal of Applied Sciences(Faisalabad)*, **10**(13), 1345–1348.

Cantournet, S., Desmorat, R. and Besson, J., (2009). Mullins effect and cyclic stress softening of filled elastomers by internal sliding and friction thermodynamics model. *International Journal of Solids and Structures*. **46**(11), 2255–2264.

Diani, J., Fayolle, B. and Gilormini, P., (2009). A review on the Mullins effect. *European Polymer Journal*. **45**(3), 601–612.

European Tyre & Rubber manufacturers' association (ETRma). (2012). Reinforcing Fillers in the Rubber Industry - Assessment as potential nanomaterials with focus on tyres. [online] Available from; http://www.etrma.org/uploads/Modules/Documentsmanager/201201-etrma-fact-sheet---carbon-black-and-silica-2.pdf

Freakley, P. K. and Payne, A. R., (1978). *Theory and practice of engineering with rubber*. Applied Science Publishers London.

Fröhlich, J., Niedermeier, W. and Luginsland, H.-D., (2005). The effect of filler–filler and filler–elastomer interaction on rubber reinforcement. *Composites Part A: Applied Science and Manufacturing*. **36**(4), 449–460.

Ganjian, E., Khorami, M. and Maghsoudi, A. A., (2009). Scrap-tyre-rubber replacement for aggregate and filler in concrete. *Construction and Building Materials*. **23**(5), 1828–1836.

Goppel, J. M. and Arlman, J. J., (1949). On the degree of crystallinity in natural rubber IV. *Applied Scientific Research*. **1**(1), 462–474.

Ho, A. C., Turatsinze, A., Hameed, R. and Vu, D. C., (2012). Effects of rubber aggregates from grinded used tyres on the concrete resistance to cracking. *Journal of Cleaner Production*. **23**(1), 209–215.

Leblanc, J. L., (2002). Rubber–filler interactions and rheological properties in filled compounds. *Progress in polymer science*. **27**(4), 627–687.

Legorju-Jago, K. and Bathias, C., (2002). Fatigue initiation and propagation in natural and synthetic rubbers. *International Journal of Fatigue*. **24**(2), 85–92.

Mars, W. V and Fatemi, A., (2006). Multiaxial stress effects on fatigue behavior of filled natural rubber. *International Journal of Fatigue*. **28**(5), 521–529.

Mavridou, S. and Oikonomou, N., (2011). Integration of end-of-life tires in the life cycle of road construction. *EU-LIFE+ Environment Policy and Governance, LIFE 09 ENV/GR/304 ROADTIRE*.

Moore, J., (1950). Some chemical and physical properties of rubber. *British Journal of Applied Physics*. **1**(1), 6.

Mullins, L., (1969). Softening of rubber by deformation. *Rubber Chemistry and Technology*. **42**(1), 339–362.

Najim, K. B. and Hall, M. R., (2010). A review of the fresh/hardened properties and applications for plain-(PRC) and self-compacting rubberised concrete (SCRC). *Construction and Building Materials*. **24**(11), 2043–2051.

185

Poompradub, S., Tosaka, M., Kohjiya, S., Ikeda, Y., Toki, S., Sics, I. and Hsiao, B. S., (2005). Mechanism of strain-induced crystallization in filled and unfilled natural rubber vulcanizates. *Journal of applied physics*. **97**(10), 103529.

Richardson, A. E., Coventry, K. A. and Ward, G., (2012). Freeze/thaw protection of concrete with optimum rubber crumb content. *Journal of Cleaner Production*. **23**(1), 96–103.

Scaffaro, R., Dintcheva, N. T., Nocilla, M. A. and La Mantia, F. P., (2005). Formulation, characterization and optimization of the processing condition of blends of recycled polyethylene and ground tyre rubber: Mechanical and rheological analysis. *Polymer degradation and stability*. **90**(2), 281–287.

Segre, N., Monteiro, P. J. M. and Sposito, G., (2002). Surface characterization of recycled tire rubber to be used in cement paste matrix. *Journal of colloid and interface science*. **248**(2), 521–523.

Shu, X. and Huang, B., (2013). Recycling of waste tire rubber in asphalt and Portland cement concrete: an overview. *Construction and Building Materials*. **67**, 217–224.

Siddique, R. and Naik, T. R., (2004). Properties of concrete containing scrap-tire rubber–an overview. *Waste Management*. **24**(6), 563–569.

Sienkiewicz, M., Kucinska-Lipka, J., Janik, H. and Balas, A., (2012). Progress in used tyres management in the European Union: a review. *Waste Management*. **32**(10), 1742–1751.

Sukontasukkul, P. and Tiamlom, K., (2012). Expansion under water and drying shrinkage of rubberized concrete mixed with crumb rubber with different size. *Construction and Building Materials*. **29**, 520–526.

Tabor, D., (1994). The bulk modulus of rubber. *Polymer*. **35**(13), 2759–2763.

Timoshenko, S., Timoshenko, S. and Goodier, J. N., (1951). *Theory of Elasticity*. McGraw-Hill book Company.

Treloar, L. R. G., (1973). The elasticity and related properties of rubbers. *Reports on progress in physics*. **36**(7), 755.

Treloar, L. R. G., (1975). *The physics of rubber elasticity*. Oxford University Press.

Zimmermann, J. and Stommel, M., (2013). The mechanical behaviour of rubber under hydrostatic compression and the effect on the results of finite element analyses. *Archive of Applied Mechanics*. **83**(2), 293–302.

Appendix B. Packing of Granular Particles

This section presents additional literature on the properties of rubber and includes excerpts from deliverable 1.1 previously prepared by the author for the Anagennisi project.

The particle packing and size distribution of concrete constituent materials has a major influence on the concrete properties, particularly its rheology, durability characteristics and strength (Kwan and Mora, 2001). With the increasing demand for advanced concretes including ultra-high strength and durability concretes, lightweight and heavyweight concretes, concretes with recycled aggregates, self-compacting and roller compacting concretes, more emphasis has been dedicated to concrete mix optimisation.

The significance of particle packing and refining the proportions of concrete granular particles has been highlighted in the literature. Early methods were based on empirical models that generate appropriate particle size distributions in an effort to achieve a densely packed mix. Some examples include the pioneering works of Feret, Powers and Fuller described in many papers (Goltermann and Johansen, 1997; Sobolev and Amirjanov, 2004; Brouwers and Radix, 2005; Kwan and Wong, 2008; Wong and Kwan, 2008c; Fung, Kwan and Wong, 2009; Kwan and Fung, 2009; Nanthagopalan and Santhanam, 2009, 2012). These models as well as many subsequent models cannot predict the actual packing densities achieved in granular mixes or account for aggregate combinations of different types and shapes. Dissimilarities in the packing behaviour of aggregates and fine cementitious materials are also rarely considered.

188

B.1 PACKING THEORY

The packing density of a granular mixture is defined as the volume of solids present in a certain bulk unit volume (De Larrard, 1999). The main rationale behind optimising packing is that a dense concrete particle packing reduces the cement paste or water required to fill the voids, resulting in higher compressive strengths in concrete mixers (Figure B.1) (Kwan and Mora, 2001). Alternatively, for the same amount of water at a higher packed mix, an improved lubrication and higher flowability is achieved (Kwan and Wong, 2008; Kwan and Fung, 2009). This results in major economic savings and a reduced concrete shrinkage.
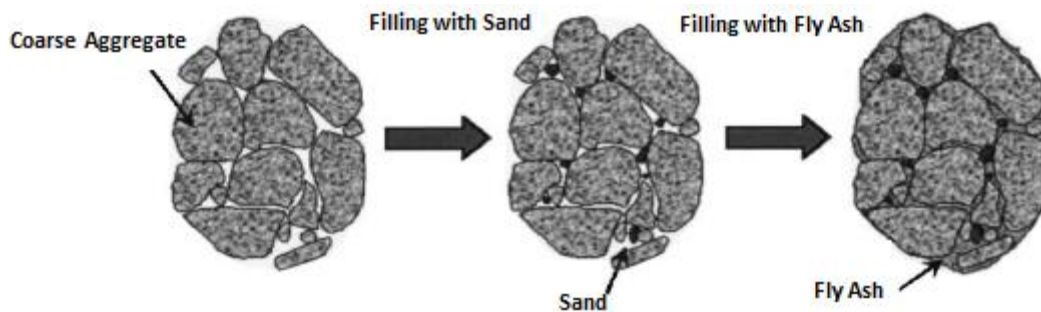
Figure B.1 A simple illustration of the reduced voids in concrete in densely paced mixtures

(Tsai et al., 2006)

The virtual density, which is the theoretical density obtained for identical particles placed one by one to the maximum possible filling of a container, has been used to approximate the packing density of a mono-sized particle mix (Kwan and Mora, 2001; Sobolev and Amirjanov, 2004; Médici *et al.*, 2012). However, particle packing is sensitive to a large number of variables such as compaction, mixing and placing techniques (Kwan and Fung, 2009; Kwan, Li and Fung, 2012; Nanthagopalan and Santhanam, 2012; Fennis, Walraven and den Uijl, 2013), moisture condition of the particles (Fung, Kwan and Wong, 2009; Kwan and Fung, 2009; Kwan, Li and Fung, 2012), concrete admixtures (Kwan and Fung, 2009; Kwan, Li and Fung, 2012) and physical properties of the particles considered (Kwan and Mora, 2001; Wong and Kwan, 2008a; Fennis, Walraven and den Uijl, 2013). The packing of fine filler particles is also influenced by the surface and inter-particle forces that control their behaviour (Wong and Kwan, 2008b;

Fennis, Walraven and den Uijl, 2013). As a result, the virtual density is always higher than the actual practical density of a granular mixes, regardless of the parameters involved (De Larrard, 1999). For example, the virtual packing density of mono-sized spheres achieved by a "face centred cubic lattice arrangement" and has a density of approximately 0.74 (Kwan and Mora, 2001; Sobolev and Amirjanov, 2004; Médici *et al.*, 2012) compared to a maximum density of 0.60/0.64 for actual mono-sized particle mixtures (De Larrard, 1999).

The physical properties that influence granular particle packing include the particle size distribution, their shape and surface texture. The particle shape is generally described by its roundness, "sphericity", elongation, and flakiness (Figure B.2) (Kwan and Mora, 2001; Médici *et al.*, 2012). The voids ratio in a granular blend tends to increase with angular particles when compared to a mix of a similar content of round aggregates (Neville, 1995). This is attributed to the higher surface area of angular (crushed) aggregates when compared to the natural round aggregates, which necessitates a higher water content to wet the grain surface and achieve the same workability (Neville, 1995; Médici *et al.*, 2012). Similarly, aggregates with high sphericities have a high water demand (Neville, 1995). Elongated and flaky coarse aggregates are undesirable since they tend to get positioned in one plane and trap air voids and bleeding water underneath(Neville, 1995). Kwan and Mora (2001) propose correlation factors that can be used to consider the combined effects of some shape factors to approximate the particles' packing density. The surface texture of the particles, particularly that of fine aggregates, has been shown to influence the particle-cement interphase and the mix water requirement (Neville, 1995). Kwan and Mora (2001), however, report that the surface texture of a particle is "one order of magnitude less" than its roundness property of the particle and therefore has negligible additional effect to that of the roundness factor.
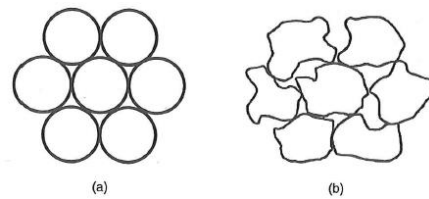
Figure B.2 A simple illustration of the influence of particle shape on the packing and void ratio; (a) spherical particles (b) particles with concave corner (Kwan and Mora, 2001)

Geometrical interactions among the aggregate particles induce loosening and "wall" effects that influence the maximum packing densities achieved in a particle mix (Figure B.3). The loosening effect is exerted by the fine grain particles on the packing of neighbouring coarse grain particles (Figure B.4b). Alternatively, the wall effect is exerted by the coarse grains (De Larrard, 1999; Fennis, Walraven and den Uijl, 2013) or by the wall of the container (Goltermann and Johansen, 1997) on the adjacent fine grain particles, inhibiting their maximum packing (Figure B.4a). The particle interactions depend on the size differences between the different grain sizes (Fennis, Walraven and den Uijl, 2013). Depending on this size difference, either complete, partial or absent interaction among the particle size groups is expected to occur. For similar sized particles, a total interaction is assumed (De Larrard, 1999).
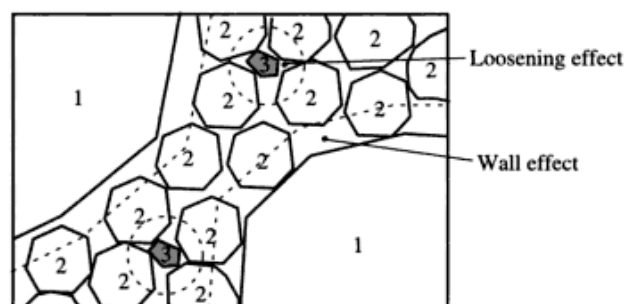
Figure B.3 Geometrical interactions between adjacent particles in a ternary mix (De Larrard, 1999)

191
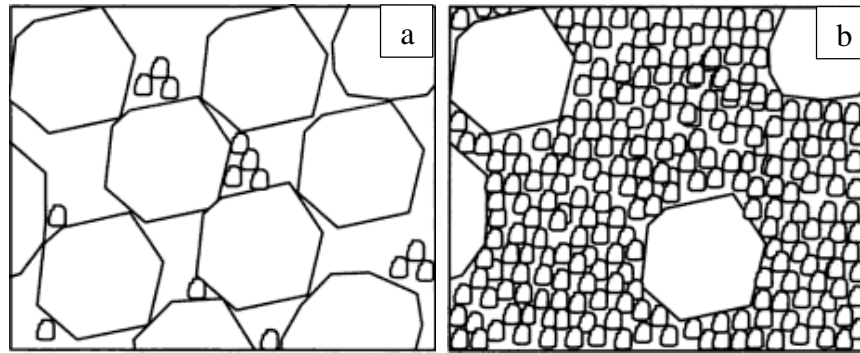
Figure B.4 Coarse grain dominant (a) and fine grain dominant (b) particle mixes

(De Larrard, 1999)

Traditionally, the packing behaviour of fine cementitious particles has been considered to be similar to that of the larger aggregate particles (Kwan and Mora, 2001). However, later studies show that the behaviour of fine powders (sizes less than 100-125 μm) is governed by surface forces rather than the gravitational forces that normally dominate particle behaviour (Wong and Kwan, 2008b). This is due to the higher surface area to mass ratio in the ultra-fine particles. The surface forces include van der Waals, electrical double layer and steric forces (Wong and Kwan, 2008b; Fennis, Walraven and den Uijl, 2013). Similar to the packing of coarse granular particles, a highly packed blend of cementitious materials has been shown to achieve an improved strength, durability and fresh properties in concrete mix (Kwan and Wong, 2008; Wong and Kwan, 2008b; Peng, Hu and Ding, 2009).

B.2   EXPERIMENTAL METHODS AND NUMERICAL MODELING

BS 812-2 (1995), BS EN 1097-3 (1998) and ASTM C29 (2009) standards propose a dry packing method to measure the packing of granular particles. The technique measures the bulk density of loose (BS EN 1097-3, 1998; ASTM C29, 2009) or compacted (ASTM C29, 2009) dry aggregates (either oven dried or SSD) and the resulting percentage of voids in the container. Goltermann and Johansen (1997) measured the bulk density of saturated surface dry granular aggregates using a "fall-table" for a certain number of cycles from a specified height. BS EN 1097-4 (2008) proposes the measurement of the bulk density of finer particles (passing the 0.063 sieve) by determining the density of the compacted dry filler. This process may not be

applied to moist filler particles (BS 812-2, 1995). An earlier approach involved suspension of the fillers in a kerosene liquid to measure the filler apparent bulk density (BS 812-2, 1995, BS EN 1097-3, 1998).

A number of parameters (described in Section B.1) are ignored in these experimental techniques. The effect of compaction is amplified in dryly packed fine-particle mixes since the probability of agglomeration and the resulting loosening effect increases with a decrease in the particle sizes involved (Kwan and Wong, 2008; Wong and Kwan, 2008c). Additionally, the packing behaviour of ultra-fine filler particles is influenced by surface and inter-particle forces (Wong and Kwan, 2008c; Fennis, Walraven and den Uijl, 2013). Therefore, due to their distinct packing behaviour, the packing of coarse and ultra-fine (cementitious) particles must be obtained differently (Nanthagopalan and Santhanam, 2009).

An indirect measurement of the voids in a concrete mix has been achieved through evaluating the level of consistency in a concrete mixture resulting from certain mix proportions. The minimum water demand to reach a standard consistency to form cement paste is used as an indication of the amount of voids in the mix and thus an indication of the degree of packing achieved (BS EN 196-3, 2005; Jones, Zheng and Newlands, 2003; Mangulkar and Jamkar, 2013). The standard consistence of the cement can be measured using the Vicat apparatus (BS EN 196-3, 2005). De Larrard (1999) proposes that the minimum amount of water could be selected visually by experimentally detecting the quantity of water below which the paste would be a humid powder. In both approaches, the presence of air in the paste or entrapped air in voids that cannot be fully saturated is neglected. It is also assumed that the minimum water content for a particular consistence is used to entirely fill the voids, which is not entirely precise (Wong and Kwan, 2008c). Subsequent experiments attempt to improve the accuracy of this indirect packing measurement by assuming a certain air content in the cement paste that is not completely filled with water (Wong and Kwan, 2008c). A comprehensive review of some direct and indirect experimental methods proposed can be found in Wong and Kwan (2008b).

The wet packing method, one of the latest developments in the experimental packing measurements, represents the real conditions of coarse and fine particles in a concrete or mortar mix with higher accuracy than the previously described direct and indirect measurements (Wong and Kwan, 2008b; Kwan and Wong, 2008; Fung, Kwan and Wong, 2009; Kwan and Fung, 2009). The typical wet packing procedure of cementitious materials is described as follows (Wong and Kwan, 2008b; Fung, Kwan and Wong, 2009; Kwan, Li and Fung, 2012). Particles are mixed with water (and any admixture) at various w/c and the corresponding mix bulk density is measured. This allows for the air content of the mix as well as the other cement constituents to be incorporated as part of the packing measurement. Compaction was applied to some of the mixes (Kwan, Li and Fung, 2012). The w/c is varied until the mix with the highest packing density is achieved (Wong and Kwan, 2008b; Kwan, Li and Fung, 2012). The procedure used to mix the particles with the water influence the packing density attained. Various mixing procedures were investigated to achieve the lowest mixing time possible without compromising the degree of packing (Wong and Kwan, 2008b). Kwan, Li and Fung (2012) observed that the influence of using the wet packing method rather than the dry packing method is higher in mixes with fine aggregates (rather than coarse granular aggregates) as an increase in packing of up to 18% is observed in the wet packing method. Blended aggregate mixes achieve a much higher packing density in wet packing method and the benefits of blending different particle sizes are more evident (Kwan, Li and Fung, 2012). Unlike the direct dry packing measurement techniques, the wet packing of fine filler particles decreases electrostatic forces and agglomeration within the particles and improves their packing capabilities (Fung, Kwan and Wong, 2009). The use of admixtures and various mixing techniques to reduce this agglomeration has also been vigorously investigated (Wong and Kwan, 2008b; Kwan and Fung, 2009). Capillary forces created in the presence of the lubricant hold particles together, which increases the density of the mixture, as in actual concrete mixtures (Fung, Kwan and Wong, 2009). As a result of the high level of packing achieved, the sensitivity of the fine particle packing to the applied compaction technique is massively reduced (Fung, Kwan and Wong, 2009).

Numerous numerical models have been developed in an effort to optimise and predict particle packing behaviour. These models include binary and ternary mixture models, multi-component mixture models, continuous models, 3D computer simulation models and digital image processing models, which are described explicitly in the literature (Fung, Kwan and Wong, 2009; Nanthagopalan and Santhanam, 2009; Mangulkar and Jamkar, 2013). As the packing of aggregates depends on several variables, the models were very difficult to develop and only a few of them match well with the experimental results. The "compressible packing model" (CPM), combines a large range of factors to show good correlation with experimental results. Nevertheless, this method is only suitable for grading curves of similar particle shape combinations and a known compaction factor value (De Larrard, 1999).

B.3   PACKING OF RUBBERISED CONCRETE CONSTITUENTS

The effect of rubber on the packing of the concrete constituents has not been investigated in the literature. Although Youssf et al. (2014) has investigated the influence of gap-graded rubber particles and others have intended to replace mineral aggregates with particles of similar gradations (Sukontasukkul, 2009; Pedro, De Brito and Veiga, 2012), no measurements for the actual packing densities in rubberised concrete currently exist in the literature. It is anticipated that blending mineral aggregates with rubber particles of different physical, chemical and mechanical properties will affect the packing of concrete constituents. The available models (calibrated with experimental results from conventional aggregate mixtures) do not apply for mixes with both rubber and mineral aggregates.

B.4   REFERENCES

ASTM. (2009). *Standard test methods for bulk density (unit weight) and voids in aggregate C29/C29-M*. West Conshohoken, P.A.: ASTM international

Brouwers, H. J. H. and Radix, H. J., (2005). Self-compacting concrete: the role of the particle size distribution. in *First International Symposium on Design, Performance and Use of SCC*. Hunan, China, 2005.

British Standards Institution., (1998). *Tests for mechanical and physical properties of*

aggregates: Determination of loose bulk density and voids BSI 1097-3:1998. London: British Standards Publications.

British Standards Institution., (2008). *Tests for mechanical and physical properties of aggregates: Determination of voids of dry compacted filler* BSI 1097-4:2008. London: British Standards Publications.

British Standards Institution., (1995). *Methods for determination of density* BSI 812-2:1995. London: British Standards Publications.

British Standards Institution., (2005). *Methods of testing cement. Determination of setting times and soundness* BSI 196-3:2005. London: British Standards Publications.

Fennis, S., Walraven, J. C. and den Uijl, J. A., (2013). Compaction-interaction packing model: regarding the effect of fillers in concrete mixture design. *Materials and structures.* **46**(3), 463–478.

Fung, W. W. S., Kwan, A. K. H. and Wong, H. H. C., (2009). Wet packing of crushed rock fine aggregate. *Materials and structures.* **42**(5), 631–643.

Goltermann, P. and Johansen, V., (1997). Packing of aggregates: an alternative tool to determine the optimal aggregate mix. *ACI Materials Journal.* **94**(5).

Jones, M. R., Zheng, L. and Newlands, M. D., (2003). Estimation of the filler content required to minimise voids ratio in concrete. *Magazine of concrete Research.* **55**(2), 193–202.

Kwan, A. K. H. and Fung, W. W. S., (2009). Packing density measurement and modelling of fine aggregate and mortar. *Cement and Concrete Composites.* **31**(6), 349–357.

Kwan, A. K. H., Li, L. G. and Fung, W. W. S., (2012). Wet packing of blended fine and coarse aggregate. *Materials and structures.* **45**(6), 817–828.

Kwan, A. K. H. and Mora, C. F., (2001). Effects of various shape parameters on packing of aggregate particles. *Magazine of concrete Research.* Thomas Telford (ICE Publishing). **53**(2), 91–100.

Kwan, A. K.H. and Wong, H. H. C., (2008). Packing density of cementitious materials: part 2—packing and flow of OPC+ PFA+ CSF. *Materials and structures.* **41**(4), 773–784.

De Larrard, F., (1999). *Concrete mixture proportioning: A scientific approach*. London, UK: E & FN Spon.

Mangulkar, M. N. and Jamkar, S. S., (2013). Review of Particle Packing Theories Used For Concrete Mix Proportioning. *International Journal Of Scientific & Engineering Research*. **4**(5), 143–148.

Médici, M. E., Benegas, O. A., Uñac, R. O. and Vidales, A. M., (2012). The effect of blending granular aggregates of different origin on the strength of concrete. *Physica A: Statistical Mechanics and its Applications*. **391**(5), 1934–1941.

Nanthagopalan, P. and Santhanam, M., (2009). Experimental investigations on the influence of paste composition and content on the properties of self-compacting concrete. *Construction and*

Building Materials. **23**(11), 3443–3449.

Nanthagopalan, P. and Santhanam, M., (2012). An empirical approach for the optimisation of aggregate combinations for self-compacting concrete. *Materials and structures*. **45**(8), 1167–1179.

Neville, A. M., (1995). *Properties of Concrete*. Essex: Pearson Education Limited.

Pedro, D., de Brito, J. and Veiga, R., (2012). Mortars Made with Fine Granulate from Shredded Tires. *Journal of Materials in Civil engineering*. **25**(4), 519–529.

Peng, Y., Hu, S. and Ding, Q., (2009). Dense packing properties of mineral admixtures in cementitious material. *Particuology*. **7**(5), 399–402.

Sobolev, K. and Amirjanov, A., (2004). A simulation model of the dense packing of particulate materials. *Advanced Powder Technology*. **15**(3), 365–376.

Sukontasukkul, P., (2009). Use of crumb rubber to improve thermal and sound properties of pre-cast concrete panel. *Construction and Building Materials*. **23**(2), 1084–1092.

Tsai, C. T., Li, L. S., Hwang, C. L., Tasi, C. T., Li, L. S. and Hwang, C. L., (2006). The effect of aggregate gradation on engineering properties of high performance concrete. *Journal of ASTM International*. **3**(3), 891–902.

Wong, H. H. C. and Kwan, A. K. H., (2008a). Packing density of cementitious materials: measurement and modelling. *Magazine of concrete Research*. **60**(3), 165–175.

Wong, H. H. C. and Kwan, A. K. H., (2008b). Packing density of cementitious materials: part 1—measurement using a wet packing method. *Materials and structures*. **41**(4), 689–701.

Wong, H. H. C. and Kwan, A. K. H. (2008c). Rheology of cement paste: role of excess water to solid surface area ratio. *Journal of Materials in Civil engineering*. **20**(2), 189–197.

Youssf, O., ElGawady, M. A., Mills, J. E. and Ma, X., (2014). An experimental investigation of crumb rubber concrete confined by fibre reinforced polymer tubes. *Construction and Building Materials*. **53**, 522–532.

Appendix C. Fresh Concrete Mixes

The original mix (O) parameters were optimised to achieve a mix that can incorporate high volumes of rubber with minimum influence on the concrete fresh performance and compressive strength. The results of this research are presented in Chapter 2 of this thesis; however, this section presents additional information and photos on the mix optimisation practice that could not be included in Chapter 2 due to space limitations.

C.1   MIX PARAMETERS

For the convenience of the reader, the original mix and the final optimised mix are presented Table C.1 and Table C.2, respectively.

Table C.1 Original mix design

Material	Quantity/m^3
CEM II – 52.5 MPa	425 kg/m^3
Aggregates 0/5mm	820 kg/m^3
Aggregates 5/10mm	364 kg/m^3
Aggregates 10/20mm	637 kg/m^3
Water	180 l/m^3
Plasticiser (Sika Viscoflow 1000)	2.5 l/m^3
Superplasticiser (Sika Viscoflow 2000)	5.1 l/m^3

Table C.2 Optimise mix proportions (no rubber replacement)

Material	Quantity/m³
CEM II – 52.5 MPa	340 kg/m³
Silica Fume (SF)	42.5 kg/m³
Pulverised Fuel Ash (PFA)	42.5 kg/m³
Aggregates 0/5mm	820 kg/m³
Aggregates 5/10mm	364 kg/m³
Aggregates 10/20mm	637 kg/m³
Water	149 l/m³
Plasticiser (Sika Viscoflow 1000)	2.5 l/m³
Superplasticiser (Sika Viscoflow 2000)	5.1 l/m³

Table C.3 presents the mix parameters that were investigated to evaluate their effect on RuC fresh performance and short-term compressive strength. For comparison purposes, a rubber content replacing 40% of the sand volume (18% of the total aggregate volume) was used in all trial mixes in the preliminary study. Some additional rubber contents were investigated for the original mix (O), mix (C), as shown below.

Table C.3 Description of mix parameters

Mix	Rubber Content* (%)	Cement (kg/m³)	SF (kg/m³)	PFA (kg/m³)	w/b	Other parameters
O1	0	425	0	0	0.423	-
O2	10	425	0	0	0.423	-
O3	40	425	0	0	0.423	-
O4	100	425	0	0	0.423	-
A1	40	425	0	0	0.35	-
A2	40	425	0	0	0.35	Rubber pre-washed with water
A3	40	425	0	0	0.38	-
A4	40	425	0	0	0.38	Rubber pre-washed with water
A5	40	425	0	0	0.35	0.01% air entraining agent added
A6	40	425	0	0	0.30	Admixtures pre-mixed with water
A7	40	425	0	0	0.32	Admixtures pre-mixed with water
A8	40	425	0	0	0.35	Admixtures pre-mixed with water

A9	40	425	0	0	0.32	Admixtures pre-mixed with water
B1	40	425	0	0	0.423	Total admixtures reduced by 20%
B2	40	425	0	0	0.423	Superplasticiser reduced by 40%
B3	40	425	0	0	0.423	Plasticiser reduced by 80%
C1	10	425	0	0	0.423	Rubber added to the mix rather than used
C2	40	425	0	0	0.423	as an aggregate replacement
C3	40	425	0	0	0.35	
C4	40	425	0	0	0.38	
D1	40	340	10	10	0.35	-
D2	40	340	10	10	0.35	pre-coating the rubber with SF
D3	40	340	10	10	0.33	-
E1	40	425	10	10	0.35	Rubber added at the last 2 minutes
I1	40	425	10	10	0.35	Additional 40kg/m^3 RTSF$^\#$

*Rubber content as a percentage of the volume of fine aggregates (sand)

$^\#$ Recycled tyre steel fibres

A more exhaustive experimental programme was adopted for the "optimum mix" D1. Rubber contents were varied from 0-100% of the fine or coarse aggregate volume. A combined replacement of 20%, 40% and 60% of the total aggregate volume was also investigated. These mixes were identified by indicating the volume followed by the type of aggregate replaced (FR for fine rubber or CR for coarse rubber). Mixes with a combined replacement of 20%, 40% and 60% of the total aggregate volume are denoted as 20CR20FR, 40CR40FR and 60CR60FR, respectively.

C.2   PHOTOS

Figure C.1 Flow table test for mix O1

Figure C.2 Flow table test for mix O4

Figure C.3 Flow table test for mix A1

Figure C.4 Flow table test for mix A1
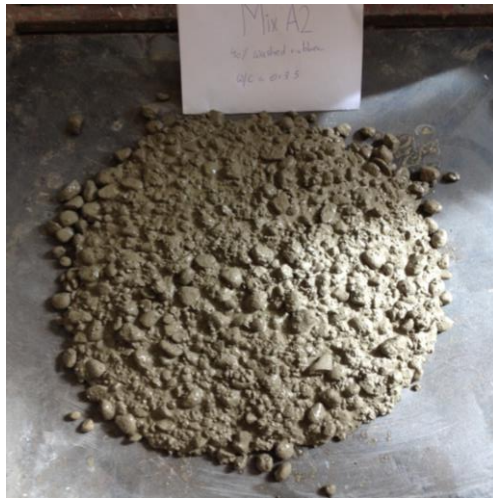
Figure C.5 Flow table test for mix A2

Figure C.6 Slump test for mix A2

Figure C.7 Flow table test for mix A3

Figure C.8 Slump test for mix A3

Figure C.9 Flow table test for mix A4

Figure C.10 Slump test for mix A4

Figure C.11 Slump test for mix A5
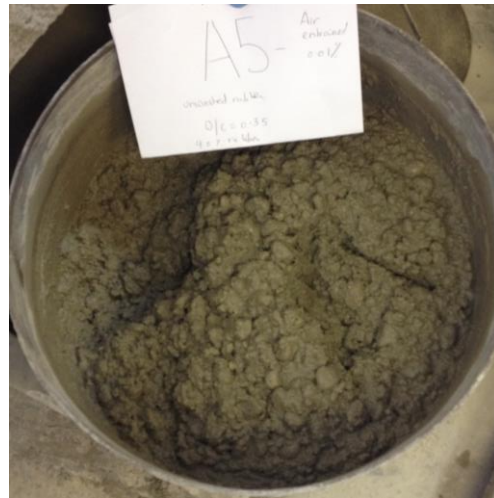
Figure C.12 Fresh appearance of mix A5

Figure C.13 Fresh appearance of mix A6

Figure C.14 Slump test for mix A7
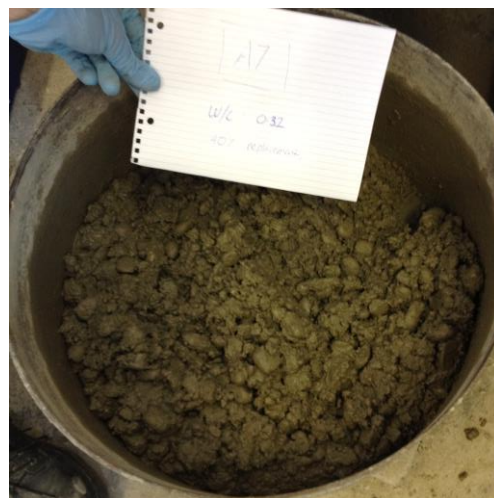
Figure C.15 Fresh appearance of mix A7

203
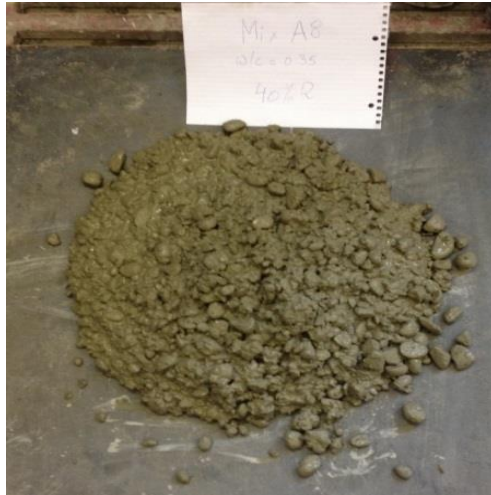
Figure C.16 Flow table test for mix A8
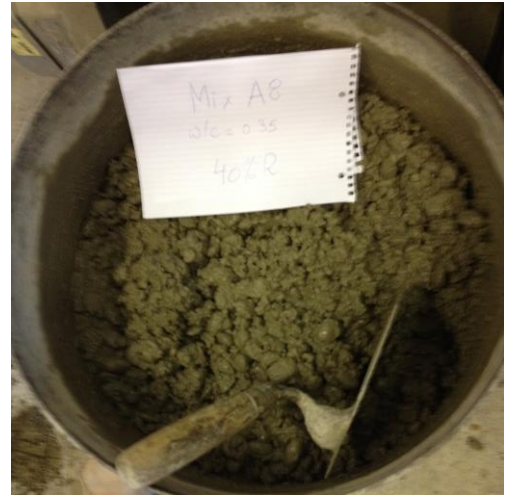
Figure C.17 Fresh appearance of mix A8

Figure C.18 Fresh appearance of mix A9

Figure C.19 Flow table test for mix B1

Figure C.20 Fresh appearance of mix B1

Figure C.21 Flow table test for mix B2
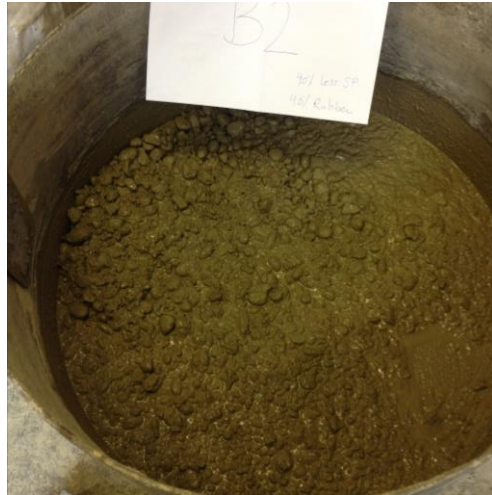
Figure C.22 Fresh appearance of mix B2

Figure C.23 Flow table test for mix B3

Figure C.24 Fresh appearance of mix B3

Figure C.25 Flow table test for mix C1

Figure C.26 Fresh appearance of mix C1

Figure C.27 Flow table test for mix C2

Figure C.28 Slump test for mix C2
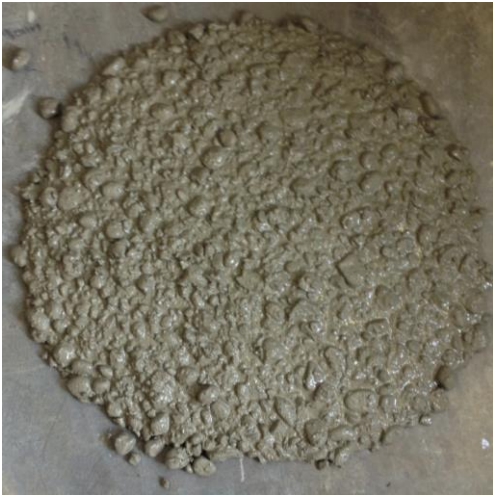
Figure C.29 Flow table test for mix D1

Figure C.30 Slump test for mix D1

Figure C.31 Flow table test for mix D2

Figure C.32 Flow table test for mix D3

Figure C.33 Slump test for mix D3

Figure C.34 Flow table test for mix E1

Figure C.35 Slump test for mix E1

Figure C.36 Appearance of fibre balling in mix I1

C.3 OPTIMISED MIX PHOTOS

C.3.1 Plain mix

Figure C.37 Flow test for plan mix (0% rubber)

Figure C.38 Slump test for plain mix (0% rubber)

C.3.2 Fine aggregate replacement

Figure C.39 Flow table test for mix 40FR

Figure C.40 Slump test for mix 40FR

Figure C.41 Flow table test for mix 60FR

Figure C.42 Slump test for mix 60FR

Figure C.43 Flow table test for 80FR

Figure C.44 Slump test for 80FR

C.3.3 Coarse aggregate replacement
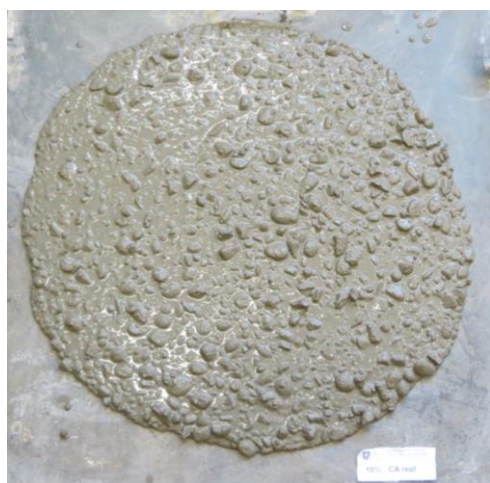
Figure C.45 Flow table test for mix 10 CR

Figure C.46 Slump table for mix 10 CR

Figure C.47 Flow table test for mix 20CR

Figure C.48 Flow table test for mix 60CR

Figure C.49 Slump test for mix 60CR

Figure C.50 Flow table test for mix 100CR

Figure C.51 Slump test for mix 100CR

C.3.4 Combined replacement of fine and coarse aggregate

Figure C.52 Flow table test for mix 20CR20FR

Figure C.53 Slump test for mix 20CR20FR
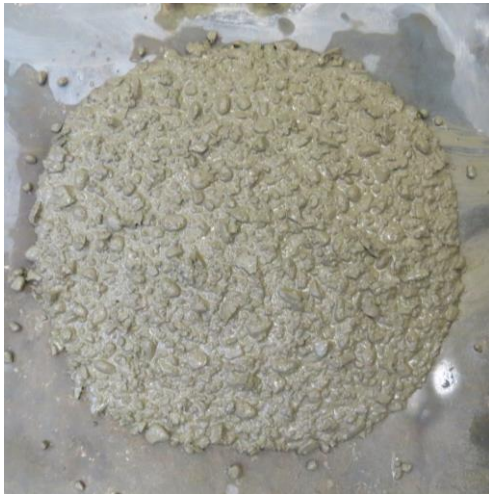
Figure C.54 Flow table test for mix 40CR40FR

Figure C.55 Slump test for mix 40CR40FR

Figure C.56 Flow table test for mix 60CR60FR

Figure C.57 Slump test for mix 60CR60FR

Figure C.58 Collapse of slump test for mix 60CR60FR

Appendix D. Instrumentation and Test Setup

The typical setup and instrumentation used on individual cylinders confined with either AFRP or CFRP subjected to monotonic or cyclic loading (from experimental programmes presented in Chapters 4 and 5) is shown in Figure 1.
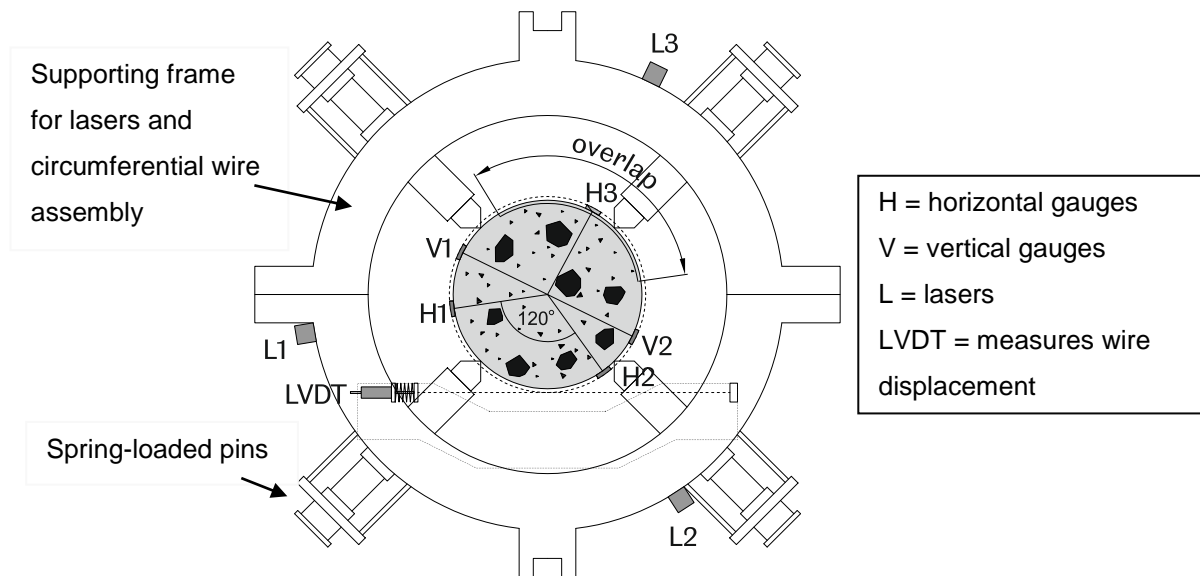
Figure 1. Schematic diagram of instrumentation and test setup

The experimental results are presented in Appendices E and F in terms of σ-ε curves of individual and average data from i) horizontal strain gauges (H1, H2, H3), ii) vertical strain gauges (V1, V2), iii) lasers (L1, L2, L3). The average volumetric ratio as well as the overall σ-ε curves, including average strains from all the aforementioned instrumentation and the envelope curves (in the case of cyclically loaded cylinders) are also presented. The final (average) axial

213

σ-ε curves were obtained, as described in Chapter 4, by using average readings from the vertical gauges (V1,V2), up to critical stress (f_{cr}), after which average measurements from the lasers (L1, L2, L3) were used. All horizontal strains were obtained from average readings from the horizontal gauges (H1, H2, H3). The LVDT connected to the circumferential wire was often not activated or the wire assembly moved during the test, leading to false readings. Therefore, its measurements were not used in the analysis and are not included in the relevant appendices (E and F).

The test cylinders (ϕ100x200) are identified according to the number of confining layers (2,3, 4 or 6), the confining material (A or AFRP or C for CFRP), the loading protocol (M for monotonic or C for cyclic) and the specimen number (1,2, or 3) in this same order. Larger cylinders (ϕ150x300) were denoted with an additional letter (L) after the specimen number. For example, specimen two of a large cylinder confined with six layers of CFRP tested monotonically is denoted as 6C-M2-L.

Appendix E. Experimental Data – Monotonic Loading

This appendix presents detailed experimental data from the monotonically loaded cylinders described in Chapters 4 and 5. A description of the instrumentation details and cylinder notation can be found in appendix D.

2A-M1
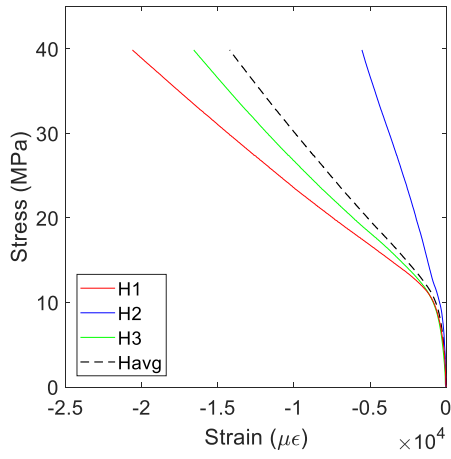
Figure E.1 σ-ε curves from H gauges
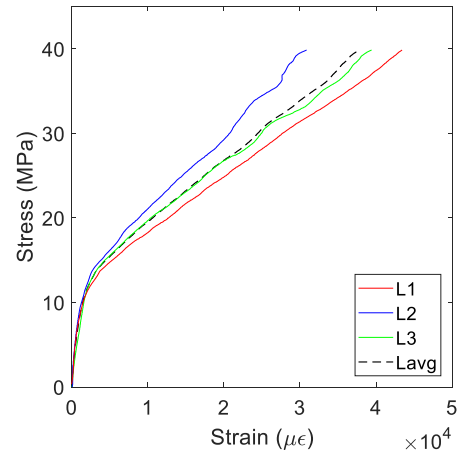
Figure E.2 σ-ε curves from lasers (L)
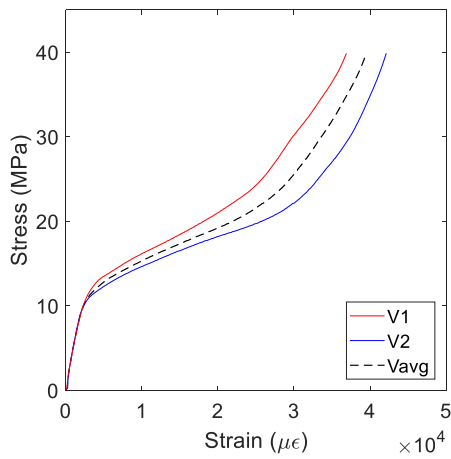
Figure E.3 σ-ε curves from V gauges
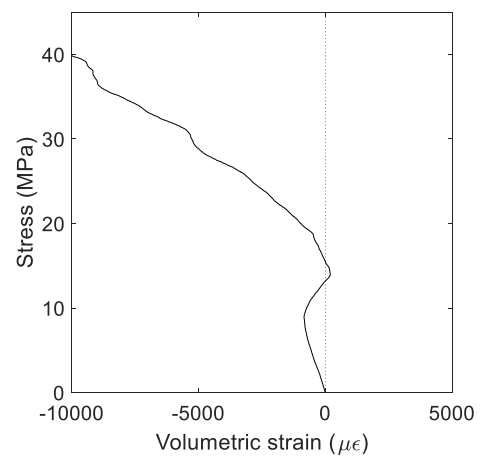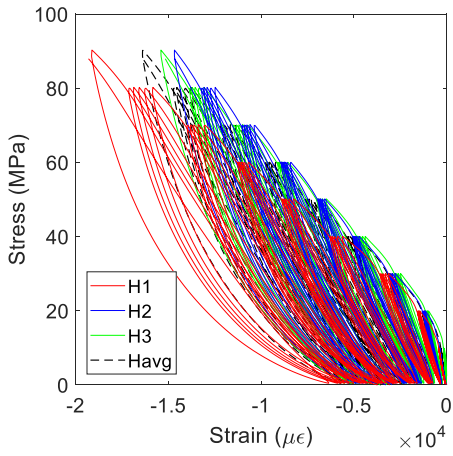

Figure E.4 Stress vs.average volumetric strain
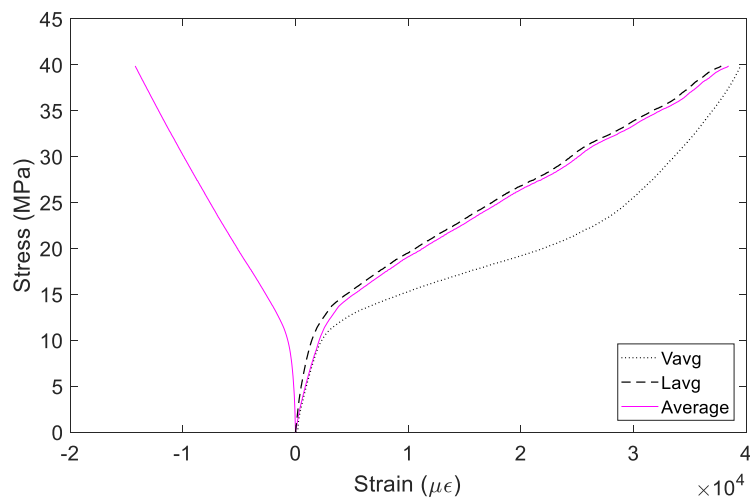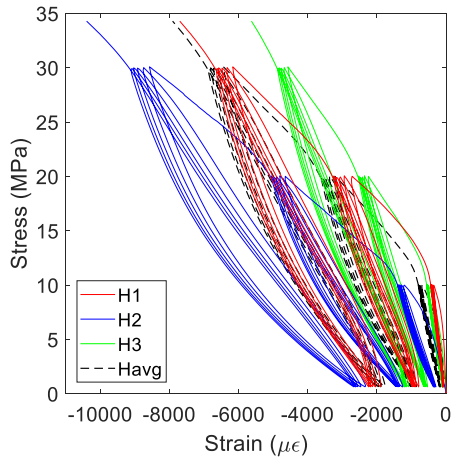

Figure E.5 Average curves

2A-M2
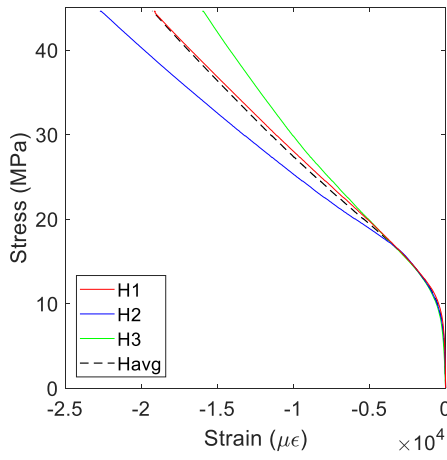
Figure E.6 σ-ε curves from H gauges
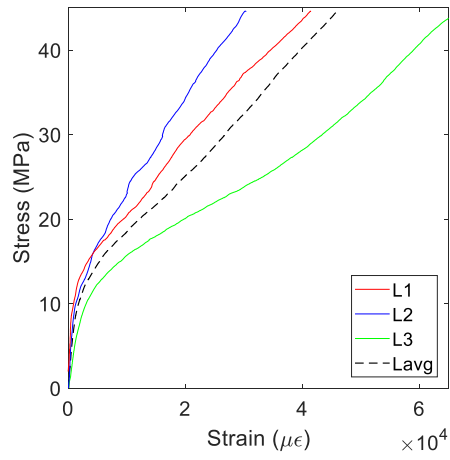
Figure E.7 σ-ε curves from lasers (L)
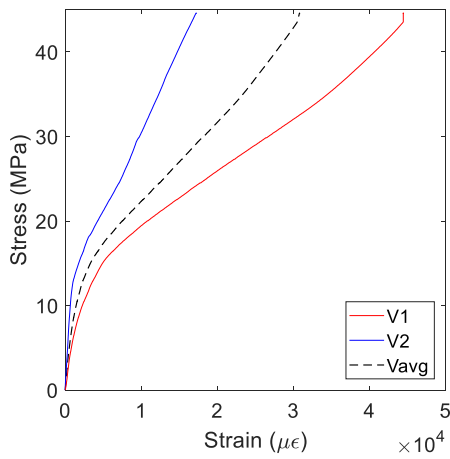
Figure E.8 σ-ε curves from V gauges
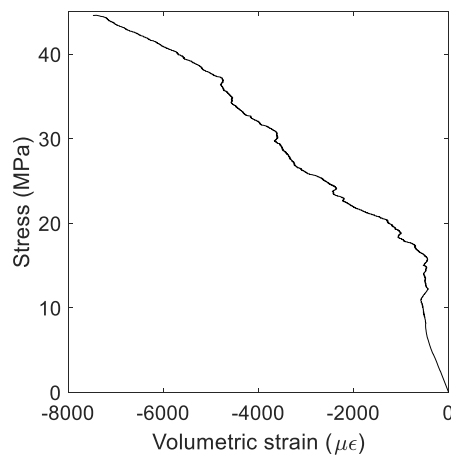
Figure E.9 Stress vs. average volumetric strain
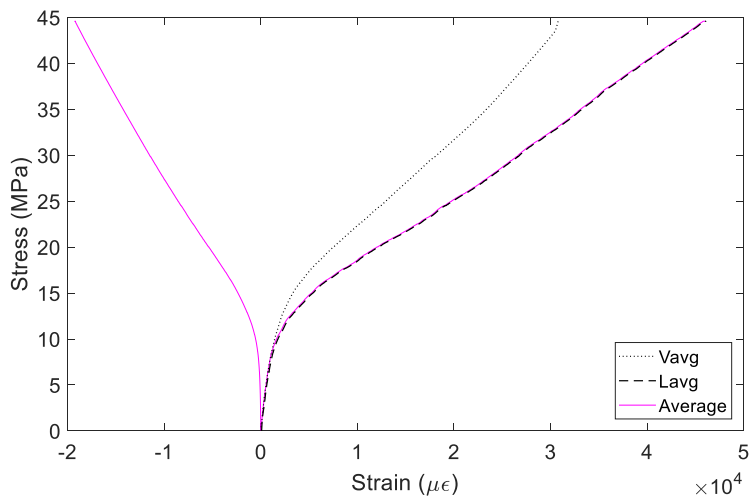
Figure E.10 Average curves

3A-M1
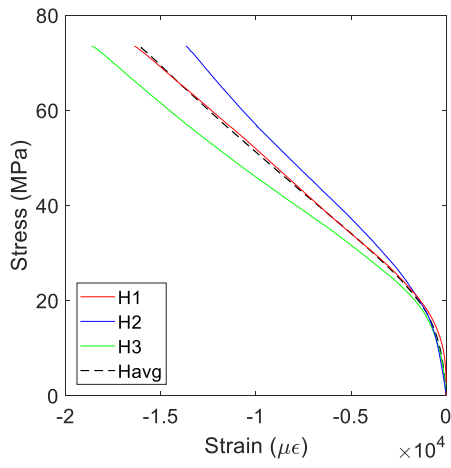
Figure E.11 σ-ε curves from H gauges
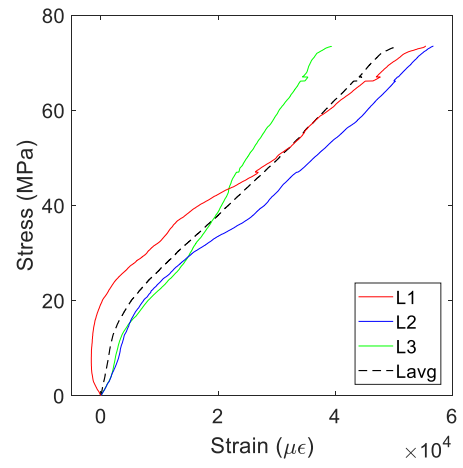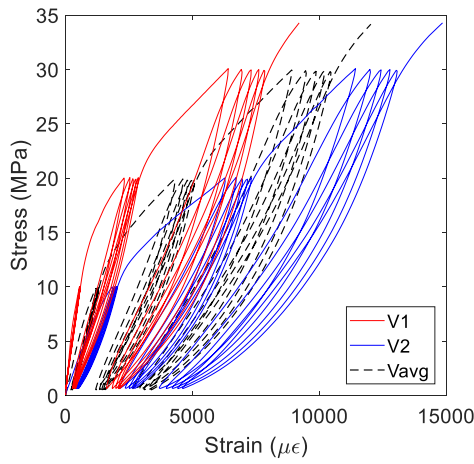

Figure E.12 σ-ε curves from lasers (L)
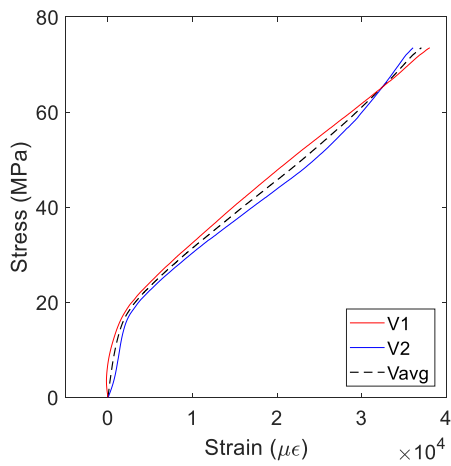
Figure E.13 σ-ε curves from V gauges
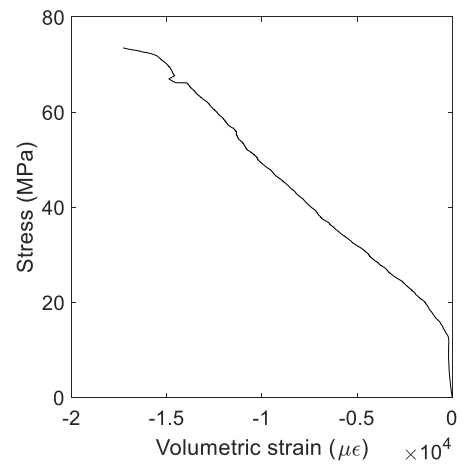
Figure E.14 Stress vs. volumetric strain
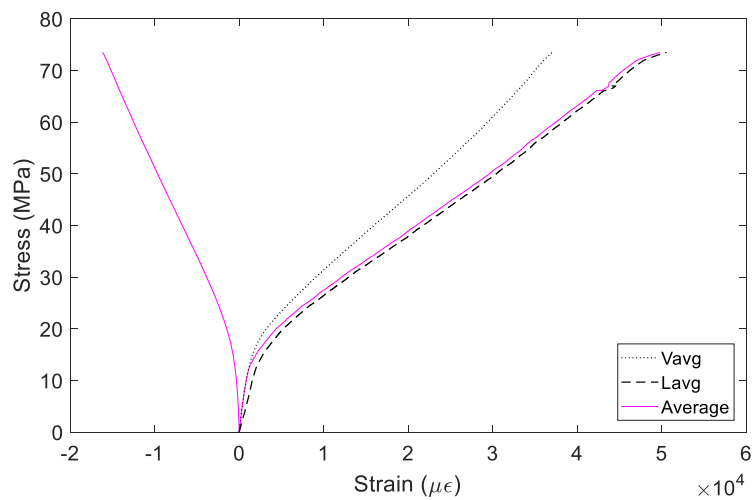
Figure E.15 Average curves

3A-M2
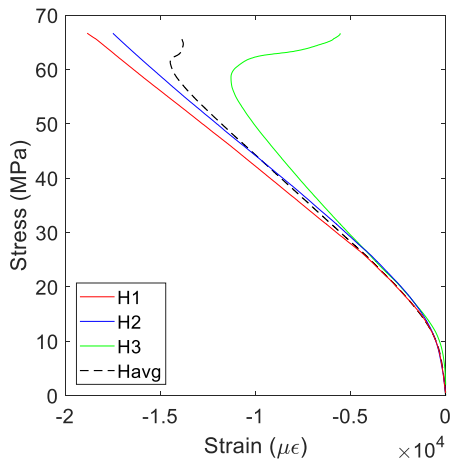
Figure E.16 σ-ε curves from H gauges
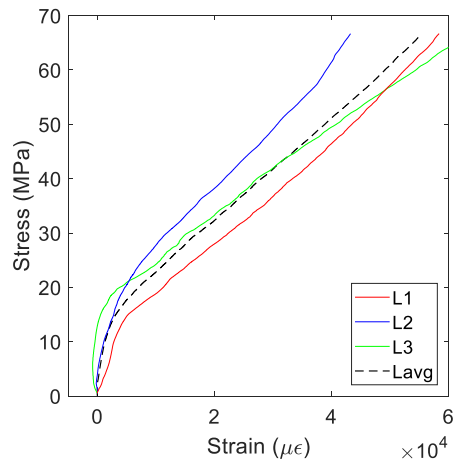
Figure E.17 σ-ε curves from lasers (L)
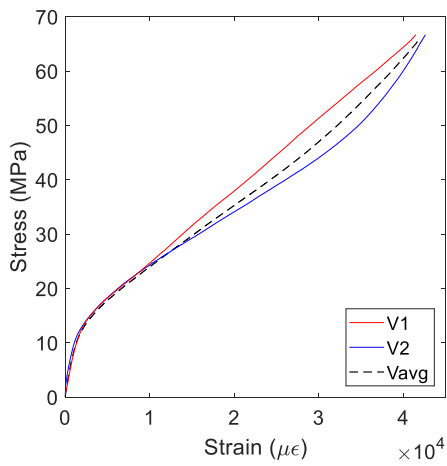
Figure E.18 σ-ε curves from V gauges
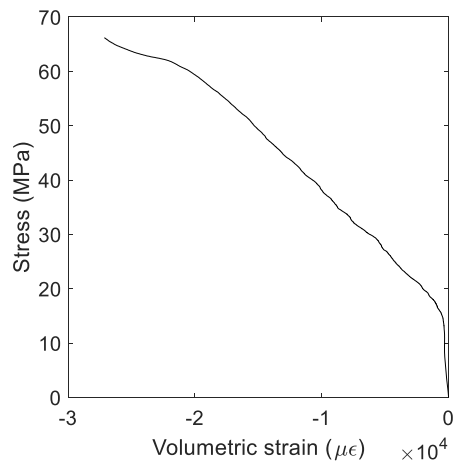
Figure E.19 Stress vs. volumetric strain
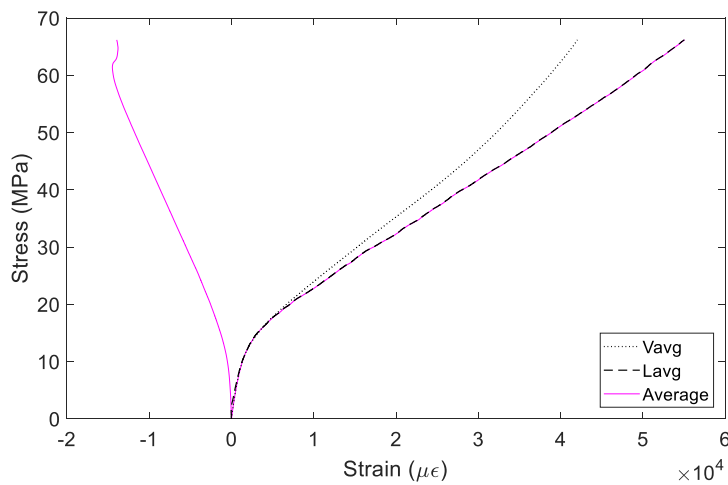
Figure E.20 Average curves

4A-M1
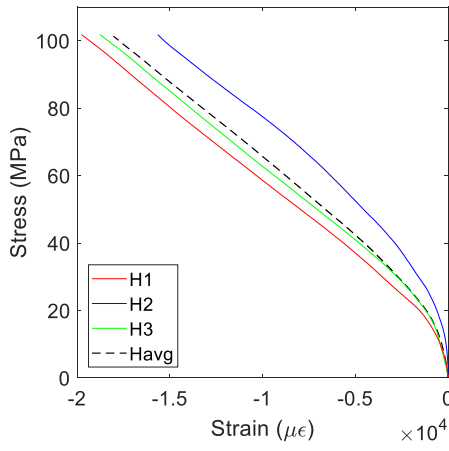
Figure E.21 σ-ε curves from H gauges
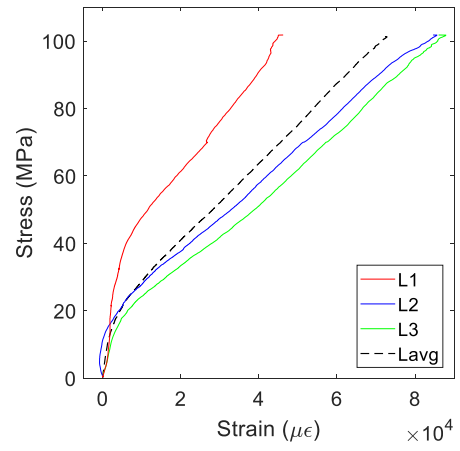
Figure E.22 σ-ε curves from lasers (L)
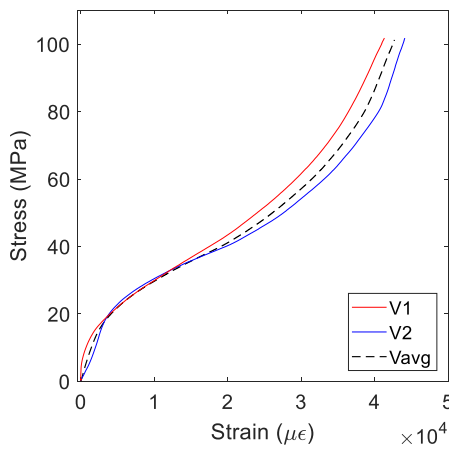
Figure E.23 σ-ε curves from V gauges
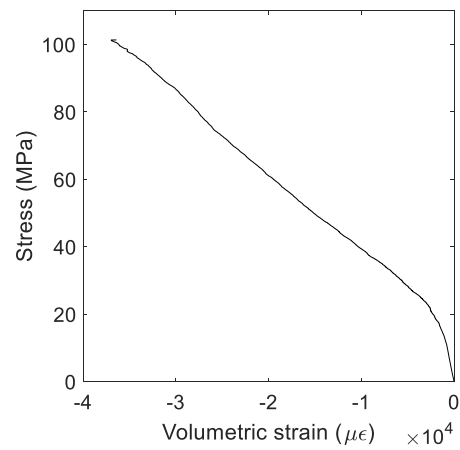
Figure E.24 Stress vs. volumetric strain
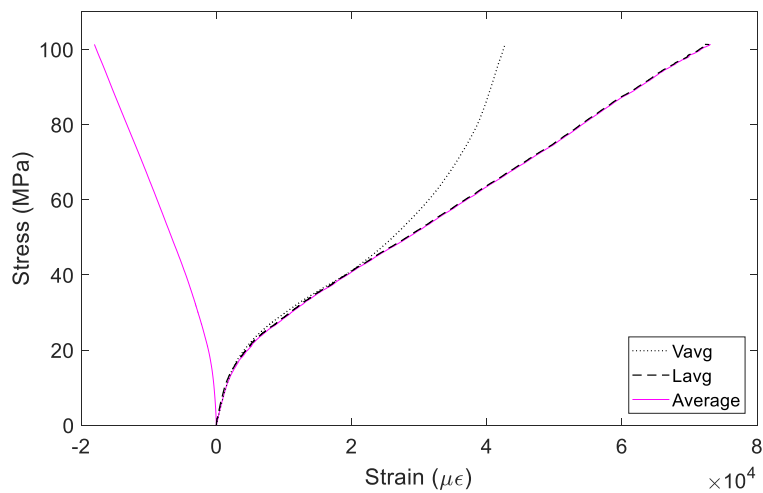
Figure E.25 Average curves

4A-M2
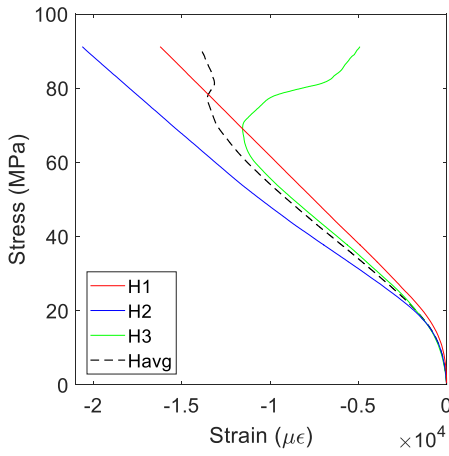
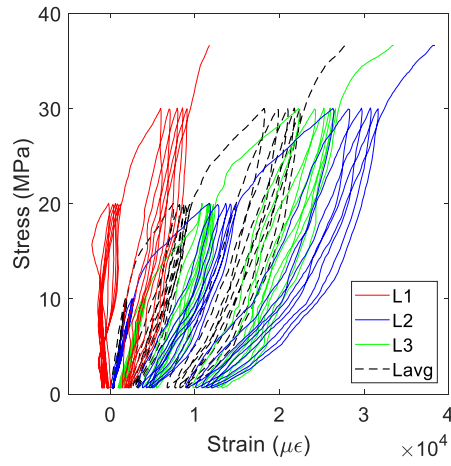**Figure E.26 σ-ε curves from H gauges**
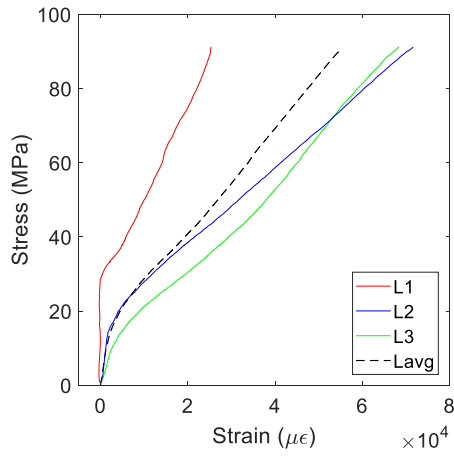
Figure E.27 σ-ε curves from lasers (L)
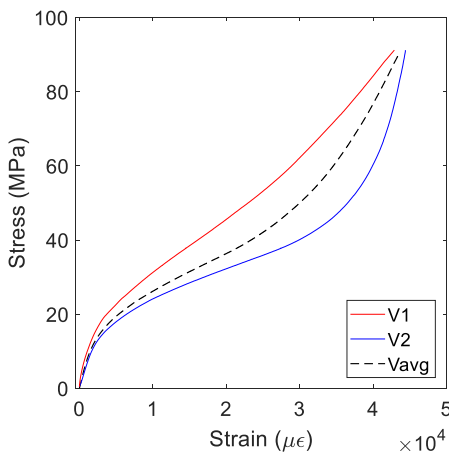
Figure E.28 σ-ε curves from V gauges
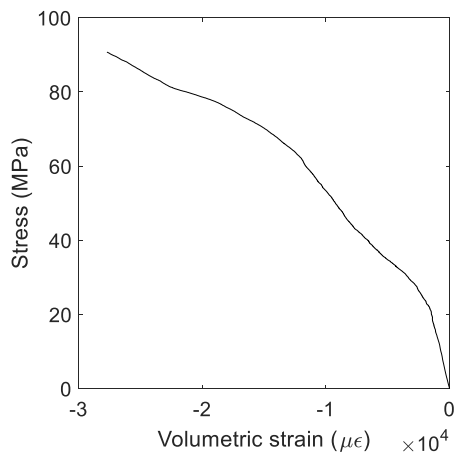
Figure E.29 Stress vs. volumetric strain
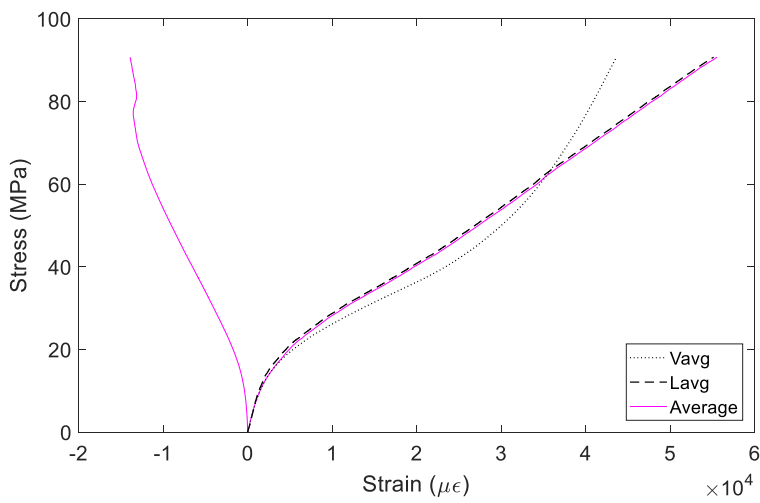
Figure E.30 Average curves

3A-M1-L
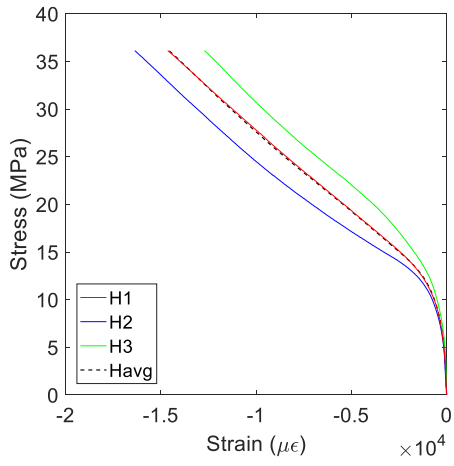
Figure E.31 σ-ε curves from H gauges
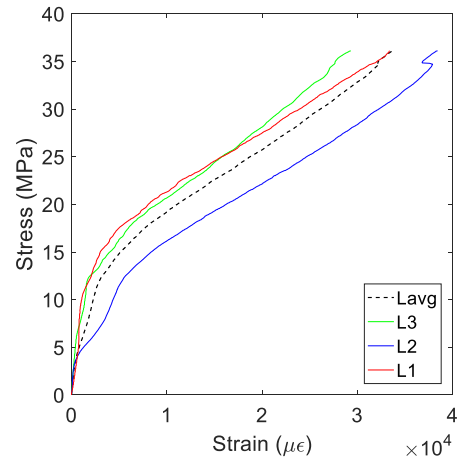
Figure E.32 σ-ε curves from lasers (L)
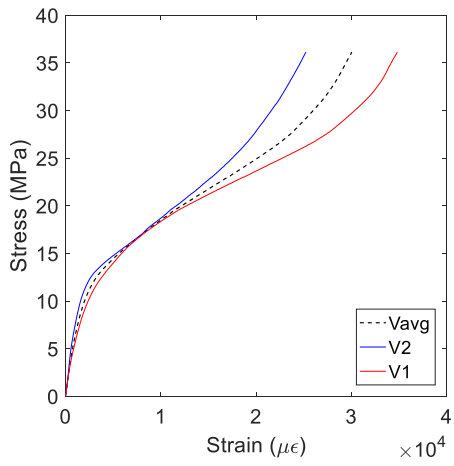
Figure E.33 σ-ε curves from V gauges
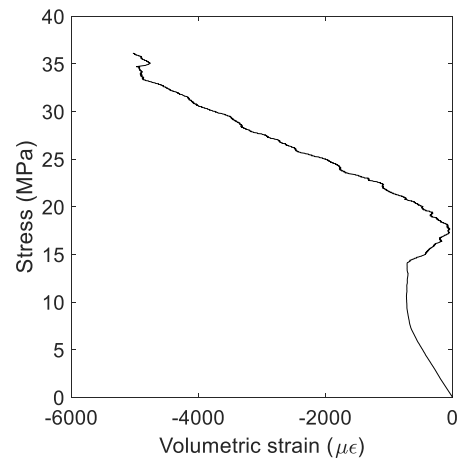
Figure E.34 Stress vs. average volumetric strain
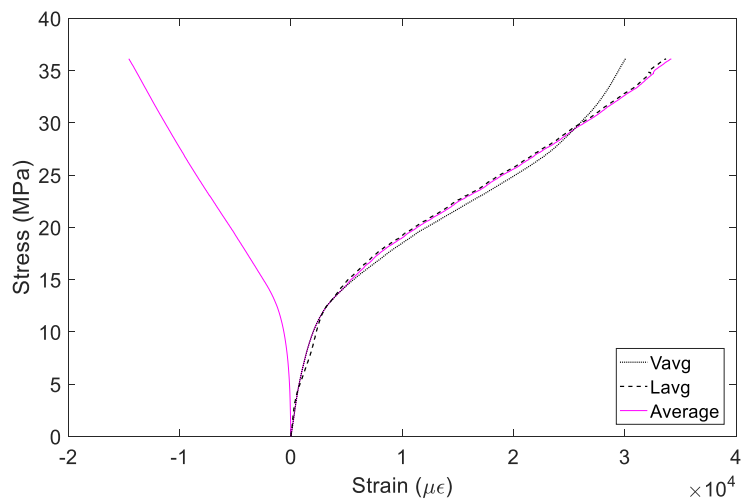
Figure E.35 Average curves

3A-M2-L
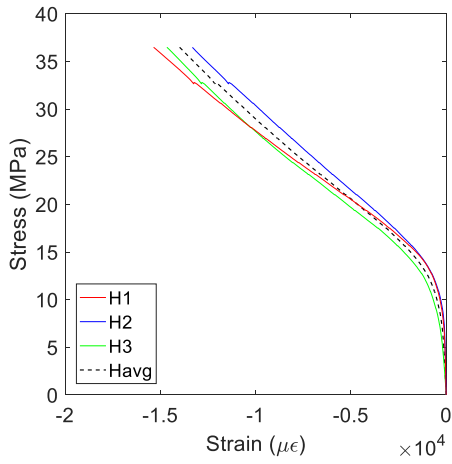
Figure E.36 σ-ε curves from H gauges
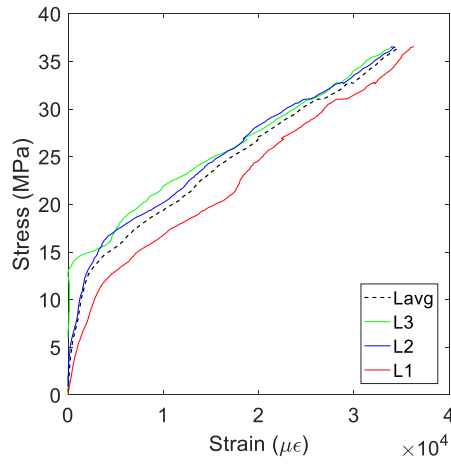
Figure E.37 σ-ε curves from lasers (L)
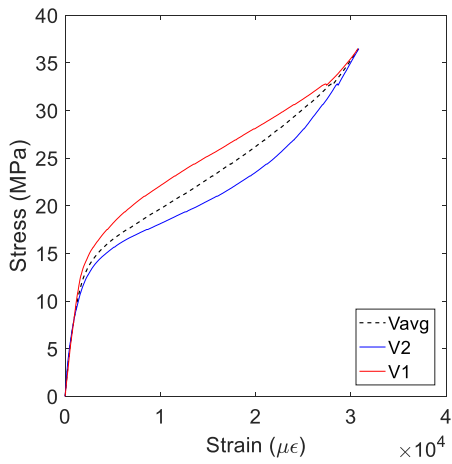
Figure E.38 σ-ε curves from V gauges
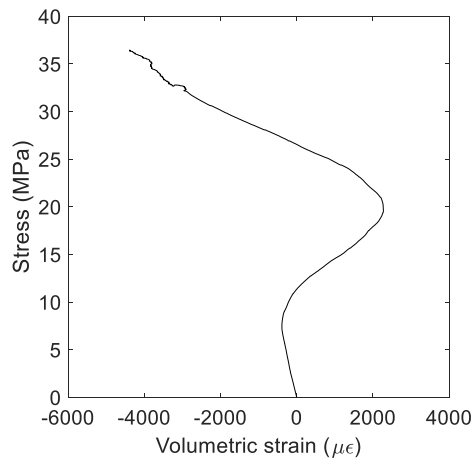
Figure E.39 Stress vs. average volumetric strain
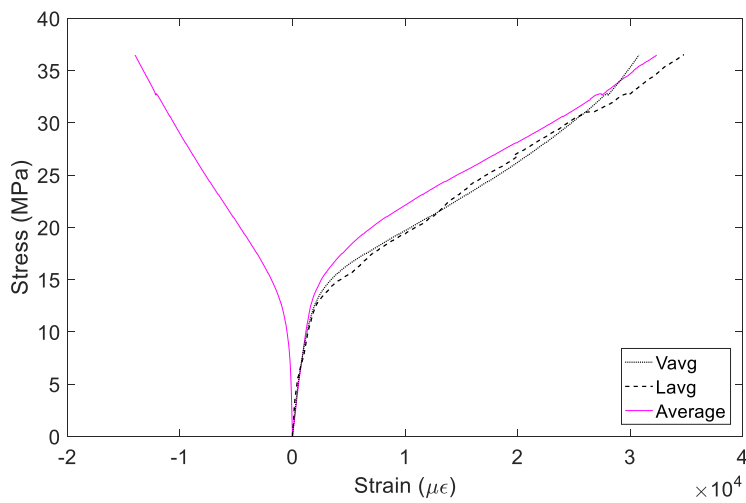
Figure E.40 Average curves

6A-M1-L
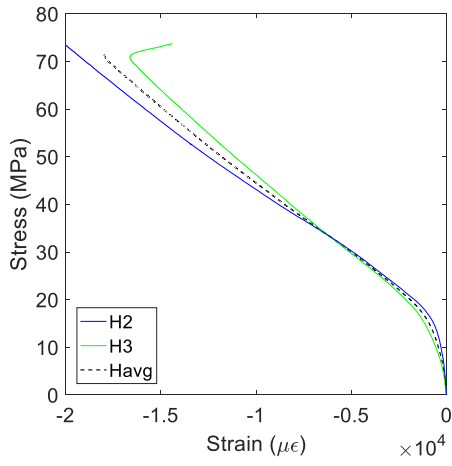
Figure E.41 σ-ε curves from H gauges
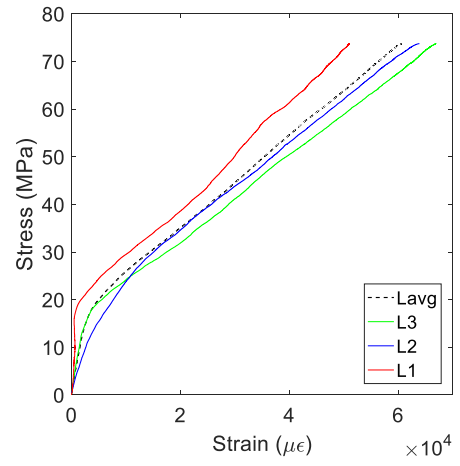
Figure E.42 σ-ε curves from lasers (L)
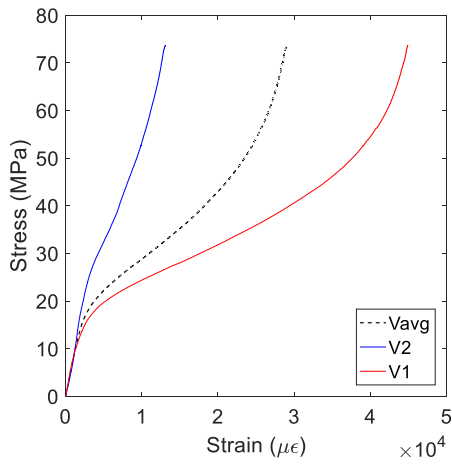
Figure E.43 σ-ε curves from V gauges
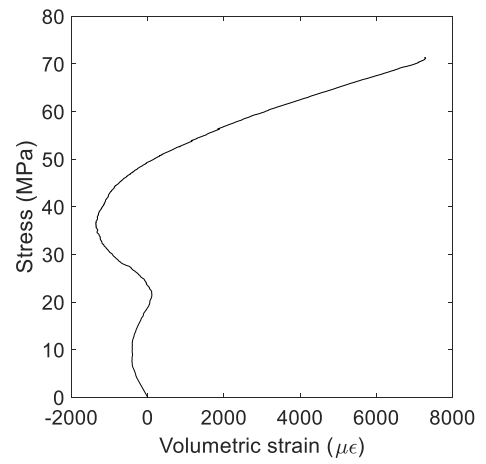
Figure E.44 Stress vs. average volumetric strain
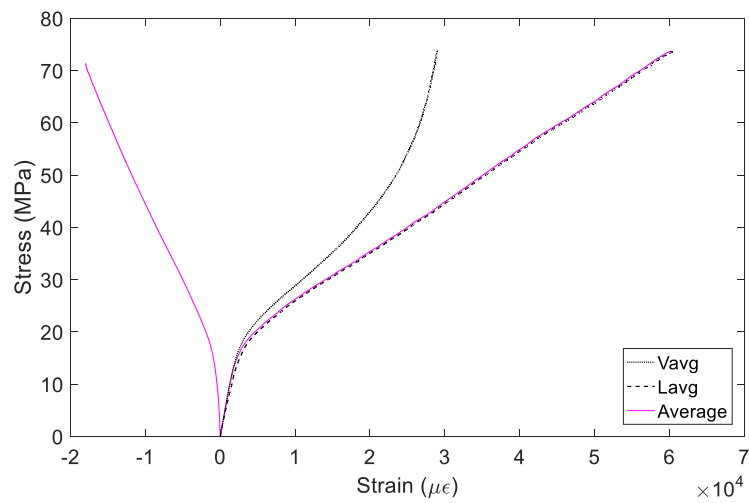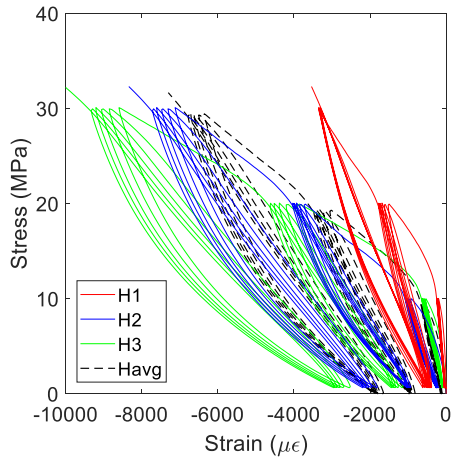

Figure E.45 Average curves

6A-M2-L
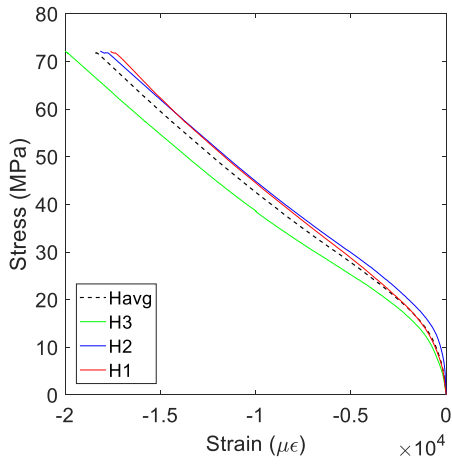
Figure E.46 σ-ε curves from H gauges
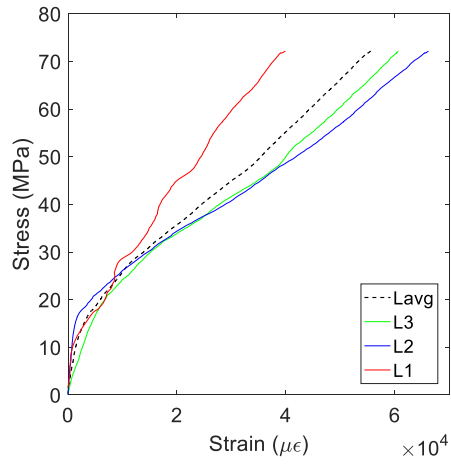
Figure E.47 σ-ε curves from lasers (L)
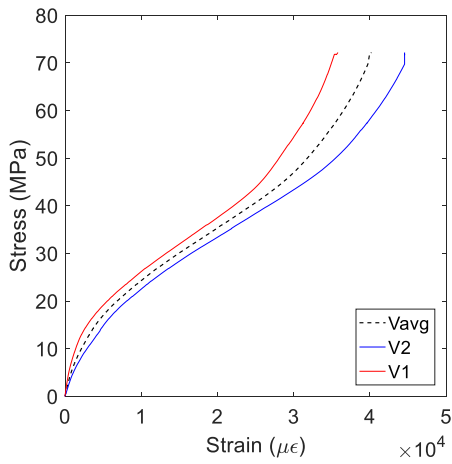
Figure E.48 σ-ε curves from V gauges
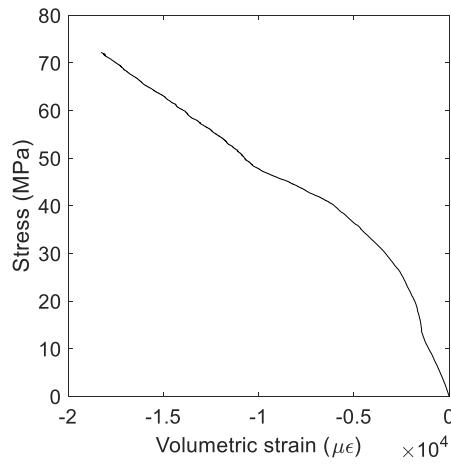
Figure E.49 Stress vs. average volumetric strain
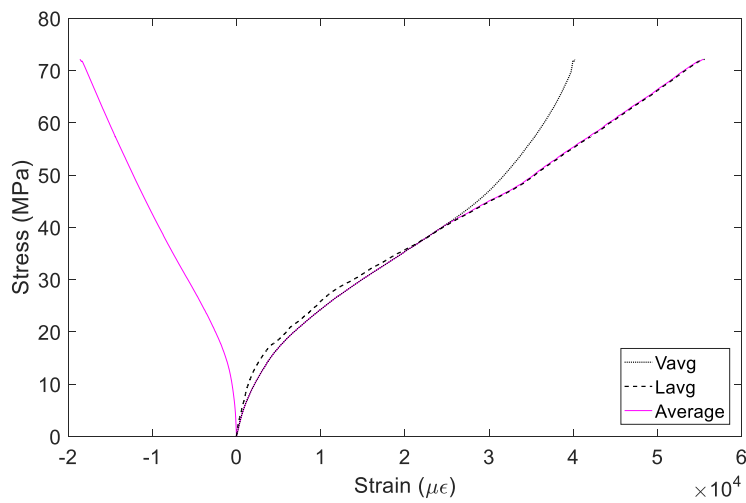
Figure E.50 Average curves

2C-M1
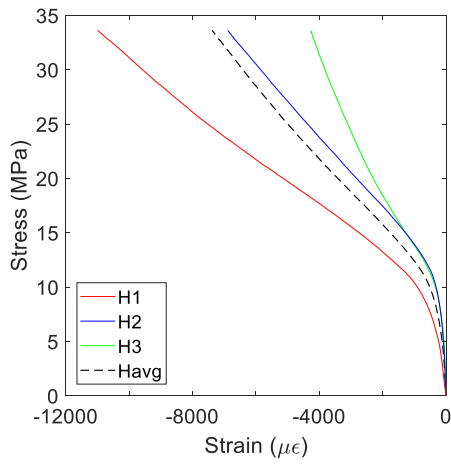
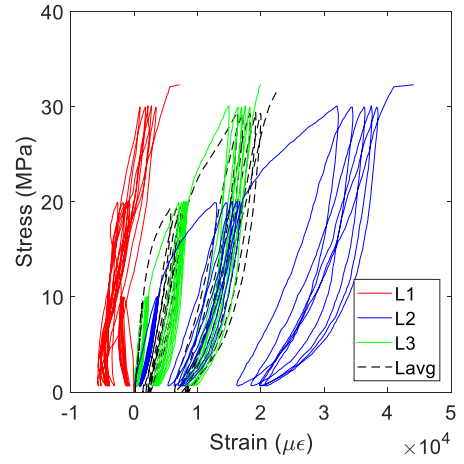**Figure E.51 σ-ε curves from H gauges**
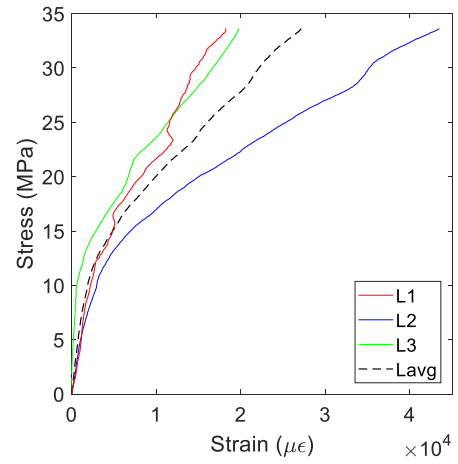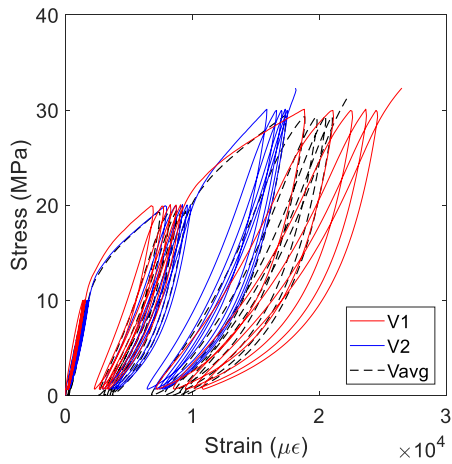

Figure E.52 σ-ε curves from lasers (L)
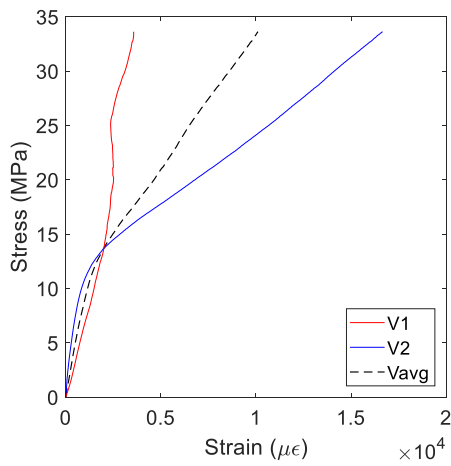
Figure E.53 σ-ε curves from V gauges
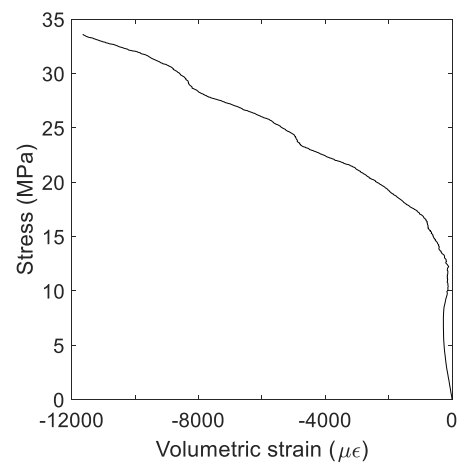
Figure E.54 Stress vs. volumetric strain
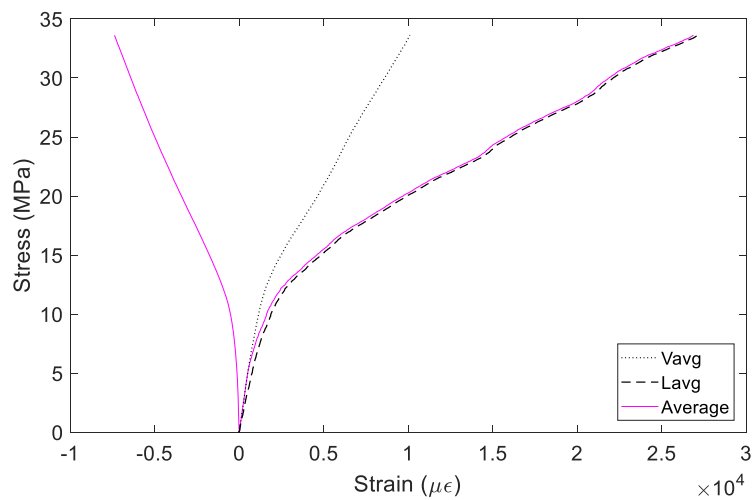
Figure E.55 Average curves

2C-M2
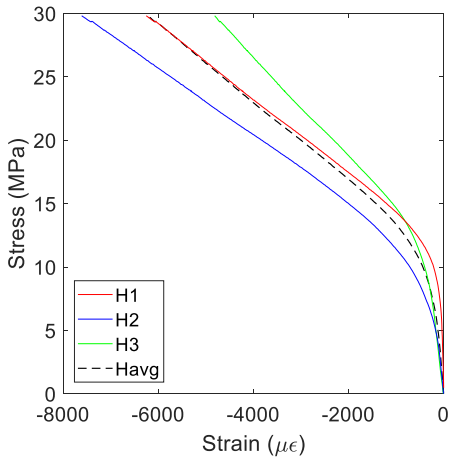
Figure E.56 σ-ε curves from H gauges
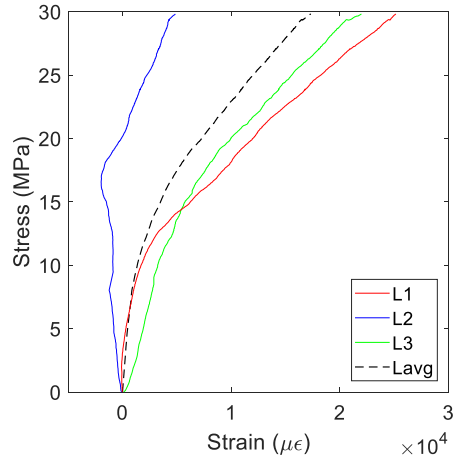
Figure E.57 σ-ε curves from lasers (L)
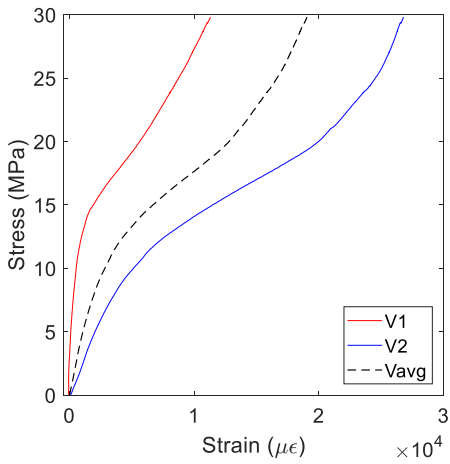
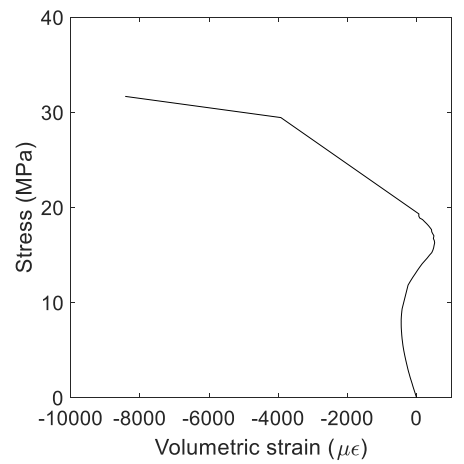**Figure E.58 σ-ε curves from V gauges**
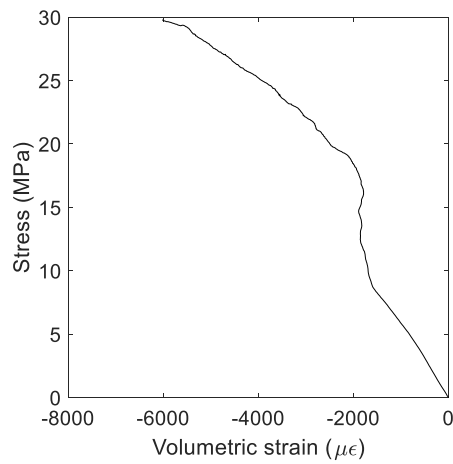
Figure E.59 Stress vs. volumetric strain
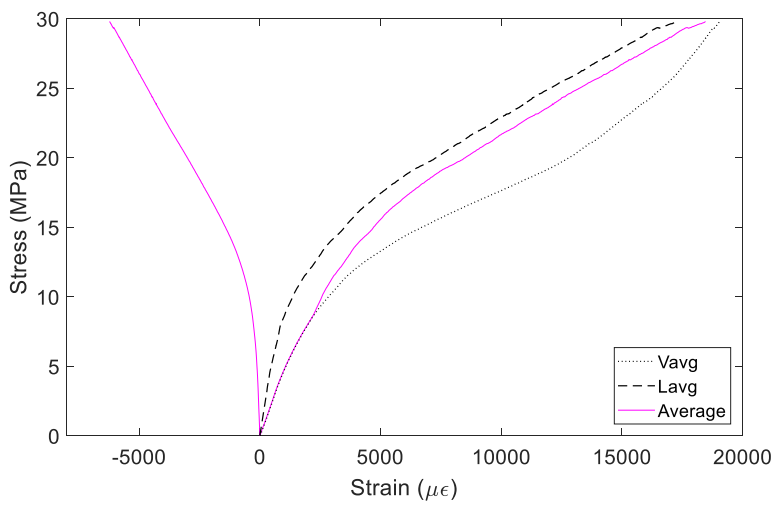
Figure E.60 Average curves

3C-M1
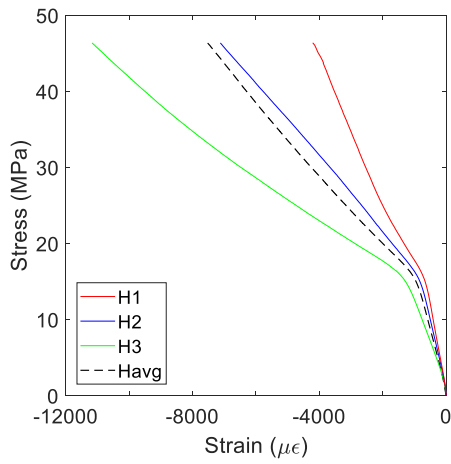
Figure E.61 σ-ε curves from H gauges
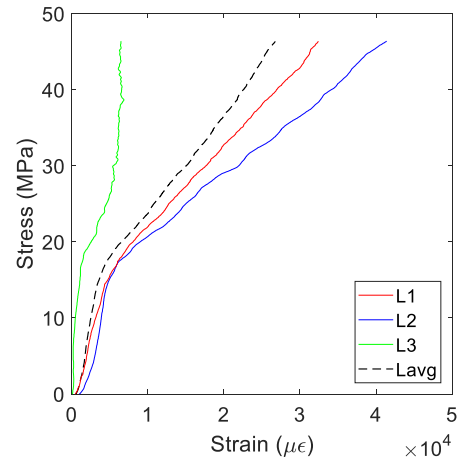
Figure E.62 σ-ε curves from lasers (L)
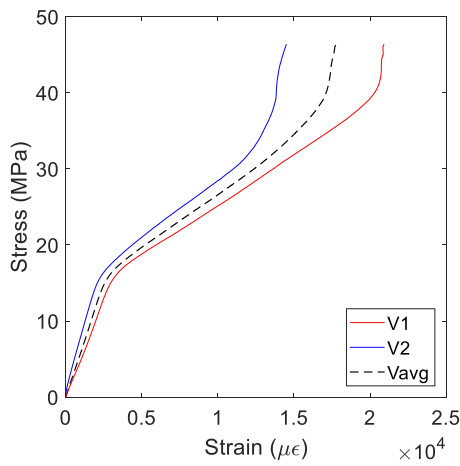
Figure E.63 σ-ε curves from V gauges
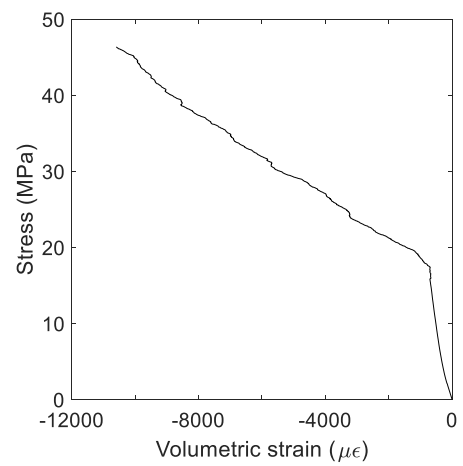
Figure E.64 Stress vs. volumetric strain
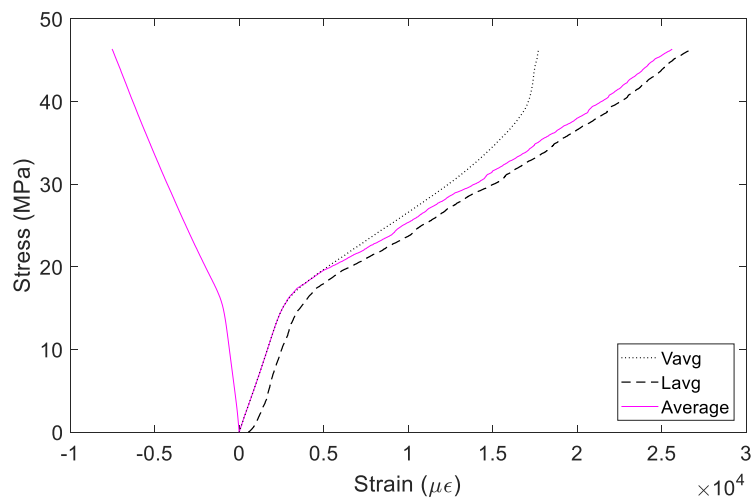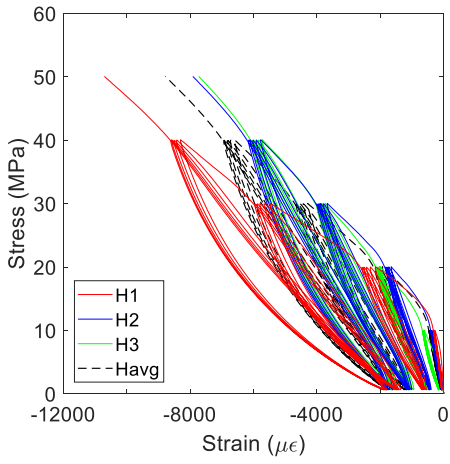

Figure E.65 Average curves

3C-M2
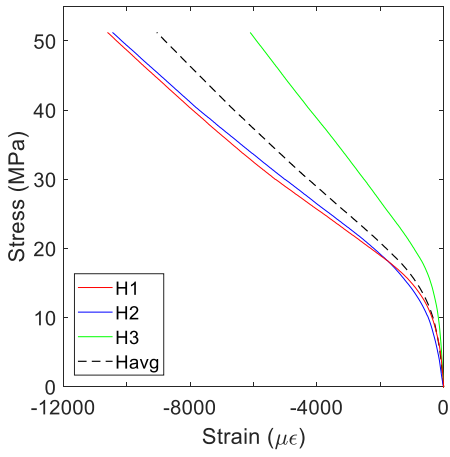
Figure E.66 σ-ε curves from H gauges
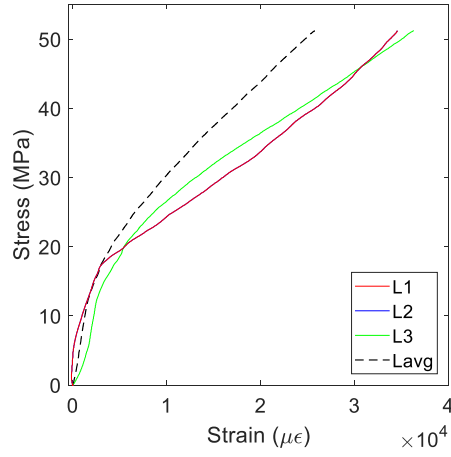
Figure E.67 σ-ε curves from lasers (L)
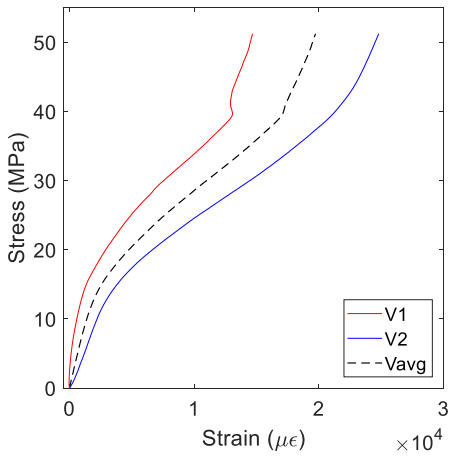
Figure E.68 σ-ε curves from V gauges
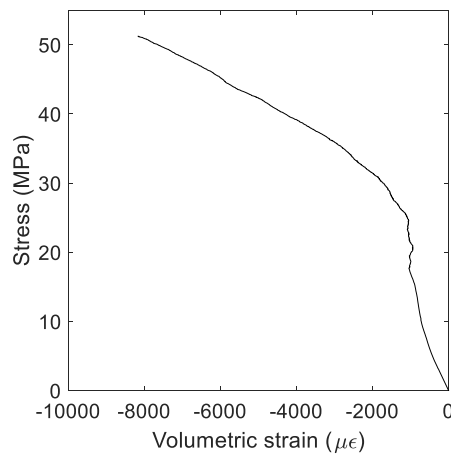
Figure E.69 Stress vs. volumetric strain
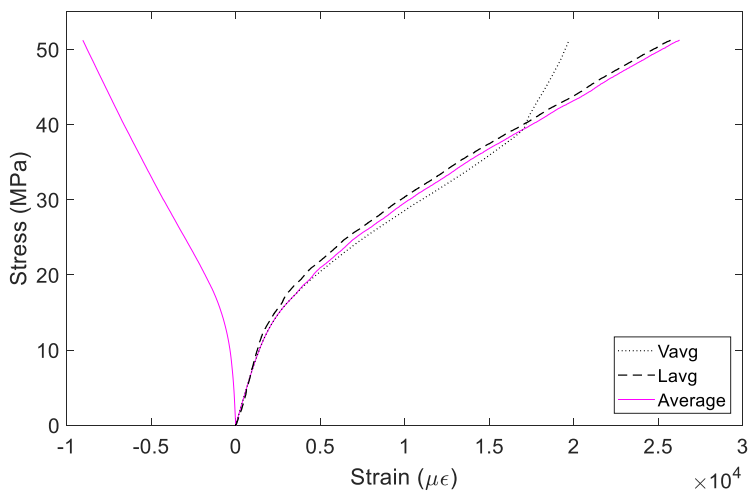
Figure E.70 Average curves

4C-M1
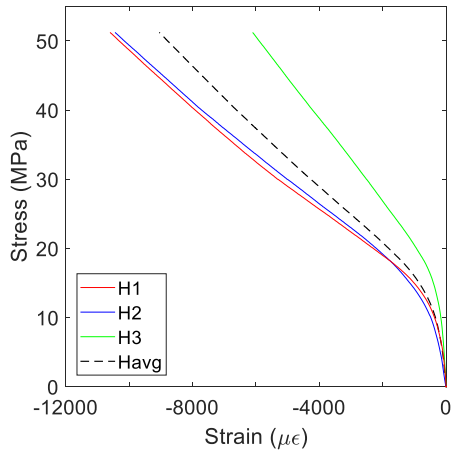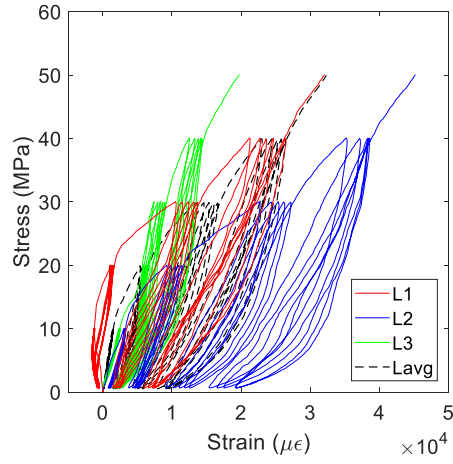

Figure E.71 σ-ε curves from H gauges
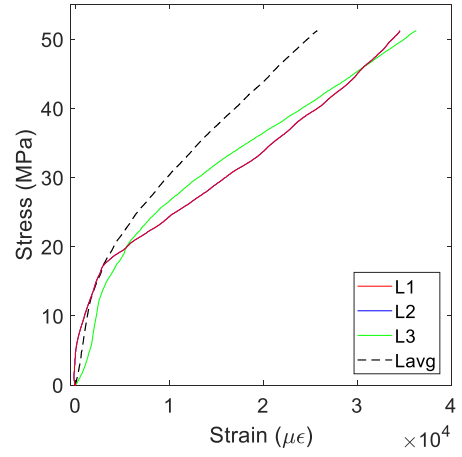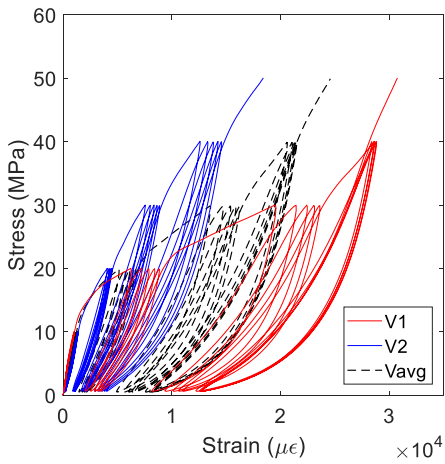

Figure E.72 σ-ε curves from lasers (L)
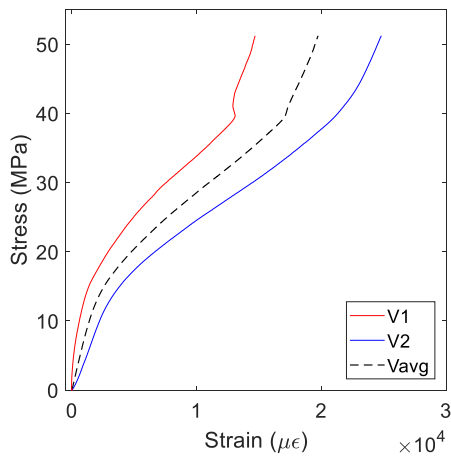
Figure E.73 σ-ε curves from V gauges
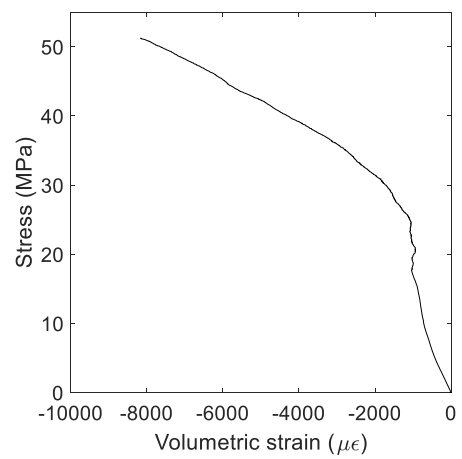
Figure E.74 Stress vs. volumetric strain
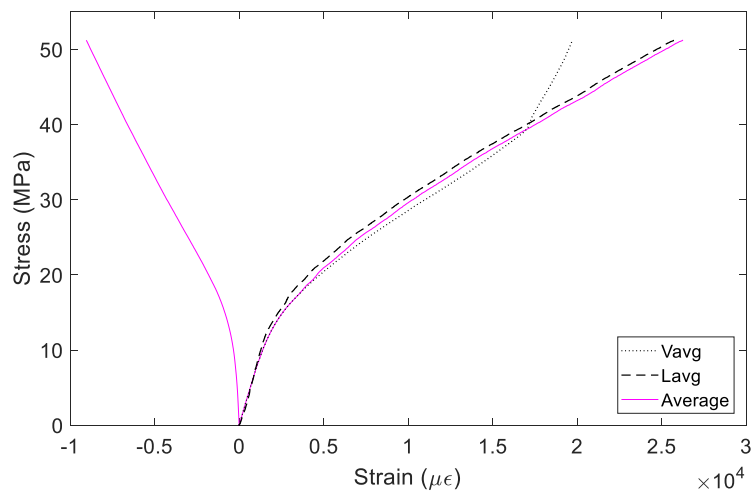
Figure E.75 Average curves

4C-M2
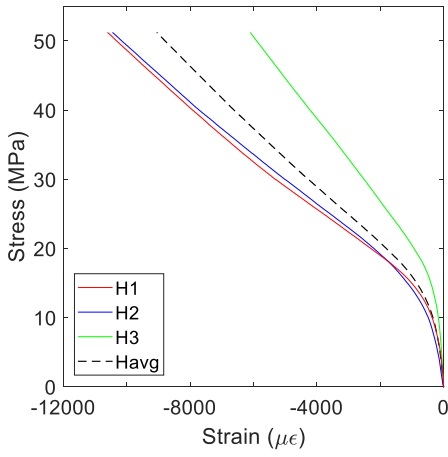
Figure E.76 σ-ε curves from H gauges
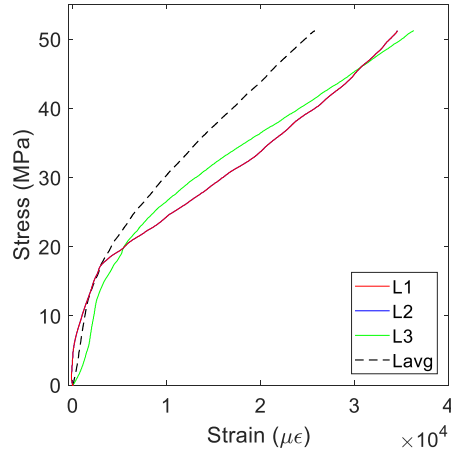
Figure E.77 σ-ε curves from lasers (L)
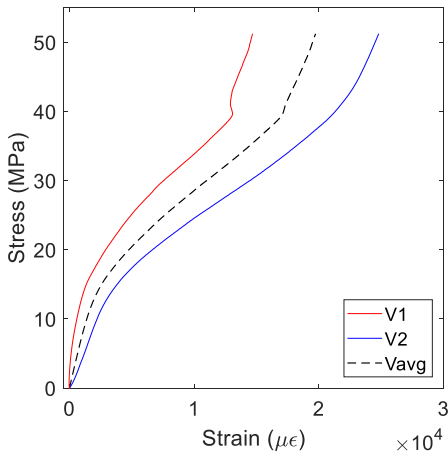
Figure E.78 σ-ε curves from V gauges
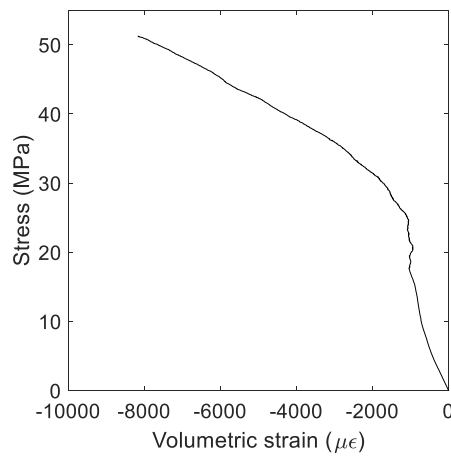
Figure E.79 Stress vs. volumetric strain
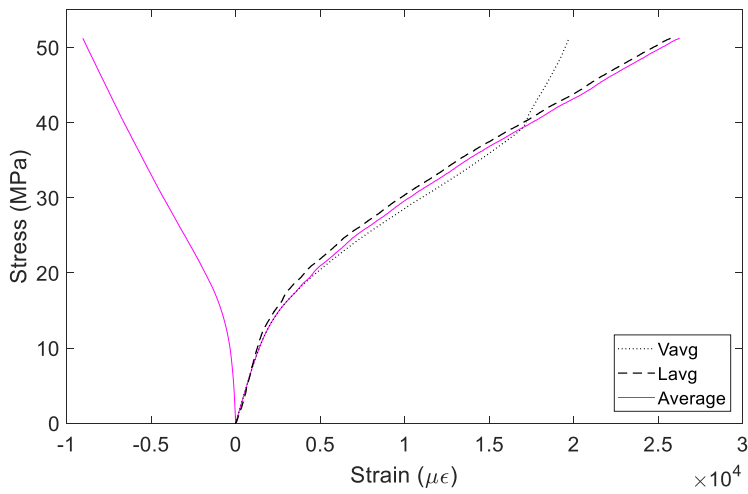
Figure E.80 Average curves

3C-M1-L
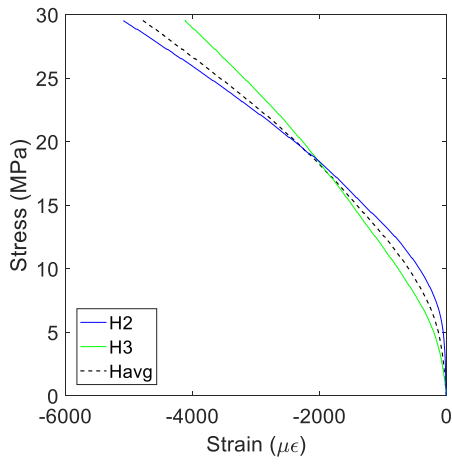
Figure E.81 σ-ε curves from H gauges
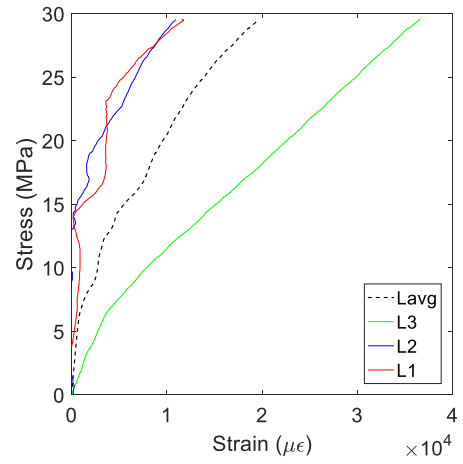
Figure E.82 σ-ε curves from lasers (L)
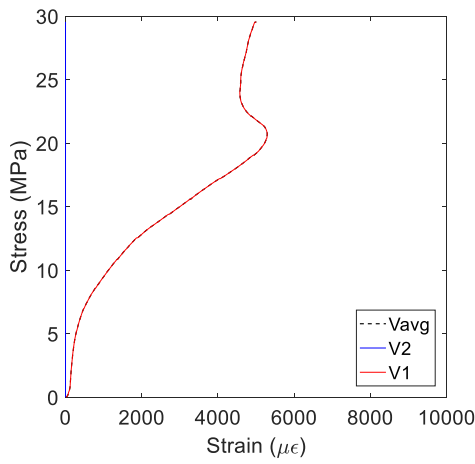
Figure E.83 σ-ε curves from V gauges
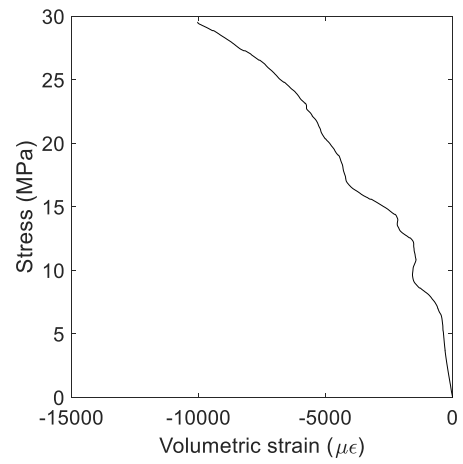
Figure E.84 Stress vs. volumetric strain
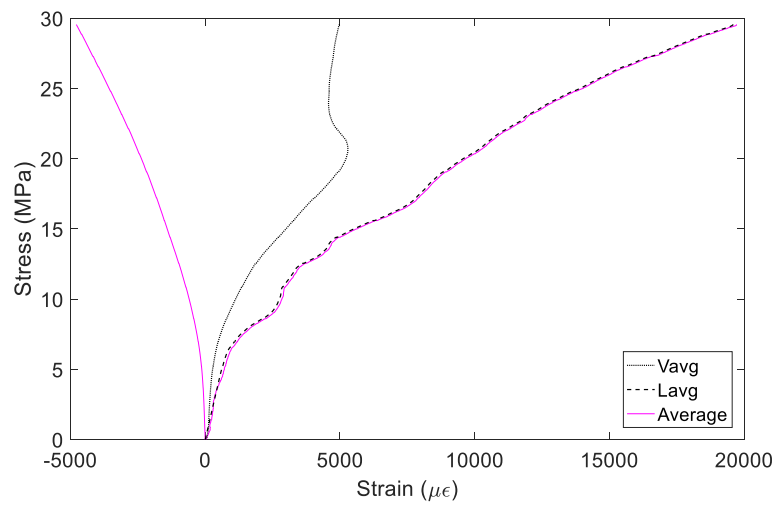
Figure E.85 Average curves
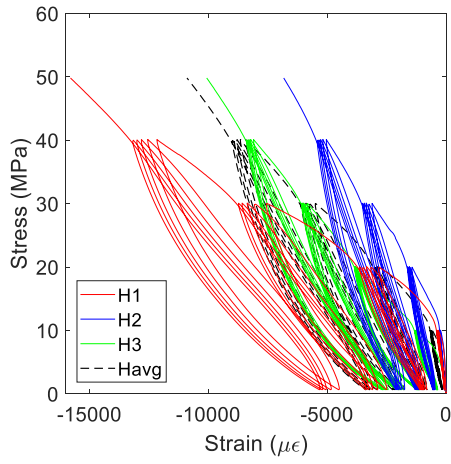
3C-M2-L
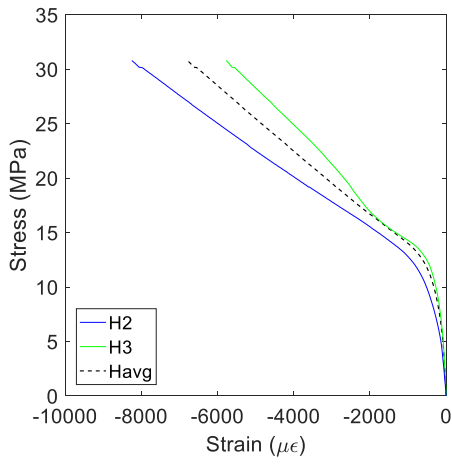
Figure E.86 σ-ε curves from H gauges
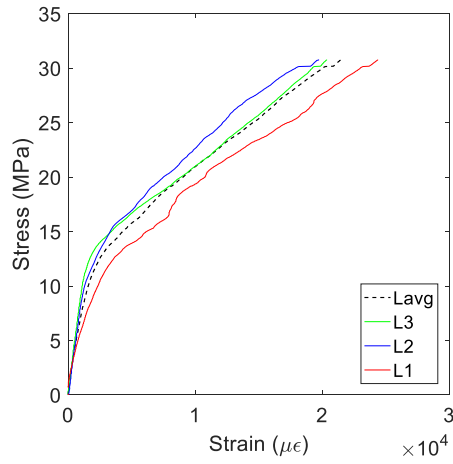
Figure E.87 σ-ε curves from lasers (L)
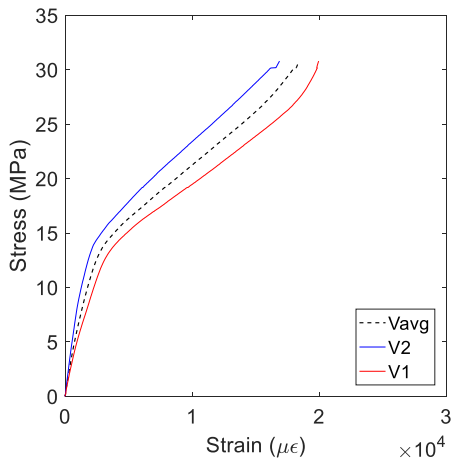
Figure E.88 σ-ε curves from V gauges
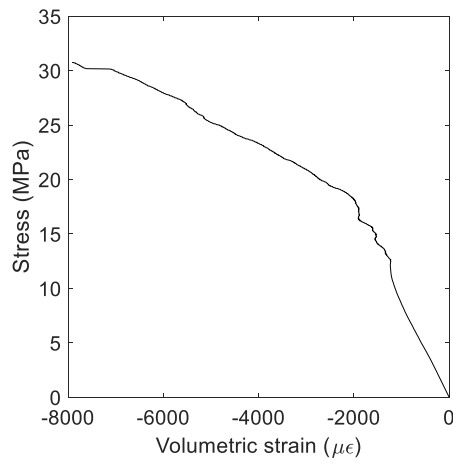
Figure E.89 Stress vs. volumetric strain
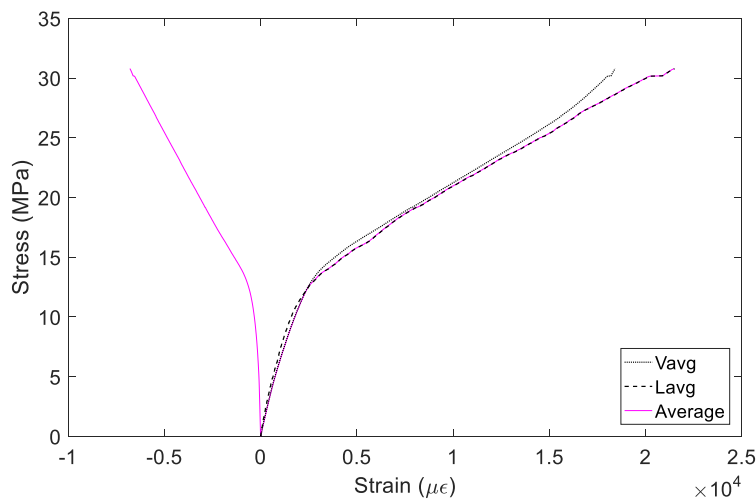
Figure E.90 Average curves

6C-M1-L
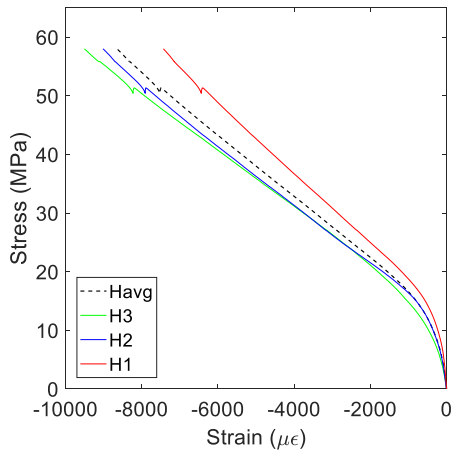
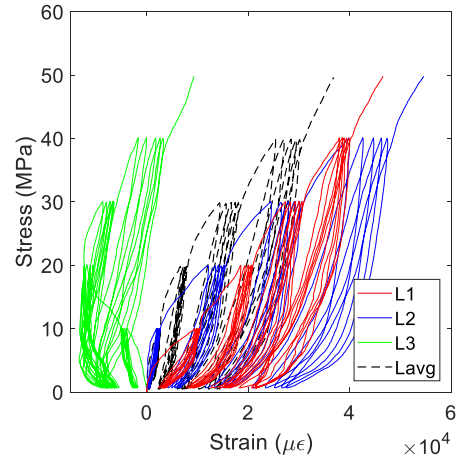**Figure E.91 σ-ε curves from H gauges**
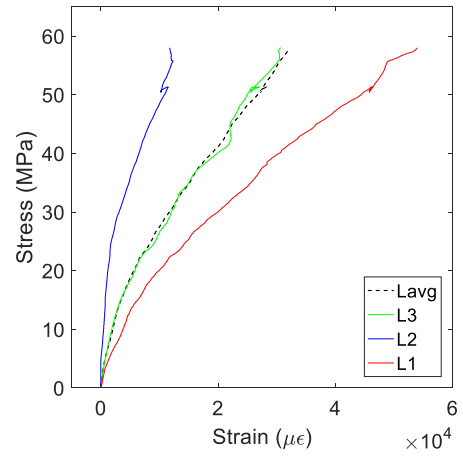
Figure E.92 σ-ε curves from lasers (L)
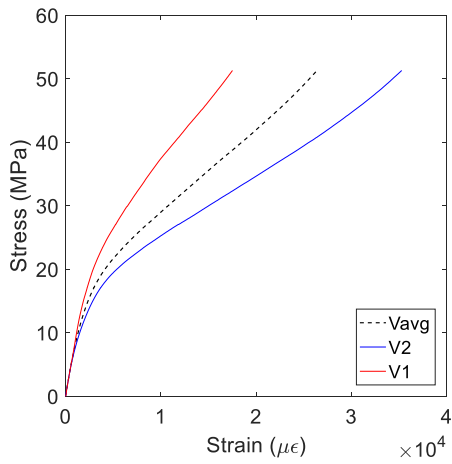
Figure E.93 σ-ε curves from V gauges
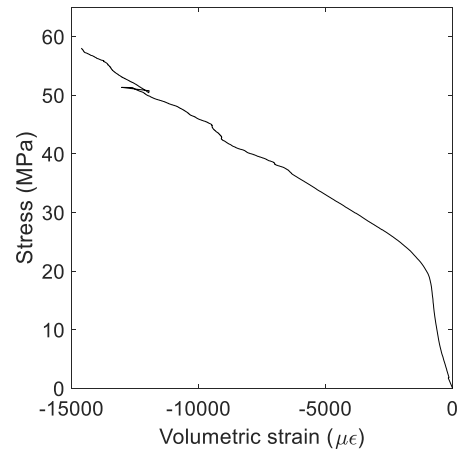
Figure E.94 Stress vs. volumetric strain
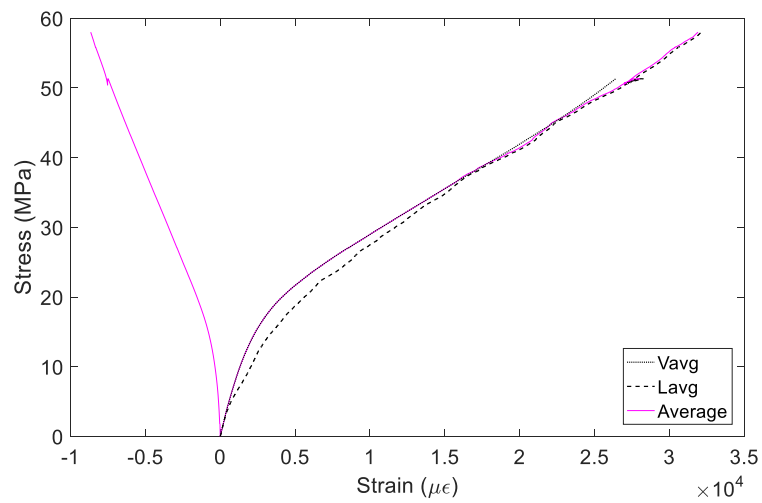
Figure E.95 Average curves

6C-M2-L
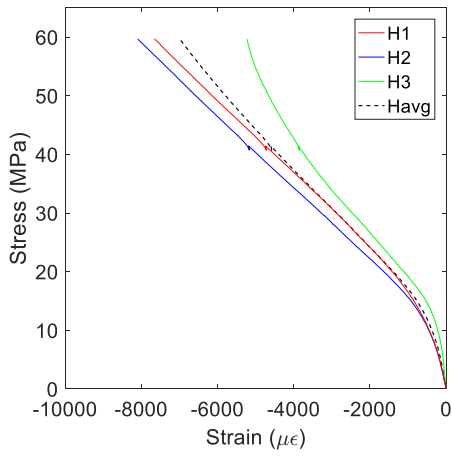
Figure E.96 σ-ε curves from H gauges
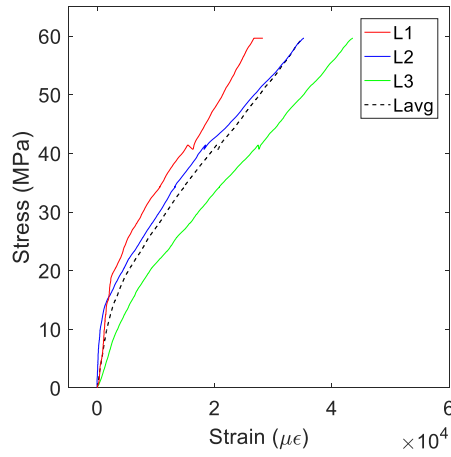
Figure E.97 σ-ε curves from lasers (L)
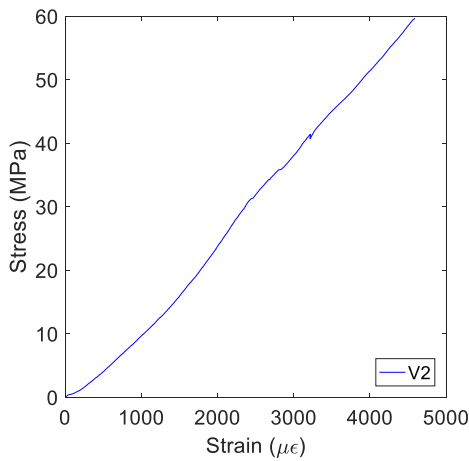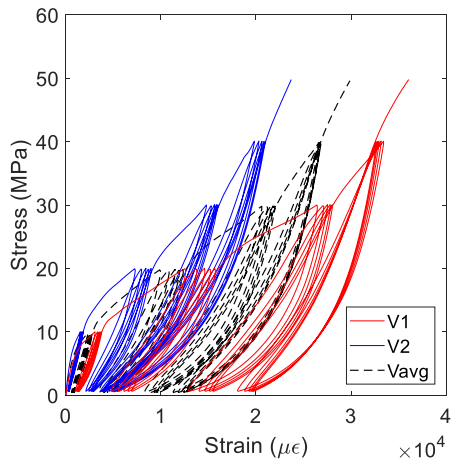

Figure E.98 σ-ε curves from V gauges
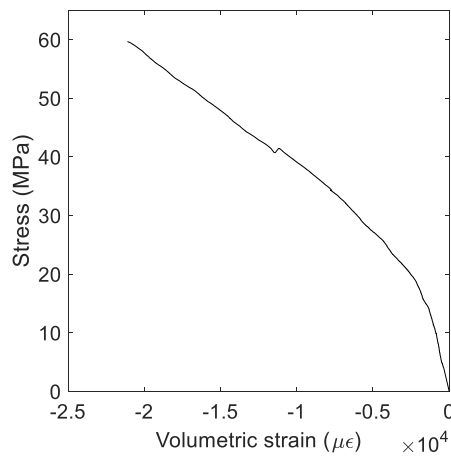
Figure E.99 Stress vs. volumetric strain
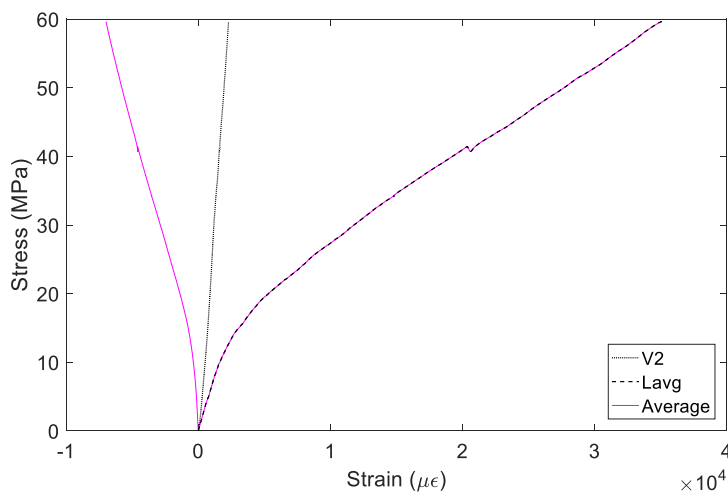
Figure E.100 Average curves

Appendix F. Experimental Data – Cyclic Loading

This appendix presents detailed experimental data from the cyclically loaded cylinders described in Chapters 4 and 5. A description of the instrumentation details and cylinder notation can be found in appendix D.

2A-C1
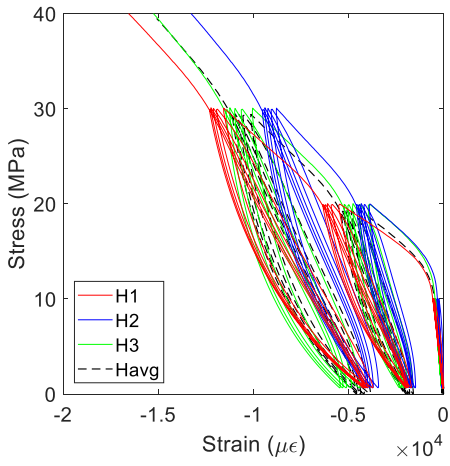
Figure F.1 σ-ε curves from H gauges
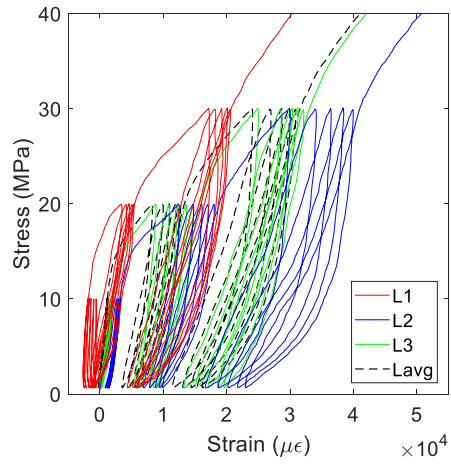
Figure F.2 σ-ε curves from lasers (L)
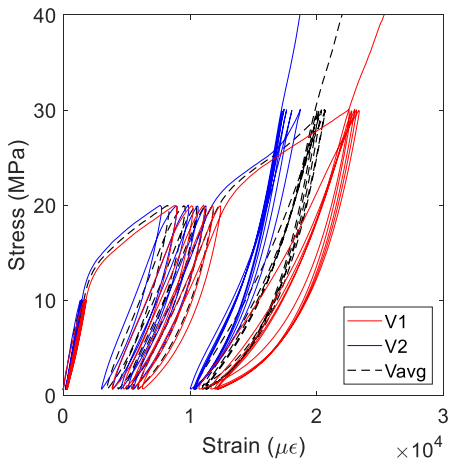
Figure F.3 σ-ε curves from V gauges
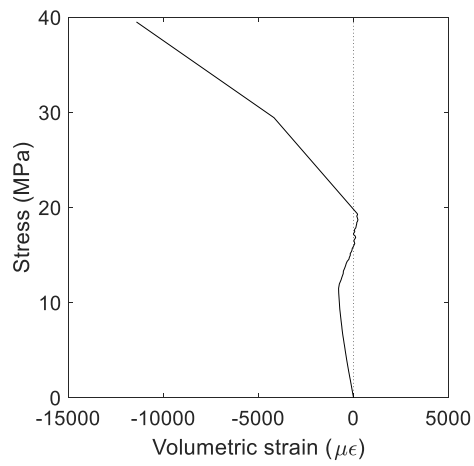
Figure F.4 Stress vs.average volumetric strain
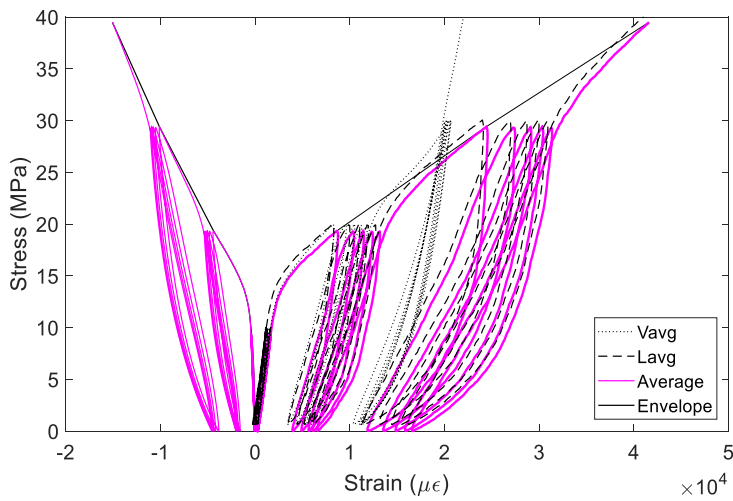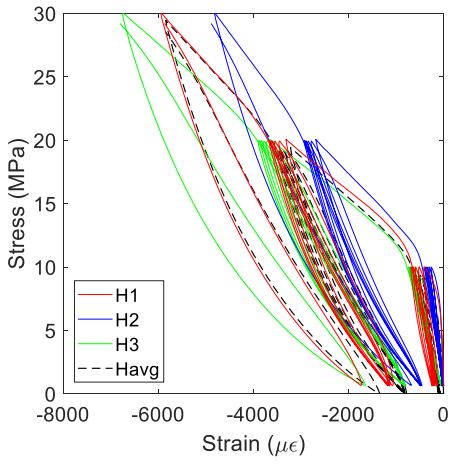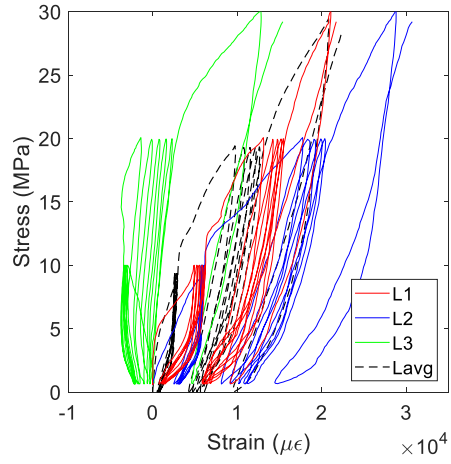

Figure F.5 Average curves

237
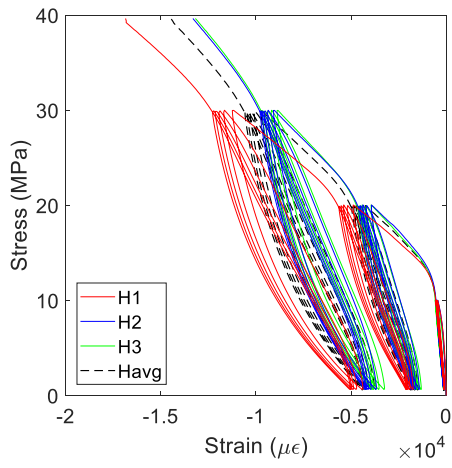
2A-C2

Figure F.6 σ-ε curves from H gauges
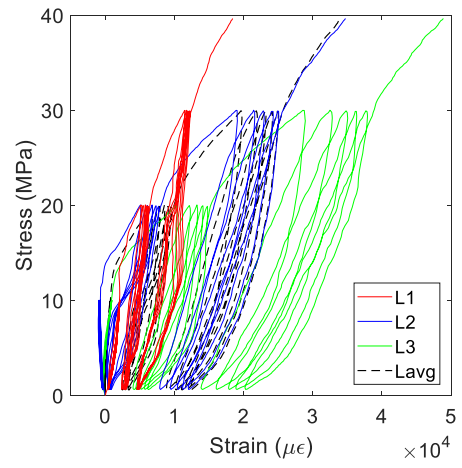
Figure F.7 σ-ε curves from lasers (L)
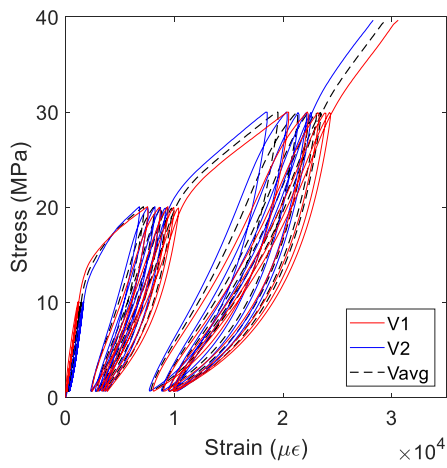
Figure F.8 σ-ε curves from V gauges
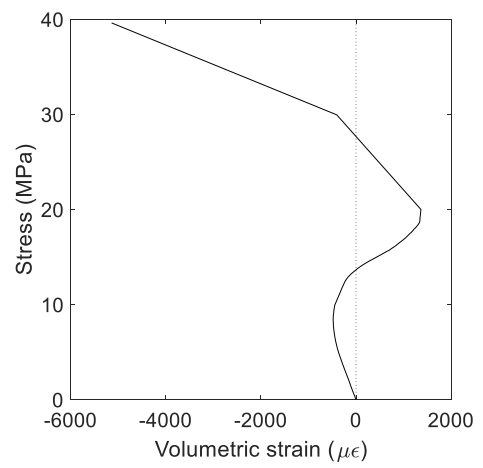
Figure F.9 Stress vs. average volumetric strain
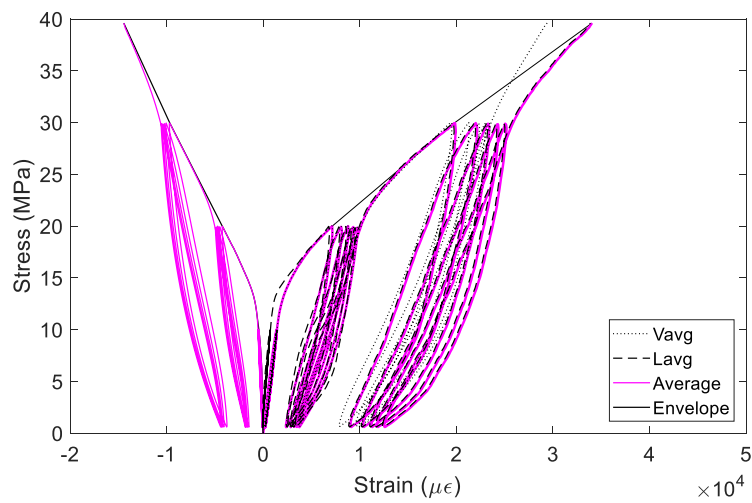
Figure F.10 Average curves

2A-C3
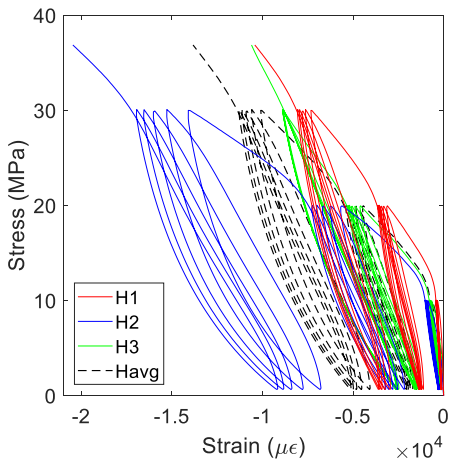
Figure F.11 σ-ε curves from H gauges
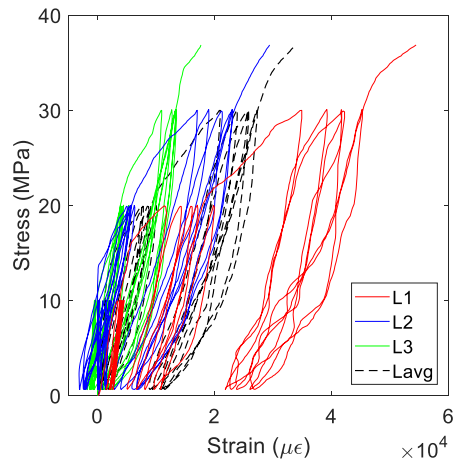
Figure F.12 σ-ε curves from lasers (L)
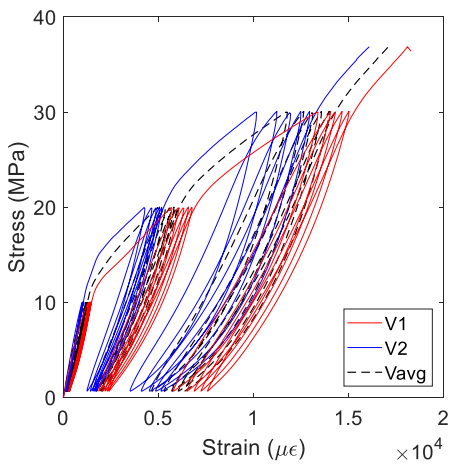
Figure F.13 σ-ε curves from V gauges
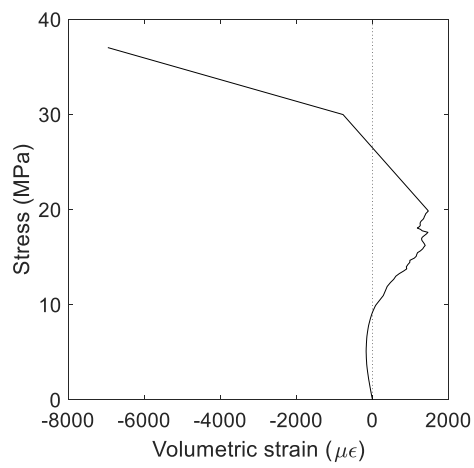
Figure F.14 Stress vs. average volumetric strain
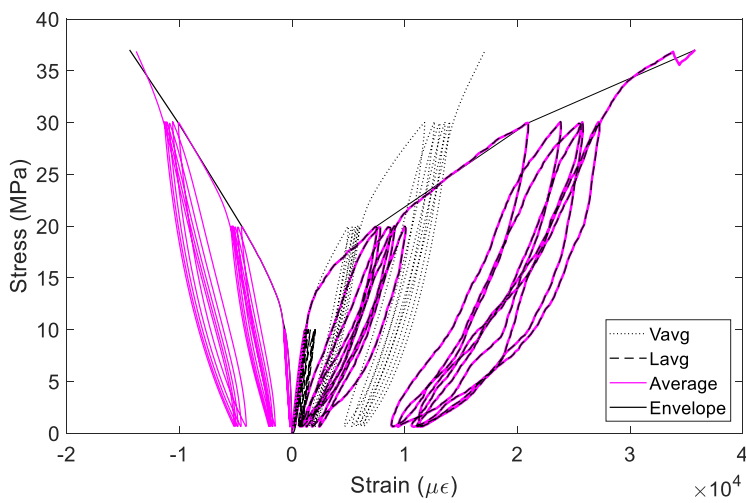
Figure F.15 Average curves

3A-C1
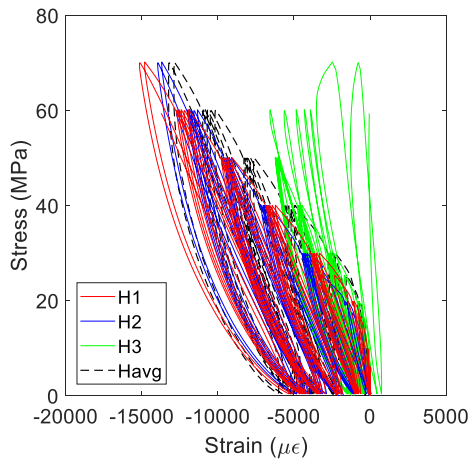
Figure F.16 σ-ε curves from H gauges
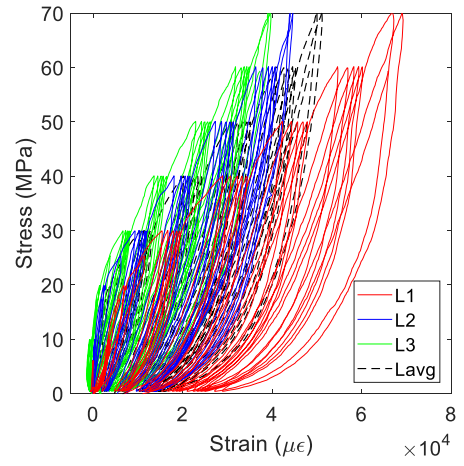
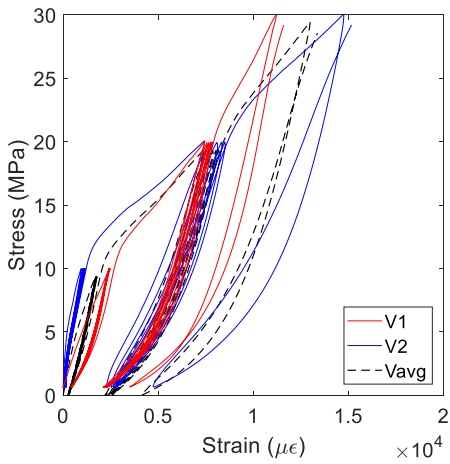**Figure F.17 σ-ε curves from lasers (L)**
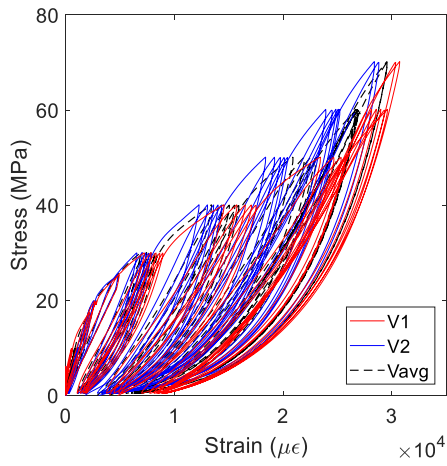
Figure F.18 σ-ε curves from V gauges
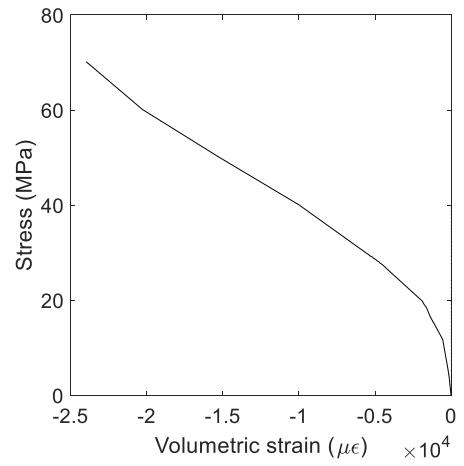
Figure F.19 Stress vs. volumetric strain
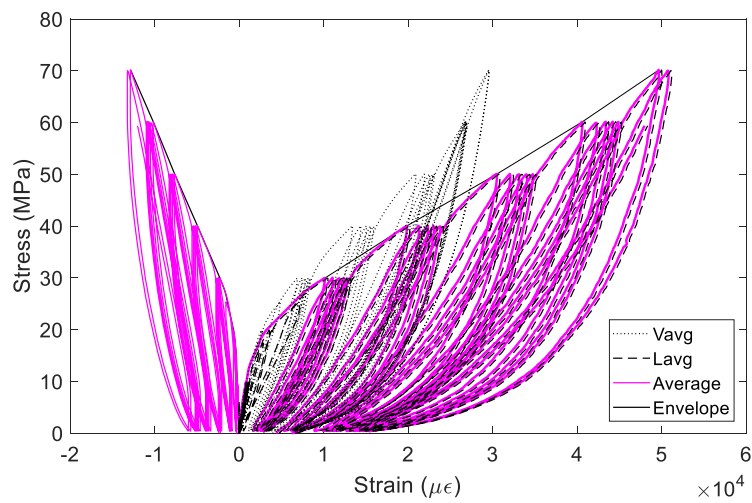
Figure F.20 Average curves

3A-C2
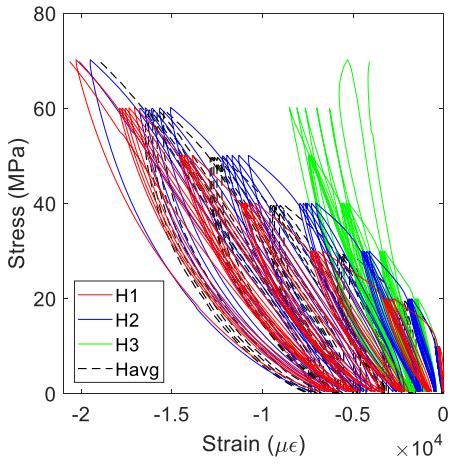
Figure F.21 σ-ε curves from H gauges
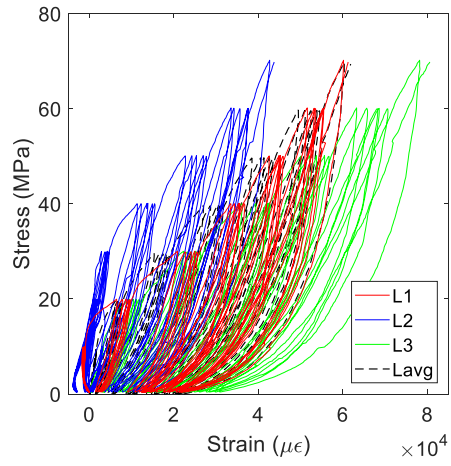
Figure F.22 σ-ε curves from lasers (L)
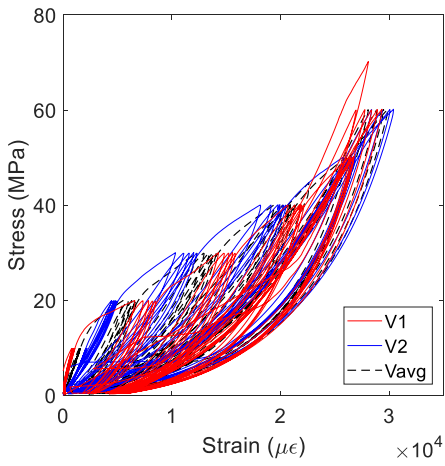
Figure F.23 σ-ε curves from V gauges
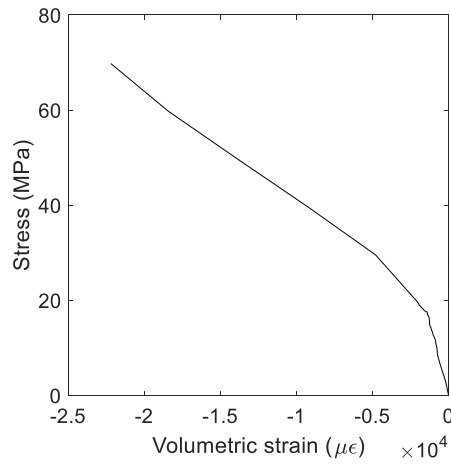
Figure F.24 Stress vs. volumetric strain
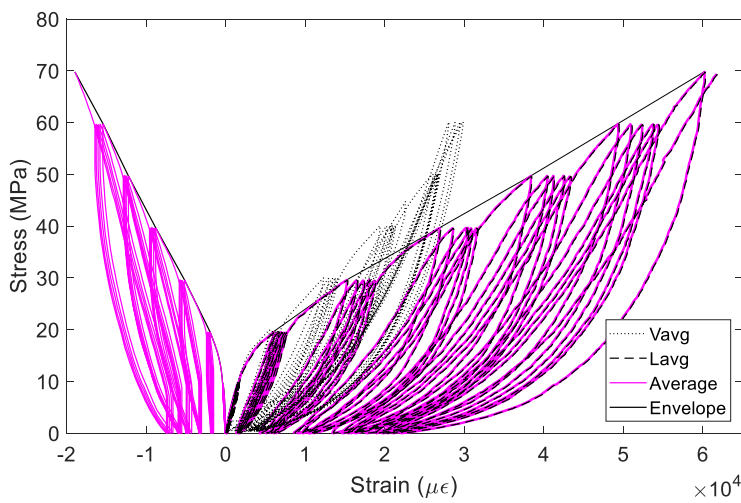
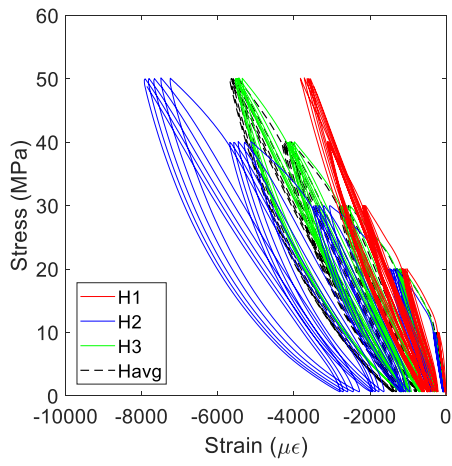**Figure F.25 Average curves**

3A-C3
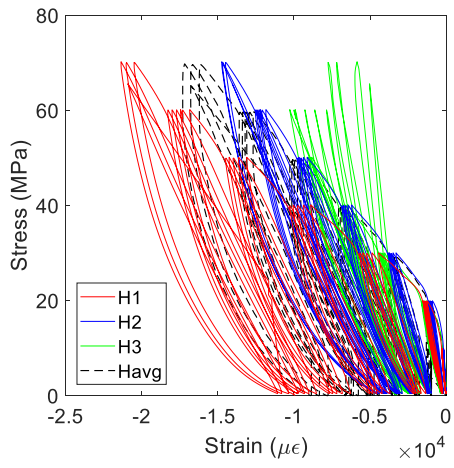
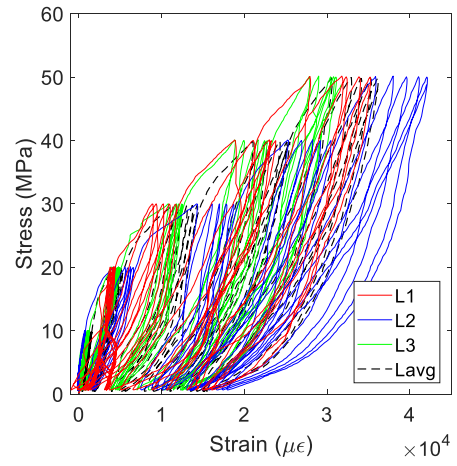**Figure F.26 σ-ε curves from H gauges**
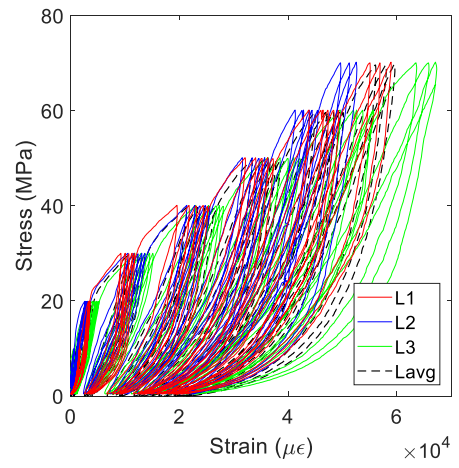
Figure F.27 σ-ε curves from lasers (L)
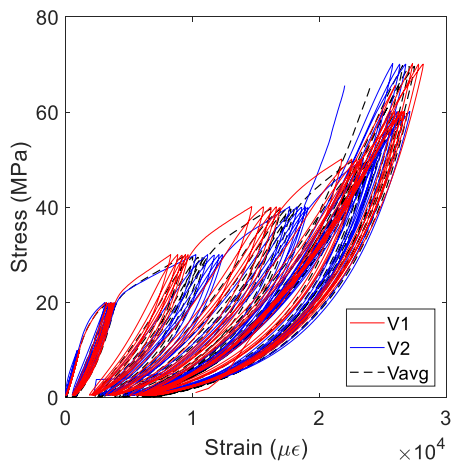
Figure F.28 σ-ε curves from V gauges
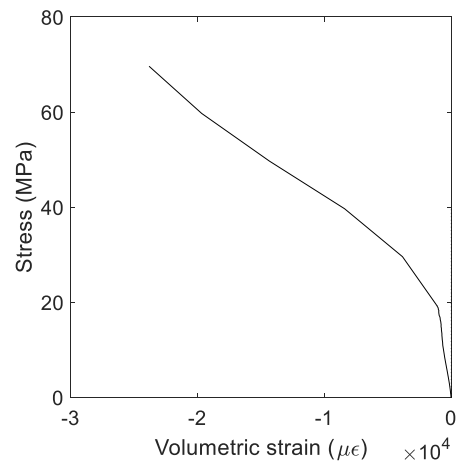
Figure F.29 Stress vs. volumetric strain
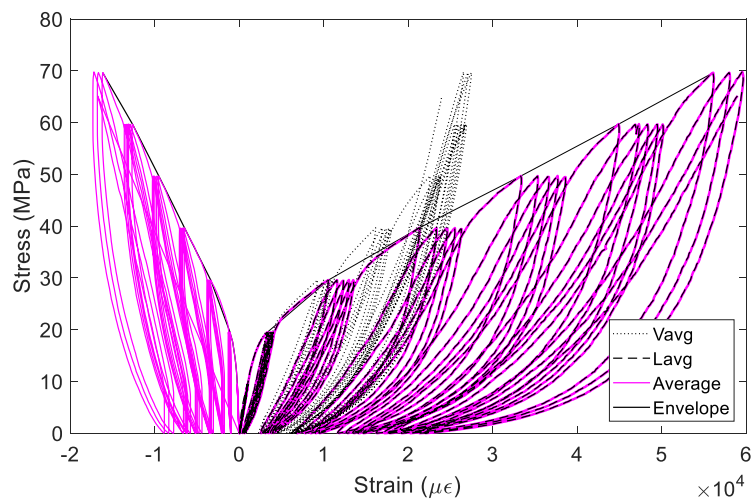
Figure F.30 Average curves

4A-C1
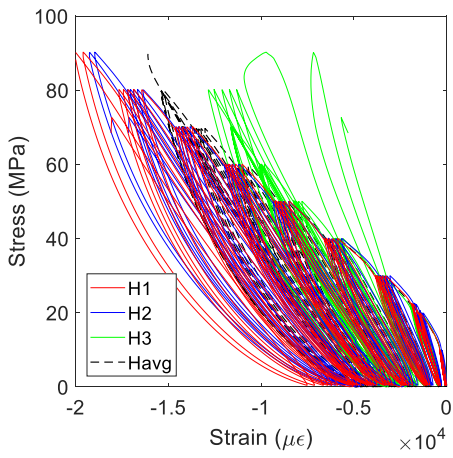
Figure F.31 σ-ε curves from H gauges
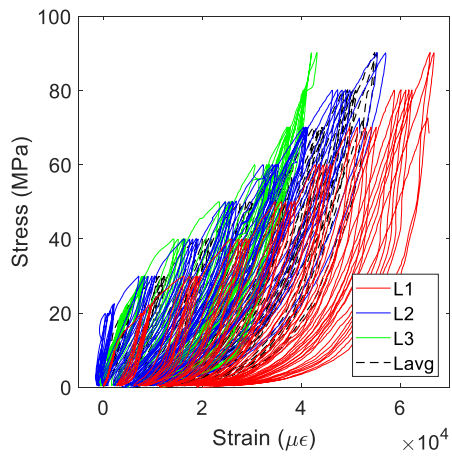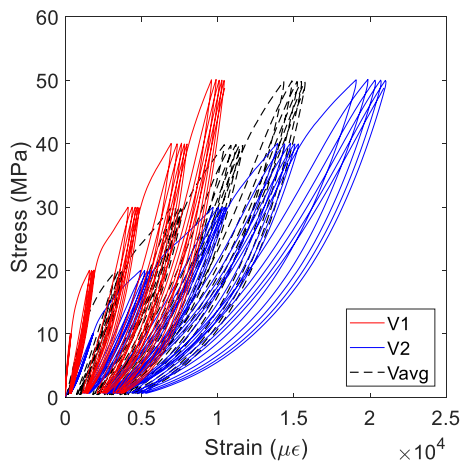

Figure F.32 σ-ε curves from lasers (L)
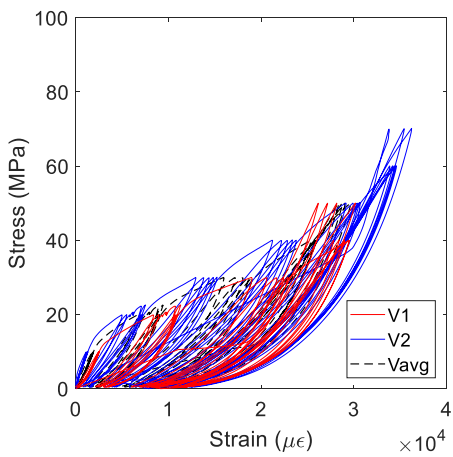
Figure F.33 σ-ε curves from V gauges
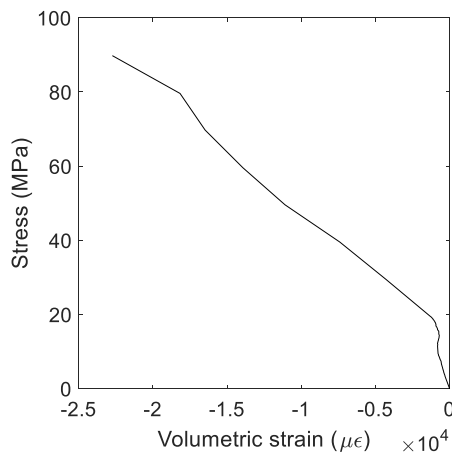
Figure F.34 Stress vs. volumetric strain
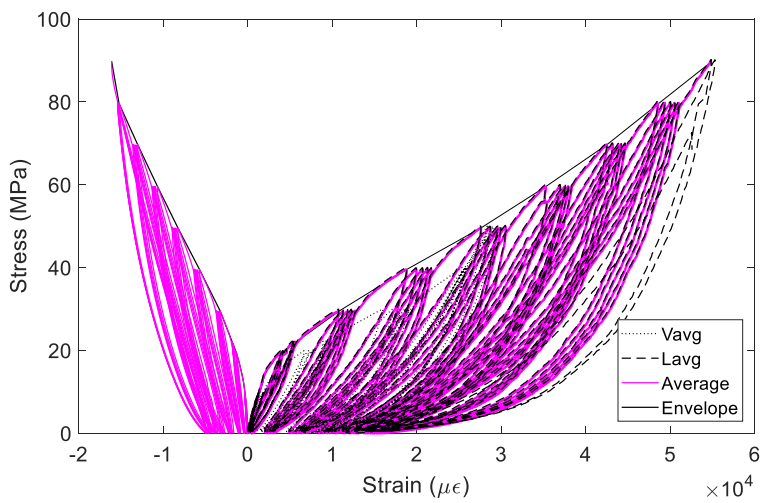
Figure F.35 Average curves

4A-C2
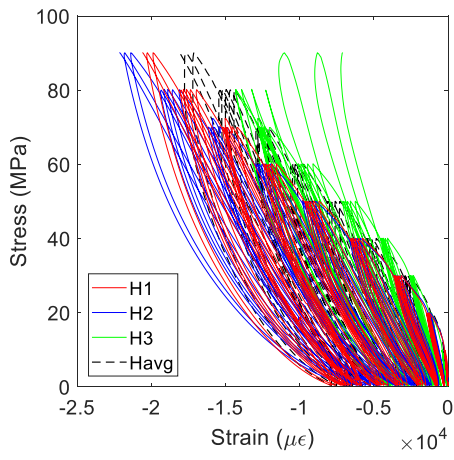
Figure F.36 σ-ε curves from H gauges
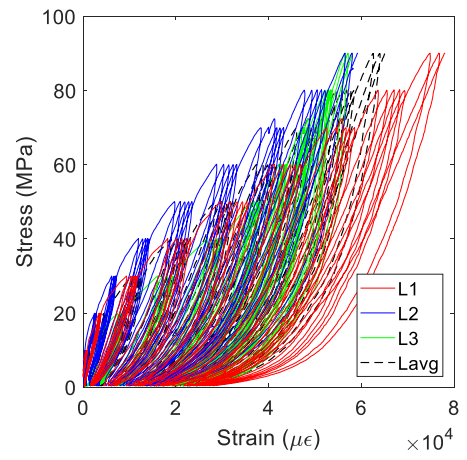
Figure F.37 σ-ε curves from lasers (L)
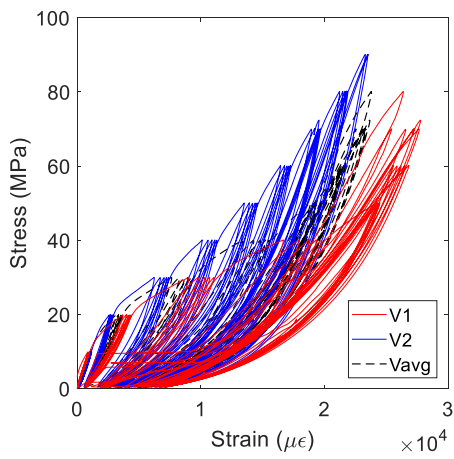
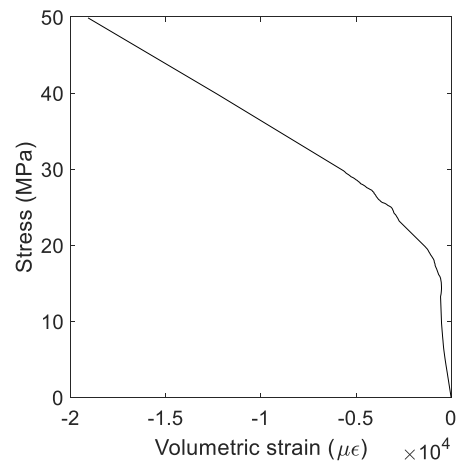**Figure F.38 σ-ε curves from V gauges**
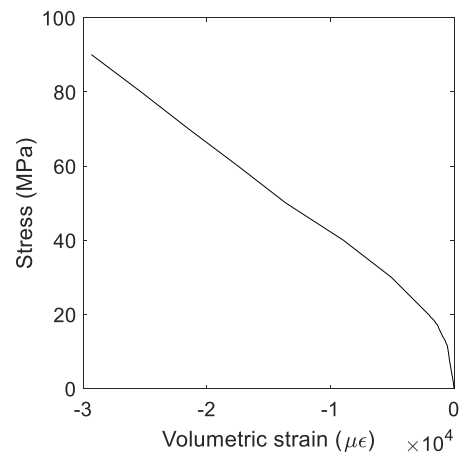
Figure F.39 Stress vs. volumetric strain
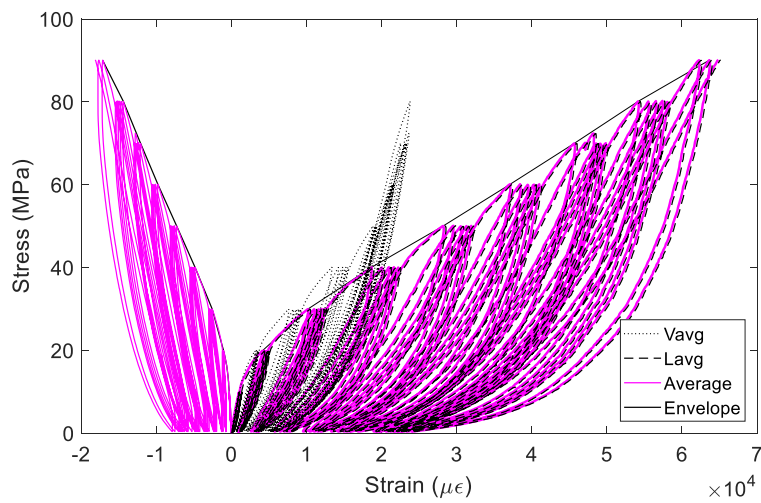
Figure F.40 Average curves

4A-C3

Figure F.41 σ-ε curves from H gauges
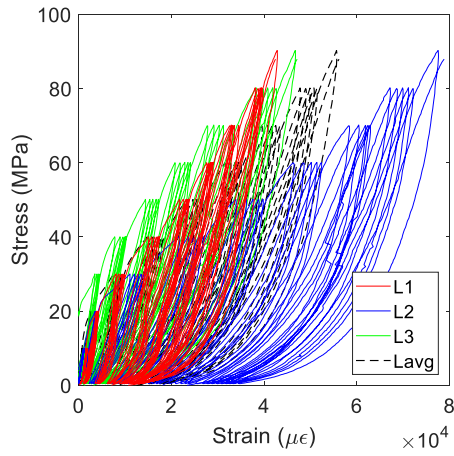
Figure F.42 σ-ε curves from lasers (L)
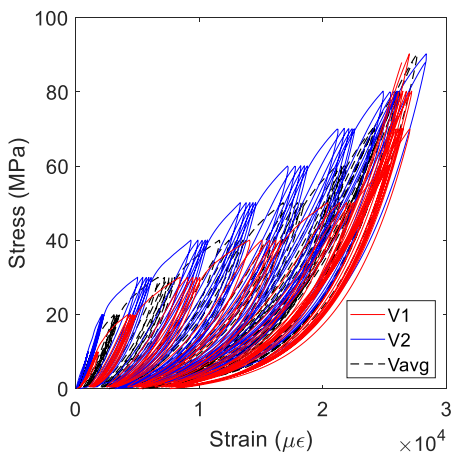
Figure F.43 σ-ε curves from V gauges
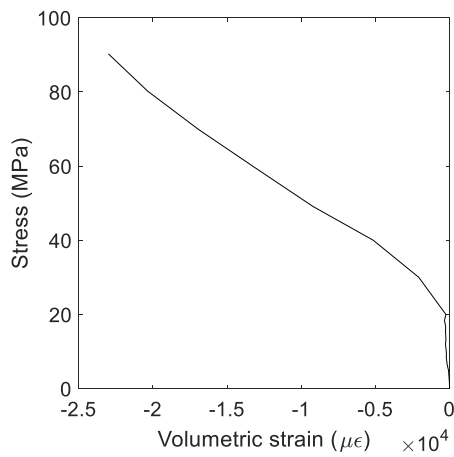
Figure F.44 Stress vs. volumetric strain
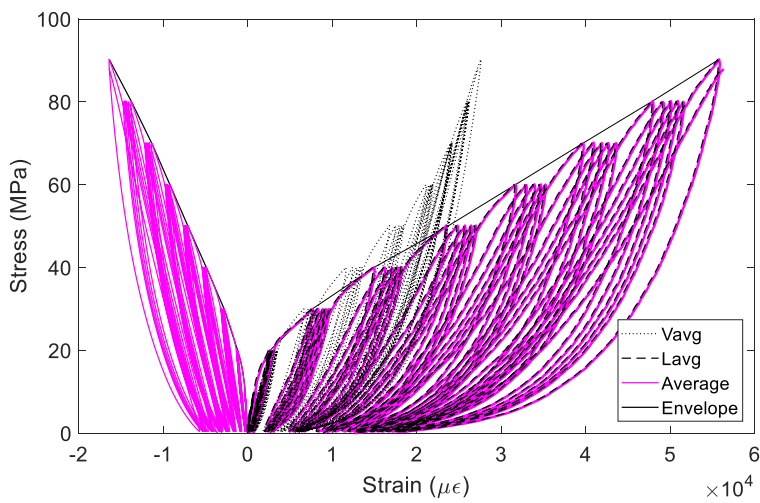
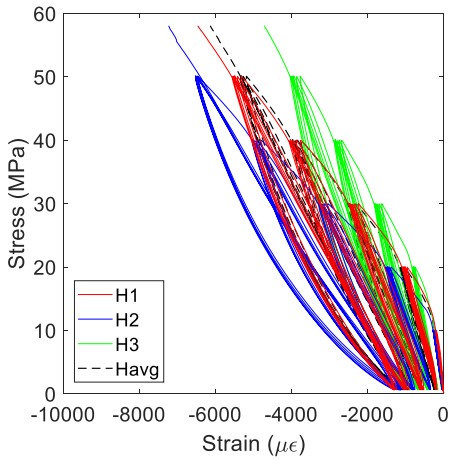**Figure F.45 Average curves**

2C-C1

Figure F.46 σ-ε curves from H gauges
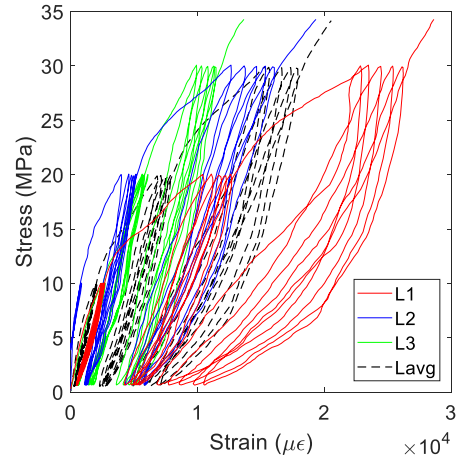
Figure F.47 σ-ε curves from lasers (L)

Figure F.48 σ-ε curves from V gauges
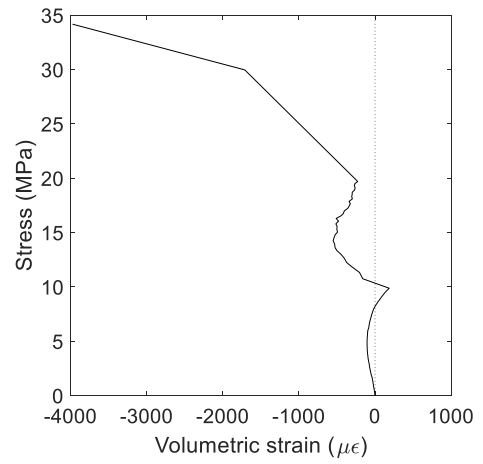
Figure F.49 Stress vs. volumetric strain
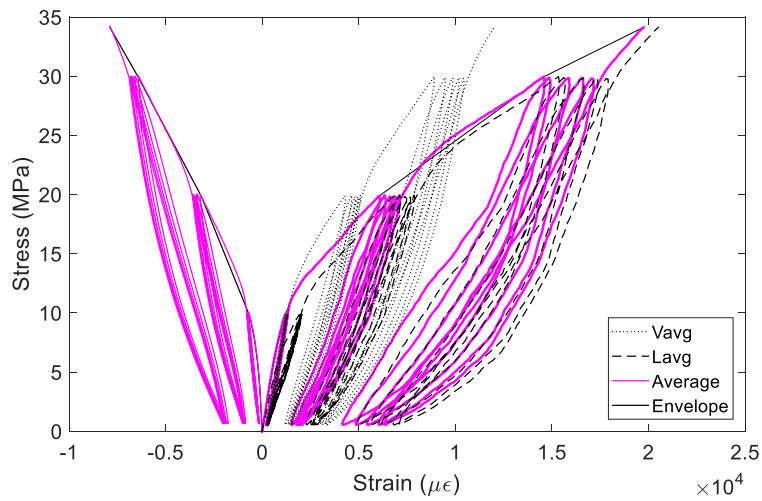
Figure F.50 Average curves

2C-C2
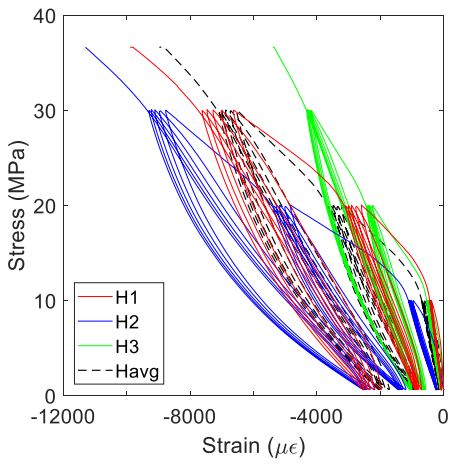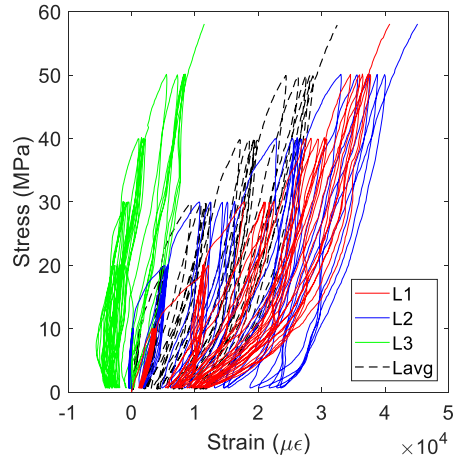

Figure F.51 σ-ε curves from H gauges
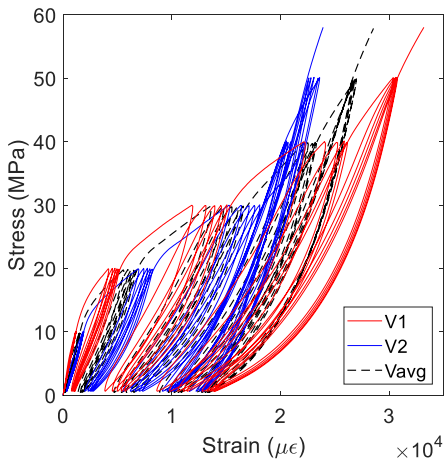

Figure F.52 σ-ε curves from lasers (L)
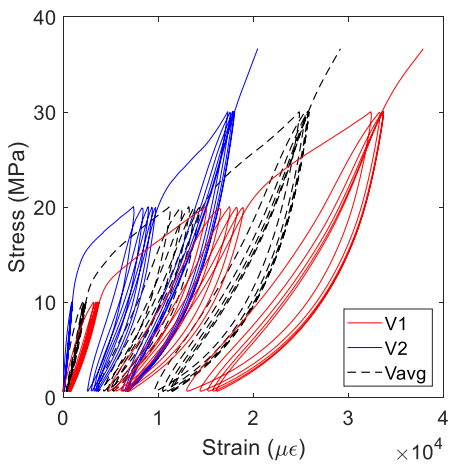
Figure F.53 σ-ε curves from V gauges
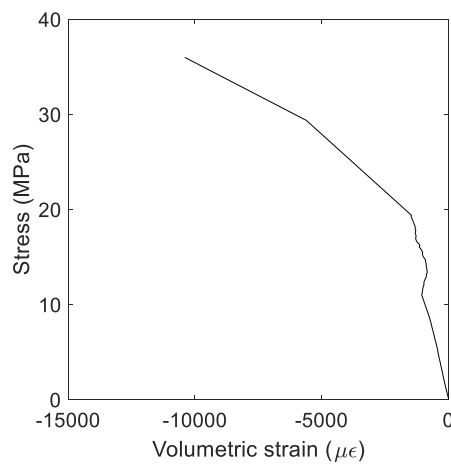
Figure F.54 Stress vs. volumetric strain
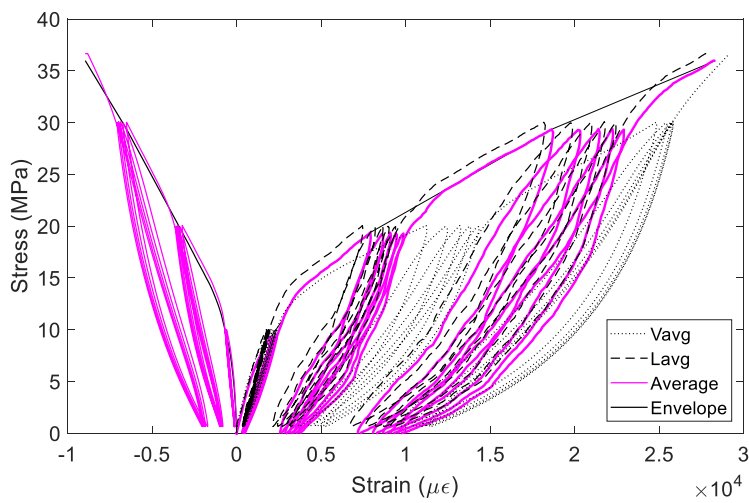
Figure F.55 Average curves

2C-C3

Figure F.56 σ-ε curves from H gauges

Figure F.57 σ-ε curves from lasers (L)

Figure F.58 σ-ε curves from V gauges

Figure F.59 Stress vs. volumetric strain
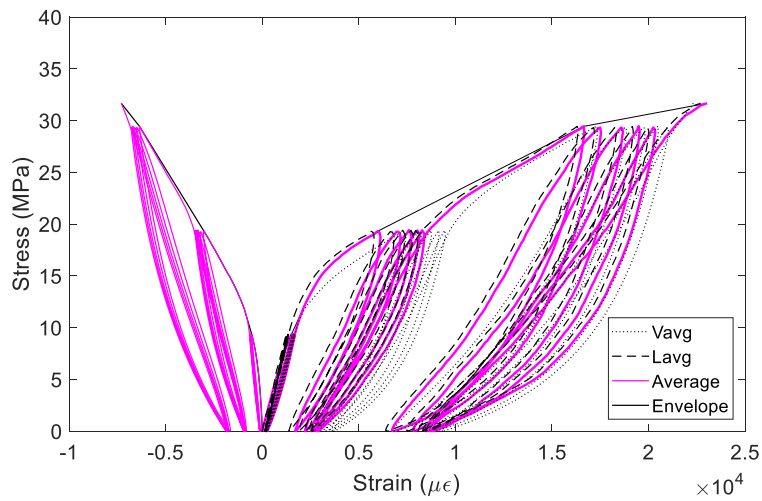
Figure F.60 Average curves

3C-C1

Figure F.61 σ-ε curves from H gauges

Figure F.62 σ-ε curves from lasers (L)

Figure F.63 σ-ε curves from V gauges
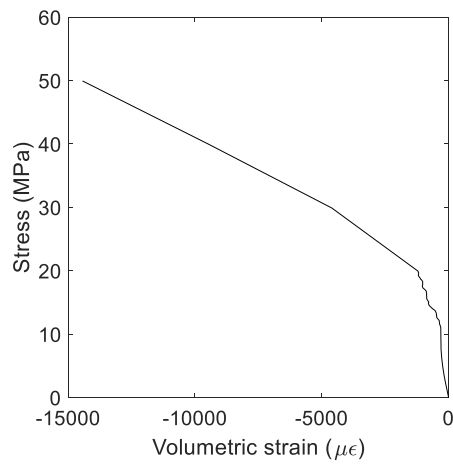
Figure F.64 Stress vs. volumetric strain
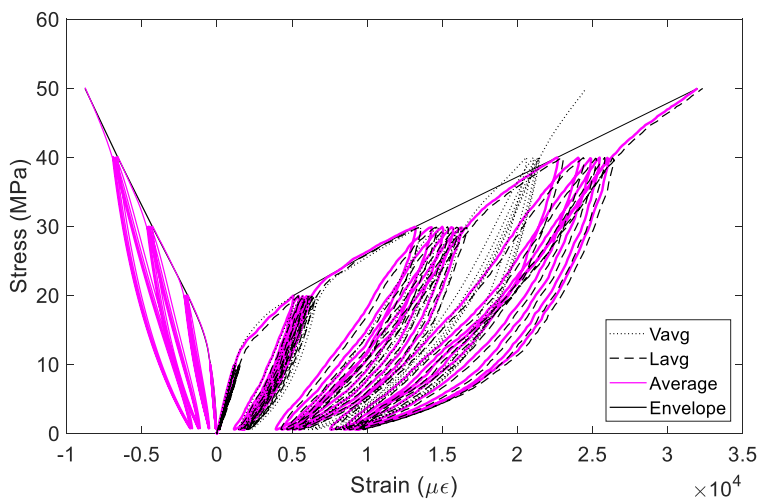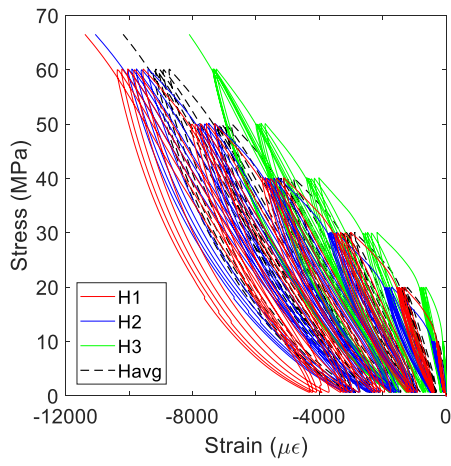

Figure F.65 Average curves

3C-C2

Figure F.66 σ-ε curves from H gauges

Figure F.67 σ-ε curves from lasers (L)

Figure F.68 σ-ε curves from V gauges
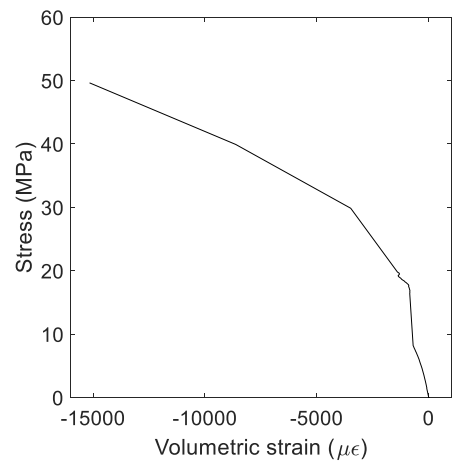
Figure F.69 Stress vs. volumetric strain
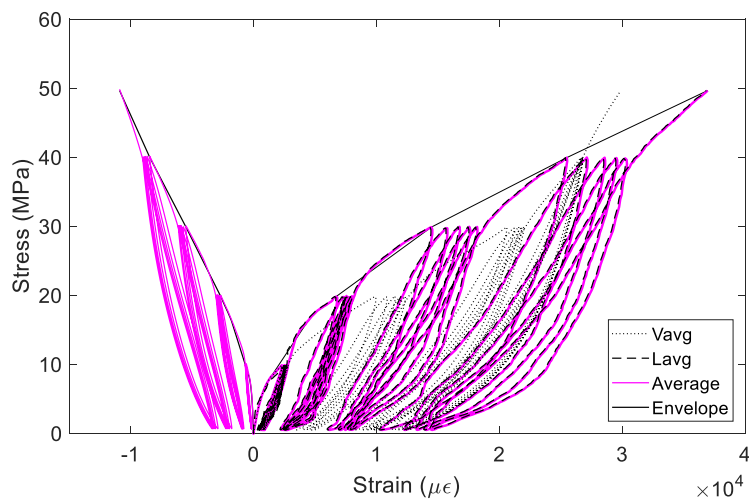
Figure F.70 Average curves

3C-C3
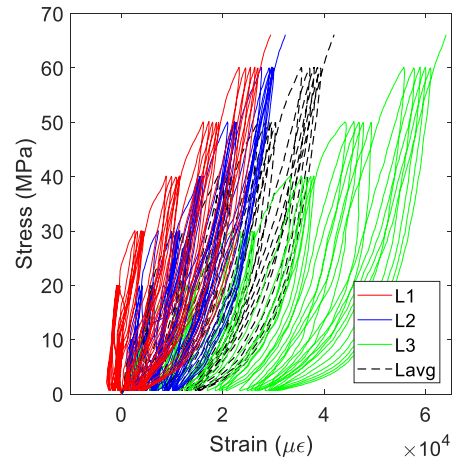

Figure F.71 σ-ε curves from H gauges

Figure F.72 σ-ε curves from lasers (L)

Figure F.73 σ-ε curves from V gauges
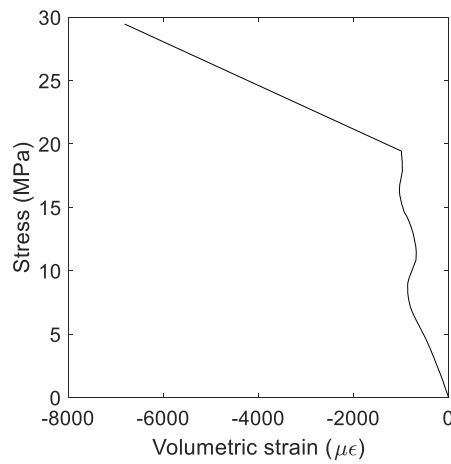
Figure F.74 Stress vs. volumetric strain
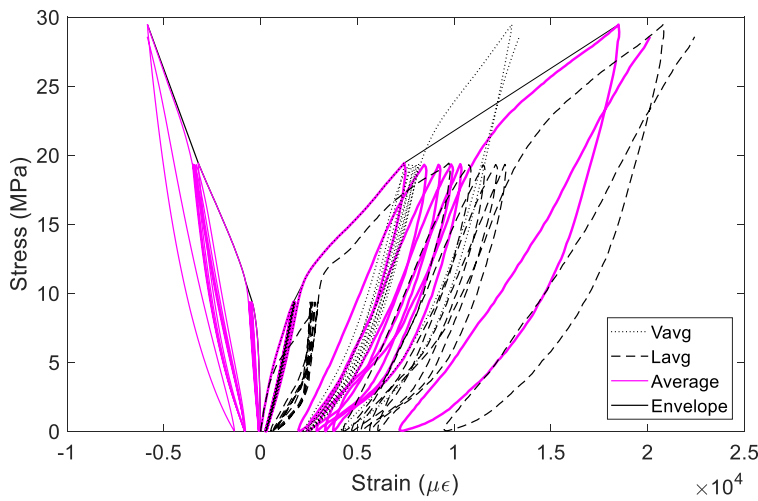
Figure F.75 Average curves

4C-C1

Figure F.76 σ-ε curves from H gauges

Figure F.77 σ-ε curves from lasers (L)

Figure F.78 σ-ε curves from V gauges

Figure F.79 Stress vs. volumetric strain
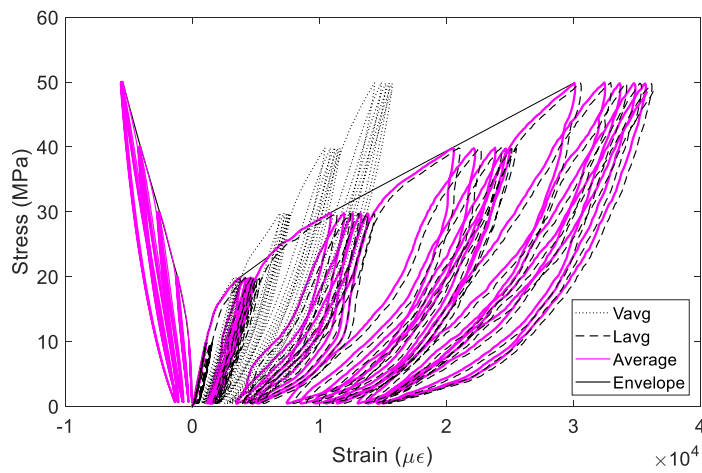
Figure F.80 Average curves

4C-C2

Figure F.81 σ-ε curves from H gauges

Figure F.82 σ-ε curves from lasers (L)

Figure F.83 σ-ε curves from V gauges
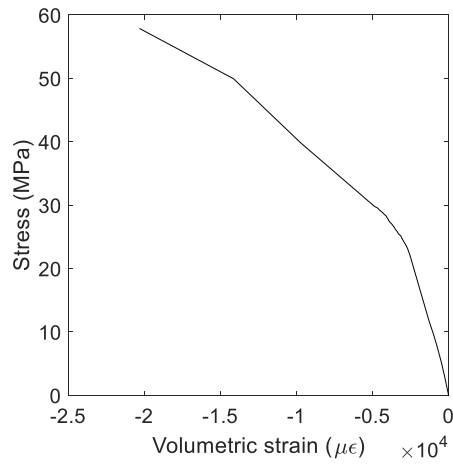
Figure F.84 Stress vs. volumetric strain
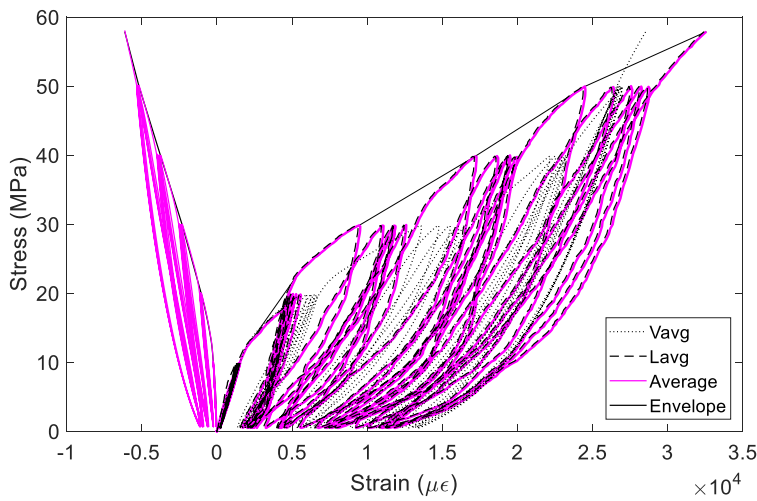
Figure F.85 Average curves

4C-C3

Figure F.86 σ-ε curves from H gauges

Figure F.87 σ-ε curves from lasers (L)
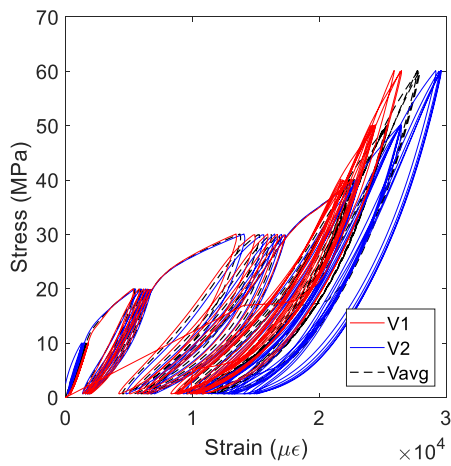
Figure F.88 σ-ε curves from V gauges
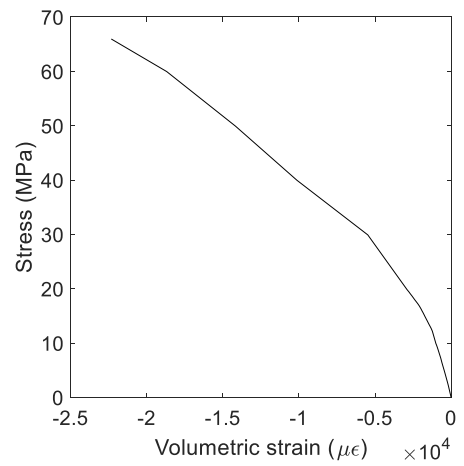
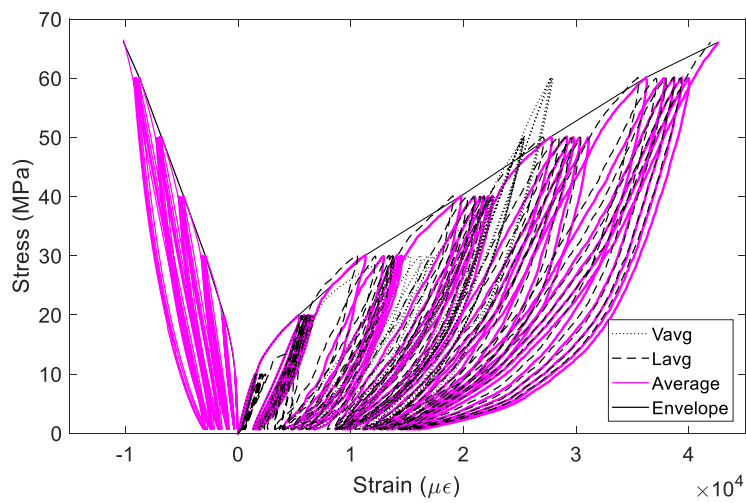**Figure F.89 Stress vs. volumetric strain**

Figure F.90 Average curves

Appendix G. Cylinder Failure Photos

This section presents additional photos for the unconfined (Chapters 2,3) and FRP-confined (Chapters 4,5) RuC cylinders taken before and after failure. Cylinder notation for the unconfined and confined RuC mixes can be found in Appendices C and D, respectively.

G.1   UNCONFINED SPECIMEN PHOTOS

Figure G.1 Failure of mix O1

Figure G.2 Failure of mix O2

Figure G.3 Failure of mix O2

Figure G.4 Failure of mix O2

Figure G.5 Failure of mix O3

Figure G.6 Failure of mix O3

Figure G.7 Failure of mix O3

Figure G.8 Mix O4 before testing

Figure Mix O4 before testing

Figure G.9 Failure of mix O4

Figure G.10 Failure of mix O4

Figure G.11 Failure of mix O2

Figure G.12 Failure of mix A1

Figure G.13 Failure of mix A5

Figure G.14 Failure of mix A5

Figure G.15 Failure of mix A7

Figure G.16 Failure of mix A8

Figure G.17 Failure of mix A8

257

Figure G.18 Failure of mix D1

Figure G.19 Failure of mix D1

Figure G.20 Mix D2 before testing

Figure G.21 Failure of mix D2

Figure G.22 Failure of mix E1

Figure G.23 Failure of mix I1

G.2   OPTIMISED MIX SPECIMEN PHOTOS

G.2.1 Plain mix

Figure G.24 Failure of plain mix

Figure G.25 Failure of plain mix

Figure G.26 Top view of plain mix

G.2.2 Fine aggregate replacement

Figure G.27 Failure of 60FR

Figure G.28 Failure of 80FR

Figure G.29 Failure of 80FR

G.2.3 Coarse aggregate replacement

Figure G.30 Top view of 10 CR
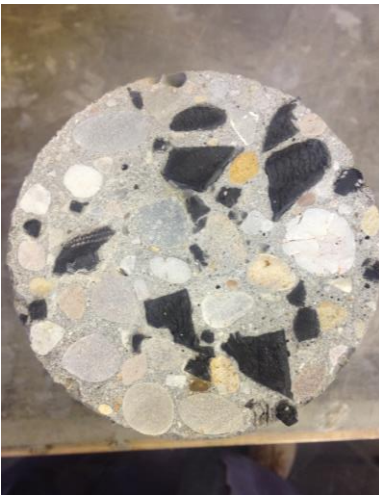

Figure G.31 Top view of 10 CR

Figure G.32 Failure of 10CR

Figure G.33 Top view of 20 CR

Figure G.34 Section of 20CR

Figure G.35 Failure of 20 CR

Figure G.36 Failure of 20CR

Figure G.37 Failure of 40 CR

Figure G.38 Top view of 40 CR

Figure G.39 Failure of 40 CR

Figure G.40 Top view of 60CR

Figure G.41 Section of 60 CR

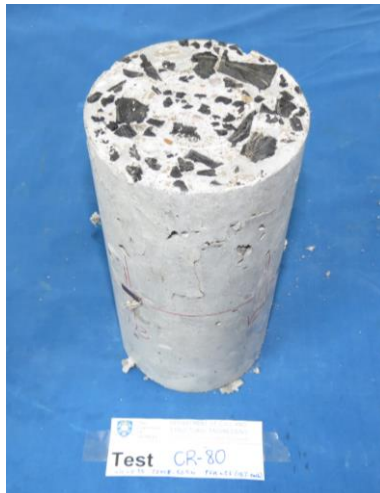
Figure G.42 Failure of 60CR

Figure G.43 Failure of 80 CR

Figure G.44 Failure of 80 CR

Figure G.45 Section view of 20CR (left), 40CR (middle) and 100 CR (right)

G.2.4 Typical failure of specimens 60CR60FR (from Chapter 3)

Figure G.46 Failure of 60CR60FR

Figure G.47 Failure of 60CR60FR

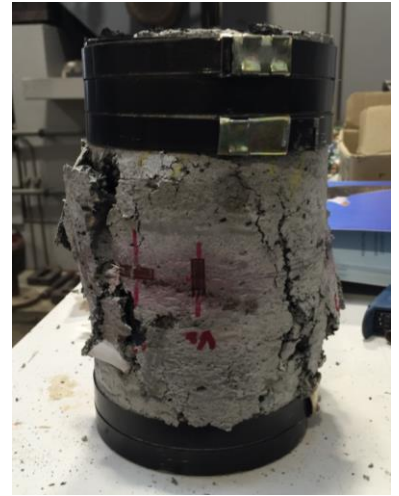**Figure G.48 Failure of 60CR60FR**

Figure G.49 Broken specimen – 60CR60FR

G.2.4 Typical failure of specimens 60CR60FR (from Chapter 4 and 5)

**Figure G.50 Failure of
60CR60FR**

**Figure G.51 Failure of
60CR60FR**

**Figure G.52 Failure of
60CR60FR**

**Figure G.53 Failure of
60CR60FR**

**Figure G.54 Failure of
60CR60FR**

**Figure G.55 Failure of
60CR60FR**

**Figure G.56 Failure of
60CR60FR**

**Figure G.57 Failure of
60CR60FR**

**Figure G.58 Failure of
60CR60FR**

G.2   CONFINED RUBBERISED CONCRETE FAILURE PHOTOS

Figure G.59 Photos of 2A-M1

Figure G.60 Photos of 2A-M1

Figure G.61 Photos of 2A-M2

Figure G.62 Photos of 2A-M2

Figure G.63 Photos of 2A-M2

Figure G.64 Photos of 2A-C1

Figure G.65 Photos of 2A-C1

Figure G.66 Photos of 2A-C2

Figure G.67 Photos of 2A-C2

Figure G.68 Photos of 2A-C3

Figure G.69 Photos of 2A-C3

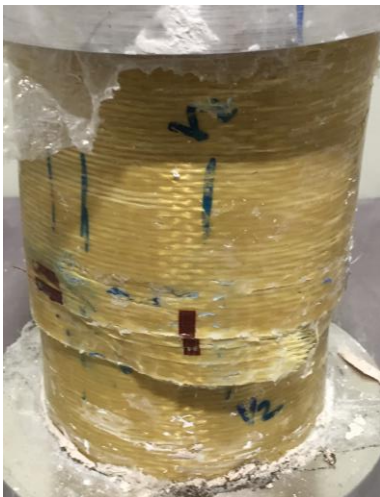**Figure G.70 Photos of 3A-M1**
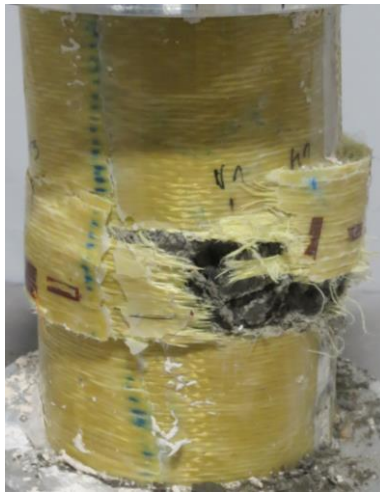

Figure G.71 Photos of 3A-M1

Figure G.72 Photos of 3A-M2

Figure G.73 Photos of 3A-M2

Figure G.74 Photos of 3A-C1

Figure G.75 Photos of 3A-C2

Figure G.76 Photos of 3A-C2

Figure G.77 Photos of 3A-C3

Figure G.78 Photos of 3A-C3

Figure G.79 Photos of 4A-M1

Figure G.80 Photos of 4A-M1

Figure G.81 Photos of 4A-M1

Figure G.82 Photos of 4A-M2
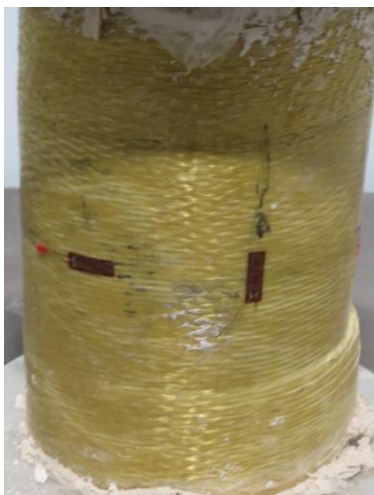

Figure G.83 Photos of 4A-M2

Figure G.84 Photos of 4A-C1

Figure G.85 Photos of 4A-C2

Figure G.86 Photos of 4A-C2

Figure G.87 Photos of 4A-C3

Figure G.88 Photos of 4A-C3

Figure G.89 Photos of 2C-M1

Figure G.90 Photos of 2C-M1
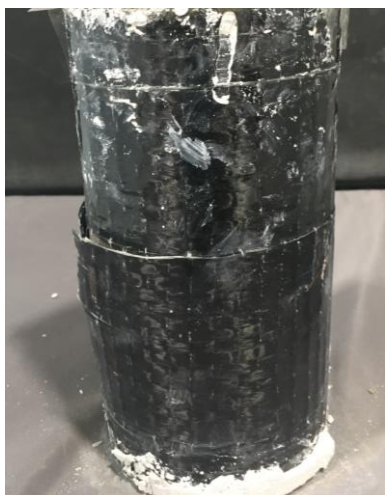

Figure G.91 Photos of 2C-M2

Figure G.92 Photos of 2C-M2

Figure G.93 Photos of 2C-C3

Figure G.94 Photos of 2C-C3

Figure G.95 Photos of 2C-C3

Figure G.96 Photos of 3C-C3

Figure G.97 Photos of 3C-C3

Figure G.98 Photos of 4C-M1

Figure G.99 Photos of 4C-C3

Figure G.100 Photos of 3C-M2